To the Graduate Council:

I am herewith submitting a dissertation written by James Alan Drakes entitled "A Mechanism For Fast Electronic Energy Transfer in Spin-Forbidden Reactions." I have examined the final copy of this dissertation for form and content and recommend that it be accepted in partial fulfillment of the requirements for the degree of Doctor of Philosophy, with a major in Physics.

Arthur A. Mason, Major Professor

We have read this dissertation
and recommend its acceptance:

W. S. McGregor

C. C. Limbaugh

H. W. Crater

Accepted for the Council:

Associate Vice Chancellor
and Dean of the Graduate School

A Mechanism For Fast Electronic Energy Transfer in Spin-Forbidden Reactions

A Dissertation

Presented for the

Doctor of Philosophy

Degree

The University of Tennessee, Knoxville

James Alan Drakes

May 1994

In memory,

Blessed is the man whose strength is in thee.
(Psalms 84:2)

M. E. Gorniak
(1931 - 1994)

ACKNOWLEDGMENTS

After a graduate career of some nine years, it must be realized that without my wife Nancy, none of this would have been possible. She has earned, without question, my unending gratitude for her patience, devotion, and tireless encouragement throughout this entire educational process.

During seven of the past nine years, my formal education has been guided by Dr. Arthur Mason. I wish to thank him for his ceaseless, positive support and guidance during this special time. Furthermore, I wish to acknowledge the professional critique received from members of my graduate committee, Drs. Crater, Lewis, and Limbaugh, beginning with the development of this research and lasting through the writing of this dissertation. In addition, I wish to thank a special member of my committee, Dr. Mac McGregor, whom I consider as a research collaborator, teacher, and friend. I am certain that he has taught me more than either of us realize.

This effort would not have been possible without the direct and indirect support of Sverdrup Technology, Inc., and most notably my supervisor for the majority of this work, Mr. C.R. Darlington. In addition, the support received in all forms, technical, clerical, etc., from the people of the Technology branch work groups EL3, headed by Dr. J. Adams, and EL5, headed by Dr. C. Pender, must be cited. It is the work environment which they provide which fosters the excitement and creativity necessary to pursue endeavors such as this research.

The United States Air Force Arnold Engineering Development Center has played a pivotal role in the completion of this work. I wish to thank the Air Force Directorate of Technology for creating a stimulating, dynamic arena in which to apply fundamental science to real-world problems.

My family members have contributed greatly to this successful outcome, including my mother, siblings, nieces, FNDs, et al. They must be credited for forcing me to complete this effort, even at times by readjusting an oft-misplaced attitude. Thank you.

I also wish to acknowledge Mr. Martin Nelius for his optimism, encouragement and support, including such things as the loan of the printer upon which this document was created.

ABSTRACT

The quenching behavior of neutral metastable species during collisions with a neutral partner is investigated. Usually, radiationless energy transfer can be described by invoking the radiation field as an intermediary between interacting molecules. However, for metastables, the dominant radiation transition moments are suppressed, most often by spin selection rules between the excited and ground energy states. The fast reaction rates for the quenching of the metastables suggest a different intermediary for such cases. Motivated by this phenomena, a two-electron exchange process is proposed as the quenching mechanism. During a collision, it is envisioned that the excited outer shell electron of the metastable effectively undergoes a change of molecular center and is replaced by an electron from the collision partner. The theoretical framework for this process is developed from first principles of quantum field theory. The electron exchange term is obtained explicitly, using the minimal-coupling method.

An application of the theory was computed for the energy transfer from the Ar metastable to N_2. This reaction has been studied in depth experimentally, and has a mean cross section of 9 A^2, with a range of measurements from 2.7 A^2 to 18 A^2. The computed theoretical cross section using the two-electron exchange interaction in the first Born approximation is 1.7 A^2, which is in good agreement with the data considering the range of measured values and the difficulty involved in interpreting the experiments.

TABLE OF CONTENTS

LIST OF TABLES

LIST OF FIGURES

FIGURE PAGE

FIGURE PAGE

FIGURE PAGE

Chapter 1

Introduction

Experimental Observations

There exists a class of bimolecular collisions which transfer electronic energy at collision rates near the gas kinetic limit. Although interesting in itself, the peculiar item about this class of collisions is that the energy transfer rate should be near zero. The class of collisions which is referred to is a subset of those reactions in which one of the collision partners is initially in an electronically metastable state. For certain reaction pairs, the electronic energy transfer rate from the metastable reactant to the collision partner is extremely large. However, in the usual methods of energy transfer in collisions, the rate should be governed by radiative polar transition moment functions of each of the collision partners, e.g. the electric dipole, magnetic dipole, electric quadrupole transition moments, etc. Hence, a paradox arises since the metastable species is defined as metastable because the radiative polar transition moment function is so small.

As a concrete example, a very well studied energy transfer reaction is the quenching of $N_2(A^3\Sigma_u^+)$ by NO. The reaction details are given by

(1.1) $$N_2(A^3\Sigma_u^+) + NO(X^2\Pi) \rightarrow N_2(X^1\Sigma_g^+) + NO(A^2\Sigma^+)$$

The reaction rate has been carefully measured by Piper, et al., [1][1] using a discharge flow reactor apparatus, and the value of 1.0×10^{-10} cm^3/sec/molecule was determined. Under those conditions, the gas kinetic rate is approximately 3.0×10^{-10}

---

[1]Numbers in brackets refer to similarly numbered references in the bibliography.

cm^3/sec/molecule. At first glance, the rate of (1.1) is not particularly exciting. However, upon closer inspection, it will be found that the N_2 undergoes a spin-forbidden transition during the electronic energy transfer process. It should be understood that the term spin-forbidden transition does not necessarily mean that the molecular transition is impossible, but in the case of the transition of N_2 from the excited $A^3\Sigma_u^+$ state to the ground $X^1\Sigma_g^+$ the terminology is quite appropriate. This is evidenced by the fact that the lifetime of the $A^3\Sigma_u^+$ state is approximately two seconds. For comparison, typical electronic lifetimes of similar states with spin-allowed transitions range in the neighborhood of 10^{-8} to 10^{-7} seconds. Clearly, the extremely fast energy transfer rate of (1.1) is incompatible with a description of energy transfer based upon radiative moments.

Another common example of a fast, but spin-forbidden energy transfer reaction is given by

(1.2) $$CO(a^3\Pi) + NO(X^2\Pi) \rightarrow CO(X^1\Sigma^+) + NO(A^2\Sigma^+)$$

In this case the excited metastable collision partner is the lowest triplet state of carbon monoxide, $CO(a^3\Pi)$, with a radiative lifetime of roughly 7 msec [2]. Once again, the longevity of the $CO(a^3\Pi)$ state is due to spin-forbidden dipole transition to ground $CO(X^1\Sigma^+)$ state [3]. The quenching of $CO(a^3\Pi)$ by ground state nitric oxide, NO, has been carefully measured by several authors [4-7]. The rate constant for (1.2) is on the order of 2.3×10^{-10} cm^3/sec/molecule, which, again, is nearly the gas kinetic rate of 3.0×10^{-10} cm^3/sec/molecule [8].

A final example of the class of fast, spin-forbidden energy transfer reactions is given by the quenching of metastable atomic argon by N_2,

(1.3) $$Ar(^3P_{0,2}) + N_2(X^1\Sigma_g^+) \rightarrow Ar(^1S_0) + N_2(C^3\Pi_u)$$

The reaction rate for (1.3) has been determined by Kolts, et al., [9] to be approximately 3.3×10^{-11} cm^3/sec/molecule, which is within an order of magnitude of the approximate

gas kinetic rate.

In every reaction, (1.1), (1.2), and (1.3), the energy is removed during the collision from an excited metastable at a tremendous rate. The usual description of energy transfer during molecular collisions asserts that the collision partners react to one another by coupling to the radiation field. However, since the radiative moments of the metastables involved in (1.1), (1.2), and (1.3) are so small, it is clear that radiative coupling between the collision partners is impossible. An alternative model of energy transfer is required to address the unique characteristics of the fast, spin-forbidden, energy transfer reactions.

Hypothesis of the Two-Electron Exchange Mechanism

Once the possibility of coupling collision partners with an intermediate photon is removed, the possibilities for a coupling mechanism are rather limited. Indeed, the only alternative is to couple the reactants directly with intermediate electrons. This is not a new concept. Single electron transfer processes are the topic of a burgeoning amount of research, predating the now classic works by Massey, et al., and many others [10,11,12]. However, while most experimental and theoretical work has concentrated upon the transfer of an electron from an atom or molecule as a target to some type of positively charged projectile, a lesser effort has examined electron transfer processes with charge neutral participants.

In the spirit of single electron transfer, the present research begins by postulating that a two-electron exchange mechanism is responsible for the anomalous fast energy transfer rates of (1.1), (1.2), and (1.3). Indeed, the main goal of this work is to develop the theoretical formalism required to describe an electron transfer process for neutral collision partners.

Any one of the three above reactions would be suitable for testing the theory. However, practical computational considerations make (1.3) the most desirable reaction on which to apply the formalism. First, reaction (1.3) is a crucial step in the operation of the UV Nitrogen laser [13]. This has made it a topic of intense research for over the past twenty-five years. Secondly, (1.3) is the least stressing in terms of the molecular wavefunctions and collision dynamics. Because Ar is an atomic species as opposed to a diatomic molecule, the level of complexity in the descriptions of components outside the newly developed theory is greatly reduced. Thus, (1.3) was chosen as a prototype reaction for the application of the two-electron exchange mechanism.

Objectives and Results

The stated objective of this research is thus twofold. The first goal is to develop the two-electron exchange mechanism for energy transfer. The second goal is to apply this mechanism to a physical system to determine if it represents a plausible energy transfer mechanism.

The interaction Hamiltonian for the two-electron exchange mechanism was obtained, based upon a first principles derivation of the fully quantized system Hamiltonian. This derivation constitutes the first occurrence of such a formalism in the literature.

The application of the two-electron exchange mechanism to the Ar-N_2 reaction successfully proved that this mechanism is a plausible explanation to the anomalous high reaction rate. The reaction cross section predicted by this mechanism is within a factor of 5 of the mean experimental measurement.

Format of the Dissertation

This dissertation is presented in two conceptual parts. The first part of the discussion is the theoretical development of the two-electron mechanism. This includes the presentation of some reference material that is necessary to complete the modeling, but which lies in fields outside the customary sources. Indeed, this dissertation research has taken a multidisciplinary approach, pulling quite heavily from the fields of molecular quantum electrodynamics, particle physics, quantum chemistry, chemical kinetics, and molecular physics. The bulk of the novel research is contained within Chapter 3 in which the two-electron exchange mechanism is derived.

The second part of the dissertation presents the application of the theory to reaction (1.3). Even though the formalism is completed in the first part, there is considerable theoretical development remaining in order to adapt it to the specifics of an actual physical system. Indeed, in Chapter 7, a novel method for solving a class of molecular integrals falls out of this development. Following the adaptation of the theory, the methodology of the application is documented. Lastly, the computational results are scrutinized and compared with data.

Chapter 2

Molecular Quantum Electrodynamics

The purpose of this research is to apply the techniques of quantum field theory to molecular scattering. It is only appropriate then, to determine the groundwork laid by previous researchers in this area. The most effective application of quantum field theory to molecular processes is the topic of molecular quantum electrodynamics (MQED). This chapter serves to define the boundaries of MQED, and provides a starting point for the present research.

The following presentation of MQED draws almost exclusively from original papers by Craig, Power, and Thirunamachandran [14-19]. It is given as supporting reference material which will be used as a foundation for the original research to be described in subsequent Chapters.

Basic Premise

Molecular quantum electrodynamics (MQED) was defined in the early 1980's as the synthesis of second quantization of the molecular Hamiltonian with the quantum field theory of radiation, in large part by a series of works by Craig, Power, and Thirunamachandran [14-19]. The goal was to advance the textbook theories to applications regarding specific interactions between atomic or molecular systems and radiation. The hallmark of the success of MQED lay in the clear descriptions of single and multiphoton processes, such as laser absorption and fluorescence. Furthermore, by introducing the radiation field as a quantum rather than classical field, Feynmann diagrams could be used to describe and calculate interactions that were previously

awkward at best. However, since molecular systems are not point particles, such as those typically used in Feynmann diagrams, several key assertions were made to apply MQED to physical systems. They were:

1.) All interactions between molecules are mediated by the quantized radiation field. This implies that both real (massless) and virtual (massive) photons are responsible for collision processes such as energy transfer. Indeed, excitation transfer is the main concern of MQED.

2.) The equations of motion are generated from a combined Hamiltonian of a spinless matter Hamiltonian with the quantized radiation Hamiltonian. The lack of electron spin is typically not a problem for most situations. This is because the intermediate particle of molecular interactions is the photon which is of unit spin, i.e. a Boson. Hence, the spin eigenspaces for the photon and the molecule are disjoint.

3.) It is usually assumed that each participating molecule, called a chromophore, behaves as if it had a single active electron. All other electrons, such as K-shell electrons, are ignored since they do not participate directly with collision processes.

4.) The formalism, as is presently developed, is nonrelativistic. Hence, it is not written in a Lorentz invariant framework. Since molecular collision systems are rarely, if ever, near relativistic energies, this is not a significant restriction, other than the loss of symmetric equations.

Clearly, these assumptions are not very restrictive to the problem of molecular collisions.

The concept of MQED is both elegant and powerful. MQED provides a foundation for the study of molecular interactions with radiation by treating both elements equally. This research used elements of MQED as a springboard to model a specific class of molecular collision. As will be shown below, MQED models molecular

collisions as a transfer of real and virtual photons. Even though this mechanism fails for fast, spin-forbidden energy transfer reactions, as will be shown below, understanding the inspiring structure of MQED is a relevant undertaking.

To understand the limitations of MQED, the interaction Hamiltonian must be derived. This goal is attained by standard field techniques after postulating an appropriate Lagrangian. The assumed Lagrangian is tested for correctness by determining the equations of motion of the fields and comparing with the known dynamical equations. The standard minimal substitution prescription is followed in order to include the interaction between the fields. The complete Hamiltonian follows directly. Although minimal substitution is useful, an equivalent multipolar formulation of the equations is given which exploits the gauge freedom of the radiation field. This is more amenable to the typical observables of atomic and molecular physics, such as the dipole and quadrupole moments. The expression of the interaction Hamiltonian in terms of molecular moments is the *coups de gras* of MQED. By examining the interaction Hamiltonian, it will become evident that at least for the class of molecular collisions of this study, the interaction is not sufficient to explain the experimental data presented in Chapter 6. A new, more applicable model must be postulated, and will be discussed in Chapter 3.

Behavior of the (Unquantized) Electron and Radiation Fields

The Minimal Substitution Lagrangian

Consider the Lagrangian for a spinless electron field in the presence of an undefined external potential,

$$L_{charge} = -\int d^3r\, \overline{\psi}(\underline{r})\left\{\frac{-\hbar^2}{2m}\nabla^2 + V(\underline{r})\right\}\psi(\underline{r}) + \frac{i\hbar}{2}\int d^3r\left\{\overline{\psi}(\underline{r})\dot{\psi}(\underline{r}) - \dot{\overline{\psi}}(\underline{r})\psi(\underline{r})\right\} \tag{2.1}$$

where $\psi(\underline{r})$ and $\overline{\psi}(\underline{r})$ are the scalar electron field operators, with the property that $\overline{\psi}(\underline{r})$ is the Hermitian conjugate to $\psi(\underline{r})$. The electron mass is given by m, and the vector $\underline{r}$ refers to three-dimensional coordinate space. The partial time derivatives are abbreviated as $\partial A/\partial t \equiv \dot{A}$. The $V(\underline{r})$ potential is due to external sources, such as the individual atomic nuclei within the molecular system. As mentioned above, electron-electron correlation effects are ignored.

To see that (2.1) is, in fact, a correct Lagrangian, the equations of motion can be obtained from the Euler-Lagrange equations in a straightforward manner, noting that the complete Lagrangian may be written as an integral over the Lagrangian density, $\mathcal{L}$,

$$L = \int d^3r\, \mathcal{L}\,(\psi, \overline{\psi}, \dot{\psi}, \dot{\overline{\psi}}; \underline{r}, t) \tag{2.2}$$

and that the equations of motion originate from the Euler-Lagrange equation,

$$\frac{d}{dt}\left(\frac{\partial \mathcal{L}}{\partial \dot{\psi}}\right) + \frac{d}{dr_i}\left(\frac{\partial \mathcal{L}}{\partial(\partial\psi/\partial r_i)}\right) - \frac{\partial \mathcal{L}}{\partial \psi} = 0 \tag{2.3}$$

The canonical momentum of $\psi(\underline{r})$ is simply

$$\frac{\partial \mathcal{L}}{\partial \dot{\psi}} = \frac{i\hbar}{2}\overline{\psi} \tag{2.4}$$

and substituting (2.4) into (2.3) yields the equation of motion for $\psi(\underline{r})$,

$$(2.5) \qquad i\hbar\dot{\psi} = \left\{\frac{-\hbar^2}{2m}\nabla^2 + V\right\}\psi$$

This is the standard Schrödinger equation for an electron field. Note that the explicit $\underline{r}$ dependence of ψ has been suppressed for clarity. Furthermore, an analogous equation may be derived for $\overline{\psi}$. Thus, the Lagrangian of (2.1) is sufficient to describe the dynamical behavior of the field and will be used as the basis for subsequent discussion.

To couple the electron and radiation fields, the standard minimal coupling prescription is used [14]. The total Lagrangian must be the sum of the uncoupled electron field Lagrangian, i.e. (2.5), an uncoupled radiation field Lagrangian, and a term which involves both the electron and radiation fields. The usual form for this Lagrangian is

(2.6)

$$\begin{aligned} L_{min} = &-\int d^3r\,\overline{\psi}\left\{\frac{1}{2m}\left(-i\hbar\nabla + \frac{e}{c}\underline{a}\right)^2 + V\right\}\psi \\ &-\frac{e^2}{2}\int d^3r\,\overline{\psi}(\underline{r})\int d^3r'\,\frac{\overline{\psi}(\underline{r}')\psi(\underline{r}')}{|\underline{r}-\underline{r}'|}\psi(\underline{r}) \\ &+\frac{i\hbar}{2}\int d^3r\left\{\overline{\psi}\dot{\psi} - \dot{\overline{\psi}}\psi\right\} \\ &+\frac{1}{8\pi}\int d^3r\left[\left(\frac{\dot{\underline{a}}}{c}\right)^2 - (\nabla\times\underline{a})^2\right] \end{aligned}$$

where, in contrast to (2.1), the interaction energy of the electron field has been accounted for in the second line. The radiation field, $\underline{a}$, is a spatial varying vector quantity. The lower case serves as a reminder that $\underline{a}$ is the microscopic radiation field.

Also, note that in (2.6) the electron charge, e, is defined as a negative value. Imposing the Coulomb gauge on $\underline{a}$ implies that

$$\nabla \cdot \underline{a} = 0 \tag{2.7}$$

meaning that $\underline{a}$ is a purely transverse vector. Thus, in this discussion, $\underline{a}$ is always taken to be the perpendicular component of the total vector potential. From standard classical electrodynamics [20], it follows that the electric field can be obtained as the time derivative of the vector potential via

$$\underline{e} = -\frac{1}{c}\dot{\underline{a}} \tag{2.8}$$

Hence, $\underline{e}$ is also a purely transverse vector in the absence of interactions with matter. Since the fields are not yet quantized, (2.8) must be valid for (2.6) to be a valid Lagrangian.

In using (2.6) rather than (2.1), the Lagrangian density is now a functional of both the radiation and the matter fields. It is important to determine if (2.6) is capable of generating the equations of motion for the radiation field. Minimizing the Lagrangian with respect to the i^{th} vector component of the radiation field results in

$$\begin{aligned} 0 = \frac{1}{c^2}\ddot{a}_i - [\nabla \times (\nabla \times \underline{a})]_i + \\ \frac{4\pi e}{mc}\int d^3r' \, \overline{\psi}(\underline{r}')\left\{-i\hbar\nabla' + \frac{e}{c}\underline{a}(\underline{r}')\right\}_j \delta_{ij}^{\perp}(\underline{r} - \underline{r}')\psi(\underline{r}') \end{aligned} \tag{2.9}$$

The transverse delta function is given by $\delta_{ij}^{\perp}(\underline{r}) \equiv \frac{2}{3}\delta_{ij}\delta(\underline{r}) - \frac{1}{4\pi r^3}\left(\delta_{ij} - 3\hat{r}_i\hat{r}_j\right)$. Note that in (2.9), ∇' refers to differentiation with respect to $\underline{r}'$. Using $\underline{b} = \nabla \times \underline{a}$, (2.9) can be rewritten as

$$\frac{1}{c}\dot{\underline{e}}(\underline{r}) = \nabla \times \underline{b}(\underline{r}) + \frac{4\pi}{c}\underline{j}^{\perp}(\underline{r}) \tag{2.10}$$

with the current defined as

$$(2.11) \qquad \left(\underline{j}^{\perp}(\underline{r})\right)_i = \frac{-e}{m}\int d^3r' \,\overline{\Psi}(\underline{r}')\left\{-i\hbar\nabla' + \frac{e}{c}\underline{a}(\underline{r}')\right\}_j \delta^{\perp}_{ij}(\underline{r}-\underline{r}')\Psi(\underline{r}')$$

It is of interest to note that (2.10) is the differential form of Ampere's law.

The equations of motion for the electron fields may also be obtained from (2.6) by performing the minimization of the Lagrangian (2.6) with respect to the electron fields, in a similar fashion as was done for the uncoupled electron field Lagrangian (2.1). This leads to an expression for the equation of motion of an electron field in the presence of the radiation field,

$$(2.12) \qquad i\hbar\dot{\psi}(\underline{r}) = \left\{\frac{1}{2m}\left(-i\hbar\nabla + \frac{e}{c}\underline{a}\right)^2 + V(\underline{r}) + e^2\int dr' \frac{\overline{\Psi}(\underline{r}')\Psi(\underline{r}')}{|\underline{r}-\underline{r}'|}\right\}\Psi(\underline{r})$$

which is simply the expected Schrödinger equation for the system. The interaction of the electron and radiation fields is given by the cross products of the first term in the brackets, while the Coulomb attraction of the nucleus is described by the external potential energy $V(\underline{r})$. The electron-electron interaction energy is described by the third term in the brackets. Thus, the minimal substitution Lagrangian (2.6) leads to the proper equations of motion for both the radiation and matter fields.

The Multipolar Lagrangian

The minimal substitution Lagrangian (2.6) fully describes the electron-radiation system. However, an alternative, but equivalent form of the electron-radiation coupling is desirable when dealing with atomic and molecular systems. Usually, the experimental observables are not the electron field, but the atomic and molecular multipole moments, e.g. the electric dipole moment. Thus, by couching (2.6) in terms of molecular parameters, a more manageable expression for the interaction Hamiltonian will result.

The multipolar formalism can be obtained in a variety of ways and has been studied by a variety of authors [21-23]. One common method of obtaining a multipolar expansion from the minimal substitution expression has been to include a total time derivative to the Lagrangian [24]. An alternative, yet equivalent, method due to Craig and Thirunamachandran is to define a phase change of the electron fields in which

$$\psi(\underline{r}) \equiv e^{iS(\underline{r})}\phi(\underline{r}) \tag{2.13}$$

where

$$S(\underline{r}) \equiv \frac{1}{\hbar c}\int d^3r'\, \underline{p}(\underline{r}',\underline{r})\cdot \underline{a}(\underline{r}') \tag{2.14}$$

and $\underline{p}(\underline{r}',\underline{r})$ is the polarization vector field due to the electron [14]. Since $S(\underline{r})$ is real, it follows that $\overline{\psi} = \overline{\phi}\, e^{-iS}$.

For bound electrons, the polarization is localized and can be determined by an expansion at a given spatial location. An example would be a system, such as an atom, with a defined center located at $\underline{R}$. The polarization may then be expanded as

$$\underline{p}(\underline{r}',\underline{r}) = -e(\underline{r}-\underline{R})\delta(\underline{r}'-\underline{R}) + \tfrac{1}{2}e(\underline{r}-\underline{R})(\underline{r}-\underline{R})\cdot\nabla'\delta(\underline{r}'-\underline{R}) + \ldots \tag{2.15}$$

where, as above, the electron charge is defined intrinsically negative. Defining the dipole moment as the vector,

$$\underline{\mu} \equiv -e(\underline{r}-\underline{R}) \tag{2.16}$$

and the quadrupole moment as a dyadic,

$$\ddot{Q} \equiv -\tfrac{e}{2}(\underline{r}-\underline{R})(\underline{r}-\underline{R}) \tag{2.17}$$

allows the polarization field to be approximated as a function dependent upon two spatial locations,

$$\underline{p}(\underline{r}',\underline{r}) \equiv \underline{\mu}(\underline{r})\delta(\underline{r}'-\underline{R}) - \ddot{Q}(\underline{r})\cdot\nabla'\delta(\underline{r}'-\underline{R}) \tag{2.18}$$

where the infinite series has been truncated. Thus, the molecular moments may now be incorporated into the derivation of the interaction Hamiltonian.

The minimal coupling Lagrangian (2.6) can be converted to a multipolar Lagrangian by substituting the phase condition (2.13) into (2.6). The substitution results in

$$
\begin{aligned}
L_{multi} = & -\int d^3r\, e^{-iS}\bar{\phi}\left\{\frac{1}{2m}\left(-i\hbar\nabla+\frac{e}{c}\underline{a}\right)^2+V+\frac{e^2}{2}\int d^3r'\frac{\bar{\phi}(\underline{r}')\phi(\underline{r}')}{|\underline{r}-\underline{r}'|}\right\}e^{iS}\phi \\
& +\frac{i\hbar}{2}\int d^3r\left\{e^{-iS}\bar{\phi}\partial_t(e^{iS}\phi)-\partial_t(\bar{\phi}e^{-iS})e^{iS}\phi\right\} \\
& +\frac{1}{8\pi}\int d^3r\left\{\left(\frac{\dot{\underline{a}}}{c^2}\right)^2-(\nabla\times\underline{a})^2\right\}
\end{aligned}
\tag{2.19}
$$

The gradient term can be pulled through the matter portion of L_{multi} using straightforward differentiation,

$$
\left(-i\hbar\nabla+\frac{e}{c}\underline{a}\right)e^{iS}\phi = e^{iS}\left(\hbar(\nabla S)\phi-i\hbar\nabla\phi+\frac{e}{c}\underline{a}\phi\right) \tag{2.20}
$$

and after considerable algebra, the square which appears in (2.19) can be obtained as

$$
\left(-i\hbar\nabla+\frac{e}{c}\underline{a}\right)^2 e^{iS}\phi = e^{iS}\left(-i\hbar\nabla+\frac{e}{c}\underline{a}+\hbar\nabla S\right)^2\phi \tag{2.21}
$$

The electron field current term of the minimal substitution Lagrangian is replaced by the second line of (2.19). Using the phase transformation and the subsequent expressions for the multipole moments, it is possible to rewrite the second line of (2.19) as

$$
\begin{aligned}
& \frac{i\hbar}{2}\int d^3r\left\{e^{-iS}\bar{\phi}\partial_t(e^{iS}\phi)-\partial_t(\bar{\phi}e^{-iS})e^{iS}\phi\right\}= \\
& \frac{i\hbar}{2}\int d^3r\left\{\bar{\phi}\dot{\phi}-\dot{\bar{\phi}}\phi\right\} \\
& -\frac{1}{c}\int d^3r\,\bar{\phi}(\underline{r})\int d^3r'\,\underline{p}(\underline{r}',\underline{r})\cdot\underline{a}(\underline{r}')\phi(\underline{r})
\end{aligned}
\tag{2.22}
$$

Putting the pieces together into the multipolar Lagrangian results in

$$L_{multi} = -\int d^3r\, \bar{\phi}\left\{\frac{1}{2m}\left(-i\hbar\nabla + \frac{e}{c}\underline{a} + \hbar\nabla S\right)^2 + V + \frac{e^2}{2}\int d^3r' \frac{\bar{\phi}(\underline{r}')\phi(\underline{r}')}{|\underline{r}-\underline{r}'|}\right\}\phi$$

$$+\frac{i\hbar}{2}\int d^3r\left\{\bar{\phi}\dot{\phi} - \dot{\bar{\phi}}\phi\right\} + \frac{1}{8\pi}\int d^3r\left\{\left(\frac{\dot{\underline{a}}}{c^2}\right)^2 - (\nabla\times\underline{a})^2\right\} \tag{2.23}$$

$$-\frac{1}{c}\int d^3r\, \bar{\phi}(\underline{r})\int d^3r'\, \underline{p}(\underline{r}',\underline{r})\cdot\dot{\underline{a}}(\underline{r}')\phi(\underline{r})$$

A very useful trick [22] is to define a function $\underline{n}(\underline{r}',\underline{r})$ as

$$\underline{n}(\underline{r}',\underline{r}) = -e(\underline{r}-\underline{R})\int_0^1 d\lambda\, \lambda\, \delta(\underline{r}'-\underline{R}-(\underline{r}-\underline{R})\lambda) \tag{2.24}$$

By expanding $\underline{n}(\underline{r}',\underline{r})$ into its leading terms, it can be related to the multipole moments defined in (2.15),

$$\underline{n}(\underline{r}',\underline{r}) = \left[-\frac{e}{2}(\underline{r}-\underline{R}) + \frac{e}{3}(\underline{r}-\underline{R})(\underline{r}-\underline{R})\cdot\nabla' + \ldots\right]\delta(\underline{r}'-\underline{R}) \tag{2.25}$$

Conversely, this implies that the polarization field (2.15) can be written in a similar form as $\underline{n}(\underline{r}',\underline{r})$. A suitable functional expression [22] for (2.15) is

$$\underline{p}(\underline{r}',\underline{r}) = -e(\underline{r}-\underline{R})\int_0^1 d\lambda\, \delta(\underline{r}'-\underline{R}-(\underline{r}-\underline{R})\lambda) \tag{2.26}$$

It can then be shown that the vector potential term of (2.23) can be written as [14]

$$\frac{e}{c}\underline{a}(\underline{r}) + \hbar\nabla S(\underline{r}) = \frac{1}{c}\int d^3r'\, \underline{n}(\underline{r}',\underline{r})\times\underline{b}(\underline{r}') \tag{2.27}$$

Physically, the integral form on the right is an expression for the transformed vector potential, consistent with the definition on the left. The compact form of $\underline{n}(\underline{r}',\underline{r})$ and its expansions provide ample justification for its seemingly ad hoc introduction.

With (2.27), some immediate approximations to the matter-radiation coupling terms of (2.23) can be demonstrated. The electric dipole coupling can be seen to give a zero contribution from

$$\begin{aligned}\frac{e}{c}\underline{a}+\hbar\nabla S &\approx \frac{e}{c}\underline{a}(\underline{R})-\frac{e}{c}\nabla\int d^3r'\,(\underline{r}-\underline{R})\cdot\underline{a}(\underline{r}')\,\delta(\underline{r}'-\underline{R}) \\ &= \frac{e}{c}\underline{a}(\underline{R})-\frac{e}{c}\nabla(\underline{r}-\underline{R})\cdot\underline{a}(\underline{R}) \\ &= 0\end{aligned} \tag{2.28}$$

while the electric quadrupole has a nonzero value given by

$$\begin{aligned}\left(\frac{e}{c}\underline{a}+\hbar\nabla S\right)_i &\approx \frac{e}{c}(\underline{r}-\underline{R})_j\nabla_j a_i(\underline{R}) \\ &\quad -\frac{e}{2c}\nabla_i\left\{(\underline{r}-\underline{R})_k(\underline{r}-\underline{R})_j\nabla_k a_j(\underline{R})\right\} \\ &= \frac{-e}{2c}\left[(\underline{r}-\underline{R})\times\underline{b}(\underline{R})\right]_i\end{aligned} \tag{2.29}$$

With these approximations for the coupling term, the total Lagrangian can be written in a form which is correct through the electric quadrupole and magnetic dipole terms of the multipolar expansion as

(2.30)

$$
\begin{aligned}
L_{multi} = &-\int d^3r\,\bar{\phi}\left\{\frac{1}{2m}\left(-i\hbar\nabla-\frac{e}{2c}(\underline{r}-\underline{R})\times\underline{b}(\underline{R})\right)^2+V\right\}\phi \\
&-\frac{e^2}{2}\int d^3r\,\bar{\phi}(\underline{r})\int d^3r'\,\frac{\bar{\phi}(\underline{r}')\phi(\underline{r}')}{|\underline{r}'-\underline{r}|}\phi(\underline{r}) \\
&+\frac{i\hbar}{2}\int d^3r\left\{\bar{\phi}\dot{\phi}-\dot{\bar{\phi}}\phi\right\}+\frac{1}{8\pi}\int d^3r\left\{\left(\frac{\dot{\underline{a}}}{c^2}\right)^2-(\nabla\times\underline{a})^2\right\} \\
&+\frac{e}{c}\int d^3r\,\bar{\phi}(\underline{r})(\underline{r}-\underline{R})\cdot\dot{\underline{a}}(\underline{R})\phi(\underline{r})
\end{aligned}
$$

This expression for the Lagrangian is particularly useful for determining interactions that depend upon the multipole moments of the electron field. The Hamiltonian is determined from the Lagrangian according to the standard manipulation,

(2.31) $$H = \sum_i p_i\dot{q}_i - L$$

where $\dot{q}_i$ represents the time derivative of the various fields, and p_i represents the corresponding field conjugate momentum. For the radiation field, the conjugate momentum density, using (2.23), is a vector quantity given by

(2.32)

$$
\begin{aligned}
\pi_i &\equiv \frac{\partial \mathcal{L}_{multi}}{\partial \dot{a}_i} \\
&= \frac{1}{4\pi c^2}\dot{a}_i - \frac{1}{c}\int d^3r'\,\bar{\phi}(\underline{r}')\,p_i^{\perp}(\underline{r}',\underline{r})\,\phi(\underline{r}') \\
&= \frac{-1}{4\pi c}\left\{\frac{-1}{c}\dot{a}_i + 4\pi\int d^3r'\bar{\phi}(\underline{r}')\,p_i^{\perp}(\underline{r}',\underline{r})\,\phi(\underline{r}')\right\} \\
&\equiv \frac{-1}{4\pi c}d_i^{\perp}
\end{aligned}
$$

which defines $\underline{d}^{\perp}$ as the transverse component of the microscopic displacement vector. Note that only the transverse portion of the polarization is considered in (2.32) since it originated as a dot product with the implicitly transverse vector potential. A similar calculation for the electron fields gives the conjugate momentum as

$$\begin{aligned} \Pi &\equiv \frac{\partial \mathcal{L}_{multi}}{\partial \dot{\phi}} \\ &= \frac{i\hbar}{2}\overline{\phi} \end{aligned} \tag{2.33}$$

and

$$\begin{aligned} \overline{\Pi} &\equiv \frac{\partial \mathcal{L}_{multi}}{\partial \dot{\overline{\phi}}} \\ &= -\frac{i\hbar}{2}\phi \end{aligned} \tag{2.34}$$

The full Hamiltonian follows directly from (2.31) as

$$H = \int d^3r \left(\underline{\pi} \cdot \dot{\underline{a}} + \Pi\dot{\phi} + \overline{\Pi}\dot{\overline{\phi}} \right) - L \tag{2.35}$$

The multipolar Hamiltonian may finally be obtained upon substitution of (2.30), (2.32), (2.33), and (2.34) into (2.35). Furthermore, additional substitution of the electric displacement vector into the multipolar Hamiltonian generates a very useful expression [14],

$$\begin{aligned} H_{multi} = & \int d^3r\, \overline{\phi}\left\{ \frac{1}{2m}\left(-i\hbar\nabla + \frac{1}{c}\int d^3r'\, \underline{n}(\underline{r}',\underline{r}) \times \underline{b}(\underline{r}') \right)^2 + V \right\}\phi \\ & + \frac{e^2}{2}\int d^3r\, \overline{\phi}(\underline{r}) \int d^3r' \frac{\overline{\phi}(\underline{r}')\phi(\underline{r}')}{|\underline{r}-\underline{r}'|}\phi(\underline{r}) \\ & + \frac{1}{8\pi}\int d^3r \left\{ (\nabla \times \underline{a})^2 + 16\pi^2 \left(c\underline{\pi} + \int d^3r'\, \overline{\phi}(\underline{r}')\underline{p}^{\perp}(\underline{r}',\underline{r})\phi(\underline{r}') \right)^2 \right\} \end{aligned} \tag{2.36}$$

Obviously, this expression can be separated into Hamiltonians for the radiation and matter fields, with the remainder being the interaction. Following some manipulation, the portion governing the radiation field is given by

$$H_{radn} = \frac{1}{8\pi}\int d^3r \left\{ \underline{b}\cdot\underline{b} + \underline{d}^{\perp}\cdot\underline{d}^{\perp} \right\} \tag{2.37}$$

while the portion governing the electron field is

$$\begin{aligned} H_{matter} = \int d^3r\, \bar{\phi}\left\{ \frac{1}{2m}(-i\hbar\nabla)^2 + V + \frac{e^2}{2}\int d^3r' \frac{\bar{\phi}(\underline{r}')\phi(\underline{r}')}{|\underline{r}-\underline{r}'|} \right\}\phi \\ +2\pi\int d^3r \left\{ \int d^3r' \bar{\phi}(\underline{r}')\underline{p}^{\perp}(\underline{r}',\underline{r})\phi(\underline{r}') \right\}^2 \end{aligned} \tag{2.38}$$

The radiation field Hamiltonian is exactly that which appears in standard texts on electromagnetism [20]. The matter Hamiltonian (2.38) consists of the expected terms for the kinetic energy, the external nuclear potential, and the electron-electron interaction. However, there is an additional term which is due to the introduction of the polarization vector. Thus, the electron-radiation interaction Hamiltonian is the sum of the remaining terms,

$$\begin{aligned} H_{int} = 4\pi c\int d^3r\, \bar{\phi}\left\{ \int d^3r'\, \underline{p}^{\perp}(\underline{r}',\underline{r})\cdot\frac{-1}{4\pi c}\underline{d}^{\perp}(\underline{r}') \right\}\phi \\ +\frac{1}{2mc}\int d^3r\, \bar{\phi}\left\{ \int d^3r' \begin{pmatrix} -i\hbar\nabla\cdot\underline{n}(\underline{r}',\underline{r})\times\underline{b}(\underline{r}') \\ +\underline{n}(\underline{r}',\underline{r})\times\underline{b}(\underline{r}')\cdot(-i\hbar\nabla) \end{pmatrix} \right\}\phi \\ +\frac{1}{2mc^2}\int d^3r\, \bar{\phi}\left\{ \int d^3r'\, \underline{n}(\underline{r}',\underline{r})\times\underline{b}(\underline{r}') \right\}^2\phi \end{aligned} \tag{2.39}$$

It is possible to write $\nabla\cdot\underline{n}(\underline{r}',\underline{r})\times\underline{b}(\underline{r}') = \nabla\times\underline{n}(\underline{r}',\underline{r})\cdot\underline{b}(\underline{r}') - \underline{n}(\underline{r}',\underline{r})\cdot\nabla\times\underline{b}(\underline{r}')$ where the second term is identically zero since $\underline{b}$ is a function of $\underline{r}'$ rather than $\underline{r}$. Another manipulation,

$$\underline{n}(\underline{r}',\underline{r})\times\underline{b}(\underline{r}')\cdot\nabla = -\underline{b}(\underline{r}')\times\underline{n}(\underline{r}',\underline{r})\cdot\nabla \qquad (2.40)$$
$$= -\underline{b}(\underline{r}')\cdot\underline{n}(\underline{r}',\underline{r})\times\nabla$$

allows the second term of the interaction Hamiltonian to be written as

$$\frac{1}{2mc}\int d^3r\,\bar{\phi}\left\{\int d^3r'\begin{pmatrix}\underline{b}(\underline{r}')\cdot(-i\hbar\nabla)\times\underline{n}(\underline{r}',\underline{r}) \\ -\underline{b}(\underline{r}')\cdot\underline{n}(\underline{r}',\underline{r})\times(-i\hbar\nabla)\end{pmatrix}\right\}\phi$$
$$= \frac{1}{2mc}\int d^3r'\,\underline{b}(\underline{r}')\cdot\int d^3r\begin{Bmatrix}-i\hbar\nabla\times\underline{n}(\underline{r}',\underline{r}) \\ -\underline{n}(\underline{r}',\underline{r})\times(-i\hbar\nabla)\end{Bmatrix}\phi \qquad (2.41)$$
$$= -\int d^3r'\int d^3r\,\bar{\phi}(\underline{r})\underline{b}(\underline{r}')\cdot\underline{m}(\underline{r}',\underline{r})\phi(\underline{r})$$

where the magnetic moment, $\underline{m}(\underline{r}',\underline{r})$, has been defined by

$$\underline{m}(\underline{r}',\underline{r}) \equiv \frac{-1}{2mc}\{(-i\hbar\nabla)\times\underline{n}(\underline{r}',\underline{r}) - \underline{n}(\underline{r}',\underline{r})\times(-i\hbar\nabla)\} \qquad (2.42)$$

Adaptation to Many-Field Problems

Although the problem of the radiation field interacting with a single electron field is of great interest and practical importance, (2.39) is not suited to describe molecular energy transfer collisions. The extension of the theory to include energy transfer is rather simplistic. The problem is modeled by assuming that each molecular center has a single active electron. The Lagrangian is then merely a summation of the exact single-center Lagrangian of (2.23), yielding

(2.43)

$$L_{multi} = -\sum_i \int d^3r\, \bar{\phi}_i \left\{ \frac{1}{2m}\left(-i\hbar\nabla + \frac{1}{c}\int d^3r'\, \underline{n}_i(\underline{r}',\underline{r}) \times \underline{b}(\underline{r}') \right)^2 + V_i + \frac{e^2}{2}\int d^3r' \frac{\bar{\phi}_i(\underline{r}')\phi_i(\underline{r}')}{|\underline{r}-\underline{r}'|} \right\} \phi_i$$
$$+ \frac{i\hbar}{2}\sum_i \int d^3r \left\{ \bar{\phi}_i\dot{\phi}_i - \dot{\bar{\phi}}_i\phi_i \right\} + \frac{1}{8\pi}\int d^3r \left\{ \left(\frac{\dot{\underline{a}}}{c^2} \right)^2 - (\nabla \times \underline{a})^2 \right\}$$
$$- \frac{1}{c}\sum_i \int d^3r\, \bar{\phi}_i(\underline{r}) \int d^3r'\, \underline{p}_i(\underline{r}',\underline{r}) \cdot \dot{\underline{a}}(\underline{r}')\phi_i(\underline{r})$$

The interaction between molecular assemblies has not been accounted for in (2.43). An additional Coulomb expression is required,

(2.44)

$$\sum_{\substack{i,j \\ i\neq j}} V_{ij} = \sum_{\substack{i,j \\ i\neq j}} \left\{ \int d^3r \bar{\phi}_i \left(\frac{-Z_j e^2}{|\underline{r}-\underline{R}_j|} + \frac{e^2}{2}\int d^3r' \frac{\bar{\phi}_j(\underline{r}')\phi_j(\underline{r}')}{|\underline{r}-\underline{r}'|} \right) \phi_i + \frac{1}{2}\frac{Z_i Z_j e^2}{|\underline{R}_i - \underline{R}_j|} \right\}$$

which involves three terms: the attraction of the electron of center i to nuclei j, the repulsion of the electron of center i from the electron of center j, and the repulsion of the nuclei j from nuclei i. Note that center i is located at $\underline{R}_i$, and that the nuclei has a charge Z_i.

In (2.43), $\underline{p}_i(\underline{r}',\underline{r})$ refers to the complete, i.e. both transverse and longitudinal, polarization density of the i^{th} molecule. Note though, that the vector potential is purely transverse. Thus, in the $\underline{p}_i(\underline{r}',\underline{r}) \cdot \dot{\underline{a}}(\underline{r}')$ term, the longitudinal component of the

polarization vector was not used. By defining $\underline{p}_i^l(\underline{r})$ as the longitudinal component of the polarization field vector (2.26) of the i^{th} molecule, i.e.

$$\underline{p}_i^l(\underline{r}) \equiv \int d^3r' \bar{\phi}_i(\underline{r}')\underline{p}_i^l(\underline{r},\underline{r}')\phi_i(\underline{r}') \tag{2.45}$$

it is possible to relate the various potentials involving a single center to the polarization vector. Also, it will be convenient to use a similar definition to (2.45) for the transverse component of the complete polarization vector, $\underline{p}_i^{\perp}(\underline{r})$. It can be shown that the intramolecular potential terms of (2.43) may be written as follows,

$$\begin{aligned} V_{intra} &= \sum_i \int d^3r\, \bar{\phi}_i \left\{ V_i + \frac{e^2}{2}\int d^3r' \frac{\bar{\phi}_i(\underline{r}')\phi_i(\underline{r}')}{|\underline{r}-\underline{r}'|} \right\} \phi_i \\ &= 2\pi \sum_i \int d^3r\, \underline{p}_i^l(\underline{r}) \cdot \underline{p}_i^l(\underline{r}) \end{aligned} \tag{2.46}$$

The intermolecular potentials may also be written in the above form, such that (2.44) takes the form,

$$\begin{aligned} V_{inter} &= \sum_{\substack{i,j \\ i\neq j}} V_{ij} \\ &= 2\pi \sum_{\substack{i,j \\ i\neq j}} \int d^3r\, \underline{p}_i^l(\underline{r}) \cdot \underline{p}_j^l(\underline{r}) \end{aligned} \tag{2.47}$$

The multipolar Lagrangian may now be obtained by completing the square in the last two terms of (2.43) and combining the intermediate result with (2.46) and (2.47). The result is

(2.48)

$$L_{multi} = -\sum_i \int d^3r\, \bar{\phi}_i \left\{ \frac{1}{2m}\left(-i\hbar\nabla + \frac{1}{c}\int d^3r'\, \underline{n}_i(\underline{r}',\underline{r}) \times \underline{b}(\underline{r}') \right)^2 \phi_i \right.$$

$$-2\pi \sum_i \int d^3r\, \underline{p}_i^l \cdot \underline{p}_i^l - 2\pi \sum_{\substack{i,j \\ i \neq j}} \int d^3r\, \underline{p}_i^l \cdot \underline{p}_j^l + \frac{i\hbar}{2} \sum_i \int d^3r \left\{ \bar{\phi}_i \dot{\phi}_i - \dot{\bar{\phi}}_i \phi_i \right\}$$

$$\left. + \frac{1}{8\pi} \int d^3r \left\{ \left(\frac{\dot{\underline{a}}}{c^2} - 4\pi \sum_i \underline{p}_i^{\perp} \right)^2 - (\nabla \times \underline{a})^2 \right\} - 2\pi \sum_{i,j} \int d^3r\, \underline{p}_i^{\perp} \cdot \underline{p}_j^{\perp} \right.$$

By splitting the last term into two parts, one corresponding to intramolecular interactions and the other to intermolecular interactions, the polarization sums of (2.48) may be combined. This results in an expression devoid of the longitudinal polarization component,

(2.49)

$$-2\pi \sum_i \int d^3r\, \underline{p}_i^l \cdot \underline{p}_i^l - 2\pi \sum_{\substack{i,j \\ i \neq j}} \int d^3r\, \underline{p}_i^l \cdot \underline{p}_j^l - 2\pi \sum_{i,j} \int d^3r\, \underline{p}_i^{\perp} \cdot \underline{p}_j^{\perp}$$

$$= -2\pi \sum_i \int d^3r\, \underline{p}_i \cdot \underline{p}_i + 2\pi \sum_{\substack{i,j \\ i \neq j}} \int d^3r\, \underline{p}_i \cdot \underline{p}_j$$

The value of (2.49) lies in the fact that the first term is not dependent upon the product of electron fields from different molecules. Thus, this term is an overall constant molecular potential of the problem. The total molecular polarization vector is localized at the molecular center. Thus, for systems in which the charge distributions do not overlap, the second term of (2.49) is identically zero.

Although this assumption of nonoverlapping charge distributions simplifies the Lagrangian greatly, it is pivotal for interpretation of the results. In fact, it is primarily

this characteristic of MQED which has led to further theoretical development of fully quantized molecule-radiation problems, as discussed in the next chapter.

The system Hamiltonian may be determined for the many-center problem in a manner analogous to that for the single center Hamiltonian (2.36). The result of calculating the analog to (2.35) is

(2.50)

$$H_{multi} = H_{rad} + \sum_i H_i + 4\pi c \sum_i \int d^3r\, \underline{\pi} \cdot \underline{p}_i^{\perp}$$
$$+ \sum_i \int d^3r\, \bar{\phi}_i \left\{ \frac{1}{2m} \left(\begin{array}{l} -i\hbar\nabla \cdot \frac{1}{c} \int d^3r'\, \underline{n}_i(\underline{r}', \underline{r}) \times \underline{b}(\underline{r}') + \\ \qquad \frac{1}{c} \int d^3r'\, \underline{n}_i(\underline{r}', \underline{r}) \times \underline{b}(\underline{r}') \cdot (-i\hbar\nabla) \end{array} \right) \right.$$
$$\left. + \left(\frac{1}{c} \int d^3r'\, \underline{n}_i(\underline{r}', \underline{r}) \times \underline{b}(\underline{r}') \right)^2 \right\} \phi_i$$

where the radiation Hamiltonian is defined as

(2.51) $$H_{rad} = \int d^3r \left\{ (4\pi \underline{\pi})^2 + (\nabla \times \underline{a})^2 \right\}$$

and the molecular Hamiltonian, explicitly writing the longitudinal polarization in in the form of the potential, is

(2.52)

$$H_i = \int d^3r\, \bar{\phi}_i \left\{ \frac{1}{2m} (-i\hbar\nabla)^2 + V_i + \frac{e^2}{2} \int d^3r' \frac{\bar{\phi}_j(\underline{r}') \phi_j(\underline{r}')}{|\underline{r} - \underline{r}'|} \right\} \phi_i$$
$$+ 2\pi \int d^3r \left| \underline{p}_i^{\perp}(\underline{r}) \right|^2$$

The assignment of the radiation and molecular Hamiltonians is based upon the fact that they depend purely upon the radiation and molecular fields alone, respectively, and not upon a mix of the radiation and molecular fields.

The Hamiltonian may be simplified by first neglecting terms of $O(1/c^2)$ and then applying (2.40) and (2.41). This results in the desired expression for the interaction Hamiltonian,

$$H_{int} = -\int d^3r \left\{ \underline{d}^{\perp}(\underline{r}) \cdot \underline{p}^{\perp}(\underline{r}) + \underline{b}(\underline{r}) \cdot \underline{m}(\underline{r}) \right\} \tag{2.53}$$

The explicit expression for the transverse polarization vector is

$$\underline{p}^{\perp}(\underline{r}) = \sum_i \int d^3r' \overline{\phi}_i(\underline{r}') \underline{p}_i^{\perp}(\underline{r}, \underline{r}') \phi_i(\underline{r}') \tag{2.54}$$

and similarly the magnetization vector is

$$\underline{m}(\underline{r}) = \sum_i \int d^3r' \overline{\phi}_i(\underline{r}') \underline{m}_i(\underline{r}', \underline{r}) \phi_i(\underline{r}') \tag{2.55}$$

The transverse displacement vector is defined as

$$\begin{aligned} \underline{d}^{\perp}(\underline{r}) &= -\dot{\underline{a}}(\underline{r}) + 4\pi \underline{p}^{\perp}(\underline{r}) \\ &= -4\pi \underline{\pi}(\underline{r}) \end{aligned} \tag{2.56}$$

The simplicity of the interaction Hamiltonian (2.53) is extremely desirable. The full power of (2.53) has not yet been realized since this expression is due to classical fields. The true beauty of MQED lies in the conversion of (2.53) to the quantum domain. At that point, calculations can be performed based upon the framework of the eigenstates of both the molecular and radiation quantum fields.

Quantization

Commutation Relations

The radiation field may be quantized based upon the defined commutation relation between the field and the conjugate momentum of the field,

$$\left[(\underline{a}(\underline{r}, t))_i, (\underline{\pi}(\underline{r}', t'))_j \right] = i\hbar \delta_{ij}^{\perp}(\underline{r} - \underline{r}') \delta(t - t') \tag{2.57}$$

The transverse delta function, defined following (2.9), is used since $\underline{a}$ is a transverse vector under the Coulomb gauge (2.7). Typically, the quantized vector potential is expanded in Fourier series form over the polarization state and the wave vector [22],

$$\underline{a}(\underline{r},t)=\sum_{\underline{k},\lambda}\sqrt{\frac{2\pi\hbar c}{Vk}}\left\{\underline{\varepsilon}_{\lambda}(\underline{k})\hat{a}_{\underline{k},\lambda}e^{i(\underline{k}\cdot\underline{r}-\omega t)}+\underline{\varepsilon}_{\lambda}^{*}(\underline{k})\hat{a}_{\underline{k},\lambda}^{+}e^{-i(\underline{k}\cdot\underline{r}-\omega t)}\right\} \tag{2.58}$$

The polarization is normalized to a box of volume V. The quantities $\hat{a}_{\underline{k},\lambda}$ and $\hat{a}_{\underline{k},\lambda}^{+}$ are interpreted as annihilation and creation operators of radiation field quantum, called photons, having polarization state λ and wave vector $\underline{k}$. The unit polarization vectors of the quantized radiation field modes are given as $\underline{\varepsilon}_{\lambda}(\underline{k})$ and its Hermitian conjugate. Recall that the field operators have the following actions on the occupation number states of the radiation field, where $|\{0\}\rangle$ denotes the radiation vacuum state, [25]

$$\begin{aligned}&\hat{a}_{\underline{k},\lambda}|\{0\}\rangle=|\{0\}\rangle\\&\hat{a}_{\underline{k},\lambda}\left|\{\cdots,n_{\underline{k}',\lambda'},\cdots\}\right\rangle=\sqrt{n_{\underline{k}',\lambda'}}\left|\{\cdots,n_{\underline{k}',\lambda'}-1,\cdots\}\right\rangle\delta(\underline{k}-\underline{k}')\delta_{\lambda,\lambda'}\end{aligned} \tag{2.59}$$

and

$$\hat{a}_{\underline{k},\lambda}^{+}\left|\{\cdots,n_{\underline{k}',\lambda'},\cdots\}\right\rangle=\sqrt{n_{\underline{k}',\lambda'}+1}\left|\{\cdots,n_{\underline{k}',\lambda'}+1,\cdots\}\right\rangle\delta(\underline{k}-\underline{k}')\delta_{\lambda,\lambda'} \tag{2.60}$$

With the above definition of the radiation field (2.58), the conjugate momentum must be designed to satisfy (2.57). Thus, it has the form,

$$\underline{\pi}(\underline{r},t)=\frac{-i}{4\pi c}\sum_{\underline{k},\lambda}\sqrt{\frac{2\pi\hbar ck}{V}}\left\{\underline{\varepsilon}_{\lambda}(\underline{k})\hat{a}_{\underline{k},\lambda}e^{i(\underline{k}\cdot\underline{r}-\omega t)}-\underline{\varepsilon}_{\lambda}^{*}(\underline{k})\hat{a}_{\underline{k},\lambda}^{+}e^{-i(\underline{k}\cdot\underline{r}-\omega t)}\right\} \tag{2.61}$$

The transverse displacement vector appears in the Hamiltonian and is related to the radiation momenta by (2.56). From (2.61), it may be written in quantized form as

$$\underline{d}^{\perp}(\underline{r},t)=i\sum_{\underline{k},\lambda}\sqrt{\frac{2\pi\hbar ck}{V}}\left\{\underline{\varepsilon}_{\lambda}(\underline{k})\hat{a}_{\underline{k},\lambda}e^{i(\underline{k}\cdot\underline{r}-\omega t)}-\underline{\varepsilon}_{\lambda}^{*}(\underline{k})\hat{a}_{\underline{k},\lambda}^{+}e^{-i(\underline{k}\cdot\underline{r}-\omega t)}\right\} \tag{2.62}$$

The electron fields must obey an anticommutation rule to preserve Fermi-Dirac statistics. Thus, assuming equal times,

(2.63) $$\left\{\bar{\phi}(\underline{r}),\phi(\underline{r}')\right\}=\delta(\underline{r}-\underline{r}')$$

Transition Probabilities

The quantized interaction Hamiltonian may be constructed from (2.58), (2.62), and (2.63). However, it does not really achieve a meaningful significance until applied to the quantized system eigenstates. In most cases, the complete eigenstates are built from a basis set determined by the direct products of the individual eigenspaces of the molecular and radiative Hamiltonians,

(2.64) $$\left|\alpha;\left\{\cdots n_{\underline{k},\lambda}\cdots\right\}\right\rangle\equiv|\alpha\rangle\otimes\left|\left\{\cdots n_{\underline{k},\lambda}\cdots\right\}\right\rangle$$

An example of the MQED formalism is the calculation of the transition matrix element for absorption of a photon by a ground state molecule. The initial state describes an excited radiation field and a ground state molecule and is given by

(2.65) $$|i\rangle=\left|\alpha_o;\left\{\cdots 0,n_{\underline{k},\lambda}=1,0\cdots\right\}\right\rangle$$

while the final state describes an excited molecule with a vacuum radiation field,

(2.66) $$|f\rangle=|\beta;\{0\}\rangle$$

Under the electric dipole approximation, only the first term of (2.18) is used. The delta function which appears in this term serves to condense the integration which occurs in the interaction Hamiltonian (2.53) to an evaluation at the molecular origin. The transition matrix can then be written as

(2.67)
$$\begin{aligned}T_{fi}&=-\left\langle\beta;\{0\}\left|\underline{\mu}\cdot\underline{d}^{\perp}(\underline{R})\right|\alpha;\left\{\cdots,n_{\underline{k},\lambda}=1,\cdots\right\}\right\rangle\\&=-\langle\beta|\underline{\mu}|\alpha\rangle\cdot\left\langle\{0\}\left|\underline{d}^{\perp}(\underline{R})\right|\left\{\cdots,n_{\underline{k},\lambda}=1,\cdots\right\}\right\rangle\\&=-\underline{\mu}^{\beta\alpha}\cdot\left\langle\{0\}\left|\underline{d}^{\perp}(\underline{R})\right|\left\{\cdots,n_{\underline{k},\lambda}=1,\cdots\right\}\right\rangle\end{aligned}$$

where $\underline{R}$ refers to the spatial position of the molecular origin. Using (2.62) for the displacement vector reduces the second matrix element because of the action of the radiation mode annihilation and creation operators,

$$\begin{aligned}\left\langle\{0\}\left|\underline{d}^{\perp}\right|\left\{\cdots,n_{\underline{k}\lambda}=1,\cdots\right\}\right\rangle = i\sum_{\underline{k}'\lambda'} g_{\underline{k}'\lambda'} \\ \left\{\underline{\varepsilon}_{\lambda'}(\underline{k}')\left\langle\{0\}\left|\hat{a}_{\underline{k}'\lambda'}\right|\left\{\cdots,n_{\underline{k}\lambda}=1,\cdots\right\}\right\rangle e^{i(\underline{k}'\cdot\underline{R})}\right. \\ \left.-\underline{\varepsilon}^{*}_{\lambda'}(\underline{k}')\left\langle\{0\}\left|\hat{a}^{+}_{\underline{k}'\lambda'}\right|\left\{\cdots,n_{\underline{k}\lambda}=1,\cdots\right\}\right\rangle e^{-i(\underline{k}'\cdot\underline{R})}\right\}\end{aligned} \tag{2.68}$$

where $g_{\underline{k}\lambda} \equiv \sqrt{\frac{2\pi\hbar ck}{V}}$. The annihilation operator reduces the expansion sum of the displacement vector to a single term, while the creation operator contributes nothing. The transition matrix element is then

$$T_{fi} = -\underline{\mu}^{\beta\alpha}\cdot ig_{\underline{k}\lambda}\underline{\varepsilon}_{\lambda}(\underline{k})e^{i(\underline{k}\cdot\underline{R})} \tag{2.69}$$

The important item to note in (2.69) is that the transition matrix element is proportional to the electric dipole transition moment between the initial and final states.

A more pertinent application of MQED to this research is the transition element for molecular energy transfer during a collision. Under this formalism, the molecule-molecule interaction is mediated only via the radiation field. That is to say, the interaction Hamiltonian of (2.53) contains no terms involving the product of molecular fields from different molecules.

Expanding the concept of the free states to include two molecules is trivial, and the form taken for the unperturbed system is

$$\left|\alpha;\beta;\left\{\cdots n_{\underline{k}\lambda}\cdots\right\}\right\rangle \equiv |\alpha\rangle\otimes|\beta\rangle\otimes\left|\left\{\cdots n_{\underline{k}\lambda}\cdots\right\}\right\rangle \tag{2.70}$$

The quantum numbers α and β refer to the distinct sets of quantum numbers appropriate to each molecule, while the $\{\cdots n_{\underline{k},\lambda}\cdots\}$ refers to the set of radiation mode occupation numbers.

As will be shown in Chapter 5, the scattering matrix is given by the evaluation of the interaction Hamiltonian across the free final state and the complete interaction solution which developed from a defined free state. Under the electric dipole assumption, the Born approximation series yields the following terms for the scattering matrix,

$$
\begin{aligned}
T = & \left\langle \alpha';\beta';\{\cdots n'_{\underline{k},\lambda}\cdots\}\right| -\sum_l \underline{\mu}_l \cdot \underline{d}^{\perp}(\underline{R}_l)\left|\alpha;\beta;\{\cdots n_{\underline{k},\lambda}\cdots\}\right\rangle \\
& +\sum_j \frac{\left\langle \alpha';\beta';\{\cdots n'_{\underline{k},\lambda}\cdots\}\right| -\sum_l \underline{\mu}_l \cdot \underline{d}^{\perp}(\underline{R}_l)\left|\alpha_j;\beta_j;\{\cdots n_{\underline{k},\lambda}\cdots\}_j\right\rangle}{E_{\alpha,\beta}-E_j} \\
& \qquad \left\langle \alpha_j;\beta_j;\{\cdots n'_{\underline{k},\lambda}\cdots\}_j\right| -\sum_l \underline{\mu}_l \cdot \underline{d}^{\perp}(\underline{R}_l)\left|\alpha;\beta;\{\cdots n_{\underline{k},\lambda}\cdots\}\right\rangle \\
& +\ldots
\end{aligned}
\tag{2.71}
$$

The summation over l refers to each of the two molecular centers. Since the initial and final radiation field states are both the vacuum, the first term in (2.71) is equal to zero. The sum over j in the second term refers to the various intermediate configurations of the system. Note that all system states contribute, even if they are not physical. This summation introduces contributions to the energy transfer process from virtual photons and molecular configurations which do not instantaneously conserve energy. Of course, the actual physical observables are constrained to conserve energy and momentum. Since the displacement vector appears only twice, (2.71) is limited to intermediate configurations in which only one photon mediates the collision. (It will require one

action of the displacement operator to create a photon and a second action of the displacement operator to remove the photon.) Clarifying (2.71) with these restrictions yields

$$
\begin{aligned}
T = \sum_j \frac{1}{E_{\alpha,\beta} - E_j} \\
&\langle \alpha'; \beta'; \{0\} | -\left(\underline{\mu}_1 \cdot \underline{d}^{\perp}(\underline{R}_1) + \underline{\mu}_2 \cdot \underline{d}^{\perp}(\underline{R}_2)\right) \left| \alpha_j; \beta_j; \left\{ \cdots n_{\underline{k},\lambda} \cdots \right\}_j \right\rangle \\
&\left\langle \alpha_j; \beta_j; \left\{ \cdots n'_{\underline{k},\lambda} \cdots \right\}_j \right| -\left(\underline{\mu}_1 \cdot \underline{d}^{\perp}(\underline{R}_1) + \underline{\mu}_2 \cdot \underline{d}^{\perp}(\underline{R}_2)\right) | \alpha; \beta; \{0\} \rangle
\end{aligned} \tag{2.72}
$$

The only intermediate states allowed are $\left|\alpha; \beta'; \left\{n_{\underline{k},\lambda} = 1\right\}\right\rangle$ and $\left|\alpha'; \beta; \left\{n_{\underline{k},\lambda} = 1\right\}\right\rangle$. Thus the scattering matrix may be written as

$$
\begin{aligned}
T = &\frac{1}{E_{\alpha,\beta} - E_{\alpha',\beta}} \langle \alpha'; \beta'; \{0\} | -\left(\underline{\mu}_1 \cdot \underline{d}^{\perp}(\underline{R}_1) + \underline{\mu}_2 \cdot \underline{d}^{\perp}(\underline{R}_2)\right) \left| \alpha'; \beta; \left\{n_{\underline{k},\lambda} = 1\right\} \right\rangle \\
&\left\langle \alpha'; \beta; \left\{n_{\underline{k},\lambda} = 1\right\} \right| -\left(\underline{\mu}_1 \cdot \underline{d}^{\perp}(\underline{R}_1) + \underline{\mu}_2 \cdot \underline{d}^{\perp}(\underline{R}_2)\right) | \alpha; \beta; \{0\} \rangle \\
&+ \frac{1}{E_{\alpha,\beta} - E_{\alpha,\beta'}} \langle \alpha'; \beta'; \{0\} | -\left(\underline{\mu}_1 \cdot \underline{d}^{\perp}(\underline{R}_1) + \underline{\mu}_2 \cdot \underline{d}^{\perp}(\underline{R}_2)\right) \left| \alpha; \beta'; \left\{n_{\underline{k},\lambda} = 1\right\} \right\rangle \\
&\left\langle \alpha; \beta'; \left\{n_{\underline{k},\lambda} = 1\right\} \right| -\left(\underline{\mu}_1 \cdot \underline{d}^{\perp}(\underline{R}_1) + \underline{\mu}_2 \cdot \underline{d}^{\perp}(\underline{R}_2)\right) | \alpha; \beta; \{0\} \rangle
\end{aligned} \tag{2.73}
$$

This expression may be reduced by moving the operators onto states of their appropriate eigenspaces. Hence, the first term of (2.73) may be addressed in the following fashion,

$$
\begin{aligned}
&\langle \alpha'; \beta'; \{0\} | \left(\underline{\mu}_1 \cdot \underline{d}^{\perp}(\underline{R}_1) + \underline{\mu}_2 \cdot \underline{d}^{\perp}(\underline{R}_2)\right) \left| \alpha'; \beta; \left\{n_{\underline{k},\lambda} = 1\right\} \right\rangle = \\
&\qquad \langle \alpha' | \underline{\mu}_1 | \alpha' \rangle \langle \beta' | \beta \rangle \langle \{0\} | \underline{d}^{\perp}(\underline{R}_1) \left| \left\{n_{\underline{k},\lambda} = 1\right\} \right\rangle \\
&\qquad + \langle \alpha' | \alpha' \rangle \langle \beta' | \underline{\mu}_2 | \beta \rangle \langle \{0\} | \underline{d}^{\perp}(\underline{R}_2) \left| \left\{n_{\underline{k},\lambda} = 1\right\} \right\rangle
\end{aligned} \tag{2.74}
$$

Because of the orthogonality of the molecular eigenstates of the second molecule, the first term of (2.74) vanishes. Applying (2.68) to (2.74) leaves

$$\left\langle \alpha';\beta';\{0\}\left|\left(\underline{\mu}_1\cdot\underline{d}^{\perp}(\underline{R}_1)+\underline{\mu}_2\cdot\underline{d}^{\perp}(\underline{R}_2)\right)\right|\alpha';\beta;\left\{n_{\underline{k},\lambda}=1\right\}\right\rangle = \underline{\mu}_2^{\beta'\beta} i g_{\underline{k},\lambda}\underline{\varepsilon}_{\lambda}(\underline{k})e^{i(\underline{k}\cdot\underline{R}_2)} \tag{2.75}$$

The remaining three terms of (2.73) may be reduced in a similar fashion, giving the resultant expression for the scattering matrix element,

$$T=\mu_1^{\alpha'\alpha}\mu_2^{\beta'\beta}\left\{\frac{-g_{\underline{k},\lambda}^2}{E_{\alpha,\beta}-E_{\alpha',\beta}}\hat{\underline{\mu}}_2^{\beta'\beta}\cdot\underline{\varepsilon}_{\lambda}(\underline{k})\hat{\underline{\mu}}_1^{\alpha'\alpha}\cdot\underline{\varepsilon}_{\underline{k},\lambda}^{*}(\underline{k})e^{-i(\underline{k}\cdot\underline{R}_{12})} + \frac{-g_{\underline{k},\lambda}^2}{E_{\alpha,\beta}-E_{\alpha,\beta'}}\hat{\underline{\mu}}_1^{\alpha'\alpha}\cdot\underline{\varepsilon}_{\lambda}(\underline{k})\hat{\underline{\mu}}_2^{\beta'\beta}\cdot\underline{\varepsilon}_{\underline{k},\lambda}^{*}(\underline{k})e^{i(\underline{k}\cdot\underline{R}_{12})}\right\} \tag{2.76}$$

where the magnitude of the dipole moments have been extracted to emphasize that the transition probability is dependent upon their product. The term in the brackets only contributes the proper scaling.

Although (2.76) was derived using the electric dipole approximation, the higher moments do not change the fact that in MQED, the energy transfer is mediated by a photon. Most importantly, the rate of the energy transfer is governed by the product of the individual molecular multipoles. In those cases where the multipole moments are suppressed, such as for a spin-forbidden transition on one of the molecules, the energy transfer rate will be expected to be small.

Summary

The topic of molecular quantum electrodynamics (MQED) has been thoroughly explored. Several key advantages of a fully quantum description of the interactions

between molecules and radiation have been illustrated, such as the dipole energy transfer mechanism. In addition, the discourse has exposed the underlying assumptions of MQED that hinder its application to classes of spin-forbidden processes. The proportionality between the transition probability and the multipole moments, along with the assumption of non-overlapping charge densities of collision partners, are important theoretical deficiencies. This is particularly true when describing fast spin-forbidden energy transfers, as the kind noted in Chapter 1. These deficiencies must be overcome for the application at hand, as is developed as part of this original research, discussed in Chapter 3.

Chapter 3

Quantum Field Theory of Electron Exchange

The primary goal of this research is to further the application of quantum field theory to molecular length scales. The adoption of some of the techniques of quantum field theory to molecular processes, such as energy transfer, has met with success for many fundamental processes, such as stimulated and spontaneous emission [22], as well as useful applications [26]. However, a fully quantal treatment of the mechanism responsible for fast forbidden energy transfer, like that described in Chapter 1, has never been attempted. This research attempts to fill that void, and this chapter presents the novel theoretical development used for that goal. Building upon the foundation of the previous chapter, an original extension of the MQED theory is given which includes the possibility of electron exchange. An explicit operator form is derived for this interaction and the groundwork is laid for a subsequent application to a physical system.

Motivation

The preceding chapter presented an elegant method of describing interacting molecular systems. MQED uses second quantization of the molecules and a quantized radiation field to describe phenomena such as spontaneous emission and absorption etc., as well as Raman and Rayleigh scattering and dispersion forces between molecules in ground states. However, in developing MQED in the multipolar framework, some limitations of the theory became apparent. Typically, the electric dipole approximation is used for most applications [27], although a recent effort by Scholes, et al., [28] has extended this method to include higher multipole interactions.

Perhaps the most significant restriction inherent to MQED for the purpose of this research is that overlapping molecular charge densities are not modeled. In fact, Scholes, et al, cite an approximate molecular separation distance of at least 10 Angstroms for their multipole results to apply. This requirement is incompatible with the nature of the fast energy transfer reaction, such as (1.3). As will be discussed in Chapter 7, several experimental papers have suggested that the rapidity of the reaction is due to an electronic collision phenomenon, be it a collision complex of ions, or a simultaneous electron exchange process.

The spectroscopic structure of the collision partners also suggests that MQED, in its present form, is inadequate to describe reactions like (1.3). In Chapter 6 it will be seen that the Ar metastable has an extremely long lifetime, from which it can be inferred that the radiation multipoles are feeble. Furthermore, there is no direct transition connecting the $N_2(X^1\Sigma_g^+)$ ground state with the $N_2(C^3\Pi_u)$ excited state. This transition is strongly spin forbidden. Based solely upon fact, it is clear that a radiative intermediary constitutes an insufficient mechanism for such a fast energy transfer reaction.

Given this experimental motivation, it is clear that an extension of MQED is necessary. In order to claim success, this extension must account for two key items: overlapping charge densities, and spin forbidden spectral transitions. It will be shown below that the application of quantum field theory to the problem of molecular collisions serves to broaden the scope of MQED. In essence, by using the modal expansion of the quantized electron field operators, it is possible to avoid the assumption of no overlapping electron fields inherent to the multipolar formalism, but essential to the fast energy transfer process. The solution is entirely worked out using the minimal coupling Hamiltonian. In doing so, the terms responsible for energy transfer via an electron intermediary become apparent.

Derivation of the Hamiltonian

The Spin-Dependent Lagrangian

Since the spin behavior of the active electrons is very important to this mechanism, perhaps (2.1) is insufficient to describe the anticipated electron field dynamics. The most obvious point to begin any discussion of quantum electrodynamics is the relativistic Lagrangian density of a classical free spin 1/2 field [29],

$$L_{s=1/2} = -\overline{\psi}(\underline{r})\gamma_4\left(\gamma_\mu\partial_\mu + m\right)\psi(\underline{r}) \tag{3.1}$$

where $\psi(\underline{r})$ and $\overline{\psi}(\underline{r})$ are interpreted as field operators, which may be realized as four component vectors, known as Dirac spinors. The γ_μ are related linearly to the set of 4 x 4 Dirac matrices [30]. Four elements are required in $\psi(\underline{r})$, and $\overline{\psi}(\underline{r})$ as well, in order to account for the spin up and spin down components of both the positive and negative energy solutions to Dirac's equation of motion. The positive energy solutions correspond to a matter wave progressing forward in time, i.e. an electron, while the negative energy solutions correspond to a matter wave progressing backward in time, i.e. an antielectron or positron.

Although (3.1) would be the most complete point of origin, clearly the extra features of a relativistic theory, such as antiparticle annihilation and creation, would not be warranted for a study of molecular collisions. In the nonrelativistic regime, it can be shown that (3.1) transforms, with the manual inclusion of an external potential, to the Pauli nonrelativistic Lagrangian density [31-33]

$$L_{charge}(\underline{r}) = \frac{-\hbar^2}{2m}\nabla\overline{\psi}(\underline{r})\cdot\nabla\psi(\underline{r}) - \overline{\psi}(\underline{r})V(\underline{r})\psi(\underline{r})$$
$$-\overline{\psi}(\underline{r})W(\underline{r})\sigma\cdot\underline{\mathbf{L}}\psi(\underline{r}) \tag{3.2}$$
$$+\frac{i\hbar}{2}\left\{\overline{\psi}(\underline{r})\dot{\psi}(\underline{r}) - \dot{\overline{\psi}}(\underline{r})\psi(\underline{r})\right\}$$

As in (2.1), this is an operator equation for the electron field operator, $\psi(\underline{r})$, and its Hermitian conjugate, $\overline{\psi}(\underline{r})$. However, in the transition from (3.1) to (3.2), the meaning of $\psi(\underline{r})$ is also transformed. Once the relativistic regime is left behind, there is no need to carry along the antiparticle components of $\psi(\underline{r})$. Hence, $\psi(\underline{r})$ now represents a two component vector field, with one component for each spin state. This interpretation is contrasted against (2.1), where the electron fields were interpreted as scalar fields.

The external potential, $V(\underline{r})$, was explicitly introduced in order to describe the nuclear Coulombic attraction of the electron field which is not incorporated into (3.1). The effects of the nuclear potential are twofold. The first result is that the electron field will have solutions leading to bound states. The second effect is that space is no longer translationally invariant, since $V(\underline{r})$ introduces a reference point. Thus, the electron fields will acquire well-defined states of orbital angular momentum to reflect this broken symmetry. Since the electron field displays an inherent spin angular momentum, regardless of the presence of an external potential, it is possible for the orbital angular momentum to couple to the spin angular momentum. This effect is described by the third term of (3.2), in which σ is the electron spin operator, $\underline{\mathbf{L}}$ is the electron angular momentum operator, and $W(\underline{r})$ represents a possible spatial dependence of the interaction.

As in Chapter 2, the litmus test for any Lagrangian density is that it generates the proper equations of motion for the fields. Based upon (3.2), the canonical momenta of the electron fields are

(3.3) $$\frac{\partial L_{charge}}{\partial \dot{\psi}(\underline{r})} = \frac{i\hbar}{2}\overline{\psi}(\underline{r})$$

and

(3.4) $$\frac{\partial L_{charge}}{\partial \dot{\overline{\psi}}(\underline{r})} = -\frac{i\hbar}{2}\psi(\underline{r})$$

Using the Euler-Lagrange equation, as written in (2.3), yields the equation of motion for $\psi(\underline{r})$,

(3.5) $$\left\{\frac{-\hbar^2}{2m}\nabla^2 + V(\underline{r}) + W(\underline{r})\sigma\cdot\underline{\mathbf{L}}\right\}\psi(\underline{r}) = i\hbar\dot{\psi}(\underline{r})$$

which is simply the standard nonrelativistic Schrödinger equation for the electron field with spin. An analogous equation exists for $\overline{\psi}(\underline{r})$.

Minimal Substitution

The radiation field can be introduced into (3.2) by using the minimal substitution coupling, as was done in (2.6). This time, however, the minimal substitution takes the form of a transformation specified by [34]

(3.6) $$\nabla\psi(\underline{r}) \rightarrow \left(\nabla - i\,{}^{e}\!/_{c}\,\underline{a}\right)\psi(\underline{r}) \equiv D\psi(\underline{r})$$

and likewise for the Hermitian conjugate,

(3.7) $$\nabla\overline{\psi}(\underline{r}) \rightarrow \left(\nabla + i\,{}^{e}\!/_{c}\,\underline{a}\right)\overline{\psi}(\underline{r}) \equiv D\overline{\psi}(\underline{r})$$

where $\underline{a}$ is the vector potential of the radiation field. As before, the minimal substitution transformation implicitly defines the interaction between matter and radiation.

With this prescription, the total Lagrangian density for the interacting molecule and radiation fields can then be written as

(3.8)

$$L(\underline{r}) = \frac{-\hbar^2}{2m} D\overline{\psi}(\underline{r}) \cdot D\psi(\underline{r}) -$$
$$\overline{\psi}(\underline{r}) \left\{ V(\underline{r}) + W(\underline{r}) \sigma \cdot \underline{\mathbf{L}} + \frac{e^2}{2} \int d^3r' \, \overline{\psi}(\underline{r}') \frac{1}{|\underline{r} - \underline{r}'|} \psi(\underline{r}') \right\} \psi(\underline{r})$$
$$+ \frac{i\hbar}{2} \left\{ \overline{\psi}(\underline{r}) \dot{\psi}(\underline{r}) - \dot{\overline{\psi}}(\underline{r}) \psi(\underline{r}) \right\}$$
$$+ \frac{1}{8\pi} \left\{ \left(\frac{\dot{\underline{a}}}{c} \right)^2 - (\nabla \times \underline{a})^2 \right\}$$

Note that the electron field-field interaction is explicitly written in anticipation of describing the particle-particle interactions [31].

Before proceeding further, it is prudent to quantize the fields. The components of the electron fields are required to obey a set of equal time anticommutators involving the field and its conjugate momentum, as given by Lee [29],

(3.9)
$$\left\{ \psi_\lambda(\underline{r}), \Pi_\mu(\underline{r}') \right\} = \frac{i\hbar}{2} \delta_{\lambda\mu} \delta(\underline{r} - \underline{r}')$$
$$\left\{ \psi_\lambda(\underline{r}), \psi_\mu(\underline{r}') \right\} = \left\{ \Pi_\lambda(\underline{r}), \Pi_\mu(\underline{r}') \right\} = 0$$

The electron field conjugate momenta are determined from (3.6) as

(3.10)
$$\Pi_\lambda(\underline{r}) = \frac{\partial L}{\partial \dot{\psi}_\lambda(\underline{r})}$$
$$= \frac{i\hbar}{2} \overline{\psi}_\lambda(\underline{r})$$

Substituting (3.10) into (3.9) yields the quantization requirements for the electron fields,

(3.11)
$$\left\{\psi_\lambda(\underline{r}),\overline{\psi}_\mu(\underline{r}')\right\}=\delta_{\lambda\mu}\delta(\underline{r}-\underline{r}')$$
$$\left\{\psi_\lambda(\underline{r}),\psi_\mu(\underline{r}')\right\}=\left\{\overline{\psi}_\lambda(\underline{r}),\overline{\psi}_\mu(\underline{r}')\right\}=0$$

As to be expected, the radiation field is required to satisfy the commutator given in (2.57).

The total interacting Hamiltonian density follows from the usual summation procedure, as in (2.35). The result is

(3.12)
$$\begin{aligned}H(\underline{r})=&\frac{\hbar^2}{2m}\nabla\overline{\psi}(\underline{r})\cdot\nabla\psi(\underline{r})+\overline{\psi}(\underline{r})\{V(\underline{r})+W(\underline{r})\sigma\cdot\underline{\mathbf{L}}\}\psi(\underline{r})\\&+\frac{e^2}{2}\overline{\psi}(\underline{r})\int d^3r'\,\overline{\psi}(\underline{r}')\frac{1}{|\underline{r}-\underline{r}'|}\psi(\underline{r}')\psi(\underline{r})\\&-\frac{ieh^2}{2mc}\{\nabla\overline{\psi}(\underline{r})\cdot\underline{a}(\underline{r})\psi(\underline{r})-\underline{a}(\underline{r})\overline{\psi}(\underline{r})\cdot\nabla\psi(\underline{r})\}\\&+\frac{e^2\hbar^2}{2mc^2}\underline{a}(\underline{r})\overline{\psi}(\underline{r})\cdot\underline{a}(\underline{r})\psi(\underline{r})\\&+\frac{1}{8\pi}\left\{\left(\frac{\dot{\underline{a}}(\underline{r})}{c}\right)^2+(\nabla\times\underline{a}(\underline{r}))^2\right\}\end{aligned}$$

The first two terms involve only the local electron fields and are elements of the molecular Hamiltonian density. The third term couples the electron field to itself. The fourth and fifth terms describe the interaction between the electron and radiation fields. The final term is simply the Hamiltonian density for the free radiation field. Thus, (3.12) may be thought of as free Hamiltonian densities for the radiation and electron fields, with three interaction terms. Two of these terms couple the radiation and electron field, while the third interaction couples the electron field to itself.

In Chapter 2 much of the effort was focused on manipulating the fourth and fifth terms of (3.12) in a practical form by the use of multipoles. The present approach is

somewhat different. The postulated energy transfer method of this research utilizes an electron intermediary. This is conceptually different than the photon intermediary discussed in Chapter 2. Consequently, further theoretical development deviates from the standard treatments of MQED, and concentrates upon the form of the electron field interactions. This marks the departure point from previous theoretical developments and this research.

Expansion of the Electron Field Operator

In the preceding chapter, the quantized radiation field was expanded as a Fourier series, i.e. plane waves, (2.58). This expansion form was chosen only because plane waves are the solutions to the free radiation Hamiltonian. It is desirable to perform a similar decomposition of the electron field operator. However, rather than expanding in a Fourier series, it is more natural to expand the electron field operators in terms of a set of complete basis functions, $\phi_m(\underline{r})$, [35]

$$\psi(\underline{r}) = \sum_m \phi_m(\underline{r}) u_m b_m \tag{3.13}$$

and

$$\overline{\psi}(\underline{r}) = \sum_m \phi_m^*(\underline{r}) u_m^+ b_m^+ \tag{3.14}$$

where b_m and b_m^+ are the annihilation and creation operators of mode m, and u_m and u_m^+ are two-component spinors. The action of the annihilation and creation operators is rather interesting. For example, in the m^{th} term of (3.13), b_m will remove an electron from the field only if it exists at position $\underline{r}$, with the spatial behavior described by the function ϕ_m, and the spin behavior described by u_m. Accordingly, in the m^{th} term of (3.14), b_m^+ will create an electron from the vacuum at position $\underline{r}$, spatially described by the function ϕ_m^*, with spin described by u_m. Thus, electrons are treated merely as

excitations in an abstract field, analogous to electromagnetic modes in a waveguide for example. The characteristics such as position, basis function, and spin simply serve to distinguish between types of excitations. Also, since b_m and b_m^+ represent fermion fields, they are required to anticommute. In contrast to (2.58), the antiparticle operators usually found in field expansions are neglected. This deletion is because the systems under study have energies much below that of the relativistic regime. Finally, the explicit time dependence of b_m and b_m^+ has been suppressed for clarity.

As yet the basis functions, $\{\ldots\phi_i\ldots\}$, are undefined. Although orthogonality of the basis functions is not required for the above expansion, it is desirable for the remaining development and it will be assumed that the functions $\{\ldots\phi_i\ldots\}$ form a complete, orthonormal set. Substituting (3.13) and (3.14) into (3.12) yields the Hamiltonian density in second quantized form,

$$
\begin{aligned}
H(\underline{r}) &= H_{rad}(\underline{r}) + H_{int}^{(1)}(\underline{r}) \\
&+ \sum_{m,n} \phi_m^*(\underline{r}) \left[\frac{-\hbar^2}{2m} \nabla^2 + V(\underline{r}) + W(\underline{r}) \sigma \cdot \underline{\mathbf{L}} \right] \phi_n(\underline{r})\, u_m^+ u_n b_m^+ b_n \\
&+ \frac{e^2}{2} \sum_{\substack{j,k, \\ l,m}} \int d^3r' \phi_j^*(\underline{r}) \phi_k^*(\underline{r}') \frac{1}{|\underline{r} - \underline{r}'|} \phi_l(\underline{r}') \phi_m(\underline{r}) u_j^+ u_k^+ u_l u_m b_j^+ b_k^+ b_l b_m
\end{aligned}
\tag{3.15}
$$

Note that the free radiation Hamiltonian has been defined as the last, or sixth, term of (3.12). Also, the Hamiltonian for the interaction between the radiation and electron fields, which is the fourth and fifth terms of (3.12), is labeled as the first interaction Hamiltonian. The terms comprising this interaction were manipulated in the previous chapter.

The next step is to integrate the Hamiltonian density over all space to obtain the total Hamiltonian. Segregating the terms which correspond to one and two electron fields gives

$$H = H_{rad} + H_{int}^{(1)} + \sum_{m,n} H_{mn}^{1P} b_m^+ b_n + \sum_{\substack{j,k,\\ l,m}} V_{jklm} b_j^+ b_k^+ b_l b_m \tag{3.16}$$

where

$$H_{mn}^{1P} = u_m^+ u_n \int d^3r\, \phi_m^*(\underline{r}) \left\{ \frac{-\hbar^2}{2m} \nabla^2 + V(\underline{r}) + W(\underline{r}) \sigma \cdot \underline{\mathbf{L}} \right\} \phi_n(\underline{r}) \tag{3.17}$$

Clearly, (3.17) represents the Hamiltonian for a single particle. Because (3.17) concerns only a single field, it is termed a noninteracting Hamiltonian, even though the electron explicitly interacts with the nuclear potential, $V(\underline{r})$. The nomenclature "noninteracting" is used because (3.17) does not describe an interaction between electron fields or between electron and radiation fields. A great simplification is found if the expansion functions are required to satisfy the single particle Hamiltonian, such that

$$\left\{ \frac{-\hbar^2}{2m} \nabla^2 + V(\underline{r}) + W(\underline{r}) \sigma \cdot \underline{\mathbf{L}} \right\} \phi_n(\underline{r}) = \omega_n \phi_n(\underline{r}) \tag{3.18}$$

Substituting (3.18) into (3.17) and using the orthogonality of the basis functions yields,

$$\begin{aligned} H_{mn}^{1P} &= u_m^+ u_n \int d^3r\, \phi_m^*(\underline{r}) \omega_n \phi_n(\underline{r}) \\ &= u_m^+ u_n \omega_n \delta_{mn} \\ &= \omega_n \delta_{mn} \end{aligned} \tag{3.19}$$

where the spinors are normalized to unity. Substituting (3.19) into (3.16) simplifies the Hamiltonian to a form,

$$H = H_{rad} + H_{int}^{(1)} + \sum_{m} \omega_m b_m^+ b_m + \sum_{\substack{j,k,\\ l,m}} V_{jklm} b_j^+ b_k^+ b_l b_m \tag{3.20}$$

The last term of (3.20) describes the interactions between the electron field operators, i.e. a particle-particle interaction. It contains an amplitude in the summation which describes the strength of the interaction for specific modes of the electron field,

$$V_{jklm} = \frac{e^2}{2} u_j^+ u_k^+ u_l u_m \iint d^3r\, d^3r'\, \phi_j^*(\underline{r})\phi_k^*(\underline{r}')\frac{1}{|\underline{r}-\underline{r}'|}\phi_l(\underline{r}')\phi_m(\underline{r}) \tag{3.21}$$

It is important to note that the spinors of (3.21) are simply mathematical representations of the spin eigenstate, and that they are not operator quantities. As such, they fully commute.

Although it may be tempting to define the third term of (3.20) as the molecular Hamiltonian, further development is desired. Yet as it stands, (3.20) explicitly demonstrates several key concepts that are required for an application to molecular scattering. The radiation field has been quantized in the first term, and the radiation field interaction with the matter field has been condensed into the second term. If we were considering photon intermediated processes, then usually the third term of (3.20) is identified as the matter Hamiltonian and the fourth term is dropped altogether. However, in those instances when the long-range radiation-matter interaction, $H_{\text{int}}^{(1)}$, is small, the last term provides a short-range interaction mechanism for electron exchange. The fact that the last term is a two particle operator is evident from the two creation and two annihilation operators. The amplitude for electron exchange can thus be determined independent of the free radiation Hamiltonian and the radiation-matter interaction Hamiltonians.

Molecular Scattering

Application of Molecular Orbital Theory

The nature of the molecular collision system justifies a partition of the basis functions, $\{\ldots\phi_i\ldots\}$, into two subsets, based upon the far-field separation of the molecular centers. For a two molecule system, let the first N_1 modes be centered on molecule 1, and the second N_2 modes be centered on molecule 2. For clarity, the partitioning of the basis functions can be written as $\{\ldots\phi_i\ldots;\ldots\phi_\alpha\ldots\}$, where the Latin indices indicate modes centered upon molecule 1, and the Greek indices indicate those centered upon molecule 2. Applying this to the expression for the Hamiltonian, (3.20), yields a lengthy, but crucial, expression in which each summation is split. The last term of (3.20) requires 16 terms because it specifies four indices. In anticipation of the application of the Fock space state vectors, the 16 terms can be grouped into three sets. The first set contains terms which act upon modes of one molecule. The second set contains terms which perform equivalent action on modes of differing molecules. Finally, the last set contains terms which perform nonequivalent action on modes of differing molecules. The full expression is

(3.22)

$$
\begin{aligned}
H = H_{rad} + H_{int}^{(1)} \\
&+\left\{\begin{array}{l}\sum_{m}\omega_m b_m^+ b_m + \sum_{\substack{j,k,\\ l,m}} V_{jklm} b_j^+ b_k^+ b_l b_m \\ +\sum_{\alpha}\omega_\alpha b_\alpha^+ b_\alpha + \sum_{\substack{\alpha,\beta,\\ \gamma,\delta}} V_{\alpha\beta\gamma\delta} b_\alpha^+ b_\beta^+ b_\gamma b_\delta\end{array}\right\} \\
&+\left\{\begin{array}{l}\sum_{\substack{j,\beta,\\ \gamma,m}} V_{j\beta\gamma m} b_j^+ b_\beta^+ b_\gamma b_m + \sum_{\substack{\alpha,k,\\ l,\delta}} V_{\alpha kl\delta} b_\alpha^+ b_k^+ b_l b_\delta \\ +\sum_{\substack{j,\beta,\\ l,\delta}} V_{j\beta l\delta} b_j^+ b_\beta^+ b_l b_\delta + \sum_{\substack{\alpha,k,\\ \gamma,m}} V_{\alpha k\gamma m} b_\alpha^+ b_k^+ b_\gamma b_m\end{array}\right\} \\
&+\left\{\begin{array}{l}\sum_{\substack{j,k,\\ \gamma,\delta}} V_{jk\gamma\delta} b_j^+ b_k^+ b_\gamma b_\delta + \sum_{\substack{\alpha,\beta,\\ l,m}} V_{\alpha\beta lm} b_\alpha^+ b_\beta^+ b_l b_m \\ +\sum_{\substack{j,k,\\ l,\delta}} V_{jkl\delta} b_j^+ b_k^+ b_l b_\delta + \sum_{\substack{j,k,\\ \gamma,m}} V_{jk\gamma m} b_j^+ b_k^+ b_\gamma b_m \\ +\sum_{\substack{j,\beta,\\ l,m}} V_{j\beta lm} b_j^+ b_\beta^+ b_l b_m + \sum_{\substack{j,\beta,\\ \gamma,\delta}} V_{j\beta\gamma\delta} b_j^+ b_\beta^+ b_\gamma b_\delta \\ +\sum_{\substack{\alpha,k,\\ l,m}} V_{\alpha klm} b_\alpha^+ b_k^+ b_l b_m + \sum_{\substack{\alpha,k,\\ \gamma,\delta}} V_{\alpha k\gamma\delta} b_\alpha^+ b_k^+ b_\gamma b_\delta \\ +\sum_{\substack{\alpha,\beta,\\ l,\delta}} V_{\alpha\beta l\delta} b_\alpha^+ b_\beta^+ b_l b_\delta + \sum_{\substack{\alpha,\beta,\\ \gamma,m}} V_{\alpha\beta\gamma m} b_\alpha^+ b_\beta^+ b_\gamma b_m\end{array}\right\}
\end{aligned}
$$

The first group of summations involves operators which act on modes centered at only one molecule. Hence, these terms collectively form the Hamiltonian for the two noninteracting molecules. In fact, upon closer inspection, the one center operators are simply the second quantized form of the Hartree-Fock Hamiltonian [36,37] for each of the two molecules. Hence, the molecular Hamiltonian may now be defined as

$$H_{mol} = \sum_{m} \omega_m b_m^+ b_m + \sum_{\substack{j,k,\\ l,m}} V_{jklm} b_j^+ b_k^+ b_l b_m$$
$$+ \sum_{\alpha} \omega_\alpha b_\alpha^+ b_\alpha + \sum_{\substack{\alpha,\beta,\\ \gamma,\delta}} V_{\alpha\beta\gamma\delta} b_\alpha^+ b_\beta^+ b_\gamma b_\delta \tag{3.23}$$

In a first quantized form, McWeeny [36] showed that the best solution for the eigenfunctions to the Hartree-Fock Hamiltonian of a many electron molecule in the self-consistent field approximation is given by the eigenfunctions to the single particle Hamiltonian. This was done in (3.18) and (3.19). Thus, we may simply take the union of the two sets of molecular orbitals of each molecule, as determined by the Hartree-Fock method, as the set of basis functions used in the expansion of the quantized electron field operator, (3.13) and (3.14).

The two particle, electron field-field interactions of (3.23), represented by the summation $\sum_{\substack{j,k,\\ l,m}} V_{jklm} b_j^+ b_k^+ b_l b_m$, is simply the combination of the customary "coulomb" and "exchange" operators for molecule 1 [38]. These operators will be better defined in Chapter 4. Likewise, the analogous term with four Greek subscripts for molecule 2 holds similar meaning for molecule 2.

Clearly, (3.23) corresponds to the problem of solving noninteracting molecular structures in the far-field, which will be discussed in Chapter 4. The key for the application of quantum field theory to molecular scattering is to use the molecular orbital solutions of (3.23) as the electron field operator expansion basis functions. Hence, the noninteracting electron field expansion amplitudes are not plane waves, as is the case for the radiation field, but rather they are the bound state solutions pertinent to each molecule.

Fock States

The complete Hamiltonian (3.22) appears rather unwieldy, but considerable simplification is possible once the eigenspace is considered in the context of the problem at hand. The focus of this research is upon molecular energy transfer during a scattering event. All scattering processes begin with an initial state and move to a final state via an interaction, as will be thoroughly discussed in Chapter 5. Usually, only solutions to the noninteracting Hamiltonian are known. Scattering theory tries to incorporate the certainty of the eigenstates into the determination of an event probability, at the expense of the explicit form of the interaction. Thus, as will be seen in Chapter 5, the free states are of great importance to scattering calculations.

Using customary notation, let $|i\rangle$ denote the initial, or free, molecular eigenstate in second quantized Fock space such that

$$|i\rangle = |n_1, n_2, \cdots, n_l, \cdots\rangle = \frac{(b_1^+)^{n_1}(b_2^+)^{n_2}\cdots(b_l^+)^{n_l}\cdots}{\sqrt{(n_1!)(n_2!)\cdots(n_l!)\cdots}}|0\rangle \tag{3.24}$$

where $|0\rangle$ denotes the physical vacuum, the numbers n_i are the occupation numbers for the individual eigenmodes, and the set of operators b_i^+ create an excitation in the subscripted eigenmode when applied to the vacuum state. In light of the above discussion, the eigenmodes are the molecular orbitals, and the operator b_i^+ creates an electron in the i^{th} mode, or spin-orbital. Likewise, the final state can be expressed as

$$|f\rangle = |n_1', n_2', \cdots, n_l', \cdots\rangle = \frac{(b_1^+)^{n_1'}(b_2^+)^{n_2'}\cdots(b_l^+)^{n_l'}\cdots}{\sqrt{(n_1'!)(n_2'!)\cdots(n_l'!)\cdots}}|0\rangle \tag{3.25}$$

The scattering problem is greatly simplified by noting that to first order, as will be seen in Chapter 5, the scattering amplitude is proportional to $\langle f|H_{\text{int}}|i\rangle$, with the initial and final number of electrons present in the system specified by (3.24) and (3.25). In this study, the interaction Hamiltonian is given by the last two groupings of terms in (3.22).

Under the restriction of a collision system where the reactant molecules and product molecules remain electrically neutral, both $|i\rangle$ and $|f\rangle$ have the same number of electrons. Thus it is *necessary* to have an equal number of creation and annihilation operators in every term of the interaction Hamiltonian. This is because the net electron production or annihilation due to the interaction must be null. Otherwise, the inner product, $\langle f|H_{int}|i\rangle$, reduces to zero. This is not true for the large class of charge transfer collisions in which one collision partner is the recipient of an electron donated from its collision partner.

Conversely, any term of (3.22) which contains an unequal number of creation and annihilation operators will, after acting on $|i\rangle$, yield a state $|i'\rangle$ which is not charge neutral. This will result in a zero inner product with a state, $\langle f|$, which is charge neutral. Applying this rule, it is easily seen that all terms of (3.22) within the last grouping will yield a zero amplitude when placed between initial and final states representing systems of neutral molecules.

Thus, for the class of collisions of interest to this study, the intermolecular electron-mediated interaction is given by the second grouping of (3.22),

$$H_{int}^{(2)} = \sum_{\substack{j,\beta,\\ \gamma,m}} V_{j\beta\gamma m} b_j^+ b_\beta^+ b_\gamma b_m + \sum_{\substack{\alpha,k,\\ l,\delta}} V_{\alpha k l\delta} b_\alpha^+ b_k^+ b_l b_\delta + \sum_{\substack{j,\beta,\\ l,\delta}} V_{j\beta l\delta} b_j^+ b_\beta^+ b_l b_\delta + \sum_{\substack{\alpha,k,\\ \gamma,m}} V_{\alpha k\gamma m} b_\alpha^+ b_k^+ b_\gamma b_m \tag{3.26}$$

The symmetry of (3.21) implies that $V_{j\beta\gamma m} = V_{\beta jm\gamma}$, where it is important to recall that the Latin and Greek indices refer to modes of different molecules. Note that the reversal of the first two indices, or the last two indices, does not affect the spinors embedded within $V_{j\beta\gamma m}$. The anticommutation relations of the creation and annihilation operators over the entire set of modes of both molecules dictates that $\{b_i, b_j\} = 0$, as well as $\{b_i^+, b_j^+\} = 0$.

Thus, $b_j^+ b_\beta^+ b_\gamma b_m = \left(-b_\beta^+ b_j^+\right)\left(-b_m b_\gamma\right) = b_\beta^+ b_j^+ b_m b_\gamma$, indicating that the first two summation terms of (3.26) may be consolidated. Likewise, the second pair of terms may be consolidated by noting that

$$\begin{aligned}\sum_{\substack{j,\beta,\\ l,\delta}} V_{j\beta l\delta} b_j^+ b_\beta^+ b_l b_\delta &= \sum_{\substack{j,\beta,\\ l,\delta}} V_{\beta j\delta l}\left(-b_\beta^+ b_j^+\right)\left(-b_\delta b_l\right) \\ &= \sum_{\substack{\alpha,k,\\ \gamma,m}} V_{\alpha k\gamma m} b_\alpha^+ b_k^+ b_\gamma b_m\end{aligned} \tag{3.27}$$

Substituting (3.27) into (3.26) yields the interaction Hamiltonian as

$$H_{int}^{(2)} = 2\sum_{\substack{\alpha,k,\\ l,\delta}} V_{\alpha kl\delta} b_\alpha^+ b_k^+ b_l b_\delta + 2\sum_{\substack{\alpha,k,\\ \gamma,m}} V_{\alpha k\gamma m} b_\alpha^+ b_k^+ b_\gamma b_m \tag{3.28}$$

If the indices are rewritten, this interaction Hamiltonian for collisional electron exchange takes on a familiar form,

$$H_{int}^{(2)} = 2\sum_{\substack{\alpha,k,\\ l,\delta}} \left(V_{\alpha kl\delta} - V_{\alpha k\delta l}\right) b_\alpha^+ b_k^+ b_l b_\delta \tag{3.29}$$

The resemblance of (3.29) with the typical form of the "coulomb" and "exchange" interactions so often encountered in attempting to solve the many-electron problem of a single molecule is striking. The most significant difference between (3.29) and the single molecule coulomb and exchange operators is the restriction over the mode summation. In fact, the factor of 2 counteracts the factor of 1/2 introduced in (3.21) to avoid over counting the pairwise interactions, since the over counting is explicitly omitted in (3.29). Only electrons of different molecules may interact in the collisional electron exchange mechanism.

Summary

This chapter encapsulated the novel extension of MQED to incorporate electron intermediaries in energy transfer collisions. It started with a derivation of the fully quantized system Hamiltonian, analogous to that found in Chapter 2 for MQED. However, the theory of this chapter treated the quantized electron field with much greater depth, while retaining the MQED results for the radiation field. The extended development was due primarily to the association of molecular orbitals with the expansion amplitudes of the electron field operator. Thus, the electron field was treated on an equivalent footing as the radiation field in the sense that both the radiation and the electron fields were expanded into eigenmodes of their respective noninteracting systems. This insight is perhaps the key contribution of this research to the theory of fast, spin-forbidden energy transfer.

The interaction Hamiltonian given in (3.29) clearly presents the electron exchange mechanism as a two particle process. This expression, which is specific to charge neutral energy transfer collisions, will be used in the calculations described in Chapter 7.

Chapter 4

Quantum Chemistry

The derivation of Chapter 3 used the union of molecular orbitals from each collision partner as a basis set upon which to expand the quantized electron field operator. Thus, in order to perform any actual calculations, such as determining the interaction Hamiltonian and cross section for reaction (1.3), it is imperative to numerically evaluate these orbitals. An entire industry has developed over the past fifteen years aimed at generating numerical expressions for molecular orbitals, and this research utilizes that information.

The following discussion will present a review of standard material. A brief theoretical overview is given, followed by specific details of computational techniques that will be used in Chapter 7.

General Self-Consistent Field Theory

Quantum chemistry is, in truth, a semi-classical theory. Indeed, the whole point to quantum chemistry is not to generate complex, fully-quantal solutions to the Hamiltonian of chemically-interesting physical systems. Rather, the focus of the technology is to solve Schrödinger's equation for chemically-interesting physical systems on a computer using a complex arrangement of solutions to simple, chemically-uninteresting physical systems. The fundamental building block of the entire approach is what is known as self-consistent field (SCF) theory.

Hartree first proposed a theory of the electronic structure of atoms in 1928. The theory was subsequently improved upon by Fock and Slater in 1930. The Hartree-Fock

method, as it is called, was a precursor to the self-consistent field model, although the distinction is a slight one. In the Hartree-Fock model, Hartree was able to write down a set of equations which approximated the solution to the many-electron wavefunction for an atom by treating the electrons as independent particles. In order to solve the equations, though, Hartree and Fock developed an iterative method. Once the iterations converged to an acceptable solution, the electronic wavefunctions were self-consistent, which lead to the nomenclature of the Hartree-Fock model as being self-consistent [39].

The Schrödinger equation for a many-electron atomic system is

$$H\Phi = E\Phi \tag{4.1}$$

in which the Hamiltonian is given by, in atomic units,

$$\begin{aligned} H &= \left(\frac{-1}{2}\sum_i \nabla_i^2 - \sum_i \frac{Z}{r_i}\right) + \sum_{i,j<i} \frac{1}{r_{ij}} \\ &= \sum_i h_i + \frac{1}{2}\sum_{i,j} \frac{1}{r_{ij}} \end{aligned} \tag{4.2}$$

The subscripting of the differential operator is to indicate the coordinate set of the i^{th} electron, and $r_{ij} \equiv \left|\underline{r_i} - \underline{r_j}\right|$. The Hartree-Fock model is a type of variational approximation to (4.2) with four key restrictions on the overall trial wavefunction: the wavefunction must satisfy the Pauli Principle, it must be composed of spin-orbital products, the spin-orbitals must form an orthonormal set, and the total wavefunction must be a solution of the angular momentum and spin angular momentum operators.

The cornerstone of the Hartree-Fock method is the variational principle, which states that any given trial solution to Schrödinger's equation will yield an energy value greater than the exact solution. If Φ represents a trial solution to Schrödinger's equation, then it can be shown that the energy is a functional of Φ [40], i.e. $E = E(\Phi) \geq E_{exact}$, with the form,

$$E(\Phi)=\frac{\langle\Phi|H|\Phi\rangle}{\langle\Phi|\Phi\rangle}>E_{exact} \tag{4.3}$$

It is instructive to outline the determination of Φ in the Hartree-Fock method. First, it is assumed that Φ is a normalized Slater determinant, with the form,

$$\Phi=\frac{1}{\sqrt{N!}}det\left|\phi_1(x_1)\ \phi_2(x_2)\ \ldots\ \phi_N(x_N)\right| \tag{4.4}$$

where x_i denotes both space and spin variables. The energy functional, using the Hamiltonian of (4.2), then becomes

$$E(\Phi)=\sum_{\alpha}\langle\phi_\alpha|h|\phi_\alpha\rangle+\frac{1}{2}\sum_{\alpha,\beta}\langle\phi_\alpha\phi_\beta\|\phi_\alpha\phi_\beta\rangle \tag{4.5}$$

where $h\equiv\sum h_i$. The last term is the customary notation for the direct and exchange terms,

$$\begin{aligned}\langle\phi_\alpha\phi_\beta\|\phi_\alpha\phi_\beta\rangle\equiv&\iint dx_1dx_2\phi_\alpha(x_1)\phi_\beta(x_2)\frac{1}{r_{12}}\phi_\alpha(x_1)\phi_\beta(x_2)\\&-\iint dx_1dx_2\phi_\alpha(x_1)\phi_\beta(x_2)\frac{1}{r_{12}}\phi_\beta(x_1)\phi_\alpha(x_2)\end{aligned} \tag{4.6}$$

where x_i refers to both spatial and spin variables. The energy may be rewritten in terms of a single summation by appropriately defining total coulomb and exchange operators as

$$J\phi(x_n)=\left(\sum_i\int dx_m\phi_i^*(x_m)\frac{1}{r_{nm}}\phi_i(x_m)\right)\phi(x_n) \tag{4.7}$$

and

$$K\phi(x_n)=\left(\sum_i\int dx_m\phi_i^*(x_m)\frac{1}{r_{nm}}\phi_i(x_n)\right)\phi(x_m) \tag{4.8}$$

With these definitions, the energy functional may then be written as

$$E(\Phi)=\sum_{\alpha}\langle\phi_\alpha|h|\phi_\alpha\rangle+\frac{1}{2}\sum_{\alpha}\langle\phi_\alpha|(J-K)|\phi_\alpha\rangle \tag{4.9}$$

It is required that the energy functional be stationary with respect to variations in the orbitals, under the conditions that basis functions are orthonormal. The variational equation for the k^{th} is

(4.10) $$\delta E(\Phi)\big|_k = \langle \delta\phi_k | h + (J-K) | \phi_k \rangle + \langle \phi_k | h + (J-K) | \delta\phi_k \rangle$$

where the factor of 1/2 present in (4.5) is eliminated in performing the variation. The quantity $F \equiv h + (J-K)$ is termed the Fock Hamiltonian. It represents the effective Hamiltonian for a single electron moving in the field due to the nuclei and the other electrons.

It can be shown that upon completing the variational procedure, in which the method of Lagrange multipliers is used to incorporate the orthonormality constraints of each of the individual orbitals, the orbitals which leave the energy functional stationary must satisfy [36]

(4.11) $$F\phi_i = \varepsilon_i \phi_i$$

where ε_i is the Lagrange multiplier, which now takes on the meaning of an eigenvalue to the Fock Hamiltonian. The set of equations given by (4.11) are called the Hartree-Fock equations. It would appear that (4.11) is a simple eigenvalue equation which may be used to determine ϕ_i, but it must be emphasized that F is an implicit function of the set of orbitals $\{\ldots\phi_k\ldots\}$ through (4.7) and (4.8). Hence, (4.11) is not a true eigenvalue equation, despite the appearance, and an iterative technique must be used to obtain ϕ_i. When the solutions for ϕ_i all converge to within an acceptable amount, the orbitals are self-consistent. The orbital energies, within the determined configuration, are then given by (4.11).

It will be important to explore the solution to (4.11) further in Chapter 7 for an atomic system. In that case, there is spherical symmetry which can be used to reduce the difficulty of solving (4.11). It can be shown that the form of the Fock Hamiltonian for a given atomic spin-orbital is [41]

$$F = \sum_{\alpha=1}^{N} \left\{ -\frac{1}{2}\nabla_\alpha^2 - \frac{Z}{r_\alpha} + V^{eff}(r_\alpha) \right\} \tag{4.12}$$

where the effective potential is a disguise for the coulomb and exchange terms, (4.7) and (4.8). In essence, the effect of the *N-1* electrons upon the spin-orbital of the i^{th} electron is taken up by the effective central potential, $V^{eff}(r)$. Since the electron spin is not explicitly present in (4.12), the electronic wavefunction might be considered as simply a product of a spin-orbital for each electron. Thus, (4.11) may be written as

$$\left[-\frac{1}{2}\nabla^2 - \frac{Z}{r} + V^{eff}(r) \right] \phi_i = \varepsilon_i \phi_i \tag{4.13}$$

Since this is a central field problem, the one-electron spin-orbitals may be separated into

$$\phi_i(r,\theta,\varphi,\sigma) = \frac{1}{r} P_i(r) Y_{l_i m_i}(\theta,\varphi) \chi_{\sigma_i} \tag{4.14}$$

where χ_σ is a spinor, and $P_i(r)$ is the solution of the radial Schrödinger equation. The radial functions must solve

$$\left[\frac{d^2}{dr^2} + \frac{2Z}{r} - 2V^{eff}(r) - \frac{l(l+1)}{r^2} - \varepsilon_i \right] P_i(r) = 0 \tag{4.15}$$

where the one-electron energy is given by ε_i. It should be noted that spatial portion of the orbital (4.14) is the spatial solution for an orbital consisting of two electrons, corresponding to two values of the spin eigenvalue. If a given spatial solution of (4.15) is assigned to both the spin up spinor, χ_+, and spin down spinor, χ_-, then the solution technique is referred to as a restricted Hartree-Fock (RHF) method. Given the above derivation, (4.14) would be an example of a RHF result. Consequently, if each spinor is assigned a unique spatial form, regardless of whether the forms are identical, the method is then referred to as unrestricted Hartree-Fock (UHF). This technique usually makes an attempt to incorporate spin into the effective potential term, thus allowing for the possibility of unique spatial solutions and eigenvalues for each value of the spinor.

The application of the Hartree-Fock method to molecules is based upon the Born-Oppenheimer approximation, which states that the nuclear motion may be ignored while solving for the electronic wavefunction. Thus, the nuclear coordinates are interpreted as free parameters during the solution of the Hartree-Fock equations. Indeed, this parametric form is exploited in order to predict molecular structures.

To oversimplify the method, the first step is to make an estimate of the nuclear coordinates. A calculation of (4.11) is then performed and the system energy is determined, as well as the gradients of the energy with respect to the nuclear coordinates. Recalling the variational principle, a slight modification of the coordinates is made, and a subsequent recalculation of (4.11) is done. This process is repeated until the system energy is found to be minimal. At this point, the nuclear coordinates specify the equilibrium geometry of the molecule.

Molecular Orbitals

There is an additional subtlety, though, in the calculation of molecular structures that does not appear in atomic Hartree-Fock. Because molecular structures are no longer a central potential problem, the exact spatial form of the molecular orbitals is not dependent on the spherical harmonics. The standard approach [42] to overcome this difficulty is to assume that the molecular orbitals may be constructed as linear combinations of atomic orbitals. This is identified as the LCAO approach. The total wavefunction (4.4) is still a Slater determinant, but now each of the orbitals, ϕ_i, consist of a sum of atomic orbitals, i.e.

$$\phi_i = \sum_{\lambda} c_{i\lambda} \varphi_\lambda \tag{4.16}$$

The variation of the energy functional still takes place with respect to the molecular orbitals, but under the restriction that the numerical description of the atomic orbitals is

fixed. Hence, only the coefficients of (4.16) are varied to determine the equilibrium structure. Furthermore, the distinction between RHF and UHF is removed from the atomic orbitals and raised to the level of the coefficients, such that (4.16) would designate a RHF expansion, while the corresponding UHF expansion would take the form,

$$\phi_i^{\alpha} = \sum_{\lambda} c_{i\lambda}^{\alpha} \varphi_{\lambda}; \qquad \phi_i^{\beta} = \sum_{\lambda} c_{i\lambda}^{\beta} \varphi_{\lambda} \tag{4.17}$$

Note that it is customary to designate the spin components as either α or β.

In performing the variation over the expansion coefficients with a fixed set of atomic orbitals, the result of the overall calculation depends heavily on having sufficient functional diversity in the type and number of atomic orbitals. It would be desirable to have an infinite set of atomic orbitals from which to create each molecular orbital. In practice, however, the atomic orbital set is restricted by the size of the computer performing the calculation. This limit marks the transition of quantum chemistry from a purely theoretical endeavor to a numerically driven analysis.

At the time when molecular structures were first being calculated, only the smallest possible basis sets were considered. Every molecular orbital was constructed as in (4.16) or (4.17) with only the fewest atomic orbitals necessary to describe the atoms within the molecule. For example, the hydrogen atom requires a 1s atomic orbital, while the oxygen atom requires 1s, 2s, and 2p atomic orbitals. Hence, a minimal basis set for water would include 5 atomic orbitals, one 1s orbital centered on each of the hydrogen nuclei, and three orbitals centered on the oxygen nucleus.

Although minimal basis sets are straightforward, they have three important deficiencies. One problem is that the number of orbitals does not depend upon the number of electrons present. Thus, both water and the amino radical, NH_2, share the same minimal basis set, even though they have different numbers of electrons. This

presents a computational scaling problem. A second problem with minimal basis sets is that the valence shell is unable to expand or contract in response to the local environment. This is the primary result of performing variations only on the coefficients of the LCAO expansion. Minimal basis sets have no mechanism for offsetting this penalty. The third problem with minimal basis sets is that they inadequately model molecules which have a high degree of anisotropy in the charge distribution. For example, the first row elements contain only spherical orbitals in their basis sets. The second row elements contain both s and p orbitals, and both are considered during the variational process. However, regardless of the amplitude of a given atomic orbital, all p type orbitals have the same spatial extent. It is quite impossible to model differences in the spatial extent of a molecular charge distribution when all the orbitals are of the same characteristic size.

One method to overcome these difficulties is to allow for additional basis functions, in particular the valence shell. By including an additional set of mathematical functions of the same symmetry as the original minimal valence orbitals, it becomes possible to account for a variation in spatial extent of the orbital. Suppose that the valence symmetry is an s orbital. If two s orbitals are present in the basis, one which is contracted, i.e. a small length scale, and one which is diffuse, i.e. a large length scale, then it is possible to linearly combine the orbitals to create a resultant s orbital of the proper length scale. Note that the adjustment of the linear combination of s orbitals is consistent with the framework for energy minimization. Charge density anisotropy occurs only for p, d, etc. orbitals, since s orbitals are spherically symmetric. Again, an additional set of valence orbitals can be used to emphasize a particular direction, without increasing the emphasis in any other direction.

A basis set which replicates all the orbitals of a minimal basis set is called a double-zeta basis. Although the overall system energy may be affected by the fine tuning

of the core orbitals, usually this is a waste of computing resources. This is because the inner core electrons do not participate in chemical bonding. A more prudent choice is to double only the set of orbitals in the valence shell of each atom. These types of bases are referred to as split-valence basis sets, and at the present time, they are the workhorses of the industry.

The representation of the atomic orbitals is of great importance for numerical computations of chemical parameters. Slater orbitals are analytical fits to the results of numerical solution of the atomic Hartree-Fock equations. The assumed form of Slater-type orbitals (STO) is [39]

$$\chi_{j,nlm}(\underline{r}) \equiv N r^{n-1} e^{-\alpha_j r} Y_{lm}(\theta,\phi) \tag{4.18}$$

Note the resemblance between the STOs and the hydrogenic wave functions, especially for large r. The most obvious difference is that STOs do not exhibit radial nodes. The STO may be used directly as an approximation of a Hartree-Fock orbital, or a linear combination of STOs may be used, as in

$$\varphi_{nlm}(\underline{r}) = \sum_j d_{nlm,j} \chi_{j,nlm}(\underline{r}) \tag{4.19}$$

By substituting (4.19) into (4.16) or (4.17), it is clear that a molecular orbital may, in practice, be expanded twice, once for the LCAO expansion, i.e. (4.16), and once for the atomic orbital expansion, i.e. (4.19).

The difficulty of STOs is that they are not well suited for numerical evaluation. This was recognized in the late 1960's, and an alternative method of representing atomic orbitals [43] was applied to the calculation of molecular chemistry [44]. This method replaced the STO of (4.18) by a gaussian function of the form,

$$g_{nlm}(\underline{r}) = N r^{n-1} e^{-\alpha r^2} Y_{lm}(\theta,\phi) \tag{4.20}$$

The nomenclature is that when (4.20) is substituted into (4.19), the resulting atomic orbital is referred to as a contracted gaussian, while (4.20) by itself is termed a primitive

gaussian. Quite often, the Cartesian form of the gaussians is used in calculations. The normalized gaussians for the 1s through the 2pz orbitals are given in Table 4.1.

The Cartesian forms of the gaussians are useful because integrals of products of gaussians do not exhibit complicated angular dependencies, and because the p orbitals form a basis for a cartesian coordinate system. The former provides for much simpler analytic manipulations. The latter means that the p orbitals transform as a vector under rotations. Note that the s orbitals are spherically symmetric and strictly speaking, also transform under rotations. This is valuable in performing rotational averages of orbital quantities, such as overlaps between charge distributions. Once all three p orbital quantities of interest have been computed, the analogous quantities evaluated at any other orientation of the p orbitals can quickly be determined by solving the rotation transformation matrix, i.e. the Euler angle transformation.

In order to form a basis set of atomic orbitals, a specification of the contraction of primitive gaussians is needed. The simplest type of basis is to approximate each atomic orbital by a STO, and then decompose the STO into primitive gaussians, hence

$$\varphi_{nlm}(\underline{r}) \cong \chi_{nlm}(\underline{r}) \cong \sum_{j=1}^{K} d_{nlm,j} g_{nlm,j}(\alpha_{nlm,j}, \underline{r}) \tag{4.21}$$

This type of basis set is denoted as STO-KG, where K refers to the number of primitive gaussians used to approximate each STO. Historically, this arrangement was referred to as a minimal basis set, having one STO for each atomic orbital of the atom. In practice, the basis set STO-3G represents the easiest, and least computationally expensive basis set to use. Hence, it is typically used for rough, first-cut calculations.

Quite often, a variation of (4.21) is used, in which a scaling parameter is also specified. This scaling parameter then allows the same orbital to be used for many

Table 4.1 Listing of Primitive Gaussians

Orbital Symmetry	Functional Form, $g_i(\alpha, \underline{r})$
1s	$\left(\frac{2\alpha}{\pi}\right)^{3/4} exp(-\alpha r^2)$
2s	$\left(\frac{2\alpha}{\pi}\right)^{3/4} exp(-\alpha r^2)$
2px	$\left(\frac{128\alpha^5}{\pi^3}\right)^{1/4} x\, exp(-\alpha r^2)$
2py	$\left(\frac{128\alpha^5}{\pi^3}\right)^{1/4} y\, exp(-\alpha r^2)$
2pz	$\left(\frac{128\alpha^5}{\pi^3}\right)^{1/4} z\, exp(-\alpha r^2)$

Source: Hehre, W.J., *J. Chem. Phys.*, **51**, 2657 (1969).

different shells, assuming that the spatial extent changed from shell to shell. This additional form of gaussian is actually the most common and is written as [45],

$$\varphi_{nlm}(\zeta,\underline{r}) = \zeta^{3/2}\varphi_{nlm}(1,\zeta\underline{r}) \tag{4.22}$$

where the scaled orbital is given by

$$\varphi_{nlm}(1,\zeta\underline{r}) = \sum_{j=1}^{K} d_{nlm,j}\, g_{nlm,j}(\alpha_{nlm,j},\zeta\underline{r}) \tag{4.23}$$

As computational power has increased in the last twenty years, so has the complexity of the basis sets. Split-valence basis sets are the standard for serious calculations, as mentioned above. Correspondingly, the extent of the atomic orbital expansion in terms of primitive gaussians has also increased over that time frame. The notation of a split-valence basis set is self-explanatory, once the scheme is identified. For example, the 4-31G basis set uses four primitive gaussians for each core atomic orbital. The valence orbitals are duplicated, and the first set is comprised of atomic orbitals, each of which are expanded into three primitive gaussians, while the second set is comprised of atomic orbitals which are approximated by a single gaussian. The 6-31G basis set is presently the basis set of choice for most calculations. The relevant parameters of this set for atoms through the second row of the Periodic Table have been developed and standardized by several authors [46-48]. Typically, a calculation will be performed using STO-3G to get a rough estimate of the results, and then the computation will be fine-tuned with the 6-31G basis set.

The GAUSSIAN90 program

So far, the discussion has been rather vague as to how the computation of molecular structures and properties is actually performed. Although there are many computer packages capable of doing calculations to varying degrees of accuracy, the

present research utilized the GAUSSIAN90, or g90, program [49]. Other programs, with varying degrees of cryptocity in their identification, include the MOLECULE-SWEDEN libraries, MOPAC, GAMESS, MINDO/3, etc. Obviously, each program has strengths and weaknesses, but one of the primary differences between the codes is the distinction between a semi-empirical and *ab initio* approach. g90 is an *ab initio* code, meaning that the modeling is done from first principles, in the manner described above, without extensive empirical data libraries. This is what makes the excellent agreement between the *ab initio* codes, such as g90, and experimental measurements, such as chemical structures, so incredible. Indeed, as computational power continues to increase, the usage of semi-empirical codes, e.g. MINDO/3, declines in favor of the *ab initio* codes.

GAUSSIAN90 is actually an eighth generation program of a project initiated in 1970 by Hehre, et al. Each revision of the program is annotated by the year of release. The full range of predictive capabilities can be found in the reference and is not of importance here. The important point to note is that g90 utilizes the above theoretical framework, i.e. the variational principle, gaussian expansions, etc., to solve chemical problems. The application of g90 to the ground state of diatomics is actually rather mundane, and with the proper basis set, can yield excellent agreement to the bond length and the vibrational and rotational frequencies. The determination of excited state parameters is also attempted by g90, using the orthogonality of the ground and upper states in the variational principle. The subsequent version of g90, i.e. g92, is the first version to compute dipole transition moment functions between an excited and ground state.

Summary

This chapter served to define two items: 1) the analytical and computational methods employed in practical solution of molecular quantum mechanics, and 2) the nomenclature used in the field of quantum chemistry. The latter is essential to comprehend the literature, including Chapter 7 of this document, while the former is useful in drawing conclusions based upon computational predictions.

Chapter 5

Scattering Theory of Molecules

In the previous chapters, reference has been made to the transition probability for energy transfer without rigorous definition. It is now necessary, prior to any application, to explicitly derive the transition probability, and more importantly the scattering cross section. The scattering cross section is a measurable, and is the goal of any scattering theory, not only those concerned with energy transfer reactions. However, in order to arrive at the cross section, the impact of the interacting and noninteracting Hamiltonians upon the states of the collision partners needs to be well defined. The following text serves as a review of standard material assimilated from several sources, including Newton [50], Goldberger [51], Messiah [52], and Merzbacher [53].

Time Evolution of Interacting Systems

The goal of any scattering problem is to determine the probability of measuring a system in a particular state either before or after an interaction has occurred, given that the system was in a prepared state either post or prior, respectively, to the interaction. In either case, it is the residual effect of some form of interaction energy that produces the initiative for transitions between eigenstates of the complete Hamiltonian of the system. To better understand the interaction Hamiltonian, it is essential to follow the evolution of the system eigenfunction as it travels from the distant past to the present and on into the distant future. For the context of this discussion, the interaction between the two systems will be confined to the present, with a non-interacting Hamiltonian governing the entire system in the distant past and distant future.

The following discussion may be outlined in several steps. First, the standard Green function solutions to both the non-interacting and interacting Hamiltonians are defined, along with the time evolution operators. From these solutions, it is possible to construct integral equation solutions, i.e. the Lippmann-Schwinger equations, for the complete system wavefunction. At that point, one can define the so-called "in" and "out" states and their relation to the complete interacting wavefunction. The Lippmann-Schwinger equations can be formulated in terms of Møller wave operators, which in turn can be related to the unitary scattering matrix. It is then shown that the scattering amplitude can be extracted from the scattering matrix by examining the asymptotic solutions of the usual expressions for quantum mechanical scattering.

Green's Functions

To begin, consider two molecular systems, A and B, such that in the distant past they are non-interacting. Both A and B can be described by distinct Hamiltonians, H_A and H_B, yielding independent eigenstates and eigenvalues for A and B. Explicitly,

(5.1) $$H_A\phi_A(a) = E_A(a)\phi_A(a)$$
$$H_B\phi_B(b) = E_B(b)\phi_B(b)$$

where a and b denote a suitable set of quantum numbers. They could represent entirely different solution spaces indicative of the differences in the respective Hamiltonians H_A and H_B. The total Hamiltonian, which includes the interaction, can be written

(5.2) $$H = H_o + H'$$

where $H_o = H_A + H_B$, and H' represents the interaction. In the following, H is termed the complete interacting Hamiltonian, while H_o is termed the complete noninteracting, or free Hamiltonian. A solution to the complete interacting time-dependent Schrödinger equation, $\Phi(t)$, then follows as

(5.3) $$i\frac{\partial}{\partial t}\Phi(t) = H\,\Phi(t)$$

where in natural units, $\hbar$=c=1.

The solution of the Schrödinger equation is facilitated by introducing the Green functions for both the complete interacting, H, and noninteracting, H_o, Hamiltonians defined by

(5.4) $$(i\frac{\partial}{\partial t} - H_o)\,G^{\pm}(t) = \delta(t)$$

(5.5) $$(i\frac{\partial}{\partial t} - H)\,g^{\pm}(t) = \delta(t)$$

subject to the initial conditions,

(5.6) $$G^{+}(t)=g^{+}(t)=0; \quad t<0$$

i.e. the $G^{+}(t)$and $g^{+}(t)$ solutions propagate the wavefunction into the future for the noninteracting and interacting Hamiltonians, respectively. Likewise, the $G^{-}(t)$ and $g^{-}(t)$ solutions propagate the system wavefunction into the distant past, based upon their respective Hamiltonians,

(5.7) $$G^{-}(t)=g^{-}(t)=0; \quad t>0$$

Both sets of Green functions can be formulated in terms of the time evolution operator as

(5.8)
$$G^{+}(t) = \left\{ \begin{array}{ll} -ie^{-iH_o t} \equiv -i\,U_o(t) & t>0 \\ 0 & t<0 \end{array} \right\}$$
$$G^{-}(t) = \left\{ \begin{array}{ll} 0 & t>0 \\ ie^{-iH_o t} \equiv i\,U_o(t) & t<0 \end{array} \right\}$$

and

$$
(5.9)\qquad
\begin{aligned}
g^{+}(t) &= \left\{ \begin{array}{lll} -ie^{-iHt} \equiv -iU(t) & t>0 \\ 0 & t<0 \end{array} \right\} \\
g^{-}(t) &= \left\{ \begin{array}{lll} 0 & t>0 \\ ie^{-iHt} \equiv iU(t) & t<0 \end{array} \right\}
\end{aligned}
$$

Note that the Green functions are constructed from operators that commute with their respective Hamiltonians, implying that the Green functions themselves commute with their respective Hamiltonians,

$$(5.10)\qquad [\, G^{\pm}(t), H_o \,] = 0$$

and

$$(5.11)\qquad [\, g^{\pm}(t), H \,] = 0$$

Further, H and H_o must be Hermitian since they correspond to physical observables. Likewise, the Green functions have the property,

$$(5.12)\qquad \overline{G^{+}}(t) = G^{-}(-t)$$

and

$$(5.13)\qquad \overline{g^{+}}(t) = g^{-}(-t)$$

where the overbar denotes Hermitian conjugation.

The primary reason for defining the Green functions for this work is their use as state vector propagators. Suppose that $\Psi_o(t)$ is some solution of the complete noninteracting Hamiltonian, H_o. Using the Green function for propagation into later times allows one to determine $\Psi_o(t')$, where $t'>t$,

$$
(5.14)\qquad
\begin{aligned}
\Psi_o(t') &= iG^{+}(t-t')\Psi_o(t) \\
&= U_o(t'-t)\Psi_o(t) \\
&= e^{-iH_o(t'-t)}\Psi_o(t)
\end{aligned}
$$

Note that $\Psi_o(t')$ is also a solution to the complete noninteracting Schrödinger equation, as can been seen by differentiating (5.14) with respect to t'.

In and Out States

As noted above, the Green functions track the evolution of the entire system wavefunction from the distant past through the present and into the distant future. Let $\Phi(t)$ be defined as the complete, interacting wavefunction of the entire system which satisfies the Schrödinger for H. In the distant past, the interaction was negligible and $\Phi(t)$ must have been equal to a wavefunction, defined as $\Phi_o(t)$, that satisfies the complete noninteracting Hamiltonian, H_o. Hence, for t_o in the distant past,

$$\Psi_o(t_o)=\Phi(t_o) \tag{5.15}$$

i.e. the noninteracting solution propagates into later times via the noninteracting Green function, $G^+(t)$,

$$\begin{aligned}\Psi_o(t) &\equiv iG^+(t-t_o)\Psi_o(t_o)\\ &=iG^+(t-t_o)\,\Phi(t_o)\end{aligned} \tag{5.16}$$

This logic can be viewed from the reverse perspective. Imagine a state, which is a solution to the free Hamiltonian, H_o, but which could also be traced back in time to be equal to a solution to the complete interacting Hamiltonian, H. This is the definition of the "in" state,

$$\Psi_{in}(t) \equiv \lim_{t' \to -\infty} i\,G^+(t - t')\,\Phi(t') \tag{5.17}$$

In this manner $\Psi_{in}(t)$ is a free state, since it is propagated via the non-interacting Hamiltonian and it is a solution to H_o. However, in the distant past $\Psi_{in}(t)$ was a state which was equal to the complete solution to the Hamiltonian, i.e. a planned coincidence. The "in" state should not be confused with the propagated solution (5.16) although its usefulness can be found by explicit substitution into the Schrödinger equation and taking time derivatives such as

$$i\frac{\partial}{\partial t'}\left\{G^{+}(t-t')\Phi(t')\right\} = -i\partial_{t'}G^{+}(t-t')\,\Phi(t') + iG^{+}(t-t')\partial_{t'}\Phi(t'). \tag{5.18}$$

Substituting the definition of $G^{+}(t)$,

$$i\frac{\partial}{\partial t}G^{+}(t) = H_o\,G^{+}(t) + \delta(t) \tag{5.19}$$

and the explicit Schrödinger equation,

$$\begin{aligned} i\frac{\partial}{\partial t}\Phi(t) &= H\,\Phi(t) \\ &= (H_o + H')\,\Phi(t) \end{aligned} \tag{5.20}$$

yields

$$\begin{aligned} i\frac{\partial}{\partial t'}\left\{G^{+}(t-t')\Phi(t')\right\} &= -\left\{H_oG^{+}(t-t') + \delta(t-t')\right\}\Phi(t') \\ &\quad + G^{+}(t-t')(H_o + H')\Phi(t') \\ &= -\delta(t-t')\Phi(t') + G^{+}(t-t')H'\,\Phi(t') \end{aligned} \tag{5.21}$$

where the commutator $[H_o, G^{+}(t-t')] = 0$. Straightforward integration of t' from -∞ to +∞ gives

$$\begin{aligned} \int_{-\infty}^{\infty} dt'\,\frac{\partial}{\partial t'}\left\{iG^{+}(t-t')\Phi(t')\right\} &= -\int_{-\infty}^{\infty} dt'\,\delta(t-t')\Phi(t') \\ &\quad + \int_{-\infty}^{\infty} dt'\,G^{+}(t-t')H'\,\Phi(t') \end{aligned} \tag{5.22}$$

Using the time behavior of $G^{+}(t-t')$ from (3.8), and the definition of $\Psi_{in}(t)$ from (5.17) simplifies this expression,

$$-\Psi_{in}(t) = -\Phi(t) + \int_{-\infty}^{\infty} dt'\,G^{+}(t-t')H'\,\Phi(t') \tag{5.23}$$

or in a more useful fashion,

$$\Phi(t) = \Psi_{in}(t) + \int_{-\infty}^{\infty} dt' G^{+}(t-t') H' \Phi(t') \tag{5.24}$$

which is the well-known Lippmann-Schwinger equation.

Just as the "in" state was defined, an analogous "out" state can be defined as the free (non-interacting) solution to H_o, which happens to coincide with the interaction solution in the distant future,

$$\Psi_{out}(t) \equiv \lim_{t' \to +\infty} -i\, G^{-}(t - t')\, \Phi(t') \tag{5.25}$$

Manipulations with $\Psi_{out}(t)$, similar to that above for $\Psi_{in}(t)$, yield an additional integral equation for the complete solution,

$$\Phi(t) = \Psi_{out}(t) + \int_{-\infty}^{\infty} dt' G^{-}(t-t') H' \Phi(t') \tag{5.26}$$

This form is less useful simply because experiments typically have well-defined pre-interaction states, rather than post-interaction states.

Yet another perspective of the relation of the "in" and "out" states and the complete solution can be obtained by recomputing the above using the complete propagator, $g^{\pm}(t)$. From the definition of the $\Psi_{in}(t)$,

$$\Phi(t) = \lim_{t' \to -\infty} -i\, g^{+}(t - t')\Psi_{in}(t') \tag{5.27}$$

The complete solution originates from $\Psi_{in}(t)$ in the distant past, but is propagated by the complete interacting evolution operator. Again taking derivatives,

$$i\frac{\partial}{\partial t'}\left\{g^{+}(t-t')\Psi_{in}(t')\right\} = i\,\partial_{t'} g^{+}(t-t')\ \Psi_{in}(t') + g^{+}(t-t')\ i\,\partial_{t'}\Psi_{in}(t') \tag{5.28}$$

Using the free Schrödinger equation,

$$i\frac{\partial}{\partial t'}\left\{g^{+}(t-t')\Psi_{in}(t')\right\} = i\partial_{t'} g^{+}(t-t')\Psi_{in}(t') + g^{+}(t-t')\, H_o \Psi_{in}(t') \tag{5.29}$$

applying the Green function definition (5.9),

$$i\frac{\partial}{\partial t'}\left\{g^{+}(t-t')\Psi_{in}(t')\right\}= \tag{5.30}$$
$$-\left\{H\,g^{+}(t-t')+\delta(t-t')\right\}\Psi_{in}(t')+g^{+}(t-t')(H-H')\Psi_{in}(t')$$

regrouping,

$$i\frac{\partial}{\partial t'}\left\{g^{+}(t-t')\Psi_{in}(t')\right\}= \tag{5.31}$$
$$\left[g^{+}(t-t'),H\right]\Psi_{in}(t')-\delta(t-t')\Psi_{in}(t')-g^{+}(t-t')H'\Psi_{in}(t')$$

and using the commutator $\left[g^{\pm},H\right]=0$, yields

$$i\frac{\partial}{\partial t'}\left\{g^{+}(t-t')\Psi_{in}(t')\right\}=-\delta(t-t')\Psi_{in}(t')-g^{+}(t-t')H'\Psi_{in}(t') \tag{5.32}$$

Subsequent integration of t' from -∞ to +∞ will then give

$$\lim_{t'\to\infty}\left(ig^{+}(t-t')\Psi_{in}(t')\right) \;-\; \lim_{t'\to-\infty}\left(ig^{+}(t-t')\Psi_{in}(t')\right)= \tag{5.33}$$
$$-\Psi_{in}(t)-\int_{-\infty}^{\infty}dt'\,g^{+}(t-t')H'\Psi_{in}(t')$$

The first term is zero from the initial conditions on $g^{+}(t)$ given in (5.9), while the second term is simply $-\Phi(t)$. Hence rewriting (5.33),

$$\Phi(t)=\Psi_{in}(t)+\int_{-\infty}^{\infty}dt'\,g^{+}(t-t')H'\Psi_{in}(t') \tag{5.34}$$

This form now describes the intuitive development of the complete interacting solution as a deviation from a noninteracting, freely propagating state. The amount of deviation is controlled by the complete interaction Hamiltonian over the time period of the interaction. In this context, $\Psi_{in}(t)$ can be thought of as an experimentally prepared state prior to the interaction. The result of the scattering on the complete interacting

wavefunction can now be traced back to a state which was non-interacting. It will become useful later to denote the complete interacting solution by its noninteracting origins, such that

(5.35) $$\Psi^{+}(\alpha,t) \equiv \Phi(t)$$

where α denotes the set of complete quantum numbers that identify the $\Psi_{in}(t)$ state. Obviously, in the distant past, $\Psi^{+}(\alpha,t)$ was equal to $\Psi_{in}(t)$.

Møller Wave Operators and the Scattering Matrix

Recall that the time evolution of $\Psi_{in}(t)$ is determined by the free Green function because it solves the free Schrödinger equation,

(5.36) $$\Psi_{in}(t') = -iG^{-}(t-t')\Psi_{in}(t)$$

such that upon substituting into (5.34), one obtains

(5.37)
$$\begin{aligned}\Phi(t) &= \Psi_{in}(t) - i\int_{-\infty}^{\infty} dt'\, g^{+}(t-t')H'G^{-}(t'-t)\Psi_{in}(t) \\ &= \left\{1 - i\int_{-\infty}^{\infty} dt'\, g^{+}(t-t')H'G^{-}(t'-t)\right\}\Psi_{in}(t)\end{aligned}$$

Since dt' runs from -∞ to +∞, the difference $t'-t \equiv \tau$ can be integrated over the same limits. This yields a clean form for the complete solution as

(5.38) $$\Phi(t) = \Omega^{+}\,\Psi_{in}(t)$$

where the Møller wave operator, Ω^{+}, is defined as [50]

(5.39) $$\Omega^{+} \equiv \left\{1 - i\int_{-\infty}^{\infty} d\tau\, g^{+}(-\tau)H'G^{-}(\tau)\right\}$$

Note that Ω^{+} is completely time independent and converts the $\Psi_{in}(t)$ state, which has evolved via the noninteracting Hamiltonian, into $\Phi(t)$, which has further evolved under the complete interacting Hamiltonian.

A similar manipulation with the $\Psi_{out}(t)$ state can be performed, resulting in the definition of the Ω^- operator as

(5.40) $$\Phi(t) = \Omega^- \Psi_{out}(t)$$

where the second Møller wave operator is defined by [50]

(5.41) $$\Omega^- \equiv \left\{ 1 + i \int_{-\infty}^{\infty} d\tau \, g^-(-\tau) H' G^+(\tau) \right\}$$

The utility of the $\Omega^{\pm}$ operators is that they connect the exact eigenstates to the unperturbed system eigenstates. To summarize the important relations,

(5.42) $$\Phi(t) = \Omega^+ \Psi_{in}(t)$$

(5.43) $$\Psi_{in}(t) = \overline{\Omega^+} \Phi(t)$$

(5.44) $$\Phi(t) = \Omega^- \Psi_{out}(t)$$

(5.45) $$\Psi_{out}(t) = \overline{\Omega^-} \Phi(t)$$

where the overbar denotes Hermitian conjugation. Hence, the "out" state is related to the "in" state by

(5.46) $$\Psi_{out}(t) = \overline{\Omega^-} \Omega^+ \Psi_{in}(t)$$

which leads to the natural definition of the scattering matrix as

(5.47) $$S \equiv \overline{\Omega^-} \Omega^+$$

with the property that

(5.48) $$\overline{S} S = 1 = S \overline{S}$$

which can be proven by inverting (5.46). In addition, the scattering matrix S is also time-independent.

Using the above definitions for the various states, the objective of a scattering problem can now be realized. Let the complete interacting system be described in the distant past by the wavefunction $\Phi(t)$, which is equal to the free wavefunction $\Psi_o(\alpha, t)$ where α denotes a particular set of quantum numbers. Hence, $\Psi_{in}(\alpha, t) = \Psi_o(\alpha, t)$.

The complete interacting system will evolve according to H, and the wavefunction can be designated $\Psi^{+}(\alpha,t)$, as described above. In the distant future, the complete interacting system can be described by another wavefunction, $\Phi(t')$, which is equal to a free wavefunction $\Psi_o(\beta,t) = \Psi_{out}(\beta,t)$, where β is used to denote a final set of quantum numbers corresponding to the free Hamiltonian. The state $\Psi_{out}(\beta,t)$ must have been propagated forward in time from a present state given by $\Psi^{-}(\beta,t)$. Thus, the probability amplitude of finding the system in the distant future in the free state $\Psi_o(\beta,t)$, given that the system was in a free state $\Psi_o(\alpha,t)$ in the distant past, is determined by the overlap of the complete interacting states describing the evolution of the interacting system in the present. Mathematically, this is described by the inner product,

$$A = \left\langle \Psi^{-}(\beta,t) \middle| \Psi^{+}(\alpha,t) \right\rangle \tag{5.49}$$

Using the above relations of the Møller operators, this can be written in terms of the free states by noting that

$$\begin{aligned} A &= \left\langle \Omega^{-}\Psi_{out}(\beta,t) \middle| \Omega^{+}\Psi_{in}(\alpha,t) \right\rangle \\ &= \left\langle \Psi_{out}(\beta,t) \middle| \overline{\Omega^{-}}\Omega^{+} \middle| \Psi_{in}(\alpha,t) \right\rangle \\ &= \left\langle \Psi_{out}(\beta,t) \middle| S \middle| \Psi_{in}(\alpha,t) \right\rangle \\ &= \left\langle \Psi_{out}(\beta,0) \middle| S \middle| \Psi_{in}(\alpha,0) \right\rangle \end{aligned} \tag{5.50}$$

where the time dependence vanishes since S commutes with H_o.

Perhaps one of the most important features of the scattering matrix S is that it may be separated into two parts, corresponding to an unscattered and a scattered amplitude. This is simply the origin of the two parts of the usual description of scattering of a plane wave. A functional form the scattering operator is then

$$S = 1 - 2\pi i T \tag{5.51}$$

This relation is the definition of the scattering T matrix, which is the piece de resistance

of formal scattering theory. It is the T matrix which is the valuable quantity in scattering problems since it describes the nature of the scattering event and disregards the unscattered probability.

Time-Independent Scattering

The Scattering Matrix

To this point, all calculations have been performed with the inclusion of time dependence of the state functions. In subsequent calculations, it is much simpler to deal with time-independent wavefunctions. The advantage gained is that most scattering experiments can be described in terms of monoenergetic beams, etc. To change coordinates between time and energy, a standard Fourier transform is done, such that,

$$\Psi(E,\alpha) = \int_{-\infty}^{+\infty} dt\, e^{iEt}\, \Psi(\alpha,t) \tag{5.52}$$

with similar definitions for all the wavefunctions determined in the preceding sections. Since the wave operators and the scattering matrix, S, are time-independent, the expressions relating the complete, interacting solutions, $\Psi^{\pm}(E,\alpha)$, with the "in" and "out" states are mostly unchanged. The exception is that the "in" and "out" states are now simply free states of the noninteracting Hamiltonian with specified quantum numbers. The distinction of "in" and "out" is now somewhat superfluous. The Lippmann-Schwinger relations for single channel scattering, where $H = H_o + H'$, now become

$$\begin{aligned} \Psi^{+}(E,\alpha) &= \Psi_o(E,\alpha) + g^{+}(E) H' \Psi_o(E,\alpha) \\ \Psi^{-}(E,\alpha) &= \Psi_o(E,\alpha) + g^{-}(E) H' \Psi_o(E,\alpha) \end{aligned} \tag{5.53}$$

or using the Møller wave operators,

$$\Psi^{\pm}(E,\alpha) = \Omega^{\pm}\Psi_o(E,\alpha) \tag{5.54}$$

These equations could also be written as the set,

$$\begin{aligned} \Psi^{+}(E,\alpha) &= \Psi_o(E,\alpha) + G^{+}(E)\ H'\Psi^{+}(E,\alpha) \\ \Psi^{-}(E,\alpha) &= \Psi_o(E,\alpha) + G^{-}(E)\ H'\Psi^{-}(E,\alpha) \end{aligned} \tag{5.55}$$

The advantage that (5.55) have over (5.53) is that the Green function for the noninteracting Hamiltonian is usually known. The disadvantage of (5.55) is that they are transcendental-style equations, however. It will be shown below that the well-known Born approximations are simply iterative approximations to the solution of (5.55).

The scattering probability amplitude takes on a form similar to the time-dependent case. Given a system initially prepared in a state $\Psi_o(E_\alpha,\alpha)$ which evolves into state $\Psi^{+}(E_\alpha,\alpha)$, the amplitude for scattering into state $\Psi_o(E_\beta,\beta)$ which evolved from $\Psi^{-}(E_\beta,\beta)$, is given by the overlap,

$$\begin{aligned} \left\langle \Psi^{-}(E_\beta,\beta) \middle| \Psi^{+}(E_\alpha,\alpha) \right\rangle &= \left\langle \Omega^{-}\Psi_o(E_\beta,\beta) \middle| \Omega^{+}\Psi_o(E_\alpha,\alpha) \right\rangle \\ &= \left\langle \Psi_o(E_\beta,\beta) \middle| S \middle| \Psi_o(E_\alpha,\alpha) \right\rangle \end{aligned} \tag{5.56}$$

Since S commutes with H_o, this expression must be proportional to a delta function over the energy when $\alpha = \beta$. Also, when $H = H_o$, there is no interaction and $S = 1$. The overlap (5.56) is simply over the free states. Thus S may be partitioned into pieces as

$$\begin{aligned} \left\langle \Psi_o(E_\beta,\beta) \middle| S \middle| \Psi_o(E_\alpha,\alpha) \right\rangle &= \left\langle \Psi_o(E_\beta,\beta) \middle| \Psi_o(E_\alpha,\alpha) \right\rangle \\ &\quad -2\pi i\,\delta(E_\beta - E_\alpha)\delta(P_\beta - P_\alpha)\,T_{\beta\alpha}(E) \end{aligned} \tag{5.57}$$

where the conservation of energy and momentum are explicitly stated. It follows straightforwardly that $T_{\beta\alpha}(E)$ takes the form,

$$T_{\beta\alpha}(E) = \left\langle \Psi_o(E_\beta,\beta) \middle| H' \middle| \Psi^{+}(E_\alpha,\alpha) \right\rangle \tag{5.58}$$

The Scattering Cross Section

The scattering cross section is a measurable quantity which parametrizes the relative efficiency of a collision. A standard derivation of the differential and total cross section is given in Appendix I. From (A1.19), the total scattering cross section is given by [50]

(A1.19) $$\sigma_{\beta\alpha}(q) = (2\pi)^4 \mu^2 \int d\Omega \left| T_{\beta\alpha}(E_i, \underline{p_i}, q, \Omega) \right|^2$$

In atomic units, $\sigma_{\beta\alpha}(q)$ will have units of $m^2 e^4 a_o^4$, which from Appendix II is equal to a_o^2 or an area, consistent with the physical intuition of the cross section as the "effective" area which a molecule presents its collision partner. In (A1.19) the transition matrix is written slightly different from (5.58). The correlation between the two can be examined by modifying the Lippmann-Schwinger equations (5.55) to contain a variable parameter, γ , which governs the interaction "strength". Then (5.55) takes the form,

(5.59) $$\Psi^+(E,\alpha) = \Psi_o(E,\alpha) + \gamma G^+(E)\ H'\ \Psi^+(E,\alpha)$$

and upon rewriting,

(5.60) $$(1 - \gamma K)\Psi^+(E,\alpha) = \Psi_o(E,\alpha)$$

where $K \equiv G^+(E)\ H'$. The scattering T operator then follows from this as

(5.61) $$T\,(1 - \gamma K) = \gamma\, H'$$

or

(5.62) $$T = \gamma (1 - \gamma K)^{-1} H'$$

One manner for solving for the operator $(1 - \gamma K)^{-1}$ is to expand it in a power series in the strength parameter γ . Then it takes the form,

(5.63) $$(1 - \gamma K)^{-1} = \sum_{n=0}^{\infty} \gamma^n K^n$$

The scattering T operator can be written as a power series as

(5.64) $$T = \gamma \{1 + \gamma K + (\gamma K)^2 + \ldots\}\ H'$$

For the case $\gamma = 1$, the power series is known as the Born series. Note that in this case,

the Lippmann-Schwinger equations are unmodified. In this instance, convergence of (5.64) is a concern. It will suffice herein to note that for the Born series to converge, K must be small in comparison to the scattering energy scales.

Born Approximation

The first Born approximation is given by the first term in (5.64) with $\gamma = 1$, which implies that $T \approx H'$. Hence, the scattering T matrix is given a form of

$$T_{\beta\alpha}(E) = \left\langle \Psi_o(E_\beta, \beta) \middle| H' \middle| \Psi_o(E_\alpha, \alpha) \right\rangle \tag{5.65}$$

where the momenta indices are suppressed. Comparing (5.65) to (5.58) one finds that the first Born approximation is equivalent to replacing the exact interacting solution of the complete Hamiltonian by a free eigenstate.

If the free eigenstates may be constructed from the outer product of plane wave solutions to the propagating particles and the eigenstate of the internal coordinates such that the free states take the form,

$$\left\langle \underline{r} \middle| \Psi_o(E_\alpha, \alpha) \right\rangle = \frac{e^{i\underline{k}_\alpha \cdot \underline{r}}}{(2\pi)^{3/2}} |\alpha\rangle \tag{5.66}$$

then the scattering matrix may be written as

$$T_{\beta\alpha}(\underline{k}_\alpha - \underline{k}_\beta) = \int d\underline{r} \; \frac{e^{i(\underline{k}_\alpha - \underline{k}_\beta)\cdot \underline{r}}}{(2\pi)^3} \langle \beta | H'(\underline{r}) | \alpha \rangle \tag{5.67}$$

where the inner product over the interaction Hamiltonian between the initial and final states explicitly displays the dependence of the scattering process upon the internal structure of the projectiles. Letting $\underline{q} \equiv \underline{k}_\alpha - \underline{k}_\beta$ illustrates that the scattering matrix is the Fourier transform of the interaction potential. This is the mathematical beauty and simplicity of the first Born approximation. Note that since $H'(\underline{r})$ has units (in the Hartree system) of e^2/a_o, and that the plane wave portion of the free state is unitless,

then the scattering matrix has units of $e^2 a_o^2$.

The most important issue surrounding the first Born approximation is the range of applicability of the approximation. As mentioned above, the first Born approximation amounts to replacing the correct interacting solution by an unperturbed solution. Hence, the system never "feels" the interaction until the moment of collision, and then evolves away from the collision without any decreasing perturbation of eigenstates. Indeed, the collision is effectively turned on and off instantaneously. Thus the Born approximation tends to mimic the behavior of high energy systems which do not have time to be influenced by collision partners. A good criterion for the validity of the Born approximation is

$$\frac{|H'|}{E}(Rk) << 1 \tag{5.68}$$

where the ratio $|H'|/E$ sets the energy scale of the interaction with the overall system energy, and (Rk) is the product of the length scale range of the potential with the system momentum. For the Coulomb potential, R is usually large enough to make (Rk) also large. Hence, for the Born approximation to be valid, we need to have the interaction energy be only a small fraction of the total system energy. However, it is an anomaly that the Born approximation gives the exact answer for pure Coulomb, i.e. $H' \propto 1/r$, scattering.

Summary

This review of scattering is intended to bring out several points from the formal theory. The first is that there is essentially three points in time which are of interest. The present, i.e. t = 0, is needed because it is when the scattering occurs. The infinite past is important because that was when the noninteracting states were equivalent to the

interacting states. The infinite future is also important for the same reason. In practice, the infinite past corresponds to the point in time when the reactants are prepared and the prepared and the infinite future corresponds to the point in time when the products are detected.

The concept was presented in which two sets of states propagate simultaneously. One set is governed by the noninteracting Hamiltonian, while the other is governed by the interacting Hamiltonian. It is this duality which allows for the definition of the scattering matrix.

Finally, the Born approximation for the scattering matrix was presented. This will be of great importance in the application of the two-electron exchange to the Ar-N_2 system.

Chapter 6

The Ar-N_2 Energy Transfer Reaction

The fast energy transfer reaction (1.3) presents a unique opportunity to investigate a seemingly paradoxical physical system. Before proceeding, however, it is imperative that the current state of experimental knowledge be revisited. It is the intent of this chapter to present, 1) a brief discourse on the usefulness of (1.3), 2) some of the intricacies of the Ar atom and the N_2 molecule as they pertain to modeling (1.3), and 3) a summary of the literature.

Utility

In addition to being an interesting physical system, the energy transfer reaction between the Ar metastable and the N_2 ground state has a direct application for the ultraviolet nitrogen laser [13]. The Ar-N_2 system was originally thought to be useful for making a gas scintillation chamber to measure radioactive particle energy [54]. Shortly thereafter, though, the first report of a laser utilizing the upper excited electronic states of N_2 was delivered by Heard in 1964 [55]. A proposal to use excited Ar to pump the upper N_2 states was subsequently made the following year [56]. This practical application spurred intense experimental investigation and kinetic modeling of (1.3).

The stimulated emission occurring in the ultraviolet nitrogen laser is due to transitions from the N_2(C, v=0) level to several vibrational levels of the N_2(B) electronic state. This band system is known as the nitrogen second positive system. Reports of N_2 lasing from the upper N_2(C, v=0) to the lower N_2(B,v=0,1,2,3) at 337 nm, 358 nm, 380 nm, and 406 nm, respectively, have been published [57-62].

Atomic and Molecular Structure

This research seeks to model (1.3) by an electron exchange mechanism. However, before the discussion of the proposed mechanism may take place, it is essential that the electronic structure of both the Ar atom and the N_2 molecule be put forth. Indeed, in the analysis described in Chapter 7, only the electronic manifolds were modeled, and no attempt was made to describe vibrational or rotational excitation or quenching.

General Atomic Wavefunctions

Before going into detail about the specific structure of Ar and N_2, it is worthwhile to discuss the origins of atomic and molecular symmetries. For quantum systems, such as atoms and molecules, the complete set of commuting observables determines the set of relevant quantum numbers. The set of quantum numbers used to describe atomic states includes the principal radial quantum number, the angular momentum, and the spin angular momentum. Each electron is assigned a unique set of quantum numbers, which is called an atomic orbital. Different atomic orbitals possess different types of symmetries based upon their quantum numbers. Recall that the spatial solution to the Schrödinger equation for a central potential takes the form,

$$\Psi(r,\theta,\phi) = \frac{1}{r} R_{nl}(r) Y_{lm}(\theta,\phi) \tag{6.1}$$

where $l \le n-1$, $|m| \le l$, and $n = \{0,1,2,\ldots\}$. The spherical harmonics are functions of two variables,

$$Y_{lm}(\theta,\phi) = (-1)^m \sqrt{\frac{2l+1}{4\pi}\frac{(l+m)!}{(l-m)!}} P_l^m(\cos\theta) e^{im\phi} \tag{6.2}$$

where $P_l^m(\cos\theta)$ is the associated Legendre polynomial.

The parity operation determines the symmetry nature of the orbital under

inversion through the origin, i.e. $\underline{r} \rightarrow -\underline{r}$. In spherical coordinates, this invokes the replacements: $r \rightarrow r$, $\theta \rightarrow \pi - \theta$, and $\phi \rightarrow \pi + \phi$. Clearly, from (6.1), the radial solution is unchanged. From (6.2), the angular portion of the orbital wavefunction will be affected by such a transformation. From standard texts [63], it can be found that the parity of the spherical harmonics is independent of m and depends upon l in the following manner,

$$Y_{lm}(\pi - \theta, \pi + \phi) = (-1)^l Y_{lm}(\theta, \phi) \tag{6.3}$$

Hence, orbital wavefunctions for which l is even are said to be even parity, those for which l is odd are said to have odd parity.

The spin angular momentum is discussed in most texts, and it should suffice to note that each electron wavefunction is the product of (6.1) with a spinor. Since the electron has spin 1/2, the spinor may have only two elements, one corresponding to the -1/2 projection along a defined spatial axis, and one element corresponding to the +1/2 projection. Thus, two electrons may be represented by the same spatial function or orbital, i.e. (6.1). It should be emphasized that the spin is a true angular momentum and is capable of coupling with the orbital angular momentum, in vector fashion, to form a resultant angular momentum.

For this research, only an understanding of the wavefunctions for $l = 0$ and 1 need to be considered. Orbitals for which $l = 0$ are referred to as *s orbitals*. From the above, s orbitals are of even parity. If $l = 0$, then m must also equal 0, and the spherical harmonic function is $Y_{00}(\theta, \phi) = 1/\sqrt{4\pi}$, i.e. a constant. Thus, s orbitals possess no angular variations and therefore they are spherically symmetric.

If $l = 1$, the orbital is referred to as a *p orbital*. They have odd parity, meaning that the wavefunction changes sign if inverted through the origin. The spherical harmonics for $l = 1$ may take three forms, depending on whether $m = 1$, 0, or -1. Explicitly writing the solutions,

$$Y_{11}(\theta,\phi) = -\sqrt{\frac{3}{8\pi}}\sin\theta e^{i\phi}$$

(6.4) $$Y_{10}(\theta,\phi) = -\sqrt{\frac{3}{4\pi}}\cos\theta$$

$$Y_{1-1}(\theta,\phi) = \sqrt{\frac{3}{8\pi}}\sin\theta e^{-i\phi}$$

which uses the phase convention of Condon and Shortley [63]. From (6.4) it may be seen that $Y_{10}(\theta,\phi)$ is proportional to the spherical coordinate representation of the Cartesian coordinate z. Furthermore, by taking linear combinations of the $Y_{1\pm1}(\theta,\phi)$ spherical harmonics, it is possible to construct quantities which are proportional to the Cartesian x and y coordinates. The resulting orbital wavefunctions are called the px, py, and the pz orbitals. Pictorially, these orbitals appear as lobes along each of the corresponding Cartesian coordinate axes. Because of the odd parity, the functional value of the wavefunction in a given lobe is opposite in sign but equal in magnitude to its opposing lobe.

The nomenclature of atomic states attempts to describe the aggregate angular and spin angular momentum of all the orbitals. In the *L-S* coupling scheme, this requires three values since angular momentum is a vector quantity. Let $\underline{L}$ denote the vector sum of the orbital angular momenta, and its magnitude be L, where $L \equiv \left|\sum \underline{l}_i\right|$. If $L = 0$, the atomic state is called a S state, while if $L = 1$, the atomic state is referred to as a P state. In a similar fashion, the magnitude of the vector sum of the spin angular momenta is defined as the quantum number S. The value of $2S+1$ is written as a pre-superscript to the base orbital angular momentum. Since it is possible for the spin angular momenta to couple to the orbital angular momenta, a more appropriate quantum number in many cases is the vector sum of the total spin and the total orbital angular momenta. The

magnitude of this total vector sum is denoted by J, and its value is typically written as a subscript to the base orbital angular momentum.

Argon

Argon (Ar) is a noble gas with 18 bound electrons and is chemically inert. A term diagram of Ar is given in Figure 6.1, and a table of relevant Ar parameters is given in Table 6.1 [64]. The ground state electronic configuration is $1s^2 2s^2 2p^6 3s^2 3p^6$. The spectroscopic notation for the ground state in the L-S coupling scheme is $^1S_0$. This electronic configuration implies that the third major shell, the M shell, is not filled. Note that the M shell may accommodate 10 additional electrons in the 3d orbital. Indeed, the first excited state, the $^3P_2$ state, is not due to the promotion of a ground state electron into the 3d orbital, but rather into the next shell, which is the 4s orbital [65]. Hence, the ^3P state has an electron configuration of $1s^2 2s^2 2p^6 3s^2 3p^5 4s$. Because of the spin-orbit coupling, the ^3P state will have two values of J: 0, and 2. From Figure 6.1, it can be seen that the two levels of the ^3P state both lie near 11.5 eV above the ground state. For this research, the splitting of the ^3P state due to spin-orbit coupling is neglected.

The lifetimes of the singlet and triplet excited states are listed in Table 6.1. It is clear from these values why the ^3P states are termed metastable. Physically, it is the dipole selection rule, which forbids transitions between states of unequal spin, that prevents the ^3P state from decaying to the ground state. As will be discussed below, this phenomenon is at the root of the problem of this research.

The $^1P_1$ excited states have the same electronic configuration as the ^3P states, but with differing spin arrangements. They have a relatively short lifetime, indicative of an allowed electric dipole radiative transition, and are not of interest to this study.

Since this study deals with the spatial distribution of the wavefunctions, perhaps the most important concept to gain from the discussion of atomic structure is the shape

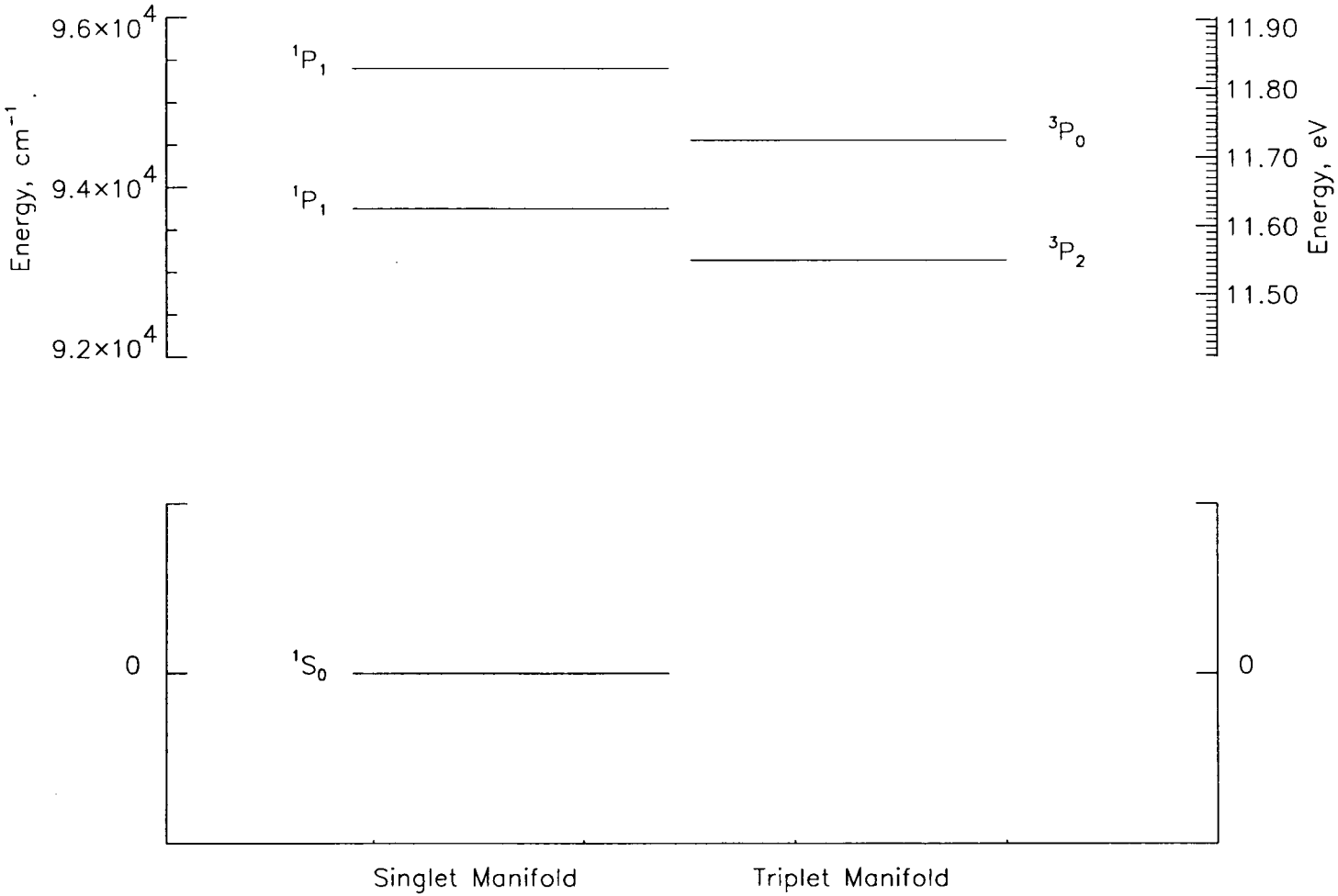

Figure 6.1 Argon Term Diagram

Table 6.1 Spectroscopic Parameters for Argon

Atomic State	Spectroscopic Term	Electronic Configuration[a]	Energy (cm^{-1})	Lifetime (sec)[b]
Ground	$^1S_0$	$3p^6$	0.0	---
First Rydberg	$^3P_2$	$3p^5 4s^1$	93143.8	Metastable
"	$^1P_1$	$3p^5 4s^1$	93750.6	8.40(-9)
"	$^3P_0$	$3p^5 4s^1$	94553.7	Metastable
"	$^1P_1$	$3p^5 4s^1$	95399.9	1.96(-9)
Second Rydberg	$^3S_1$	$3p^5 4p^1$	104102.1	
Third Rydberg	$^3P_2$	$3p^5 5p^1$	117183.7	6.90(-7)
"	$^3F_4$	$3p^5 5p^1$	122036.1	4.07(-7)

(a) A base configuration of $1s^2 2s^2 2p^6 3s^2$ is assumed.
(b) The appropriate power of 10 is given in the parentheses.
Source: Lentz, J. M., PhD dissertation, University of Tennessee (1970).

of the ground and metastable wavefunctions. Although the ground state is ^1S, the active electrons are located in the 3p orbital. Hence, the shape of the ground state for the purpose of this work is three orthogonal lobe pairs. Each lobe pair defines an axis in the Ar reference frame. From the above, a given lobe will be symmetric to its partner, with the exception of a sign change.

The excited metastable state has a term notation of ^3P. However, the electron of interest in this configuration is in the 4s orbital. Hence, the shape of the wavefunction for the ^3P excited state is a spherical ball.

General Diatomic Molecule Wavefunctions

Since molecules are comprised of atoms, much of the above discussion of atomic symmetries may be applied to diatomic molecules. However, there are a few slight modifications which need to be addressed. A comprehensive discourse on diatomic molecules is given by Herzberg [3], and should be considered as a first source for information. Only those topics pertinent to subsequent discussion in this work will be reviewed here.

The most obvious difference between atomic structure and diatomic structure is the presence of the internuclear axis. This seemingly mundane observation is actually a profound distinction. The internuclear axis breaks the spherical symmetric coordinate system of the atom by defining a preferred direction of the molecule.

It has been found that the total orbital angular momentum, $\underline{L}$, of the electrons does not necessarily lie along the internuclear axis, but will precess around it due to the electrostatic field of the nuclei. Only the component of $\underline{L}$ along the internuclear axis will be a constant of the motion. This vector component is defined as $\underline{\Lambda}$, with a magnitude given by Λ. The values of Λ are integer numbers 0, 1, 2, ..., and according to the value of Λ, the electronic state is denoted as Σ, Π, Δ, ..., respectively. Clearly, this is an

analog to the atomic term notations, but with a subtle difference. Since Λ denotes the magnitude of $\underline{\Lambda}$, the actual vector may lie either parallel or antiparallel to the internuclear axis. In the absence of coupling of orbital angular momenta, these two options are indistinguishable, and hence, degenerate.

The spin multiplicity of the diatomic wavefunction is directly analogous to an atomic spin multiplicity. The total spin vector of all the electrons is denoted by $\underline{S}$, which has a magnitude given as S. The orbital motion of the electrons creates a magnetic field which in turn causes $\underline{S}$ to precess about the internuclear axis, similar to $\underline{L}$. Hence, the stationary component of $\underline{S}$ along the internuclear axis gives rise to a conserved vector, $\underline{\Sigma}$. In contrast to $\underline{\Lambda}$, the quantum number Σ is defined as the magnitude and direction of $\underline{\Sigma}$. This is in analogy to the m_S quantum number of the individual electron spin. It is possible for Σ to assume $2S+1$ values, from $-S$ to S, which is called the multiplicity of the diatomic wavefunction.

With these definitions, the symmetries of a diatomic molecule may be considered. First, note that any plane containing the internuclear defines a plane of symmetry. When the wavefunction is not degenerate, as for Σ states, then it is required that the wavefunction be either symmetric or antisymmetric upon reflection across this plane. Thus, Σ states are classified as either Σ^+ or Σ^-, based upon their symmetric or antisymmetric reflection property across any plane containing the internuclear axis. For the case of the degenerate states, i.e. Π, Δ, etc., this symmetry is not required. The diatomic wavefunctions need only transform into any combination of the set of degenerate wavefunctions.

Another molecular symmetry of interest occurs for homonuclear diatomics, such as N_2. Because the electrostatic field due to the nuclei is now symmetric with respect to inversion at the origin, the diatomic wavefunction must exhibit the same behavior. Obviously, the origin is located at the center of the internuclear axis. If the wavefunction

is symmetric with respect to inversion through the origin, i.e. $\underline{r} \rightarrow -\underline{r}$, then the wavefunction is denoted as "gerade," which is the German word for even. Otherwise, the wavefunction must be antisymmetric with respect to inversion at the origin, and it is denoted as "ungerade." Note that this symmetry property holds for homonuclear diatomics, regardless of the Λ or Σ quantum numbers, since no amount of angular momenta coupling will change the fact that the nuclei are identical.

In addition to the symmetries for the molecular wavefunctions, it will be important to visualize the structure of the molecular orbitals composing the total wavefunction. This is analogous to examining the spatial dependence of the various atomic orbitals. However, in the case of atomic orbitals, their properties were determined by solutions to a central potential, yielding the spherical harmonics. In general, every molecular orbital belongs to the irreducible representation of the symmetry point group determined by the nuclear framework [42,66,67]. Although this can become rather complex for intricate molecules, the diatomic molecules belong to the $C_{\infty v}$ point group. This means that every diatomic molecule has an infinite number of symmetry planes which contain the internuclear axis. The molecular orbitals must also mirror this fact.

The standard nomenclature for identifying the orbitals is to label them by their irreducible representation, with a numeric integer prefix to denote the energy ordering of like orbitals. Two of the irreducible representations for the $C_{\infty v}$ point group are denoted as σ and π. A sketch of the nature of these orbitals is given in Figure 6.2. Molecular orbitals having cylindrical symmetry about the internuclear axis are termed σ orbitals. Those orbitals which have a nodal line along the internuclear axis are referred to as π orbitals [68]. Often, if the orbital is an antibonding orbital, then it is denoted with a superscript *. When the diatomic is homonuclear, the orbitals must possess the additional inversion symmetry of the nuclei. This additional symmetry property is

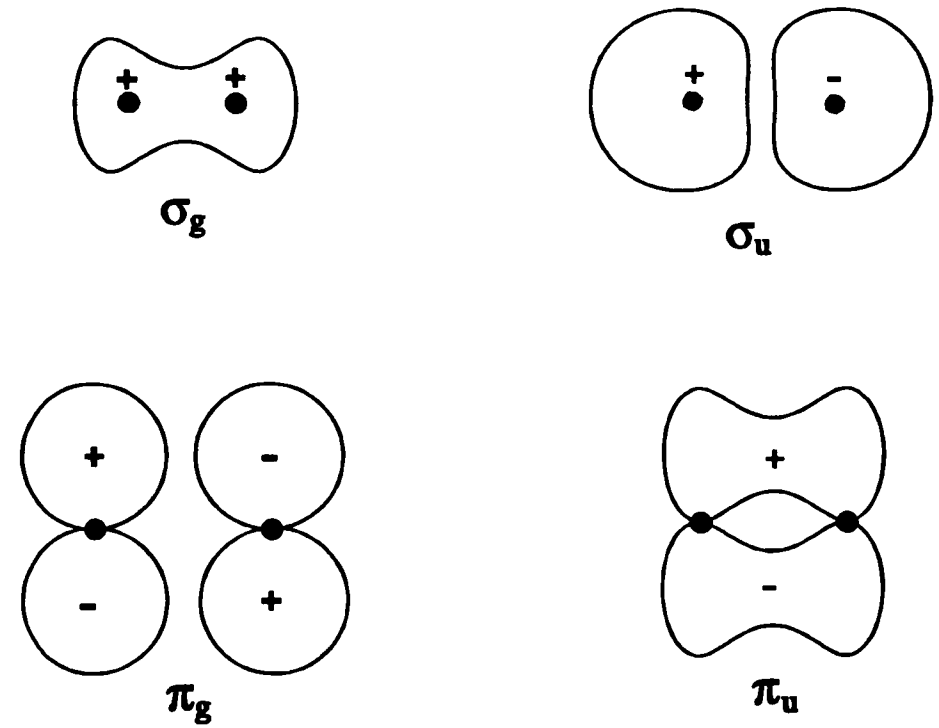

Figure 6.2 Spatial Character of Several N_2 Molecular Orbitals

denoted by a subscripted "g" when the wavefunction is symmetric under inversion, and subscripted "u" when the wavefunction is antisymmetric under inversion.

Molecular Nitrogen

The structure of N_2 is somewhat more complex than that of Ar due to the nature of molecular orbitals in general. To begin, a term diagram for N_2 is given in Figure 6.3. The upper electronic state of interest to this research is the $N_2(C^3\Pi_u)$ state. This state is excited by a transition from the ground state, denoted as $X^1\Sigma_g^+$. The $N_2(C^3\Pi_u)$ state can be seen from Figure 6.3 to lie at 11.05 eV above the $X^1\Sigma_g^+$ state. Thus there is an energy resonance of the vibration-rotation manifold of $N_2(C^3\Pi_u)$ with the $Ar(^3P_{0,2})$ state.

Table 6.2 presents some spectroscopic parameters for various states of N_2. According to Lofthus and Krupenie [69], the ground state electronic configuration consists of $1\sigma_g^2 1\sigma_u^2 2\sigma_g^2 2\sigma_u^2 1\pi_u^4 3\sigma_g^2$, while the $C^3\Pi_u$ state has a configuration of $1\sigma_g^2 1\sigma_u^2 2\sigma_g^2 2\sigma_u 1\pi_u^4 3\sigma_g^2 1\pi_g$. Hence, the excitation of N_2 is not a simple Rydberg excitation of the outer electron. This can be seen by looking at the ground state configuration. Since the last electron is in a gerade sigma orbital, promotion to the $1\pi_g$ orbital would make the overall wavefunction gerade, even though the angular momentum would change to Π. Indeed, this is exactly the configuration of the $B^3\Pi_g$ state. Further promotion of this electron leads to the very high energy $E^3\Sigma_g^+$ state [69]. Hence, it is energetically cheaper to promote from a core shell orbital. The next orbital below the $3\sigma_g$ orbital is the $1\pi_u$ orbital. Promotion of an electron from that orbital into another π orbital, while conserving momentum, would lead to an overall Σ wavefunction with ungerade symmetry, i.e. the $a'^1\Sigma^-_u$ state. The next inner shell orbital, from which to promote, is the $2\sigma_u$ orbital, which leads to the $C^3\Pi_u$ state.

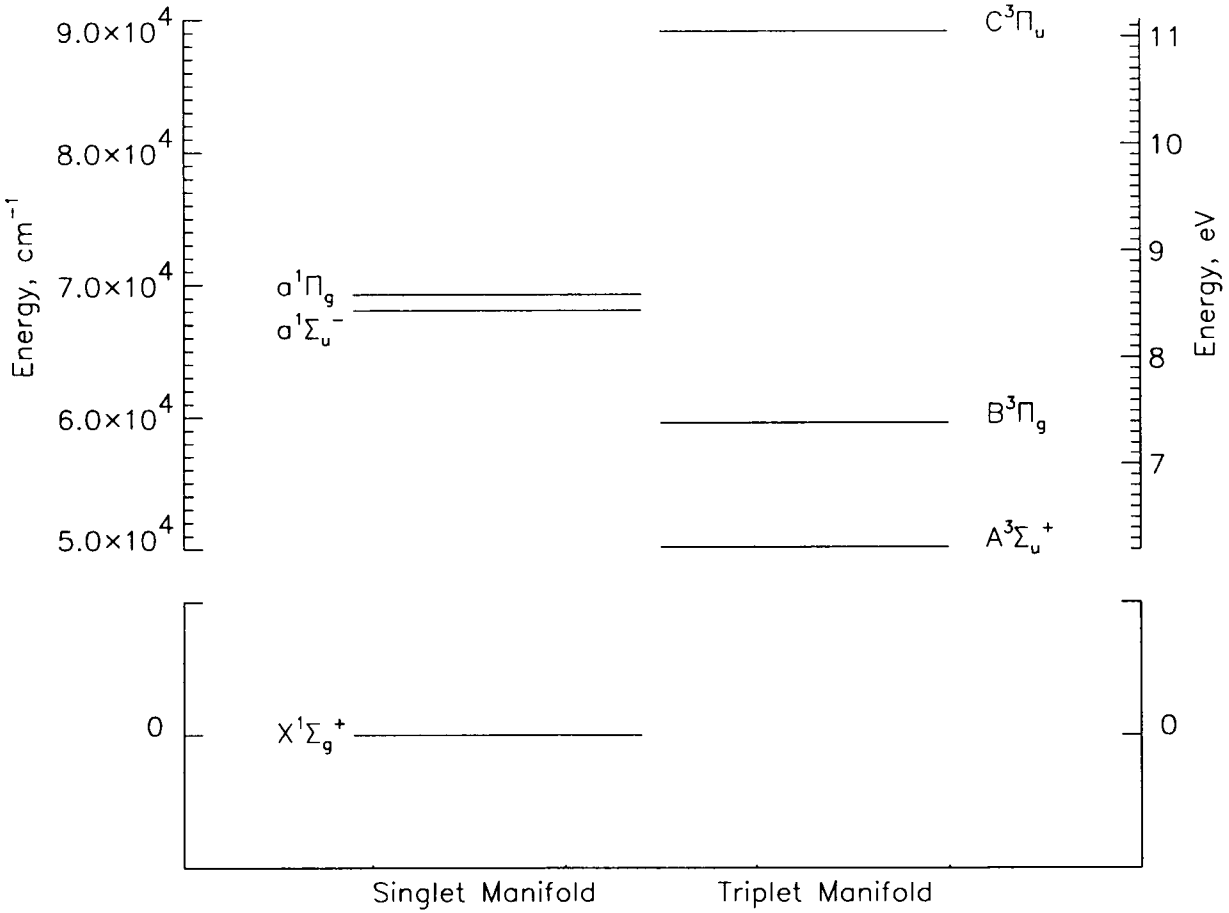

Figure 6.3 N_2 Term Diagram

Table 6.2 Spectroscopic Parameters for N_2

Molecular State	Electronic Configuration[a]	Energy (eV)[b]	Lifetime (sec)[c]	Remarks
$X^1\Sigma_g^+$	$2\sigma_u^2 1\pi_u^4 3\sigma_g^2$	0.0	---	
$A^3\Sigma_u^+$	$2\sigma_u^2 1\pi_u^3 3\sigma_g^2 1\pi_g$	6.22	1.3 to 2.5 (0)	Metastable
$B^3\Pi_g$	$2\sigma_u^2 1\pi_u^4 3\sigma_g 1\pi_g$	7.39	5 (-6)	Decays to $A^3\Sigma^+_u$ (First Positive Sys.)
$a'^1\Sigma_u^-$	$2\sigma_u^2 1\pi_u^3 3\sigma_g^2 1\pi_g$	8.44	1.3 (-2)	Decays to $X^1\Sigma^+_g$ (Ogawa-Tanaka-Wilkinson-Mulliken Sys.)
$a^1\Pi_g$	$2\sigma_u^2 1\pi_u^4 3\sigma_g 1\pi_g$	8.59	100 (-6)	Decays to $a'^1\Sigma^-_u$ (McFarlane Infrared Sys.)
$C^3\Pi_u$	$2\sigma_u 1\pi_u^4 3\sigma_g^2 1\pi_g$	11.05	35 to 41 (-9)	Decays to $A^3\Sigma^+_u$ (Second Positive Sys.)

(a) A base configuration of $1\sigma_g^2 1\sigma_u^2 2\sigma_g^2$ is assumed. Ref [A&K]
(b) This refers only to the electronic energy. In the notation of Hertzberg, this quantity is T_e.
(c) The appropriate power of 10 is given in the parantheses. All lifetimes quoted from [Hz].
Source: Huber, K.P., and Hertzberg, G., *Molecular Structure and Molecular Structure. IV. Constants of Diatomic Molecules*, Van Nostrand Reinhold (1979).

The spatial distributions of the orbitals of interest to this study are given by the forms of the $2\sigma_u$ and the $1\pi_g$ orbitals, which are occupied in the ground, $X^1\Sigma_g^+$, and excited, $C^3\Pi_u$, states respectively. It is relevant to note that the $2\sigma_u$ orbital possesses cylindrical symmetry about the internuclear axis, even though the sign of the wavefunction changes by inverting through the midpoint of the internuclear axis, as shown in Figure 6.2. The change in wavefunction sign prompts the identification of the $2\sigma_u$ as an antibonding orbital. Likewise, the $1\pi_g$ orbital is also an antibonding orbital because it has a nodal plane orthogonal to the internuclear axis. It also has two nodal planes which contain the internuclear axis, giving it the spatial form of eight lobes. Letting the origin correspond to the midpoint of the internuclear axis, it is clear that every octant would contain one of the lobes.

Cross Section Data

There have been many measurements of the energy transfer cross section for reaction (1.3). The literature reports five different techniques: discharge flow reactor, arc-jet, pulsed electron impact, crossed molecular beams, and single metastable beam experiments. A summary of the following experimental results is given in Table 6.3.

One of the earliest reports of the cross section was that of Schultz [70] in 1966, using an α-bombardment experiment. His reported value was 5 ± 1 A^2, although the technique used was not selective in determining the excitation. Three years later, McGregor [71] inferred the cross section as 2.7 ± 1.4 A^2 from an arc-jet experiment. McGregor's experiment passed flowing Ar through an arc-jet into a low density cell. A mixture of Ar and N_2 was bled in around the expanding plume of the jet. The interaction region was monitored spectroscopically for the N_2 second positive bands.

Table 6.3 Summary of Published Cross Section Data for Reaction (1.3)

Year	Experimenter(s)	Technique	Cross Section, (A^2)	Remarks[a]
1966	Schultz	α bombardment	5 ± 1	[70]
1969	McGregor	Arc-jet	2.7 ± 1.4	[71]
1977	Kolts, et al.	Discharge Flow Tube	a) NA b) 3.2 c) 5.8	a) Measured quenching rate.[9] b) Inferred by Parr and Martin [72]. c) Parr and Martin's value corrected by Tyndall, et al.[74].
1978	Bennett and Flint	Electron Impact Excitation	9.4 ± 1.0	[75]
1973	Winicur and Fraites	Crossed Beams	11.8 ± 3.5	Measured at 0.051 eV [79].
1975	Lee and Martin	Crossed Beams	6	[80]
1978	Parr and Martin	Crossed Beams	14	Peak value at 0.25 eV [72]. (including correction)
1986	Tabayashi and Shobatake	Crossed Beams	11	Peak value at 0.7 eV, sharply decreasing for higher energies [82].(including correction)
1990	Vredenbregt, et al.	Crossed Beams	18	Peak value at 0.2 eV [83].

(a) When energies are quoted, they refer to the center-of mass energy of the Ar-N_2 system. Numbers in brackets refer to similarly numbered references in the bibliography.

Discharge flow reactor experiments were performed over a time span of eight years by a group at the University of Kansas headed by Setser. This set of experiments actually determined the rate of the reaction (1.3), and not the reaction cross section. Experimentally, Ar was excited by a low pressure discharge and allowed to pass through a low density, flowing N_2 environment. The reaction was monitored spectroscopically for emission from the $N_2(C)$ and $N_2(B)$ states. The rate of photon detection was related to the quenching rate of Ar*. In these measurements, no separation of the $Ar(^3P_0)$ and $Ar(^3P_2)$ components was possible. The results were corrected accordingly by using a measured ratio of the two components as 1:7. The agreement of the reaction rates published in their last report with those of other researchers is rather good. Kolts, Brashears, and Setser reported, in 1977, a quenching rate for $Ar(^3P_2)$ of $3.3 \pm 0.5 \times 10^{-11}$ cm^3-$molecule^{-1}$-sec^{-1} [9]. In Table I of that work, they quoted two other measurements of the quenching rate and both were well within the experimental uncertainty of their measurement. For reference, the gas kinetic rate at STP is usually on the order of 10^{-10} cm^3-$molecule^{-1}$-sec^{-1}[8]. No attempt was made by the authors to convert the reaction rate measurement into cross section. However, subsequent analysis of their data by Parr and Martin [72] inferred a value of 3.2 A^2 for the cross section by assuming that the reaction occurred at room temperature. Furthermore, Sadegi and Setser [73] recently reported a new measurement of the quenching rate which is 1.8 times that measured by Kolts, et al. A recent literature review by Tyndall, et al., [74] proposed that the cross section inferred by Parr and Martin needed to be scaled upwards by a factor of 1.8. This yielded a value of 5.8 A^2 for the cross section.

A study done by Bennet and Flint [75] in 1978 determined the reaction cross section for $Ar(^3P_2)$ quenching as 9.4 ± 1.0 A^2. They used pulsed electron bombardment to excite the Ar in an Ar/N_2 mixture. The N_2 second positive emission bands were then monitored spectroscopically. The experiment took place at a temperature of 663 K. In

actuality, the second positive decay rate related the $Ar(^3P_2)$ quenching rate to $N_2(C)$. The cross section was then inferred from the expression $k = \sigma\sqrt{8k_BT/\pi\mu}$, where k is the measured rate constant, and μ is the reduced mass.

Parr and Martin [72] conducted a pulsed beam experiment in which three different methods of producing Ar* and selecting its velocity are reported. Their cross sections for (1.3) are thus a function of the center-of-mass kinetic energy, which can be quite high. Their results show a factor of 2 difference in the cross section, depending upon the excitation and selection technique. Based upon the measured cross section curves for each technique, their best estimate of the reaction cross section is 6.4 A^2. Note that this experiment is incapable of distinguishing between the $^3P_2$ and the $^3P_0$ components of the excited Ar beam.

By far, the most popular experimental technique is the method of crossed beams in which a beam of $Ar(^3P_{0,2})$ intersects a beam of $N_2(X^1\Sigma_g^+)$ at a 90 degree angle. This arrangement has the advantage of a well defined collision energy, but with the drawback that the collision energies are often much higher than that which corresponds to 300K. Several experiments were done solely to determine the relative cross section as a function of collision energy [76-78]. Absolute values of the cross sections could be determined by normalizing the cross section to a previously measured absolute cross section at a particular energy.

Perhaps the seminal crossed beam measurement was that due to Winicur and Fraites [79]. Their technique typifies the method of crossed beams. A beam of argon was excited by a discharge and then passed through an expanding supersonic nozzle, to achieve speeds of Mach 20. The expansion was sampled by a collimator to produce a beam of fast Ar*. This beam then intersected a slow beam of ground state N_2 at right angles. The N_2 second positive bands were used to monitor the energy transfer reaction. From this measurement, they obtained a probability for energy transfer as a function of

the scattering angle. A five parameter double Lennard-Jones intermolecular potential was then fitted to the data to determine a radius at which the potential is a minimum. The energy transfer cross section was then obtained from a direct numerical integration of the energy transfer probability written as a function of the reduced impact parameter, i.e. b/r_{minima}. Winicur and Fraites achieved a probability data fit by a second order polynomial, which was used for the numerical integration. Their result for the cross section was 11.8 ± 3.5 A^2.

A second absolute cross section measurement using crossed beams was performed by Lee and Martin [80]. Again, the experiment actually measured the probability of quenching as a function of collision energy. A scaling of the measured data by a comparison of the inferred quenching rate constant with that determined by Piper, et al, [81] was performed, in a manner similar to that done by Winicur and Fraites. The final result was a calculated cross section of 6 A^2 at 0.051 eV. Note that this value is roughly half of the value given by Winicur and Fraites.

More recent crossed beam experiments include that of Tabayashi and Shobatake [82] and Vredenbregt, et al., [83]. The work by Tabayashi and Shobatake was restricted to relatively high collision energies, above roughly 0.7 eV. They found that the relative cross section was a monotonically decreasing function. The maximum measured value of the relative cross section occurred for the lowest available energy. To obtain an absolute cross section, Tabayashi and Shobatake scaled their results with the value inferred by Parr and Martin since the shapes of the relative cross section agree favorably for overlapping collision energies. As pointed out in Tyndall, et al., the Parr and Martin value is incorrect by a factor of 1.8. If the data of Tabayashi and Shobatake are scaled by an additional factor of 1.8, the maximum cross section approaches 11 A^2.

The relative cross section data of Parr and Martin covers a lower energy range than that of Tabayashi and Shobatake, ranging from near zero to over 0.08 eV. There is

a distinct maximum in the curve at a collision energy of roughly 0.025 eV. The value of the cross section at this energy is roughly 14 A^2, after accounting for the factor of 1.8.

The most recent measurement was that of Vredenbregt, et al., [83]. Experimentally, this effort was similar to the others, but with expanded coverage of the absolute, vibrationally resolved reaction cross section. Their data agree very favorably with that of Tabayashi and Shobatake for energies greater than 0.07 eV. The Vredenbregt data also agree fairly well with that of upper energy range of the Parr and Martin data. A discrepancy occurs as the energy is lowered below 0.03 eV. As noted above, the Parr and Martin data peak at 0.25 eV with a value of 14 A^2. In contrast, the Vredenbregt data continue to climb until 0.009 eV, where it has a peak value of 18 A^2. Below this maximum the cross section falls very quickly.

Perhaps one of the most interesting reports did not attempt to measure the reaction cross section at all. A recent paper by Tyndall et al, in 1987, describes a single beam experiment designed to measure the rotational alignment of the product $N_2(C)$ with the initial velocity vector of the Ar [84]. They passed Ar through a discharge and used a time-of-flight method to select the desired Ar kinetic energy. The beam then entered a chamber of N_2, and the subsequent $N_2(C)$ emission was monitored. The collisional energy spanned by this experiment ranged from 42 to 460 meV. Recall that room temperature corresponds to roughly 25 meV. Although the intent of this paper was to document an experiment to measure the product rotational alignment, a review of the cross section literature was included. The interesting item of this paper was the proposal that the excitation transfer occurs by an exchange of electrons from the Ar 4s orbital to the N_2 $1\pi_g$ orbital, and from the N_2 $2\sigma_u$ orbital to the Ar 3p orbital. This mechanism was proposed to explain the observed rotational alignment of the product $N_2(C)$ with the initial Ar wavevector. Note though, that it was not evident from the data

as to whether this electron exchange was coincident, or whether it occurred sequentially via an intermediate reaction complex.

Summary

The intent of this chapter was to provide background information on three topics: the atomic structure of Ar, the molecular structure of N_2, and experimental measurements of the energy transfer cross section. From the standpoint of modeling (1.3) as an electron transfer event, it was seen that the orbitals of interest are the 3p and 4s orbitals of Ar, and the $2\sigma_u$ and $1\pi_u$ of N_2. The symmetry of the orbitals was discussed as a prelude to calculating the interaction Hamiltonian.

The experimental work showed that the energy transfer cross section is large, varying between 2.7 and 18 A^2, depending upon the measurement technique. To date, proposals to explain these experiments have included two-electron exchange, but the exact nature of the energy transfer has been debated without resolution.

Chapter 7

Application of Quantum Field Theory to Ar-N_2 Scattering

The following text documents the methods used to apply the theoretical results of Chapter 3 to the fast spin-forbidden energy transfer reaction of (1.3). In particular, the approach taken to solve the problem is presented, followed by the direct application of (3.29). The remainder of the chapter details the various computational techniques utilized to obtain the interaction Hamiltonian and the scattering cross section.

Overview

Objective

The clear goal of this calculation was to apply the formalism of the previous chapters to a real, physical system and determine whether the two-electron exchange process is plausible. The most significant physical observable in a bimolecular collision is the scattering cross section. Thus, the objective of this calculation was to determine the scattering cross section for energy transfer via the two-electron exchange mechanism.

As with any endeavor, there are a myriad of possible paths which arrive at the same destination. In this research, the point of origin for all paths was the two-electron exchange hypothesis developed in Chapter 3. From there, however, several alternative routes were possible. The path taken is described schematically in Figure 7.1. The first step was to apply the interaction Hamiltonian of (3.29) to the Ar-N_2 system. The choice was made to postulate that the inner shell electrons need not be considered for the

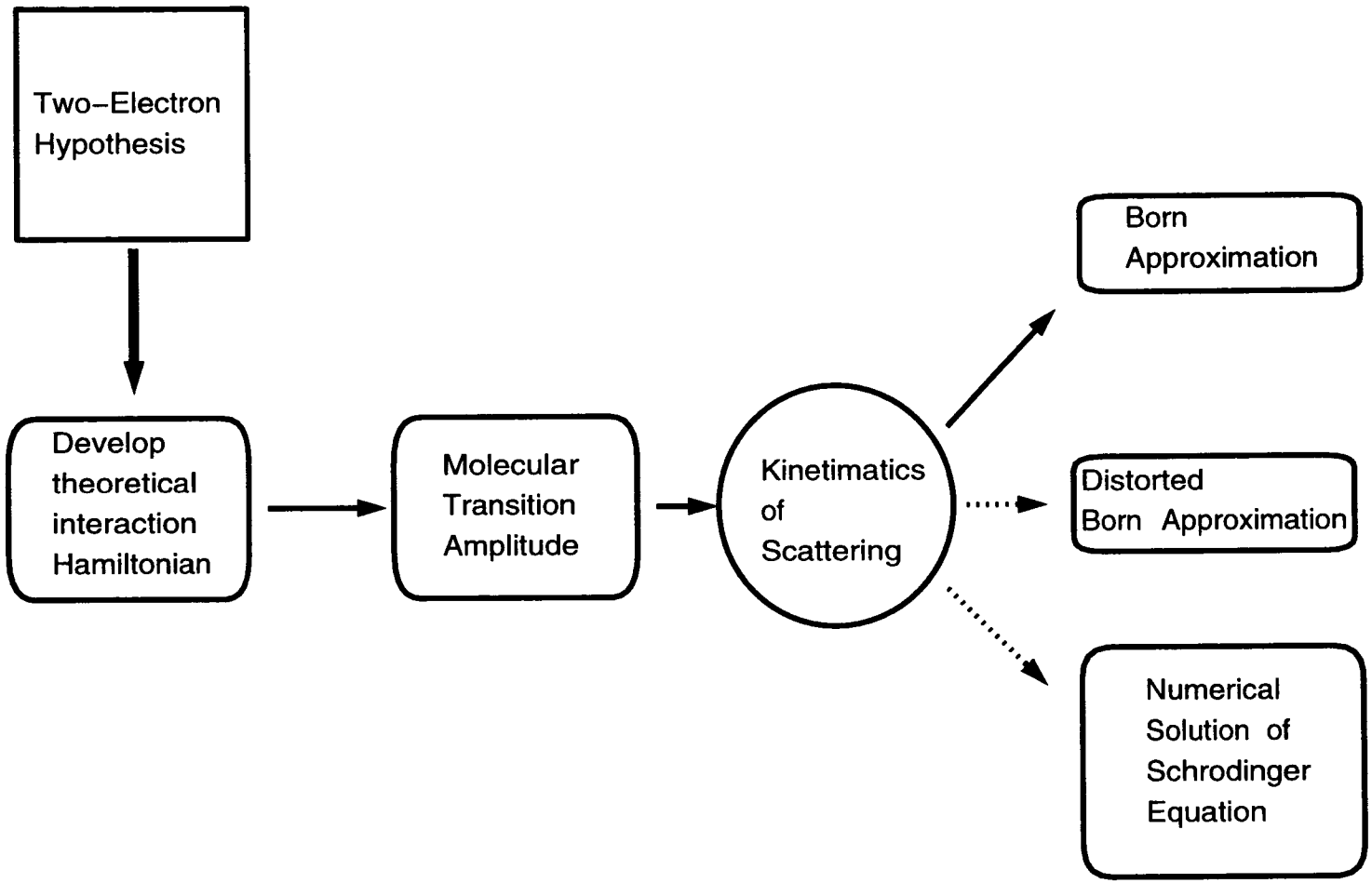

Figure 7.1 Flow Chart for the Calculation

interaction. Furthermore, it was decided to use *ab initio* electronic wavefunctions to describe both Ar and N_2.

The next step was to calculate the molecular transition amplitude for the interaction. It was decided to neglect any coupling of the vibrational and rotational modes to the electronic wavefunctions. Note that the vibrational state resolved measurements of Vredenbregt, et al., [83] indicated no anomalous dependencies of the cross section upon vibrational modes. Furthermore, any perturbations of the $N_2(C^3\Pi_u)$ state by other electronic states were neglected.

Since the electronic and kinetic eigenstates were assumed independent, the next crossroad was to choose a representation of the system kinematics. In contrast to the above modeling decisions, the description of the kinematics had no obvious choice. For that reason, the options are exhibited explicitly on Figure 7.1. The Born approximation is by far the easiest to implement numerically, although the distorted Born approximation has a reputation for greater accuracy than the first Born approximation. The final option, direct numerical solution of the kinematic Schrödinger equation should yield near-exact results, with a very high computational price tag.

The first Born approximation was chosen for a variety of reasons. Since the objective of this numerical exercise was to exhibit the plausibility of the two-electron mechanism, it was deemed inappropriate to choose a kinematic technique which would serve to complicate the anticipated results. The first Born approximation can make use of the Fast Fourier Transform (FFT) which is a simple, reliable numerical algorithm. Thus, more effort could be expended upon understanding the physics of the interaction. Also, from Chapter 5, it was possible that the scattering conditions might be quite appropriate for the first Born approximation. In the final analysis, because the exact nature of the interaction was unknown, it was important to not complicate the calculation unnecessarily.

Geometry

A well defined orientation is essential for solving the scattering equations. The interaction Hamiltonian was computed using the geometrical arrangement shown in Figure 7.2. It is important to have this orientation in mind while trying to interpret the result of computing the interaction Hamiltonian. Since the individual molecular wavefunctions of N_2 and Ar were defined with respect to their geometric centers, the problem consisted of two reference frames: the N_2 coordinate system, and the Ar coordinate system. These two reference frames are unconstrained to translate and rotate with respect to each other. The interaction Hamiltonian is thus a function of six independent coordinates. To simplify the calculation of the interaction Hamiltonian, the N_2 molecule was fixed in space with the internuclear axis coincident with the z axis. The midpoint of the internuclear axis was placed at the origin, such that the N atoms are located at the points (0, 0, ±0.55 Angstroms), or equivalently, (0, 0, ±1.04 au). The position of the Ar atom was varied with respect to the N_2 molecule to determine the entire three-dimensional potential map. The relative orientation of the Ar reference frame with respect to the N_2 reference frame was taken into account in the manner described below.

The Interaction Hamiltonian for Ar-N_2

Theoretical Development

The second quantized form of the Hamiltonian was given in (3.22) where it was noted that applying (3.23) to systems which remained charge neutral throughout the

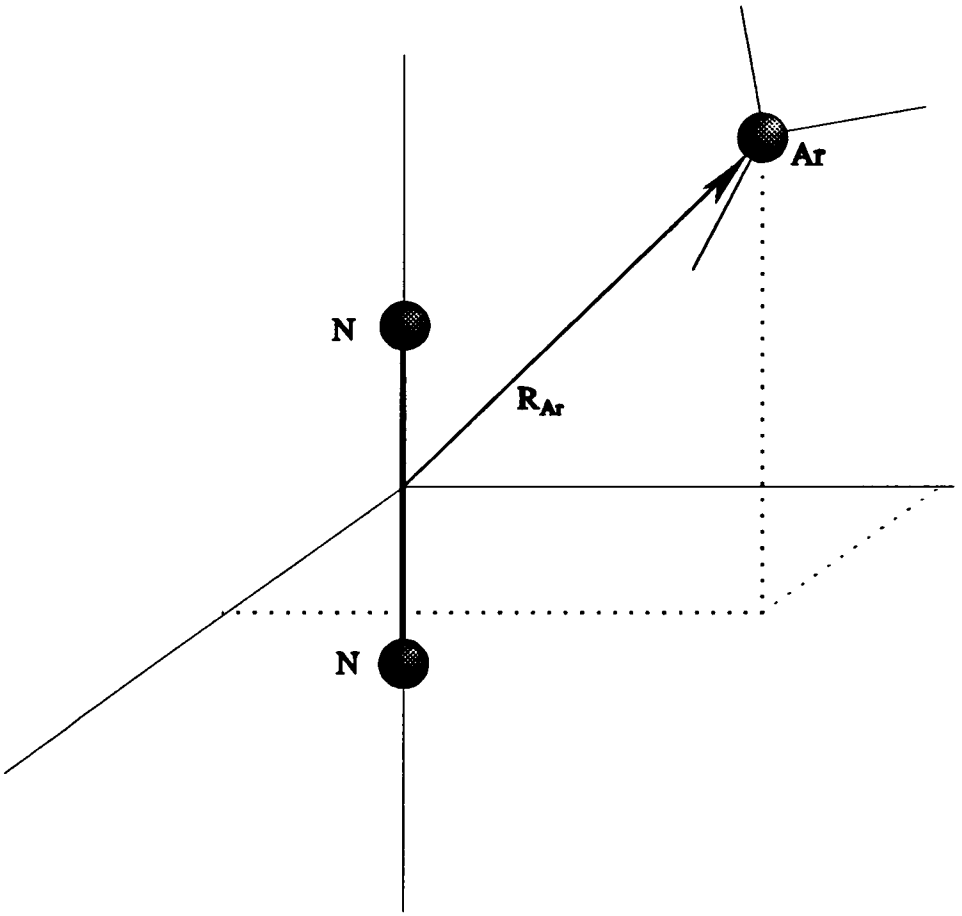

Figure 7.2 Geometrical Arrangement of Ar - N_2 Interaction

interaction would simplify things greatly. The Ar-N_2 collision system fell into this category because neither the Ar nor the N_2 is ionized before or after the collision. Thus, the Hamiltonian may be written as

$$H = H_{rad} + H_{mol} + H_{int}^{(1)} + 2\sum_{\substack{\alpha,k,\\ l,\beta}} (V_{\alpha k l \delta} - V_{\alpha k \delta l}) b_\alpha^+ b_k^+ b_l b_\delta \tag{7.1}$$

As discussed in Chapter 3, $H_{int}^{(1)}$ was due to the interaction of the radiation field with the electron field. Because the Ar ^3P state is metastable, it follows that Ar does not couple to the radiation field and that $H_{int}^{(1)}$ may be neglected.

Since a collision involves bodies in motion, it was important to include the kinetic energy of the molecules in the expression for the Hamiltonian. It can be shown that the center-of-mass momentum and kinetic energy may be separated from the absolute quantities [51,84]. As usual, the kinetic energy of the absolute reference frame was of no interest and was neglected in subsequent analysis. The resulting Hamiltonian governing the energy transfer reaction between Ar ^3P and N_2 is

$$H = H_o + H' \tag{7.2}$$

where

$$H_o = H_{CM} + H_{mol} + H_{rad} \tag{7.3}$$

and

$$H' = 2\sum_{\substack{\alpha,k,\\ l,\beta}} (V_{\alpha k l \delta} - V_{\alpha k \delta l}) b_\alpha^+ b_k^+ b_l b_\delta \tag{7.4}$$

where the mode indices specify a basis function and spinor.

Noting that the noninteracting Hamiltonian is a sum of three terms, the noninteracting wavefunctions must correspond to a tensor product of eigenstates in the three respective eigenspaces. Furthermore, since the radiation interactions have been

neglected, the radiative eigenstates may be suppressed for clarity. Based upon H_o, the eigenstates may be written as

(7.5) $$|m\rangle = \left|\underline{k_m}\right\rangle \otimes \left|\{\ldots n_{Ar}\ldots\}_m\right\rangle \otimes \left|\{\ldots n_{N_2}\ldots\}_m\right\rangle$$

where $\left|\underline{k_m}\right\rangle$ are eigenstates of the center-of-mass Hamiltonian and $\left|\{\ldots n_{Ar}\ldots\}_m\right\rangle$ and $\left|\{\ldots n_{N_2}\ldots\}_m\right\rangle$ are the second quantized form of the molecular eigenstates as discussed in Chapter 3. Thus, the initial eigenstate of the noninteracting system is

(7.6) $$|i\rangle = \left|\underline{k_i}\right\rangle \otimes |i\rangle_{Ar} \otimes |i\rangle_{N_2}$$

and the final eigenstate is

(7.7) $$|f\rangle = \left|\underline{k_f}\right\rangle \otimes |f\rangle_{Ar} \otimes |f\rangle_{N_2}$$

As given in (3.24) and (3.25), the initial and final molecular states can be expressed in terms of the creation and annihilation operators. For this study, a mechanistic bias was imposed upon the physical nature of the scattering process. It was deemed necessary to only include those orbitals in the description of the molecular states which take an active part in the energy transfer. The remaining electrons were essentially "frozen" out of the interaction. This model was proposed on the basis of the fast energy transfer rate. For the purpose of this research, the initial states may be written as

(7.8) $$|i\rangle_{Ar} = b^{+}_{Ar(i)}|0\rangle$$

(7.9) $$|i\rangle_{N_2} = b^{+}_{N2(i)}|0\rangle$$

with analogous expressions for the final molecular states. Thus the entire initial Ar state is described by creating an electron in the *Ar(i)* orbital, which in this case is the 4s orbital. Likewise, the entire initial N_2 state is described by creating only one electron in the pertinent orbital, i.e. the $2\sigma_u$ orbital.

In general, the matrix elements of interaction Hamiltonian can be determined by combining (7.6), (7.7), (7.8), and (7.9) to yield

(7.10) $$\langle f|H'|i\rangle = \left\langle \underline{k}_f \middle| H'(\underline{R}) \middle| \underline{k}_i \right\rangle$$

where the molecular portion is defined as

(7.11) $$\begin{aligned} H'(\underline{R}) &= {}_{N2}\langle f|\otimes_{Ar}\langle f|H'|i\rangle_{Ar}\otimes|i\rangle_{N2} \\ &= \langle 0|b_{N2(f)}b_{Ar(f)}\, H'\, b^{+}_{Ar(i)}b^{+}_{N2(i)}|0\rangle \end{aligned}$$

and where the implicit dependence upon the molecular geometry is denoted by $\underline{R}$. Substitution of the interaction specified by (7.4) into (7.11) then gives the general expression for the molecular interaction Hamiltonian as

(7.12) $$H'(\underline{R}) = 2\sum_{\substack{\alpha,k,\\ l,\beta}} \left(V_{\alpha k\beta} - V_{\alpha k\delta l}\right)\langle 0|b_{N2(f)}b_{Ar(f)}b^{+}_{\alpha}b^{+}_{k}b_{l}b_{\delta}b^{+}_{Ar(i)}b^{+}_{N2(i)}|0\rangle$$

The modal summation of (7.12) may be reduced by using the anticommutation relation for the creation and annihilation operators. The first step is to switch adjacent operators in an effort to move the creation operators to the left and the annihilation operators to the right. This gives an intermediate result which serves to illustrate the strategy,

(7.13)

$$\begin{aligned} H'(\underline{R}) &= 2\sum_{\substack{\alpha,k,\\ l,\beta}} \left(V_{\alpha k\beta} - V_{\alpha k\delta l}\right) \\ &\quad \langle 0|b_{N2(f)}(\delta_{\alpha;Ar(f)} - b^{+}_{\alpha}b_{Ar(f)})b^{+}_{k}b_{l}(\delta_{\delta;Ar(i)} - b^{+}_{Ar(i)}b_{\delta})b^{+}_{N2(i)}|0\rangle \\ &= 2\sum_{\substack{\alpha,k,\\ l,\beta}} \left(V_{\alpha k\beta} - V_{\alpha k\delta l}\right) \\ &\quad \langle 0|b_{N2(f)}\{\delta_{\alpha;Ar(f)}\delta_{\delta;Ar(i)}b^{+}_{k}b_{l} - \delta_{\alpha;Ar(f)}b^{+}_{k}b_{l}b^{+}_{Ar(i)}b_{\delta} \\ &\qquad -\delta_{\delta;Ar(i)}b^{+}_{\alpha}b_{Ar(f)}b^{+}_{k}b_{l} + b^{+}_{\alpha}b_{Ar(f)}b^{+}_{k}b_{l}b^{+}_{Ar(i)}b_{\delta}\}b^{+}_{N2(i)}|0\rangle \end{aligned}$$

Continued application of the anticommutation relations and use of the action of the annihilation and creation on the vacuum state gives the result, after considerable algebra,

$$
\begin{aligned}
H'(\underline{R}) = 2\sum_{\substack{\alpha,k,\\ l,\beta}} \left(V_{\alpha k l \delta} - V_{\alpha k \delta l}\right) \Big\{ & \delta_{\alpha;Ar(f)}\delta_{k;N2(f)}\delta_{l;N2(i)}\delta_{\delta;Ar(i)} \\
& -\delta_{\alpha;Ar(f)}\delta_{k;N2(f)}\delta_{l;Ar(i)}\delta_{\delta;N2(i)} \\
& -\delta_{\alpha;N2(f)}\delta_{k;Ar(f)}\delta_{l;N2(i)}\delta_{\delta;Ar(i)} \\
& +\delta_{\alpha;N2(f)}\delta_{k;Ar(f)}\delta_{l;Ar(i)}\delta_{\delta;N2(i)} \Big\} \langle 0|0\rangle
\end{aligned}
\tag{7.14}
$$

The summation can be reduced by applying the delta functions. This results in

$$
\begin{aligned}
H'(\underline{R}) = 4\big(& V_{Ar(f),N2(f),N2(i),Ar(i)} - V_{Ar(f),N2(f),Ar(i),N2(i)} \\
& - V_{N2(f),Ar(f),N2(i),Ar(i)} + V_{N2(f),Ar(f),Ar(i),N2(i)} \big)
\end{aligned}
\tag{7.15}
$$

The symmetry of the mode amplitudes, V_{abcd}, can be used to simplify this expression. It is useful to rewrite the defining equation for V_{abcd}, (3.21) by extracting the spinors from the spatial integration,

$$
\begin{aligned}
V_{ijkl} &\equiv u_i^+ u_j^+ u_k u_l \; f_{ijkl} \\
&= \delta_{jk}^{(S)} \delta_{il}^{(S)} \; f_{ijkl}
\end{aligned}
\tag{7.16}
$$

where the superscripted Kronecker deltas summarize the spin requirements, such that $\delta_{+,+}^{(S)} = \delta_{-,-}^{(S)} = 1$ and $\delta_{+,-}^{(S)} = \delta_{-,+}^{(S)} = 0$. Since the molecular orbitals are real functions, the ordering of the subscripts for f_{ijkl} refers only to the variable of integration used in (3.21). As they are defined in (3.21), the indices referring to a common variable of integration are grouped together as the inner pair and the outer pair. Thus, it can easily be seen that

$$
f_{ijkl} = f_{ikjl} = f_{ljki} = f_{lkji} = f_{jilk} = f_{jlik} = f_{kilj} = f_{klij} \tag{7.17}
$$

Applying this symmetry to (7.15) results in the final expression for the molecular interaction Hamiltonian,

$$H'(\underline{R}) = 8\left(\delta^{(S)}_{N2(f),N2(i)}\delta^{(S)}_{Ar(f),Ar(i)}\, f_{N2(f),Ar(f),Ar(i),N2(i)} - \delta^{(S)}_{N2(f),Ar(i)}\delta^{(S)}_{Ar(f),N2(i)}\, f_{N2(f),Ar(f),N2(i),Ar(i)}\right) \tag{7.18}$$

In the case that the initial states were equal to the final states, the first term would be a coulomb energy and the second term would be an exchange energy. However, since the collision is modeled with four unique molecular states, the interaction Hamiltonian is reduced from (7.4) to a difference between a "coulomb-like" and an "exchange-like" term.

Spatial and Spin State Degeneracies

For the purpose of computing the interaction Hamiltonian, the initial and final molecular eigenstates are denoted by the active orbital modes before and after the collision. The complete specification of the spatial and spin character of an orbital is termed a reaction channel. In order to compute the probability of transition for a given entrance channel, the transition amplitudes for all the possible exit channels must be summed. If there exists more than one channel that defines the initial state, then total transition probability is a weighted average of the individual entrance channel transition probabilities, usually according to the probability of occurrence of each entrance channel.

The spatial and spin degeneracies serve to complicate the calculation of the reaction probability by introducing multiple entrance and exit channels. The possibilities for the initial and final states are illustrated in Figure 7.3, which is based upon a similar drawing by Lents [64]. The arrows denote the orbital occupancy and the electron spin direction. For simplicity, it is assumed that, in the absence of any significant coupling between the spin and any other angular momentum, the spin eigenstates of both the Ar and N_2 may be taken as coaligned.

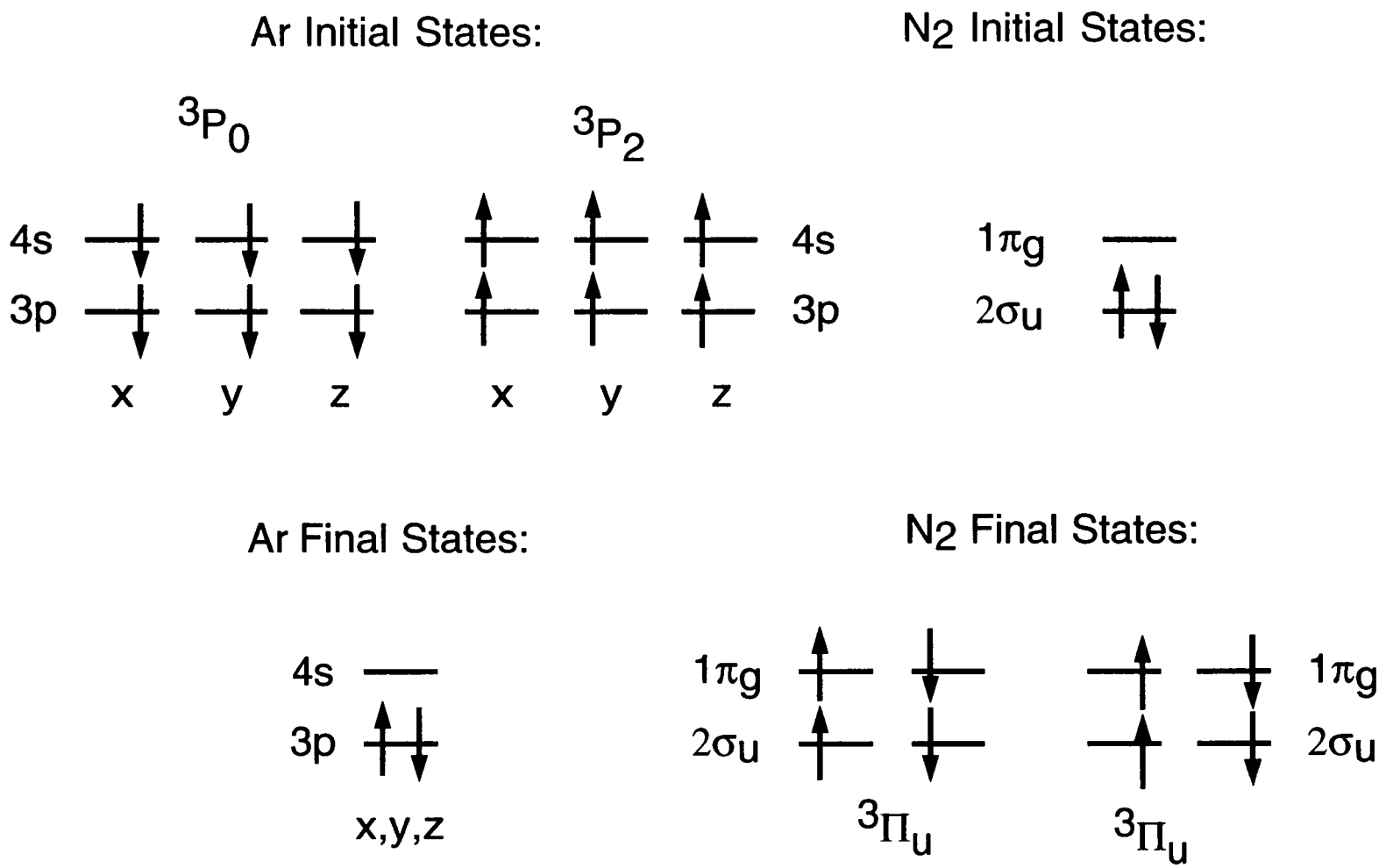

Figure 7.3 Initial and Final Ar and N_2 Spatial and Spin Configurations

The spatial degeneracies are perhaps simpler to account for than the spin degeneracies. For example, as shown in Figure 7.3, the initial Ar state consists of one 4s electron and a vacancy, or hole, in either the 3px, 3py, or 3pz orbital, which is referred to in this study as a spatial degeneracy. This spatial degeneracy is thus three-fold in the entrance channel. Similarly, the final N_2 state is the double degenerate $1\pi_g$ orbital and for notation purposes, the $1\pi_g$ orbitals are labeled as $1\pi_g(a)$ and $1\pi_g(b)$. However, neither the initial N_2 state, the $2\sigma_u$ orbital, nor the final Ar state, the completely filled 3p orbital, is spatial degenerate. Hence, due to spatial degeneracies alone, there are three entrance channels, each with two possible exit channels, for a total of six possible sets of entrance and exit channel pairs.

The spin degeneracies of each of the above entrance and exit channels further complicate matters. However, because there is no explicit spin dependence contained in the interaction Hamiltonian, each pair of spatially resolved entrance and exit channels will have the same spin fine structure. As an example, the details of the 3px-$1\pi_g(a)$ channel pair are given in Table 7.1. Each column refers to the spin state of the active electron within a specific orbital. Since there are four orbitals involved in the collision, i.e. two initial and two final, and the electron can have two spin states, there are $2^4 = 16$ possible arrangements. In the first eight rows, the 4s electron has positive spin. In order for the Ar to be in the metastable triplet state initially, this implies that the electron remaining in the 3px orbital also have positive spin. From Figure 7.3, this entrance channel then is a part of the Ar $^3P_2$ initial state. A similar situation applies to the final N_2 $1\pi_g(a)$ orbital. The electron in the $1\pi_g(a)$ orbital is free to choose the spin as either positive or negative. In either case, though, the electron remaining in the $2\sigma_u$ orbital must have the same spin orientation as the electron in the $1\pi_g(a)$ orbital in order to create the final N_2 $C^3\Pi$ state.

Table 7.1 Spin Degeneracies Associated with the 3px-$1\pi_g$(a) Reaction Channel-Pair[a]

$\|i\rangle_{Ar}$	$\|i\rangle_{N2}$	$\|f\rangle_{Ar}$	$\|f\rangle_{N2}$	Result of Spin Conservation
4s+	2σ+	3px+	$1\pi_g$(a)+	nonzero
4s+	2σ+	3px+	$1\pi_g$(a)-	0
4s+	2σ+	3px-	$1\pi_g$(a)+	0
4s+	2σ+	3px-	$1\pi_g$(a)-	nonzero
4s+	2σ-	3px+	$1\pi_g$(a)+	0
4s+	2σ-	3px+	$1\pi_g$(a)-	nonzero
4s+	2σ-	3px-	$1\pi_g$(a)+	nonzero
4s+	2σ-	3px-	$1\pi_g$(a)-	0
4s-	2σ+	3px+	$1\pi_g$(a)+	0
4s-	2σ+	3px+	$1\pi_g$(a)-	nonzero
4s-	2σ+	3px-	$1\pi_g$(a)+	nonzero
4s-	2σ+	3px-	$1\pi_g$(a)-	0
4s-	2σ-	3px+	$1\pi_g$(a)+	nonzero
4s-	2σ-	3px+	$1\pi_g$(a)-	0
4s-	2σ-	3px-	$1\pi_g$(a)+	0
4s-	2σ-	3px-	$1\pi_g$(a)-	nonzero

(a) The spatial orbital is noted along with the sign of the electron spin.

The fifth column of Table 7.1 indicates the result of explicit spin conservation by applying the Kronecker deltas of (7.18). Since the Kronecker deltas involve pairs of spin states, any combination of spin states in which there is an unequal number of up and down states will lead to a zero amplitude. This eliminates half of the reaction possibilities. Thus, the transition probability amplitude for the Ar $^3P_2[3px]$ - N_2 $C^3\Pi[1\pi_g(a)]$ channel is a sum of the remaining four terms.

Transition Probability Amplitude

In anticipation of the application of the first Born approximation, the transition amplitude for any given reaction channel pair is equal to the interaction Hamiltonian taken between the pair. Applying this to the example of the Ar $^3P_2[3px]$ - N_2 $C^3\Pi_u[1\pi_g(a)]$ reaction channel determines the transition probability amplitude as a sum of four terms which results in

$$A^{^3P_2:3px}_{^3\Pi:1\pi_g(a)} = 16\left(f_{1\pi a,3px,4s,2\sigma} - f_{1\pi a,3px,2\sigma,4s}\right) \tag{7.19}$$

Note that the analogous transition probability amplitude for the Ar $^3P_2[3px]$ - N_2 $C^3\Pi_u[1\pi_g(b)]$ channel is a similar summation, such that the total probability amplitude for the Ar $^3P_2[3px]$ - N_2 $C^3\Pi_u$ reaction is

$$\begin{aligned} A^{^3P_2:3px}_{^3\Pi_u:1\pi_g} &= 16\left(f_{1\pi a,3px,4s,2\sigma} - f_{1\pi a,3px,2\sigma,4s}\right) \\ &\quad +16\left(f_{1\pi b,3px,4s,2\sigma} - f_{1\pi b,3px,2\sigma,4s}\right) \end{aligned} \tag{7.20}$$

As stated above, the total transition amplitude requires summing over all the exit channels for a given entrance channel, and then averaging over all entrance channels. Since the interaction Hamiltonian is not explicitly spin dependent, the three entrance channels corresponding to the Ar $^3P_2$ state and the three entrance channels corresponding to the Ar $^3P_0$ state must yield identical transition amplitudes. Combining

all possible channels, the total transition probability amplitude for the Ar $^3P_{0,2}$ - N_2 C^3 Π_u energy transfer reaction, under the two-electron exchange hypothesis, then becomes

$$A_{^3\Pi_u}^{^3P_{0,2}} = \frac{16}{3}\left\{\left(f_{1\pi a,3px,4s,2\sigma} - f_{1\pi a,3px,2\sigma,4s}\right)+\left(f_{1\pi b,3px,4s,2\sigma} - f_{1\pi b,3px,2\sigma,4s}\right)\right.$$
$$\left(f_{1\pi a,3py,4s,2\sigma} - f_{1\pi a,3py,2\sigma,4s}\right)+\left(f_{1\pi b,3py,4s,2\sigma} - f_{1\pi b,3py,2\sigma,4s}\right) \quad (7.21)$$
$$\left.\left(f_{1\pi a,3pz,4s,2\sigma} - f_{1\pi a,3pz,2\sigma,4s}\right)+\left(f_{1\pi b,3px,4s,2\sigma} - f_{1\pi b,3pz,2\sigma,4s}\right)\right\}$$

Computational Methods

Calculation Overview

The calculation of the scattering cross section using field theoretical techniques was broken into four phases. The first phase was to numerically determine the electronic wavefunctions of the orbitals used in (7.21). This research used g90, discussed in Chapter 6, to compute orbital wavefunctions for both N_2 and Ar.

The second phase of this research was to determine the solution to the atomic integrals which are used in the approximation of the molecular orbitals in atomic orbitals. In a standard molecular structure calculation of chemistry, the calculation of atomic integrals consumes the majority of the computational requirements. Elaborate schemes have been developed to optimize the calculation efficiency (see [49] and references therein). Since this collision calculation was not a typical use of the g90 code, a more open, albeit less efficient, approach to the atomic integrals was desired. A novel analytic technique was derived for that purpose which reduces the integrals to a closed form solution. This approach precluded g90 for the collision calculation, while using the optimized g90 wavefunctions. Analytic solutions are preferable to numerical quadrature because the integral solution is not dependent upon the quality of the numerical

approximation. The key to numerically evaluating the results of this method was using the *Mathematica* [85] symbolic manipulator software.

The third phase of the calculation was to numerically determine the transition amplitude (7.21) given the algorithm to solve the atomic integrals. This quantity is a function of six spatial coordinates, three due to the relative orientation of the Ar atom to the N_2 molecule, and three due to the translation of the Ar coordinate system with respect to the N_2 coordinate system. At each position in 6-space, a value of the interaction must be determined. It is believed that this result is the first of its kind.

The fourth phase was to relate the transition probability amplitude to the scattering matrix (5.58) in order to attempt an estimate of the reaction cross section. In the Born approximation, this amounts to taking a Fourier transform of the interaction Hamiltonian. The computational speed of the Fast Fourier Transform (FFT) technique was essential in solving for the scattering matrix. The total cross section (A1.19) then followed from the scattering matrix as a straightforward numerical integration.

Electronic Wavefunctions

The application of quantum field theory to molecular collisions was the key conceptual development of the electron exchange Hamiltonian, (3.29). Even though the derived interaction appears very tidy, the difficulty lies in computing the amplitudes for mode transitions, i.e. the f_{ijkl} of (7.21).

The structure of Ar was, in fact, calculated via two avenues. Primarily because of the relative simplicity of atomic structures as opposed to molecular structures, atomic wavefunctions may be quickly calculated by direct numerical solution of the Schrödinger equation. At the level of SCF calculations, considerable work has been published on solutions to the Schrödinger equation. One such solution algorithm is the Hartree-Fock code written by Froese-Fischer of the Chemistry Department at Vanderbilt University

[41]. The algorithm solves the SCF equations for the radial functions, $P(r)$, given in (4.15). (As an aside, it might be noted that Froese-Fischer was a student of D.R. Hartree, who with his father, W. Hartree, were among the first to examine atomic structures numerically.)

Froese-Fischer's Hartree-Fock program was successfully used for Ar. Note that the spin orbitals are solutions of the electronic Hamiltonian only, and no consideration has been given to fine structure of the electronic manifold. The results of the radial equation for the ground Ar configuration, ^1S, are shown in Figure 7.4, where the radial wave function amplitude, $P(r)$, is plotted as a function of radial distance from the nucleus. There are five orbitals corresponding to the 1s, 2s, 2p, 3s, and 3p orbitals. Clearly, the behavior of the solutions is that of screened hydrogenic functions. Notice that the number of zero-crossings for each orbital of principal quantum number, n, is $n-l-1$, in accord with the standard rule [39].

An alternative method of understanding the physical nature of the Ar structure may be examining a plot of the radial density as a function of radius for the five orbitals, as shown in Figure 7.5. Recall that the radial density is given by $r^2|P(r)|^2$, such that

$$\int_0^\infty dr\, r^2|P(r)|^2 = 1 \tag{7.22}$$

In this plot, the shell nature of the atom is very evident by noting that the K shell density peaks near 0.05 au, the L shell density peaks near 0.34 au, and the outer M shell density peaks near 1.2 au.

It is also possible to use the Hartree-Fock code to describe virtual (unoccupied) orbitals which comprise the excited electronic states. The code was run for the ^3P state of Ar, and the results are shown in Figure 7.6, where the amplitude of the radial wavefunction, $P(r)$, is plotted as a function of radial distance. The lower five orbitals

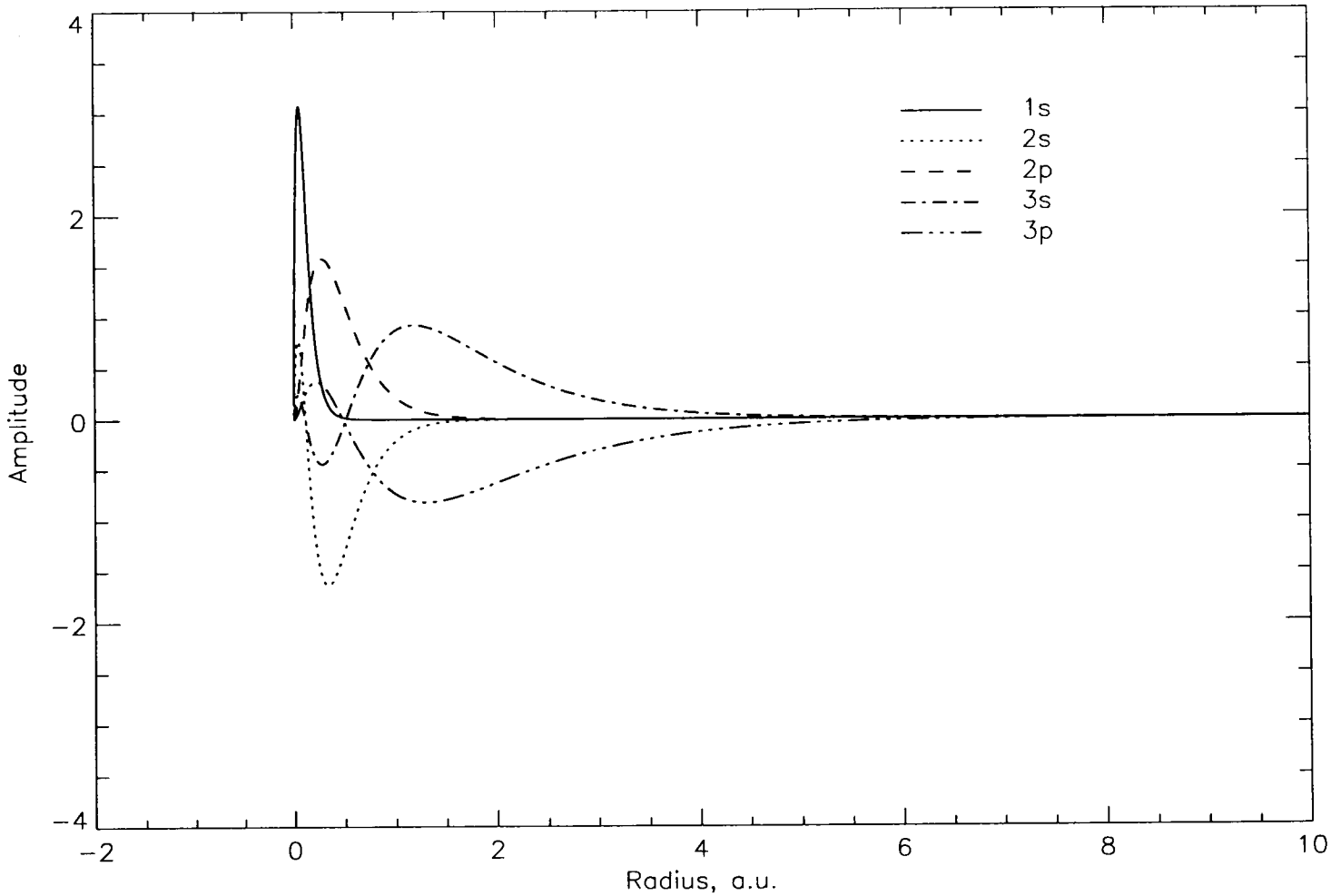

Figure 7.4 Radial Wavefunction Amplitudes for Ground State Ar(^{1}S)

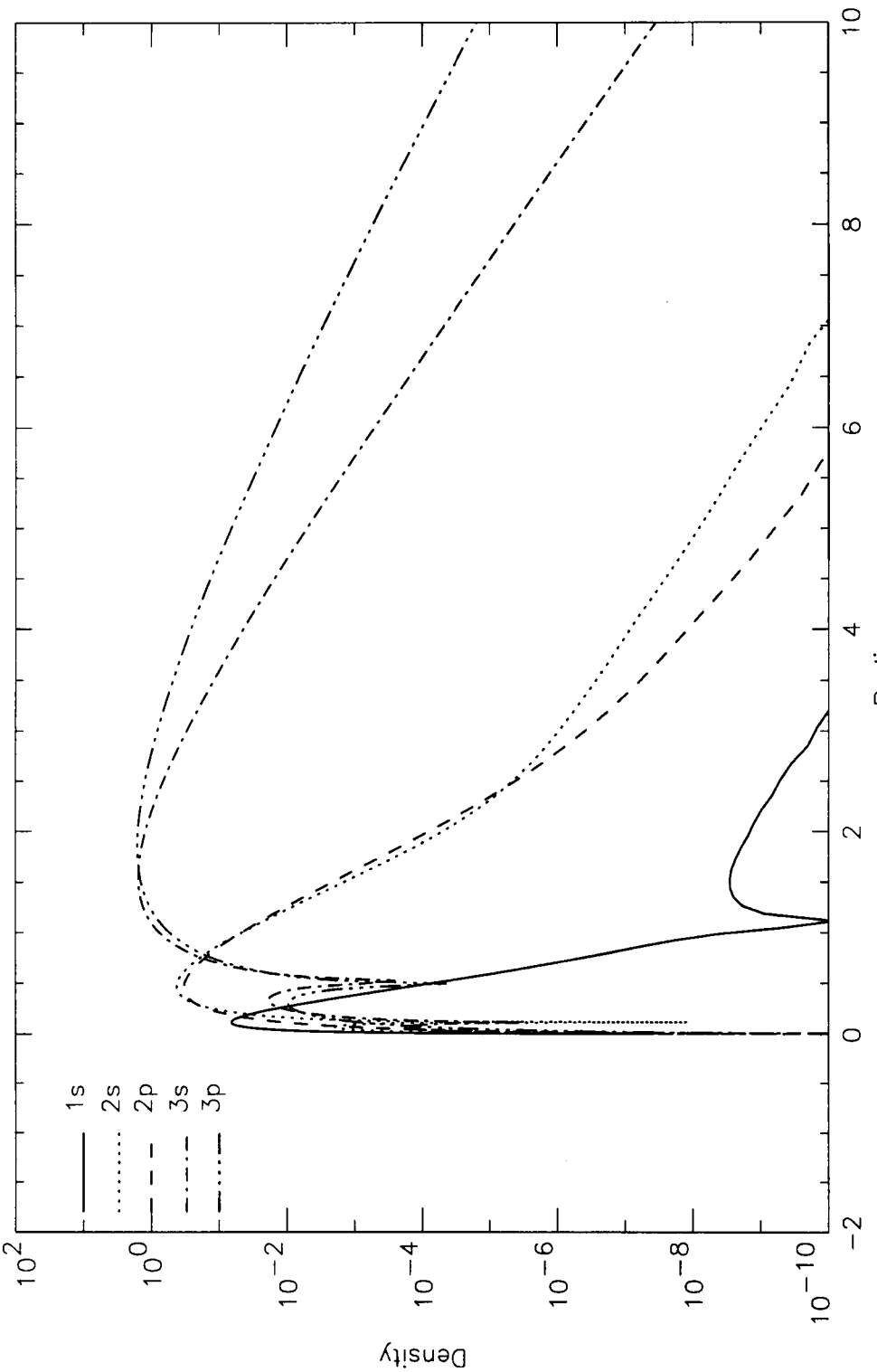

Figure 7.5 Radial Densities for Ground State Ar(^{1}S)

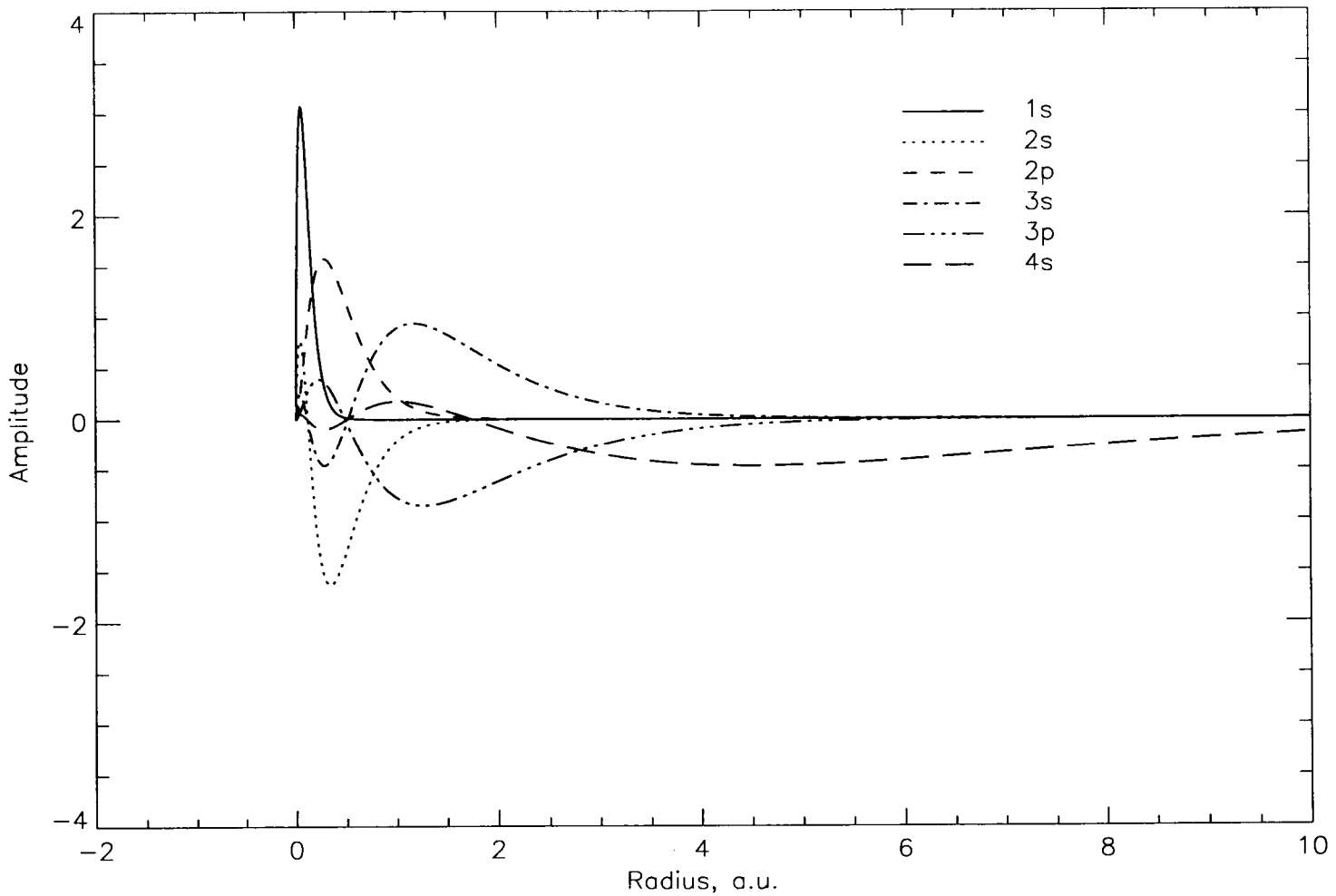

Figure 7.6 Radial Wavefunction Amplitudes for Excited State Ar(^{3}P)

are unchanged in this approximation from the calculation of the ^1S ground state. In addition to these five, however, the 4s orbital is also calculated. From Figure 7.6, the three zero-crossings are evident, corresponding to the $n-l-1$ rule. The most obvious feature of the 4s wavefunction, though, is the great spatial extent of the orbital. This facet is perhaps better portrayed by the orbital radial density function, shown in Figure 7.7. Once again, the K, L, and M shells are peaked at roughly 0.05 , 0.34, and 1.2 au, respectively. In addition, though, the N shell, consisting of 4s orbital, exhibits a peak at approximately 4.5 au, almost twice as far out as the M shell. This feature of the ^3P state of Ar orbital is consistent with the intuition that the 4s electron is so far removed from the core of the Ar atom that an exchange of molecular centers during a collision is plausible.

Even though much information was gained from the Hartree-Fock code calculation concerning the nature of the Ar states, the numerical wavefunctions produced were incompatible with the formalism needed to generate N_2 molecular orbitals. Hence, to retain a consistent and numerically efficient method, the atomic orbitals of Ar utilized in subsequent calculations were determined by g90, as described in Chapter 4.

A listing of the necessary 6-31G basis set parameters for Ar is given in Table 7.2, where the nature of the 6-31G expansion is evident. The table consists of the atomic orbital, the gaussian exponent used for each of the expansion functions, and the coefficient for the expansion gaussian. The notation is consistent with (4.20). Also, the orbital denoted 2p, for example, contains the information for all 2p orbitals, i.e. the 2px, the 2py, and the 2pz orbitals. As suggested by the name of the basis, the orbitals of the core shell, i.e. 1s, 2s, and 2p, are expanded via six gaussians, while the valence shell for which $n=3$, is split into two sets. The valence shell consists of the 3s and 3p orbitals. The first valence set is expanded in terms of three gaussians. The second valence set,

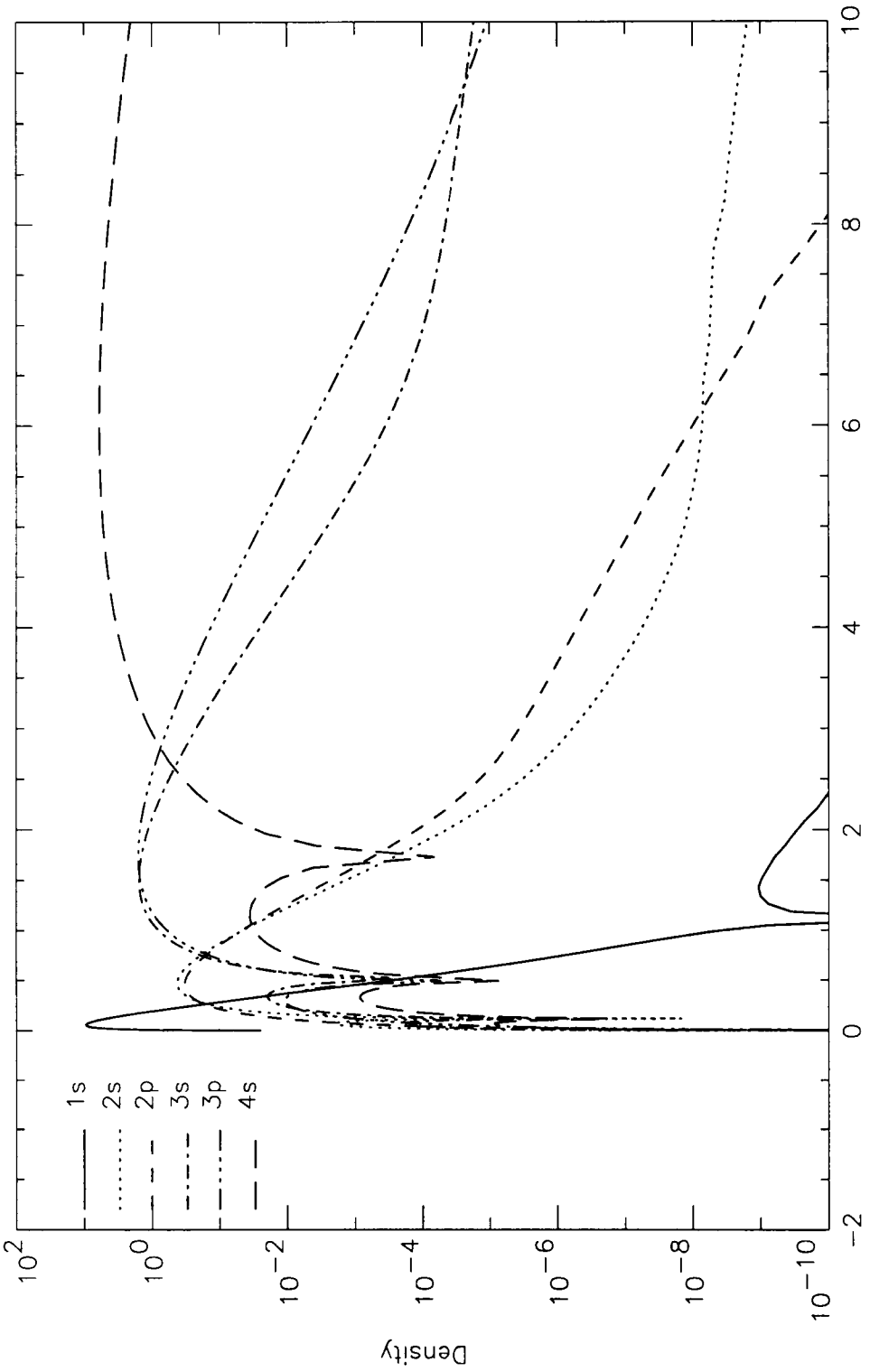

Figure 7.7 Radial Densities for Excited State Ar(^{3}P)

Table 7.2 6-31G Basis Set Expansion Parameters for Argon

Atomic Orbital	Exponent[a], α	Coefficient[a] $d_{ns,j}$	Coefficient[a] $d_{np,j}$
1s	0.283483(5)	0.182526(-2)	---
	0.425762(4)	0.139686(-1)	---
	0.969857(3)	0.687073(-1)	---
	0.273263(2)	0.236204(0)	---
	0.873695(2)	0.482214(0)	---
	0.296867(2)	0.342043(0)	---
2s	0.575891(3)	-0.215972(-2)	---
	0.136816(3)	-0.290775(-1)	---
	0.438098(2)	-0.110827(0)	---
	0.162094(2)	0.276999(-1)	---
	0.646084(1)	0.577613(0)	---
	0.265114(1)	0.488688(0)	---
2p	0.575891(3)	---	0.380665(-2)
	0.136816(3)	---	0.292305(-1)
	0.438098(2)	---	0.126467(0)
	0.162094(2)	---	0.323510(0)
	0.646084(1)	---	0.454896(0)
	0.265114(1)	---	0.256630(0)

Table 7.2 (continued)

Orbital	Exponent, α	Coefficient $d_{ns,j}$	Coefficient $d_{np,j}$
3s	0.386028(1)	-0.255592(0)	---
	0.141373(1)	0.378066(-1)	---
	0.516646(0)	0.108056(1)	---
3p	0.386028(1)	---	-0.159197(-1)
	0.141373(1)	---	0.324646(0)
	0.516646(0)	---	0.743990(0)
3s'	0.173888(0)	0.100000(1)	---
3p'	0.173888(0)	---	0.100000(1)

(a) The appropriate power of ten is noted in the parantheses.

denoted with a prime, is approximated by a single gaussian. Furthermore, it may be noted that the gaussian exponent, α, is identical for s and p orbitals of the same shell.

The g90 program was used with the 6-31G basis set in the unrestricted Hartree-Fock model to obtain molecular orbital coefficients. Since Ar is an atomic species, this may seem odd at first. However, to maintain consistency of the formalism with the N_2 structure, it was necessary to create an LCAO expansion for the atomic orbitals. In actuality, this merely allowed the g90 code to optimize the inherent gaussian expansion coefficients by mixing gaussians. The results of the atomic orbital optimization are shown in Table 7.3. Perhaps the most interesting point to make is that in the calculation of the Ar "molecular" orbitals, the atomic symmetry is preserved. For example, the 3py orbital is composed of p orbitals, and there is no contribution from s orbitals. Thus, any numeric factors from different shells merely rescale the spatial extent, but not the symmetry of the atomic orbitals. The excited 4s orbital is seen to be composed of large and near equal contributions of the 3s and 3s' orbitals. Because the 3s' has a much larger spatial extent than the 3s, based upon the parameters of Table 7.2, the split-valence basis set can model the virtual 4s orbital rather well.

The dual calculation of the Ar orbitals afforded the opportunity to compare the accuracy of the gaussian approximation technique with a direct numerical integration of the Schrödinger equation. A comparison of the standard 6-31G basis set against the numerical Hartree-Fock (nHF) solution, and also against the "effective" Ar molecular orbitals, is given in Figures 7.8 through 7.11 for each of the s orbitals, 1s, 2s, 3s, and 4s, respectively. In each of the plots, two key features are displayed. The most notable feature is probably the large disagreement between the nHF model and the g90 model near the origin. This represents the result of the tradeoff to describe the features at larger radii. It should be noted that the abscissa on Figures 7.8 through 7.11 is a logarithmic scale. The peaks located at the larger radii are responsible for chemical

Table 7.3 Optimized Argon Orbitals Using the 6-31G Basis Set

Base Atomic Orbital	g90 Optimized Coefficient Set 3px	3py	3pz	4s
1s	0.00000	0.00000	0.00000	-0.08572
2s	0.00000	0.00000	0.00000	0.13855
2px	-0.29387	0.05013	-0.01315	0.00000
2py	-0.04514	-0.21034	0.20680	0.00000
2pz	-0.02547	-0.20565	-0.21473	0.00000
3s	0.00000	0.00000	0.00000	-1.66999
3px	0.74130	-0.12646	0.03318	0.00000
3py	0.11386	0.53059	-0.52166	0.00000
3pz	0.06425	0.51875	0.54165	0.00000
3s'	0.00000	0.00000	0.00000	1.74680
3px'	0.38219	-0.06520	0.01710	0.00000
3py'	0.05870	0.27355	-0.26895	0.00000
3pz'	0.03313	0.26745	0.27926	0.00000

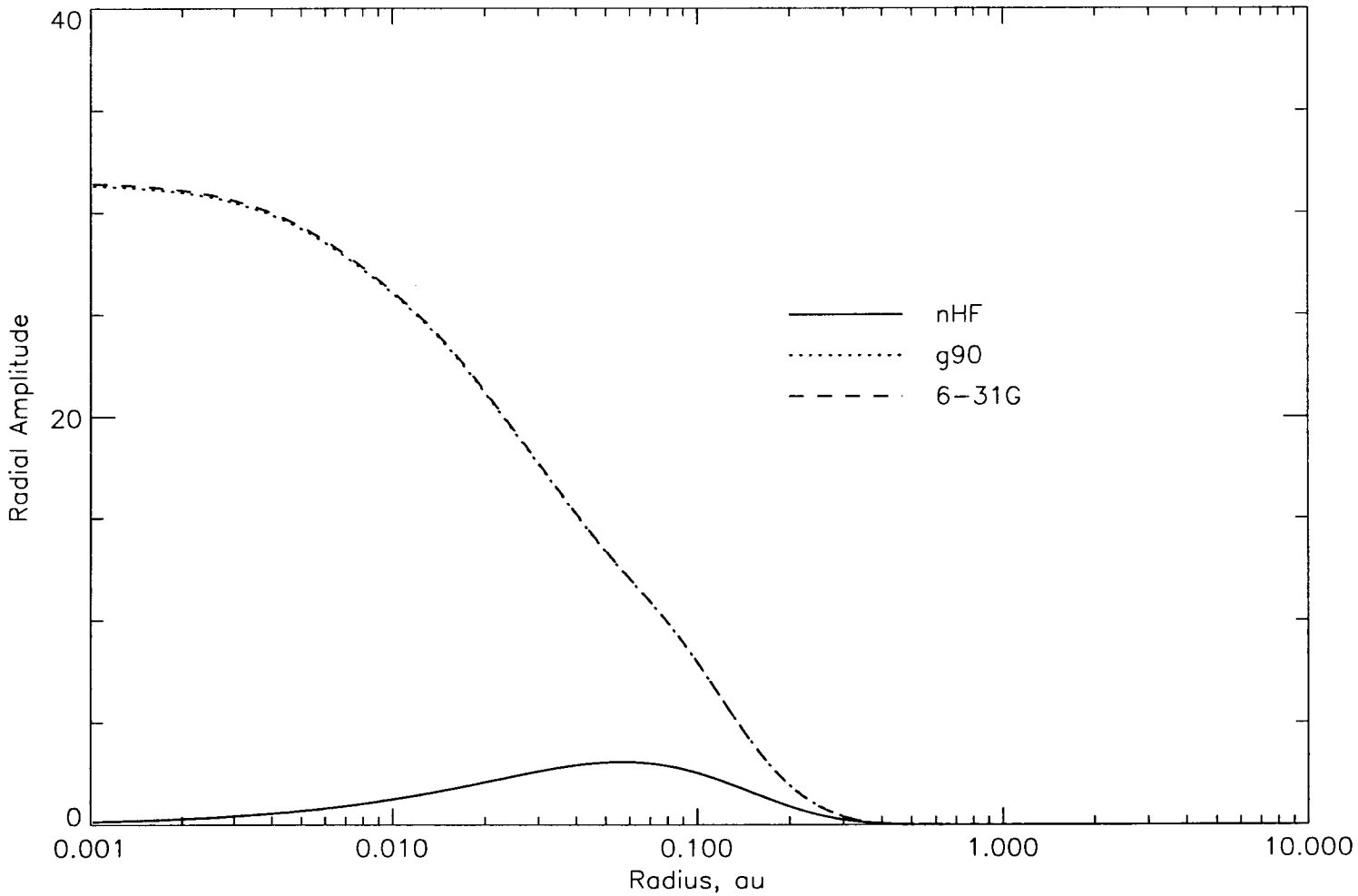

Figure 7.8 Comparison of the Ar 1s Atomic Orbital Radial Wavefunction Amplitude as Determined by the Numerical Hartree-Fock Model, the 6-31G Basis Set, and the g90 Optimization

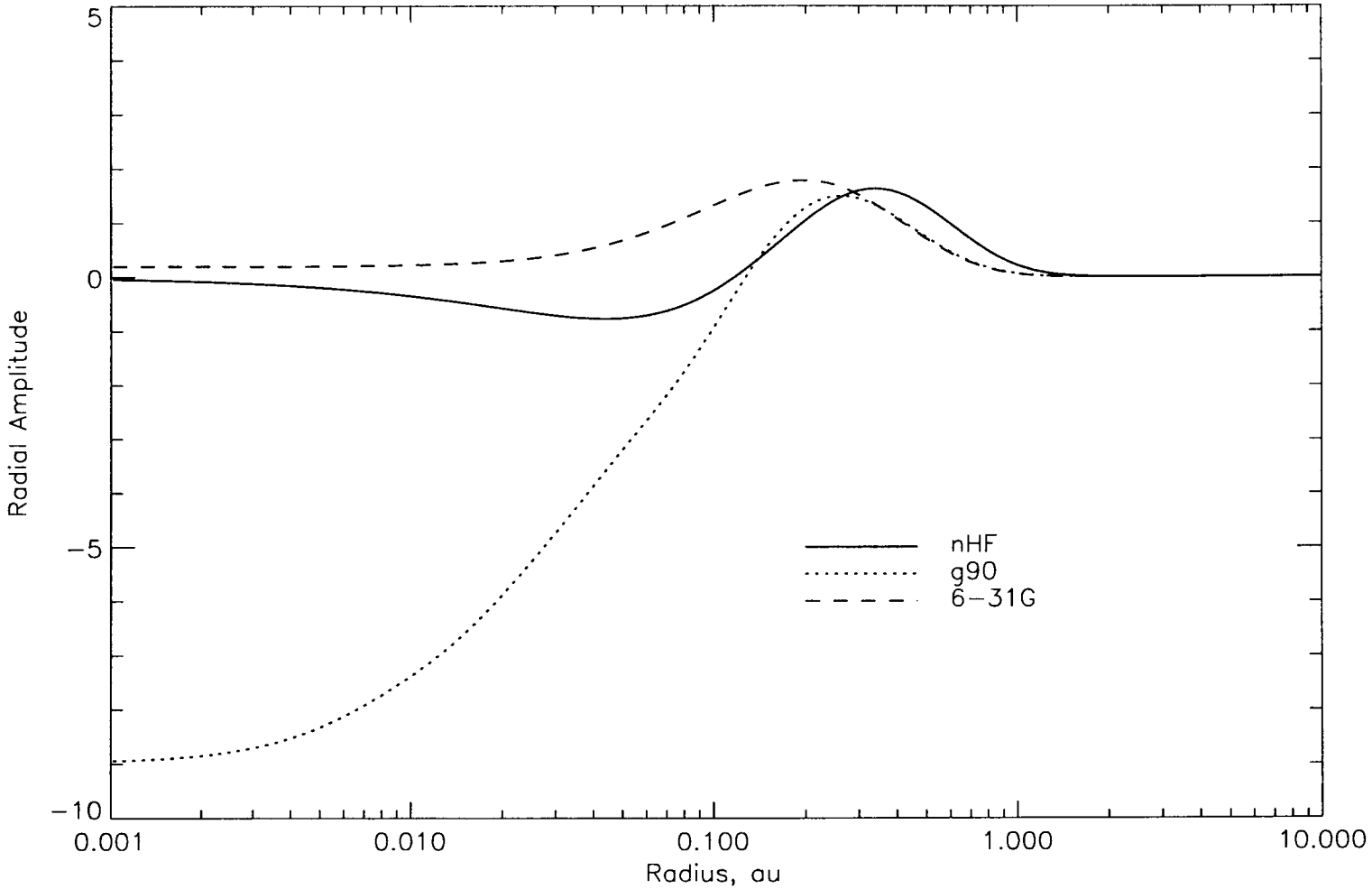

Figure 7.9 Comparison of the Ar 2s Atomic Orbital Radial Wavefunction Amplitude as Determined by the Numerical Hartree-Fock Model, the 6-31G Basis Set, and the g90 Optimization

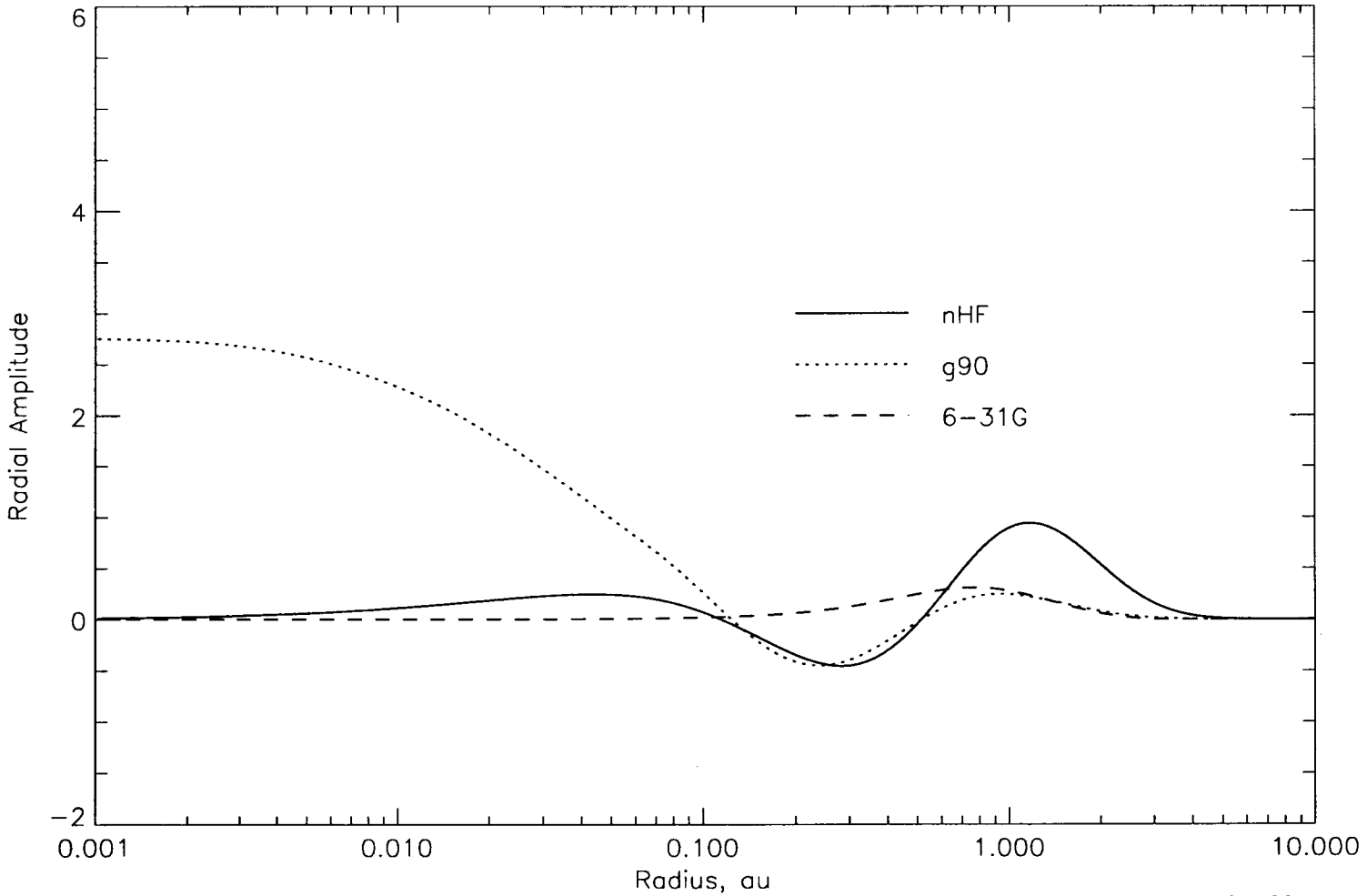

Figure 7.10 Comparison of the Ar 3s Atomic Orbital Radial Wavefunction Amplitude as Determined by the Numerical Hartree-Fock Model, the 6-31G Basis Set, and the g90 Optimization

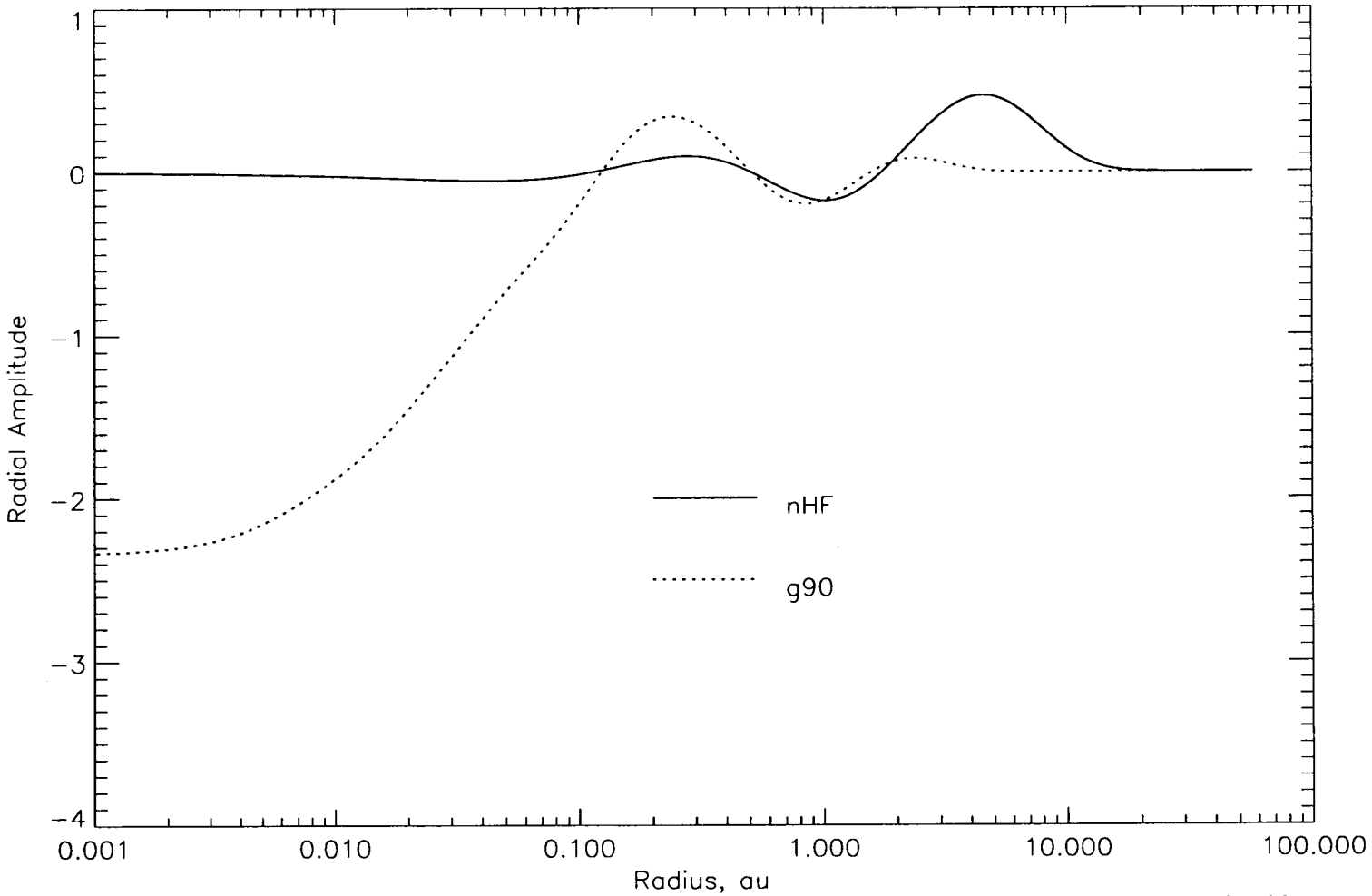

Figure 7.11 Comparison of the Ar 4s Atomic Orbital Radial Wavefunction Amplitude as Determined by the Numerical Hartree-Fock Model, and the g90 Optimization

processes such as molecular structure, bonding, and collisions. For these radii, the g90 amplitudes mimic the nHF model fairly well. Indeed, there is very good agreement between the two models near the radii corresponding to peaks in the radial density functions. In contrast, the 6-31G amplitudes appear much to stiff to be capable of describing the nHF model results. This is especially evident for the 4s orbital, where the 6-31G amplitude is flat. The nHF 2s orbital was approximated well by the 6-31G amplitude, but the 6-31G amplitudes were significantly different than the nHF 3s and 4s orbitals from 1 to 10 au. Note that a direct comparison of the nHF results and the 6-31G basis set is an opportunity to evaluate the gaussian expansion scheme. Thus, it appears that using the g90 optimization of the 6-31G basis set resulted in an improved description over using the 6-31G coefficients directly. Clearly, the g90 optimization of the 6-31G basis set was designed with the goal of minimizing the amplitude discrepancy for radii ranging from 0.1 to 1 au where chemical activity is greatest. This optimization was apparently performed at the expense of the amplitude discrepancies near the origin, $r < 0.1$ au, since this spatial location does not play a role in atomic interactions.

In truth, the reason for choosing the 6-31G model was not necessarily agreement with the Ar nHF wavefunction, but rather, consistency with the representation of the N_2 molecular orbitals. As discussed in Chapter 4, the minimal basis sets typically do a poor job of describing the spatial extent of virtual molecular orbitals, such as the virtual $1\pi_g$ orbital of N_2 which leads to the $N_2(C\ ^3\Pi_u)$ state. The alternative was to use a split-valence basis set. This led to the use of the 6-31G basis since it is the most robust and straightforward split-valence basis set available for atoms through the third row of the periodic table. The standard parameters used for describing the atomic N orbitals are given in Table 7.4. Contrasted against Ar, atomic N has only one core shell, such that only the 1s orbital is expanded into six gaussians. The $n = 2$ shell is the valence shell, containing the 2s and 2p orbitals. Hence, it is seen in Table 7.4 that the 2s and 2p

Table 7.4 6-31G Basis Set Expansion Parameters for Nitrogen

Atomic Orbital	Exponent[a], α	Coefficient[a] $d_{ns,j}$	Coefficient[a] $d_{np,j}$
1s	0.417351(4)	0.183477(-2)	---
	0.627458(3)	0.139946(-1)	---
	0.142902(3)	0.685866(-1)	---
	0.402343(2)	0.232241(0)	---
	0.128202(2)	0.469070(0)	---
	0.439044(1)	0.360455(0)	---
2s	0.116264(2)	-0.114961(0)	---
	0.271628(1)	-0.169117(0)	---
	0.772218(0)	0.114585(1)	---
2p	0.116264(2)	---	0.675797(-1)
	0.271628(1)	---	0.323907(0)
	0.772218(0)	---	0.740895(0)
2s'	0.212031(0)	0.100000(1)	---
2p'	0.212031(0)	---	0.100000(1)

(a) The appropriate power of ten is noted in the parantheses.

orbitals are approximated by three gaussians, while the 2s' and 2p' orbitals are approximated by a single gaussian.

The g90 program solved the SCF equations using the unrestricted Hartree-Fock method with the 6-31G basis set. The output was a set of coefficients that defined the "best" linear combination of atomic orbitals to describe the N_2 molecular orbitals. The results for the $2\sigma_u$ and the $1\pi_g$ orbitals are summarized in Table 7.5. The molecular orbitals are composed of 18 atomic orbitals, nine centered at each of the N atoms. In Table 7.5, the N atoms are distinguished by placing one at $\underline{R}_A$ and the other at $\underline{R}_B$. It is interesting to note that the symmetry of the molecular orbital is essentially derived by the symmetry of the constituent atomic orbitals. For example, the $2\sigma_u$ orbital is an antibonding orbital, with axial symmetry along the internuclear axis. Without considering sp hybridization for the moment, the $2\sigma_g$ and $2\sigma_u$ molecular orbitals result from the combination of the 2s orbitals from each N atom. The $2\sigma_g$ orbital is the bonding orbital, and the $2\sigma_u$ orbital is the antibonding orbital. The results of the g90 calculation reflect this fact for the $2\sigma_u$ orbital, as shown in Table 7.5. The large coefficients for the 2s and 2s' atomic orbitals from each atom indicate that the $2\sigma_u$ orbital is mostly due to the 2s atomic orbitals. Further, the sign of the coefficient from opposite atoms is different, which will construct the $2\sigma_u$ molecular orbital with a sign change across the midplane, as is illustrated qualitatively in Figure 6.2. The spherical symmetry of the 2s orbitals converts into the cylindrical symmetry of the $2\sigma_g$ and $2\sigma_u$ orbitals.

It may be noted in Table 7.5 that the $2\sigma_u$ orbital is not purely due to the 2s orbitals. It also has contributions from the 1s and 2pz orbitals as well. The former is simply a numerical artifact of the minimization process in order to achieve the proper spatial size of the final orbital by combining several differently scaled orbitals. The latter, though, is chemically interesting because it represents hybridization of the atomic s and p

Table 7.5 Optimized N_2 Molecular Orbitals Using the 6-31G Basis Set

Atomic Center	Base Atomic Orbital	g90 Optimized Coefficient Set $2\sigma_u$	$1\pi_g$	$1\pi_g$
N @ $\underline{R}_A$	1s	-0.14830	0.00000	0.00000
	2s	0.34470	0.00000	0.00000
	2px	0.00000	-0.29843	0.33767
	2py	0.00000	0.33767	0.29843
	2pz	0.19413	0.00000	0.00000
	2s'	0.55233	0.00000	0.00000
	2px'	0.00000	-0.42364	0.47934
	2py'	0.00000	0.47934	0.42364
	2pz'	0.03109	0.00000	0.00000
N @ $\underline{R}_B$	1s	0.14830	0.00000	0.00000
	2s	-0.34470	0.00000	0.00000
	2px	0.00000	0.29843	-0.33767
	2py	0.00000	-0.33767	-0.29843
	2pz	0.19413	0.00000	0.00000
	2s'	-0.55233	0.00000	0.00000
	2px'	0.00000	0.42364	-0.47934
	2py'	0.00000	-0.47934	-0.42364
	2pz'	0.03109	0.00000	0.00000

orbitals [68]. This is possible because the 2s and 2pz both have the cylindrical symmetry with respect to the N_2 molecule, even though they are of different symmetry with respect to an N atom.

Neglecting sp hybridization, the 2p orbitals, 2px, 2py, and 2pz, combine to form 4 molecular orbitals, the $3\sigma_g$, the $1\pi_u$, the $1\pi_g$, and the $3\sigma_u$ orbitals. Because the 2pz orbitals lie along the internuclear axis, they possess cylindrical symmetry and are referred to as $p\sigma$ atomic orbitals. The additive combination of these atomic orbitals is responsible for forming the $3\sigma_g$ orbital, whereas the difference between the pair of 2pz orbitals results in the very high energy $3\sigma_u$ orbital.

In a similar manner, the 2px and 2py orbitals are referred to as $p\pi$ atomic orbitals since they have a nodal plane which, when the N-N bond is formed, corresponds to the direction of the internuclear axis. The 2px and 2py orbitals combine additively to form a pair of degenerate $1\pi_u$ molecular orbitals. An example of a $1\pi_u$ molecular orbital is sketched qualitatively in Figure 6.2. Thus, the pair of $1\pi_u$ orbitals resembles a set of four hot dogs, lying with their axes parallel to the internuclear axis. The two degenerate antibonding $1\pi_g$ orbitals are due to the difference in the 2px and 2py wavefunctions. Thus, each $1\pi_g$ orbital will have four lobes. The sketch of Figure 6.2 illustrates one set of the $1\pi_g$ orbitals, with spheres indicating the orbital amplitudes. The pair of $1\pi_g$ orbitals may be thought of as eight spatially identical "spheres" placed uniformly around the midpoint of the internuclear axis. The coefficients of Table 7.5 lend credence to this intuitive picture. The first $1\pi_g$ orbital is formed by generating a linear combination of the 2px and 2py orbitals on the N atom at $\underline{R}_A$, and then subtracting the identical linear combination centered at the N atom at $\underline{R}_B$. The second $1\pi_g$ orbital is formed in the same fashion. Since the $1\pi_g$ orbitals are formed from p orbitals, and as mentioned in Chapter 6, p orbitals behave as vector quantities, another method of obtaining the second

$1\pi_g$ orbital is simply to rotate the coordinate system about the internuclear axis by $\pi/2$ radians.

Since the basis set was 6-31G, 18 atomic functions were used to create the N_2 molecular orbitals. The atomic orbitals constitute an orthonormal set in the 18 dimensional vector space, thus there are 18 possible molecular orbitals of N_2, of which only seven are occupied in the ground state. If the calculation had employed a minimal basis set, such as the STO-3G basis set consisting of 10 atomic orbitals, it would have been possible to describe only two virtual orbitals. Table 7.6 shows a comparison of selected results from a calculation of N_2 using the STO-3G and the 6-31G basis sets. Note that the 6-31G basis lowers the energy eigenvalue of the $2\sigma_u$ orbital from the STO-3G value of -0.72752 hartree to -0.77211 hartree. After accounting for the approximate 1.5 percent lowering of the ground state, the $2\sigma_u$ orbital was lowered an additional 1.1 percent. The virtual $1\pi_g$ orbital, however, was only lowered a true 0.6 percent after accounting for the ground state lowering.

As shown in Table 7.6, the STO-3G basis set predicted a ground state configuration of $1\sigma_g 1\sigma_u 2\sigma_g 2\sigma_u 1\pi_u 1\pi_u 3\sigma_g$ ($1\pi_g$), where the parentheses refer to a virtual orbital. This ordering agrees with that given by Lofthus and Krupenie [69], which should not be surprising since their conclusion was drawn from a study consisting of a minimal basis set. (Recall from Chapter 6 that the STO-3G is also a minimal basis set.) The 6-31G basis set, however, predicted a ground state configuration of $1\sigma_g 1\sigma_u 2\sigma_g 2\sigma_u 3\sigma_g 1\pi_u 1\pi_u$ ($1\pi_g$). Physically, the demotion of the $3\sigma_g$ orbital is probably due to a better description of the sp hybridization of the 2s and 2p orbitals, as discussed above. From Table 7.6, though, it is seen that the $3\sigma_g$ orbital is very close energetically to the $1\pi_u$ in both the STO-3G and the 6-31G calculation. Thus, the ordering change of the molecular orbitals due to the choice of basis set should not be

Table 7.6 Comparison of N_2 Molecular Orbital Energies Using the STO-3G and 6-31G Basis Sets

Orbital	STO-3G Energy	6-31G Energy	Orbital
$1\sigma_g$	-15.50634	-15.71562	$1\sigma_g$
$1\sigma_u$	-15.50497	-15.71204	$1\sigma_u$
$2\sigma_g$	-1.40853	-1.53376	$2\sigma_g$
$2\sigma_u$	-0.72752	-0.77211	$2\sigma_u$
$1\pi_u$	-0.54863	-0.63038	$3\sigma_g$
$3\sigma_g$	-0.53027	-0.62586	$1\pi_u$
$1\pi_g$	0.26534	0.15560	$1\pi_g$
$3\sigma_u$	1.04092	0.59294	$3\sigma_u$
---	---	0.80362	$4\sigma_g$
---	---	0.85550	$2\pi_u$
---	---	0.94131	$5\sigma_g$
---	---	1.00067	$2\pi_g$
---	---	1.10289	$4\sigma_u$
---	---	1.51861	$5\sigma_u$

Note: All energies are in atomic units, i.e hartrees.

interpreted as a radical departure in the character of the solutions, but rather as an incremental improvement in the numerical description of the electronic configuration.

Molecular Integrals

Using the numerical representation of the molecular orbitals, the expression for the transition amplitude (7.21) was solved. The determination of the electron transfer amplitudes, V_{abcd}, as written in (3.21), was the major source of difficulty. Indeed, several routes were fully explored before arriving at the present method for solving the integration. One of the more promising possibilities was to examine the functional form of (3.21), written here with the spinors and the factor of $e^2/2$ suppressed for clarity,

$$U_{jklm} \equiv \iint d^3r\, d^3r'\, \phi_j^*(\underline{r})\phi_k^*(\underline{r}')\frac{1}{|\underline{r}-\underline{r}'|}\phi_l(\underline{r}')\phi_m(\underline{r}) \tag{7.23}$$

Note that two of the orbitals are from Ar and two are from N_2. If the orbitals are of a general, unspecified form, then perhaps the first approach to solving (7.23) would be to attempt to solve it directly by transforming the integration into the momentum domain. It may then be rewritten as a single three-dimensional integral,

$$U_{jklm} = 4\pi\int d\underline{q}\,\tilde{\Omega}_{jm}(\underline{q})\frac{1}{q^2}\tilde{\Omega}_{kl}(\underline{q}) \tag{7.24}$$

where $\Omega_{ij}(\underline{r}) = \phi_i^*(\underline{r})\phi_j(\underline{r})$ and $\tilde{\Omega}_{ij}(\underline{q}) = \int d\underline{r}\, e^{-i\underline{q}\cdot\underline{r}}\phi_i^*(\underline{r})\phi_j(\underline{r})$. This was a standard approach in the mid-1960's [86], primarily due to the simplistic wavefunctions used at the time. Note that this approach moves the singularity of $1/|\underline{r}-\underline{r}'|$ to $1/q^2$ in the energy domain. This would allow one to impose numerical integration limits, if needed, based upon the energy scale of the problem. If (7.24) is performed in spherical coordinates, then it becomes

$$U_{jklm} = 4\pi\int_0^\infty dq\, q^2\int_0^{2\pi} d\varphi\int_0^{\pi} sin\theta d\theta\,\tilde{\Omega}_{jm}(q,\theta,\varphi)\frac{1}{q^2}\tilde{\Omega}_{kl}(q,\theta,\varphi) \tag{7.25}$$

where it is seen that the $1/q^2$ term is eliminated by the volume element. The major problem with this technique is that it buries the difficulty into the Fourier transform of the orbital product, $\Omega_{ij}(\underline{r})$. If the individual STOs share the same center, a closed form solution is obtained, whereas if the STOs are centered at different spatial locations, the solution may only be reduced to quadrature.

Since molecular orbitals are usually comprised of a combination of atomic orbitals centered across more than one atom, the quadrature solution for $\tilde{\Omega}_{ij}(\underline{q})$ usually results. This leads to significantly large computational time requirements, and was one of the main drivers for the gaussian approximation scheme introduced in Chapter 4. Recall that the basic assumption was that the molecular orbitals are composed of functions of the form,

$$\phi(\underline{r},\underline{A}) \propto (x-A_x)^i (y-A_y)^j (z-A_z)^k e^{-a_\lambda^2 |\underline{r}-\underline{A}|} \tag{7.26}$$

for an orbital referring to an atom spatially located at $\underline{A}$. Note that the Cartesian coordinate form of the gaussian has been chosen over the equivalent spherical coordinate form. This allows for separation of the volume integral into three similar integrations, whereas a spherical integration does not possess this functional symmetry.

Consider the amplitude defined in (3.21) for the Coulomb interaction,

$$\left\langle \phi_\mu^{N_2}, \phi_\delta^{Ar} \middle\| \phi_\varepsilon^{Ar} \phi_\nu^{N_2} \right\rangle \equiv \iint d^3r\, d^3r'\, \phi_\mu^{N_2}(\underline{r}) \phi_\delta^{Ar}(\underline{r}') \frac{1}{|\underline{r}-\underline{r}'|} \phi_\varepsilon^{Ar}(\underline{r}') \phi_\nu^{N_2}(\underline{r}) \tag{7.27}$$

where the functions refer to molecular orbitals of N_2 and Ar. The double bar inner product symbol denotes that the integration contains the $1/r$ term. The N_2 molecular orbitals are written as a sum of N_f atomic orbitals,

$$\phi_\mu^{N_2}(\underline{r}) = \sum_{i=1}^{N_f} c_{\mu i} f_i(\underline{r},\underline{R}_i) \tag{7.28}$$

where the atomic orbitals, $f_i(\underline{r},\underline{R}_i)$, are referenced to each atomic center. As stated in Chapter 4, the solution of the SCF Hamiltonian leads to the optimal values of the $c_{\mu i}$

coefficients. From (4.22) and (4.23), the atomic orbitals are subsequently expanded into gaussians as

$$f_i(\underline{r},\underline{R_i}) = \sum_{n=1}^{K} d_{i,n} g_{i,n}(\xi_i^N, \alpha_{i,n}; \underline{r} - \underline{R_i}) \tag{7.29}$$

The choice of basis set determines the value of N_f, as well as K. Thus, substituting (7.29) into (7.28) yields the working expression for the N_2 molecular orbitals,

$$\phi_\mu^{N_2}(\underline{r}) = \sum_{i=1}^{N_f} c_{\mu i} \sum_{n=1}^{K} d_{i,n} g_{i,n}(\xi_i^N, \alpha_{i,n}; \underline{r} - \underline{R_i}) \tag{7.30}$$

Of course, a similar expression holds for the Ar orbitals.

Combining the Ar and N_2 orbitals leads to the first complete expression of the Coulomb amplitude,

$$\begin{aligned} \left\langle \phi_\mu^{N_2} \phi_\lambda^{Ar} \middle\| \phi_\kappa^{Ar} \phi_\nu^{N_2} \right\rangle = & \sum_{\gamma,\beta=1}^{N_f} c_{\mu\gamma} c_{\nu\beta} \sum_{\delta,\varepsilon=1}^{M_f} c_{\lambda\delta} c_{\kappa\varepsilon} \sum_{n=1}^{K^{Ar}} \sum_{m=1}^{K^{Ar}} \sum_{p=1}^{K^N} \sum_{q=1}^{K^N} d_{\delta,n}^{Ar} d_{\varepsilon,m}^{Ar} d_{\gamma,p}^{N} d_{\beta,q}^{N} \\ & \left\langle g_{\gamma,p}^{N}(\xi_\gamma^N, \alpha_{\gamma,p}; \underline{r} - \underline{R_\gamma}) g_{\delta,n}^{Ar}(\xi_\delta^{Ar}, \alpha_{\delta,n}; \underline{r'} - \underline{R_\delta}) \right| \\ & \left| g_{\varepsilon,m}^{Ar}(\xi_\varepsilon^{Ar}, \alpha_{\varepsilon,m}; \underline{r'} - \underline{R_\varepsilon}) g_{\beta,q}^{N}(\xi_\beta^N, \alpha_{\beta,q}; \underline{r} - \underline{R_\beta}) \right\rangle \end{aligned} \tag{7.31}$$

The gaussians may be completely written out, such that they become

$$\begin{aligned} g_{\lambda,n}(\xi_\lambda^A, \alpha_{\lambda,n}; \underline{r} - \underline{R_\lambda}) \equiv & \eta_\lambda (x - R_{\lambda,x})^{l_1} (y - R_{\lambda,y})^{l_2} (z - R_{\lambda,z})^{l_3} \\ & (\xi_\lambda^A)^{3/2 + l_1 + l_2 + l_3} \exp\left\{ -\alpha_{\lambda,n} \left(\xi_\lambda^A \left| \underline{r} - \underline{R_\lambda} \right| \right)^2 \right\} \end{aligned} \tag{7.32}$$

where the normalization factor is

$$\eta_\lambda = \begin{Bmatrix} (2\alpha_{\lambda,n}/\pi)^{3/4} \\ (128\alpha_{\lambda,n}^5/\pi)^{1/4} \end{Bmatrix} \text{ for } |\lambda| = \begin{Bmatrix} 0; \text{ s orbitals} \\ 1; \text{ p orbitals} \end{Bmatrix} \tag{7.33}$$

in agreement with Table 4.1.

The orbital index, λ , may be considered as a three-component vector given by $\lambda \equiv w\underline{l}$, where w is the type of orbital, i.e. $w = 0$ for s orbitals etc., and $\underline{l}$ is the vector of orbital coordinate exponents. The final expansion extracts the atomic centers from the inner product using the binomial expansion. Thus, the entire inner product may be written as

(7.34)

$$\left\langle \phi_{\mu}^{N_2}\phi_{\lambda}^{Ar} \middle\| \phi_{\kappa}^{Ar}\phi_{\nu}^{N_2} \right\rangle = \sum_{\gamma,\beta=1}^{N_f} c_{\mu\gamma}c_{\nu\beta} \sum_{\delta,\varepsilon=1}^{M_f} c_{\lambda\delta}c_{\kappa\varepsilon} \sum_{n=1}^{K^{Ar}}\sum_{m=1}^{K^{Ar}}\sum_{p=1}^{K^{N}}\sum_{q=1}^{K^{N}} d_{\delta,n}^{Ar} d_{\varepsilon,m}^{Ar} d_{\gamma,p}^{N} d_{\beta,q}^{N} \eta_{\gamma,p}^{N} \eta_{\beta,q}^{N} \eta_{\delta,n}^{Ar} \eta_{\varepsilon,m}^{Ar}$$

$$\left(\xi_{\gamma}^{N}\right)^{3/2+l_1^{\gamma}+l_2^{\gamma}+l_3^{\gamma}} \left(\xi_{\beta}^{N}\right)^{3/2+l_1^{\beta}+l_2^{\beta}+l_3^{\beta}} \left(\xi_{\delta}^{Ar}\right)^{3/2+l_1^{\delta}+l_2^{\delta}+l_3^{\delta}} \left(\xi_{\varepsilon}^{Ar}\right)^{3/2+l_1^{\varepsilon}+l_2^{\varepsilon}+l_3^{\varepsilon}}$$

$$\sum_{h_\gamma=0}^{l_1^{\gamma}} \binom{l_1^{\gamma}}{h_\gamma} \left(-R_{\gamma,x}\right)^{l_1^{\gamma}-h_\gamma} \sum_{i_\gamma=0}^{l_2^{\gamma}} \binom{l_2^{\gamma}}{i_\gamma} \left(-R_{\gamma,y}\right)^{l_2^{\gamma}-i_\gamma} \sum_{j_\gamma=0}^{l_3^{\gamma}} \binom{l_3^{\gamma}}{j_\gamma} \left(-R_{\gamma,z}\right)^{l_3^{\gamma}-j_\gamma}$$

$$\sum_{h_\beta=0}^{l_1^{\beta}} \binom{l_1^{\beta}}{h_\beta} \left(-R_{\beta,x}\right)^{l_1^{\beta}-h_\beta} \sum_{i_\beta=0}^{l_2^{\beta}} \binom{l_2^{\beta}}{i_\beta} \left(-R_{\beta,y}\right)^{l_2^{\beta}-i_\beta} \sum_{j_\beta=0}^{l_3^{\beta}} \binom{l_3^{\beta}}{j_\beta} \left(-R_{\beta,z}\right)^{l_3^{\beta}-j_\beta}$$

$$\sum_{h_\delta=0}^{l_1^{\delta}} \binom{l_1^{\delta}}{h_\delta} \left(-R_{\delta,x}\right)^{l_1^{\delta}-h_\delta} \sum_{i_\delta=0}^{l_2^{\delta}} \binom{l_2^{\delta}}{i_\delta} \left(-R_{\delta,y}\right)^{l_2^{\delta}-i_\delta} \sum_{j_\delta=0}^{l_3^{\delta}} \binom{l_3^{\delta}}{j_\delta} \left(-R_{\delta,z}\right)^{l_3^{\delta}-j_\delta}$$

$$\sum_{h_\varepsilon=0}^{l_1^{\varepsilon}} \binom{l_1^{\varepsilon}}{h_\varepsilon} \left(-R_{\varepsilon,x}\right)^{l_1^{\varepsilon}-h_\varepsilon} \sum_{i_\varepsilon=0}^{l_2^{\varepsilon}} \binom{l_2^{\varepsilon}}{i_\varepsilon} \left(-R_{\varepsilon,y}\right)^{l_2^{\varepsilon}-i_\varepsilon} \sum_{j_\varepsilon=0}^{l_3^{\varepsilon}} \binom{l_3^{\varepsilon}}{j_\varepsilon} \left(-R_{\varepsilon,z}\right)^{l_3^{\varepsilon}-j_\varepsilon}$$

$$I$$

where the integral factor is simply

(7.35)

$$I \equiv \iint d^3r\, d^3r' \frac{1}{|\underline{r}-\underline{r}'|}$$
$$x^{h_\gamma} y^{i_\gamma} z^{j_\gamma} exp\left\{-\alpha_{\gamma,p}\left(\xi_\gamma^N \left|\underline{r}-\underline{R}_\gamma\right|\right)^2\right\}$$
$$x^{h_\beta} y^{i_\beta} z^{j_\beta} exp\left\{-\alpha_{\beta,q}\left(\xi_\beta^N \left|\underline{r}-\underline{R}_\beta\right|\right)^2\right\}$$
$$x'^{h_\delta} y'^{i_\delta} z'^{j_\delta} exp\left\{-\alpha_{\delta,n}\left(\xi_\delta^{Ar} \left|\underline{r}-\underline{R}_\delta\right|\right)^2\right\}$$
$$x'^{h_\varepsilon} y'^{i_\varepsilon} z'^{j_\varepsilon} exp\left\{-\alpha_{\varepsilon,m}\left(\xi_\varepsilon^{Ar} \left|\underline{r}-\underline{R}_\varepsilon\right|\right)^2\right\}$$

The exponents in (7.35) are limited in their possible values due to the symmetry of the individual atomic orbitals which comprise a given molecular orbital. For example, if γ referred to a 2px orbital, then $0 \leq h_\gamma \leq 1$.

At this point, the problem consists of an integral evaluation deeply nested inside several layers of expansions. There were two possible approaches to solve the problem. The first was to attempt to incorporate the highly optimized scheme used in the g90 code, or secondly, to independently reduce (7.35) analytically and then develop an appropriate computer program. The latter approach was chosen because it was felt that the g90 scheme was much too deeply ingrained within the specifics of the g90 code structure. It was deemed more worthwhile to develop an alternate, physically tractable solution scheme, even at the expense of computational efficiency. Thus, a novel method of solving (7.35) was derived.

Proceeding forward, the solution of (7.35) then involves a summation of integrations with each individual integration taking the general form,

$$I \equiv \iint d^3r\, d^3r' \frac{1}{|\underline{r}-\underline{r}'|} x^h y^i z^j e^{-a_A^2|\underline{r}-\underline{A}|^2} e^{-a_B^2|\underline{r}'-\underline{B}|^2} x'^l y'^m z'^n e^{-a_C^2|\underline{r}'-\underline{C}|^2} e^{-a_D^2|\underline{r}-\underline{D}|^2} \tag{7.36}$$

Note that the exponents for the atomic orbitals have been combined, based upon the proper integration variable. Building upon the above example where γ refers to the 2px orbital, let β refer to a 2py orbital. In that case, $0 \le h \equiv h_\gamma + h_\beta \le 1$, and $0 \le i \equiv i_\gamma + i_\beta \le 1$. If, on the other hand, β also referred to a 2px orbital, then $0 \le h \le 2$, and $i = 0$. The gaussian width parameters of (7.35) have been ungraciously lumped together as generic arguments which will be sorted out later in the derivation.

The key to reducing (7.36) is to use the identity [87],

$$\frac{1}{|\underline{r}-\underline{r}'|} = \frac{1}{2\pi^2} \int d^3k \frac{e^{i\underline{k}\cdot(\underline{r}-\underline{r}')}}{k^2} \tag{7.37}$$

as well as performing the transformations $\underline{r}-\underline{A} \equiv \underline{u}$ and $\underline{r}'-\underline{B} \equiv \underline{u}'$. Substitution of these into (7.36) leads to

$$\begin{aligned} I = & \frac{1}{2\pi^2} \int d^3k \frac{1}{k^2} e^{i\underline{k}\cdot\underline{AB}} \\ & \int d^3u\, e^{i\underline{k}\cdot\underline{u}} (u_x + A_x)^h (u_y + A_y)^i (u_z + A_z)^j e^{-a_A^2 u^2} e^{-a_D^2|\underline{u}+\underline{AD}|^2} \\ & \int d^3u'\, e^{-i\underline{k}\cdot\underline{u}'} (u'_x + B_x)^l (u'_y + B_y)^m (u'_z + B_z)^n e^{-a_B^2 u'^2} e^{-a_C^2|\underline{u}'+\underline{BC}|^2} \end{aligned} \tag{7.38}$$

where $\underline{AB} \equiv \underline{A}-\underline{B}$, etc. It is clear that I is composed of two similar integrals over $\underline{u}$ and $\underline{u}'$. Each minor integral, denoted as I_m, may be simplified by expanding the binomials, yielding

$$\begin{aligned} I_m = & \sum_{\alpha=0}^{h} \sum_{\beta=0}^{i} \sum_{\gamma=0}^{j} \binom{h}{\alpha} \binom{i}{\beta} \binom{j}{\gamma} \int du_x\, e^{ik_1 u_x} u_x^\alpha A_x^{h-\alpha} e^{-a_A^2 u_x^2} e^{-a_D^2(u_x+AD_x)^2} \\ & \int du_y\, e^{ik_2 u_y} u_y^\beta A_y^{i-\beta} e^{-a_A^2 u_y^2} e^{-a_D^2(u_y+AD_y)^2} \\ & \int du_z\, e^{ik_3 u_z} u_z^\gamma A_z^{j-\gamma} e^{-a_A^2 u_z^2} e^{-a_D^2(u_z+AD_z)^2} \end{aligned} \tag{7.39}$$

Obviously, the constants A_x, A_y, and A_z may be pulled through the integrals. Also, recall the standard trick of expressing $e^{ik_1 u_x} u_x^{\alpha}$ as a multiple partial derivative of an integral over just the $e^{ik_1 u_x}$ portion. Performing both of these actions gives the minor integral the form,

(7.40)

$$I_m = \sum_{\alpha=0}^{h}\sum_{\beta=0}^{i}\sum_{\gamma=0}^{j}\binom{h}{\alpha}\binom{i}{\beta}\binom{j}{\gamma} A_x^{h-\alpha} A_y^{i-\beta} A_z^{j-\gamma}$$
$$\frac{\partial^{\alpha}}{\partial(ik_1)^{\alpha}} \int du_x \, e^{ik_1 u_x} e^{-a_A^2 u_x^2} e^{-a_D^2 (u_x + AD_x)^2}$$
$$\frac{\partial^{\beta}}{\partial(ik_2)^{\beta}} \int du_y \, e^{ik_2 u_y} e^{-a_A^2 u_y^2} e^{-a_D^2 (u_y + AD_y)^2}$$
$$\frac{\partial^{\gamma}}{\partial(ik_3)^{\gamma}} \int du_z \, e^{ik_3 u_z} e^{-a_A^2 u_z^2} e^{-a_D^2 (u_z + AD_z)^2}$$

The integrals have closed form solutions given by the identity [88],

(7.41)
$$\int dx \, e^{ikx} e^{-ax^2} e^{-b(x+x_o)^2} = \sqrt{\frac{\pi}{a+b}} \, e^{-abx_o^2/(a+b)} \, e^{-k^2/4(a+b)} \, e^{-ikbx_o/(a+b)}$$

Thus, the minor integral takes the form,

$$I_m = \sum_{\alpha=0}^{h}\sum_{\beta=0}^{i}\sum_{\gamma=0}^{j}\binom{h}{\alpha}\binom{i}{\beta}\binom{j}{\gamma} A_x^{h-\alpha} A_y^{i-\beta} A_z^{j-\gamma} \left(\frac{\pi}{b_{AD}^2}\right)^{3/2}$$

(7.42)
$$exp\left\{-\frac{a_A^2 a_D^2}{b_{AD}^2} AD^2\right\} \frac{\partial^{\alpha}}{\partial(ik_1)^{\alpha}} exp\left\{\frac{-k_1^2 - 4ia_D^2 AD_x k_1}{4b_{AD}^2}\right\}$$
$$\frac{\partial^{\beta}}{\partial(ik_2)^{\beta}} exp\left\{\frac{-k_2^2 - 4ia_D^2 AD_y k_2}{4b_{AD}^2}\right\} \frac{\partial^{\gamma}}{\partial(ik_3)^{\gamma}} exp\left\{\frac{-k_3^2 - 4ia_D^2 AD_z k_3}{4b_{AD}^2}\right\}$$

where $b_{AD}^2 \equiv a_A^2 + a_D^2$. By substituting (7.42) into (7.38) twice, the total integral may be written as a lengthy, but important, summation,

$$I = \frac{\Omega}{2\pi^2} \sum_{\alpha,\beta,\gamma\alpha',\beta',\gamma'} \sum \binom{h}{\alpha}\binom{i}{\beta}\binom{j}{\gamma}\binom{l}{\alpha'}\binom{m}{\beta'}\binom{n}{\gamma'} A_x^{h-\alpha} A_y^{i-\beta} A_z^{j-\gamma} B_x^{l-\alpha'} B_y^{m-\beta'} B_z^{n-\gamma'}$$

$$\int d^3k \frac{e^{i\underline{k}\cdot\underline{AB}}}{k^2} \left\{ \frac{\partial^\alpha}{\partial(ik_1)^\alpha} \frac{\partial^\beta}{\partial(ik_2)^\beta} \frac{\partial^\gamma}{\partial(ik_3)^\gamma} exp\left\{ -\frac{k^2 + 4ia_D^2 \underline{k}\cdot\underline{AD}}{4b_{AD}^2} \right\} \right\} \tag{7.43}$$

$$\left\{ \frac{\partial^{\alpha'}}{\partial(-ik_1)^{\alpha'}} \frac{\partial^{\beta'}}{\partial(-ik_2)^{\beta'}} \frac{\partial^{\gamma'}}{\partial(-ik_3)^{\gamma'}} exp\left\{ -\frac{k^2 - 4ia_C^2 \underline{k}\cdot\underline{BC}}{4b_{BC}^2} \right\} \right\}$$

where Ω consolidates the pre-exponentials as

$$\Omega \equiv \frac{\pi^3}{b_{AD}^3 b_{BC}^3} exp\left\{ -\frac{a_A^2 a_D^2}{b_{AD}^2} AD^2 - \frac{a_B^2 a_C^2}{b_{BC}^2} BC^2 \right\} \tag{7.44}$$

As it is written, (7.43) would seem to appear relatively useless. However, notice that it is comprised of derivatives of exponentials, similar to the generating function of the Hermite polynomials [63]. It needs to be stressed that this similarity is strictly due to the use of gaussians as the approximation functions, and is not an indicator of any underlying physics. (Recall that the Hermite polynomials are the general solutions to the harmonic oscillator.) The Hermite polynomials are defined by

$$H_n(x) = (-1)^n e^{x^2} \frac{d^n}{dx^n}\left(e^{-x^2}\right) \tag{7.45}$$

so that some manipulation of (7.43) must be done before the Hermite polynomials may be inserted. First, expand the vector notation into component form and complete the square for each component. Thus,

$$exp\left\{-\frac{k^2+4ia_D^2\underline{k}\cdot\underline{AD}}{4b_{AD}^2}\right\}=exp\left\{-\frac{a_{AD}^4AD_x^2}{b_{AD}^2}\right\}exp\left\{-\left(\frac{k_1+2ia_D^2AD_x}{2b_{AD}}\right)^2\right\}$$

(7.46)
$$exp\left\{-\frac{a_{AD}^4AD_y^2}{b_{AD}^2}\right\}exp\left\{-\left(\frac{k_2+2ia_D^2AD_y}{2b_{AD}}\right)^2\right\}$$

$$exp\left\{-\frac{a_{AD}^4AD_z^2}{b_{AD}^2}\right\}exp\left\{-\left(\frac{k_3+2ia_D^2AD_z}{2b_{AD}}\right)^2\right\}$$

and likewise for the exponential over $\underline{k}\cdot\underline{BC}$. A temporary change of variables is implemented where $\eta_i=(k_i+2ia_D^2\,AD_i)/2b_{AD}$ and $\eta_i'=(k_i-2ia_C^2\,BC_i)/2b_{BC}$. The differentials of (7.43) may then be expressed as

(7.47)
$$\frac{\partial}{\partial(ik_i)}=\frac{\partial\eta_i}{\partial(ik_i)}\frac{\partial}{\partial\eta_i}=\frac{1}{2ib_{AD}}\frac{\partial}{\partial\eta_i}$$

and

(7.48)
$$\frac{\partial}{\partial(-ik_i)}=\frac{\partial\eta_i'}{\partial(-ik_i)}\frac{\partial}{\partial\eta_i'}=\frac{-1}{2ib_{BC}}\frac{\partial}{\partial\eta_i'}$$

The molecular orbital integral (7.43) may then be written as

(7.49)

$$I=\frac{\Omega}{2\pi^2}\sum_{\alpha,\beta,\gamma\alpha',\beta',\gamma'}\binom{h}{\alpha}\binom{i}{\beta}\binom{j}{\gamma}\binom{l}{\alpha'}\binom{m}{\beta'}\binom{n}{\gamma'}A_x^{h-\alpha}A_y^{i-\beta}A_z^{j-\gamma}B_x^{l-\alpha'}B_y^{m-\beta'}B_z^{n-\gamma'}$$
$$\left(\frac{1}{2ib_{AD}}\right)^{\alpha+\beta+\gamma}\left(\frac{-1}{2ib_{BC}}\right)^{\alpha'+\beta'+\gamma'}exp\left\{-\frac{a_D^4}{b_{AD}^2}AD^2-\frac{a_C^4}{b_{BC}^2}BC^2\right\}$$
$$\int d^3k\frac{e^{i\underline{k}\cdot\underline{AB}}}{k^2}\left\{\frac{\partial^\alpha}{\partial(\eta_1)^\alpha}\frac{\partial^\beta}{\partial(\eta_2)^\beta}\frac{\partial^\gamma}{\partial(\eta_3)^\gamma}e^{-\eta_1^2}e^{-\eta_2^2}e^{-\eta_3^2}\right\}$$
$$\left\{\frac{\partial^{\alpha'}}{\partial(\eta_1')^{\alpha'}}\frac{\partial^{\beta'}}{\partial(\eta_2')^{\beta'}}\frac{\partial^{\gamma'}}{\partial(\eta_3')^{\gamma'}}e^{-\eta_1'^2}e^{-\eta_2'^2}e^{-\eta_3'^2}\right\}$$

which simplifies greatly by introducing the Hermite polynomials of the differential operators such that

(7.50)

$$I=\frac{\Omega}{2\pi^2}\sum_{\alpha,\beta,\gamma\alpha',\beta',\gamma'}\binom{h}{\alpha}\binom{i}{\beta}\binom{j}{\gamma}\binom{l}{\alpha'}\binom{m}{\beta'}\binom{n}{\gamma'}A_x^{h-\alpha}A_y^{i-\beta}A_z^{j-\gamma}B_x^{l-\alpha'}B_y^{m-\beta'}B_z^{n-\gamma'}$$
$$\left(\frac{i}{2b_{AD}}\right)^{\alpha+\beta+\gamma}\left(\frac{1}{2ib_{BC}}\right)^{\alpha'+\beta'+\gamma'}$$
$$\int d^3k\frac{e^{-\lambda^2k^2}}{k^2}exp\left\{i\underline{k}\cdot\left[\underline{AB}-\frac{a_D^2}{b_{AD}^2}\underline{AD}+\frac{a_C^2}{b_{BC}^2}\underline{BC}\right]\right\}$$
$$H_\alpha(\eta_1)H_\beta(\eta_2)H_\gamma(\eta_3)H_{\alpha'}(\eta_1')H_{\beta'}(\eta_2')H_{\gamma'}(\eta_3')$$

where $\lambda^2\equiv\frac{1}{4}\left(\frac{1}{b_{AD}^2}+\frac{1}{b_{BC}^2}\right)$. The oscillating portion of the integrand can be written as a vector product, such as

$$\underline{W} \equiv \left\{ \underline{AB} - \frac{a_D^2}{b_{AD}^2}\underline{AD} + \frac{a_C^2}{b_{BC}^2}\underline{BC} \right\}$$

(7.51)

$$= \left\{ \frac{a_A^2 \underline{A} + a_D^2 \underline{D}}{b_{AD}^2} - \frac{a_B^2 \underline{B} + a_C^2 \underline{C}}{b_{BC}^2} \right\}$$

where the second line exhibits the inherent symmetry. This leaves the integration in a reasonably simple form,

$$I = \frac{\Omega}{2\pi^2} \sum_{\alpha,\beta,\gamma} \sum_{\alpha',\beta',\gamma'} \binom{h}{\alpha}\binom{i}{\beta}\binom{j}{\gamma}\binom{l}{\alpha'}\binom{m}{\beta'}\binom{n}{\gamma'} A_x^{h-\alpha} A_y^{i-\beta} A_z^{j-\gamma} B_x^{l-\alpha'} B_y^{m-\beta'} B_z^{n-\gamma'}$$

(7.52)

$$\left(\frac{i}{2b_{AD}}\right)^{\alpha+\beta+\gamma} \left(\frac{1}{2ib_{BC}}\right)^{\alpha'+\beta'+\gamma'} \int d^3k \frac{e^{-\lambda^2 k^2}}{k^2}$$

$$H_\alpha(\eta_1) H_\beta(\eta_2) H_\gamma(\eta_3) H_{\alpha'}(\eta_1') H_{\beta'}(\eta_2') H_{\gamma'}(\eta_3') exp\{i\underline{k} \cdot \underline{W}\}$$

The key is to recall that the Hermite polynomials may be represented as differential operators.

In (7.52) the Hermite polynomials are a function of the variables η , which are linearly related to the integration variable. It is possible to use the phase term, $e^{i\underline{k}\cdot\underline{W}}$, and convert the partial derivatives with respect to k into partial derivatives with respect to W. The resulting integral has a closed form solution. This is perhaps the most important trick in the entire derivation because it totally eliminates the need for numerical integration. Furthermore, the original problem is reduced to a closed form solution.

Specifically, in (7.52) the Hermite polynomials are imposed upon the phase factor as such

$$H_\alpha(\eta_i)e^{i\underline{k}\cdot\underline{W}} = H_\alpha\left(\frac{k_i + 2ia_D^2 AD_i}{2b_{AD}}\right)e^{i\sum k_i W_i}$$

(7.53)

$$= H_\alpha\left(\frac{\partial/\partial(iW_i) + 2ia_D^2 AD_i}{2b_{AD}}\right)e^{i\underline{k}\cdot\underline{W}}$$

Thus by converting all the Hermite polynomials from a function of the integration variable, $\underline{k}$, to a function of the constant, $\underline{W}$, they may then be pulled through the integration. This leaves the integration term of (7.52) in the form,

(7.54) $$\int d^3k\, e^{i\underline{k}\cdot\underline{W}}\frac{e^{-\lambda^2 k^2}}{k^2} = \frac{2\pi^2}{W}erf\left(\frac{W}{2\lambda}\right)$$

The importance of (7.54) cannot be overstated, and the proof is given in Appendix III. To simplify the algebra, it would be advantageous to define a vector $\underline{T} \equiv \underline{W}/2\lambda$. Furthermore, note that for $T = \sqrt{T_1^2 + T_2^2 + T_3^2}$ the partial derivatives may be written as

$$\frac{\partial}{\partial T_i} = \frac{\partial T_i}{\partial T}\frac{\partial}{\partial T}$$

(7.55)

$$= \frac{T_i}{T}\frac{\partial}{\partial T}$$

which allows the differentiation to be simplified. However, the arguments of the Hermite operator are proportional to the logarithmic derivative, $\partial T/T$. To eliminate this, a final transformation is made, defining $U \equiv T^2$, which cleans up the differentiation. The final result is

(7.56)

$$I = \frac{\Omega}{2\lambda} \sum_{\alpha,\beta,\gamma} \sum_{\alpha',\beta',\gamma'} \binom{h}{\alpha}\binom{i}{\beta}\binom{j}{\gamma}\binom{l}{\alpha'}\binom{m}{\beta'}\binom{n}{\gamma'} A_x^{h-\alpha} A_y^{i-\beta} A_z^{j-\gamma} B_x^{l-\alpha'} B_y^{m-\beta'} B_z^{n-\gamma'}$$
$$\left(\frac{i}{2b_{AD}}\right)^{\alpha+\beta+\gamma} \left(\frac{1}{2ib_{BC}}\right)^{\alpha'+\beta'+\gamma'}$$
$$H_\alpha\left[\frac{T_1}{2i\lambda b_{AD}}\partial_U + \frac{ia_D^2}{b_{AD}} AD_x\right] H_\beta\left[\frac{T_2}{2i\lambda b_{AD}}\partial_U + \frac{ia_D^2}{b_{AD}} AD_y\right]$$
$$H_\gamma\left[\frac{T_3}{2i\lambda b_{AD}}\partial_U + \frac{ia_D^2}{b_{AD}} AD_z\right] H_{\alpha'}\left[\frac{T_1}{2i\lambda b_{BC}}\partial_U - \frac{ia_C^2}{b_{BC}} BC_x\right]$$
$$H_{\beta'}\left[\frac{T_2}{2i\lambda b_{BC}}\partial_U - \frac{ia_C^2}{b_{BC}} BC_y\right] H_{\gamma'}\left[\frac{T_3}{2i\lambda b_{BC}}\partial_U - \frac{ia_C^2}{b_{BC}} BC_z\right]$$
$$\frac{erf\sqrt{U}}{\sqrt{U}}$$

At first glance, (7.56) would not appear to be computationally useful, due to the ungainly combination of Hermite polynomials having differential operators as arguments. Clearly, this is not a functional form handled by most standard programming languages. It is possible, at least theoretically, to evaluate (7.56) for each set of exponents $\{h,i,j,l,m,n\}$ by manually computing the derivatives. Since the Ar-N_2 system uses atomic orbitals through 2p, the highest power of a spatial coordinate for any orbital is one. The exponents $\{h,i,j,l,m,n\}$ of the original integration (7.29) refer to the sum of the powers for a given spatial coordinate, hence any given exponent must be restricted to the range $0 \le exponent \le 2$. This would seem to give $3^6 = 729$ possibilities. However, the sum of the exponents of the primed or the unprimed integration variable is also limited to the range $0 \le \sum exponent \le 2$, which limits the possible combinations to exactly 100. It is an understatement to state that manually obtaining 100 closed form expressions for (7.56) would be a non-trivial task.

One method to obtain the derivatives is to use a symbolic manipulator to calculate a closed form for each of the 100 sets of relevant exponents. The *Mathematica* package [85] was used to solve (7.56) for two key reasons: the first is the ability to generate the Hermite polynomials with differential operators as arguments, and the second was the ability of *Mathematica* to generate FORTRAN77 code from internal expressions.

While the latter capability is extremely desirable, it was the former capability which provided the novel approach to difficult numerical problem solving. The first step in achieving a solution was to literally "teach" *Mathematica* how to evaluate Hermite polynomials with the unusual characteristic of having differential operators for arguments. This would have been a near impossible task for most standard high-level programming languages. The second step, the generation of FORTRAN77 code, was merely a mechanical action, albeit a very useful one.

The *Mathematica* script used to solve (7.56) is presented in Figure 7.12. With the exception of a few parameters, the script directly mimics (7.56). Note that in the script, λ is replaced by the variable alpha, the summation variables $\alpha', \beta',$ and γ' were renamed as δ, ε, and η, and the exponent h was replaced with f. It is quite an amazing feat that roughly 20 lines of script generated over 8,000 lines of FORTRAN77 source code.

Transition Amplitude

The exact form of the transition amplitude for electron exchange was defined in (7.21). This form was numerically evaluated using the results of (7.21) and (7.56), and the geometrical reference frame discussed above. Note that, as written, the transition amplitude is a function of six independent variables: three to translate from the N_2 frame to the Ar frame, and three to rotate the Ar within its frame. Furthermore, the spatial

```
ip[f_, i_, j_, l_, m_, n_, g_][u] :=
  FortranForm[
  Collect[Collect[Factor[Sum[Binomial[f, alp]*Binomial[i, bet]*
       Binomial[j, gam]*Binomial[l, del]*Binomial[m, eps]*Binomial[n, eta]*
       ax^(f - alp)*ay^(i - bet)*az^(j - gam)*bx^(l - del)*by^(m - eps)*
       bz^(n - eta)*(I/(2*bAD))^(alp + bet + gam)*
       (1/(2*I*bBC))^(del + eps + eta)*
       h[alp, t1/(2*I*alpha*bAD), (I*aD^2*adX)/bAD,
         h[bet, t2/(2*I*alpha*bAD), (I*aD^2*adY)/bAD,
          h[gam, t3/(2*I*alpha*bAD), (I*aD^2*adZ)/bAD,
           h[del, t1/(2*I*alpha*bBC), -((I*aC^2*bcX)/bBC),
            h[eps, t2/(2*I*alpha*bBC), -((I*aC^2*bcY)/bBC),
             h[eta, t3/(2*I*alpha*bBC), -((I*aC^2*bcZ)/bBC), g]]]]]][u],
      {alp, 0, f}, {bet, 0, i}, {gam, 0, j}, {del, 0, l}, {eps, 0, m},
      {eta, 0, n}]], Exp[u]], Erf[Sqrt[u]]]
   ]

g[u] := Erf[Sqrt[u]]/Sqrt[u]

h[n_, c1_, c2_, g_][u] :=
  Sum[coef[n, s]*Binomial[n - 2*s, i]*c2^(n - 2*s - i)*c1^i*D[g[u], {u, i}],
   {s, 0, Floor[n/2]}, {i, 0, n - 2*s}]

coef[n_, s_] := ((-1)^s*2^(n - 2*s)*n!)/((n - 2*s)!*s!)
```

Figure 7.12 Mathematica Script Used to Calculate Two-Electron Integrals

dependence of the transition amplitude arises solely from the amplitude terms, V_{abcd}, of (7.21).

Conceptually, the evaluation consisted of several steps. Given that the N_2 molecule was fixed in space with the internuclear axis coincident to the z axis, a location in space was chosen for the center of the Ar atom. The coordinate axes of the Ar frame were then positioned commensurate with those of the N_2 frame. The interaction amplitudes of (7.21), i.e. the coulomb-like and exchange-like amplitudes, were then determined for the defined configuration. To reduce the transition amplitude to a function of three variables, a rotational average was carried out over the three degrees of freedom associated with the position of the Ar atom within the Ar reference frame. As discussed in Chapter 4, the p orbitals constitute a basis set, such that any rotational configuration may be determined by a rotational transformation from the reference configuration. The rotational average assumed that each configuration was equally probable.

The evaluation took place on an evenly spaced cubic grid. The grid was 8 Angstroms on each side, with 39 grid points in each direction. Because the evaluation of (7.21) at 39x39x39 points was anticipated to require significant amounts of computer time, the main grid was broken into 8 subcubes of 20x20x20 grid points, having the same spacing as the main grid. The solution of (7.21) in each of the subcubes was done by a suite of workstation-class computers in both a scalar and distributed mode of operation.

The scalar code was a straightforward application of FORTRAN77 to equations (7.21), (7.27), and (7.56). As mentioned above, the solution to (7.56) was written as FORTRAN77 by *Mathematica*. The code was placed into a subroutine which was called at every iteration of (7.27). The complete interaction was accomplished by two evaluations of (7.56) at each iteration of (7.27), one for each of the coulomb-like and

exchange-like terms. The rotational averaging was done by applying a rotational transformation algorithm using the Euler angles, as in Goldstein [84].

The early calculations were done on an IBM RS6000 Model 340 workstation. It was discovered that each grid point required roughly 95 CPU seconds, indicating that a subcube with 8000 points would require 760,000 CPU seconds, or 8.8 CPU days. At that point, the code was reformulated using the Express [89] distributed computing software package. This commercial package is a high-level message-passing scheme which resembles the structure of a FORTRAN subroutine library. Function calls are made to Express subroutines to establish the computational topography, and to transfer data between computational nodes. This code was written under the master-slave paradigm. Thus, a main workstation is the master and is responsible for distributing data to the computational nodes, one of which may be the master itself. Each of the nodes is capable of responding to the needs of the other nodes by communication performed by the master. The main drawback of any distributed computing effort is the increased amount of network communication required to perform the task. However, the solution of (7.21) was ideally suited for distributed computing since it was a local evaluation, i.e. the solution of (7.21) at one grid point did not require any information from any other grid point.

A cluster of four IBM RS6000 workstations (Model Numbers 340, 320H, and two 320s) was used to solve five of the eight subcubes. Table 7.7 lists the required CPU time involved for each subcube calculation. The aggregate performance of the cluster may be estimated at approximately 43 MFLOPS (Million Floating Point Operations per Second, is one of many estimates of computer performance) by summing together the MFLOPS of each node. Obviously, that value is purely theoretical since communication between nodes degrades computational performance. The actual performance of the cluster was not closely monitored, but it is believed to be near the theoretical "linear

Table 7.7 Perfomance of Computational Environment in Calculating the Ar-N_2 Transition Amplitude

Subcube #	Computer	Technique	MFLOPS	Aggregate CPU Time (Seconds)	Wall Time (Days)
1	Cluster	Distributed with equal loading	<43>	1,042,000	3.5
2	a) DEC Alpha b) SGI Indigo	a) Scalar b) Scalar		856,695	9.9
3	a) Cluster b) IBM 340	a) Distributed with equal loading b) Scalar	a) <43> b) 15	1,012,551	2.9
4	Cluster	Distributed with dynamic loading	<43>	1,023,603	2.9
5	a) IBM 320 b) SGI Indigo	a) Scalar b) Scalar	a) 15 b)	1,237,320	14.3
6	Cluster	Distributed with dynamic loading	<43>	1,030,382	3.0
7	SGI Indigo	Scalar		~500,000	5.8
8	Cluster	Distributed with dynamic loading	<43>	1,041,090	3.0

speedup." Typical wall clock times for computing a subcube were on the order of 3.5 days for an equally distributed load.

Also noted in Table 7.7 is the technique used in the distributed computing. Initially, the subcube was solved assuming a uniform computational topography, in that each node received an equal share of work. Due to the performance differences in the four workstations that comprised the cluster, this meant that the fastest workstation (the Model 340) would finish much quicker than the slowest workstation (the Model 320). Hence, the Model 340 would be idle until the Model 320 finished. To alleviate this discrepancy, a dynamic load balancing scheme was devised in which the cluster solved the subcube by sequentially computing two-dimensional planes. At the conclusion of each plane, the workstations were polled to determine their relative performance. Based upon the polling, the next two-dimensional plane was partitioned across the four nodes. Note that, in addition to dynamic load leveling, this technique also accounted for the potential loss of performance of a workstation due to time sharing with an outside user. The dynamic load balancing decreased the wall clock time required to run a subcube from roughly 3.5 days to approximately 3.0 days. It should be noted that these figures are for comparison only. The effect of network traffic upon cluster performance was not quantified. In contrast to a scalar code, the CPU time quoted for a distributed code inherently includes the effects of variations in network performance during the code operation.

The scalar version of the code figured prominently in the overall calculation, accounting for the solution of 3 subcubes. The workstations which ran the scalar code were outside the configured cluster and were used simultaneously with the cluster to bring the overall calculation to a close. Note that several subcubes utilized two machines for calculation. The code was written with a re-start capability, and as the faster machines became available, the job was migrated, by hand, from the slower machine to a

faster one. For instance, the calculation of subcube #2 on a DEC Alpha Model 500 was estimated to require ~20 days, since the time required for each grid point was 225 CPU seconds. The CPU time required per grid point using the SGI Indigo with the R4400 chip was found to be 60 CPU seconds. By starting the calculation of subcube #2 on the DEC Alpha Model 500 and finishing the calculation on the SGI Indigo, the average time required per grid point was reduced to 107 CPU seconds.

The final step in the calculation of (7.21) was to assemble all of the subcubes into the main grid. This grid constituted the complete spatial dependence of the transition amplitude for the electron exchange process.

Scattering Cross Section

Once the transition amplitude was evaluated at each of the grid points, the scattering matrix in the Born approximation, (5.67), was calculated. Following from the derivation of the transition amplitude in combined Fock and coordinate space, the scattering matrix takes the explicit form,

$$T_{\beta\alpha}(\underline{k}_\alpha - \underline{k}_\beta) = \int d\underline{r}\ \frac{e^{i(\underline{k}_\alpha - \underline{k}_\beta)\cdot\underline{r}}}{(2\pi)^3}\langle\beta|\, H'(\underline{r})\,|\alpha\rangle \tag{7.57}$$

where the Fock states are given as in (7.6) and (7.7) Hence, from a kinematic viewpoint, the plane waves describe a heavy system particle of mass $\mu = 10.67$ amu, or 1.89×10^4 times the electron mass. Note that in the Born approximation, the momentum transfer between the collision partners falls naturally out of (7.57), and the scattering matrix is independent of the initial or final collision momentum.

The clear advantage of the Born approximation, in this study, was manifested by the fact that the scattering matrix was an FFT of the transition amplitude, with the proper scale factors. The FFT is a very computationally efficient algorithm, and one implementation was found in the commercial data analysis software, PV-Wave [90].

Another amenity of the PV-Wave algorithm was that it performed the FFT over an arbitrary number of dimensions, which avoided some lengthy FORTRAN coding. For this study, the original 39x39x39 potential grid was interpolated to a 32x32x32 grid to aid in the manipulation of the resultant scattering matrix grid. The potential grid was also interpolated to a 156x156x156 grid to check the numerical stability of the FFT. Once the scattering matrix was determined, the appropriate factors were applied to obtain the differential cross section, (AI.18).

The evaluation of the total scattering cross section was done by numerical quadrature of the differential scattering cross section on shells of constant momentum transfer. Since the differential scattering cross section was defined upon a three-dimensional Cartesian grid, the numerical integration used a three-dimensional linear interpolation scheme to obtain values at specified momentum shell values. This step was done with FORTRAN77.

Chapter 8

Computational Results

The result of computing the transition amplitude (7.21) provides a very rich three-dimensional potential for the Ar-N_2 interaction. For large separations between the Ar and N_2, the interaction mimics the coulomb potential between localized atomic Ar and N_2 molecular orbitals. As the Ar approaches the N_2, the orbitals begin to overlap, and this is reflected by the appearance of a deep well structure in the interaction potential. For small distances between the Ar and N_2, the interaction resembles a three-dimensional spherical well. A crude model of the potential as a spherical well supports the analysis and provides a qualitative understanding of the interaction. The results of computing the differential cross section using the first Born approximation are discussed. A correlation is made between the features of the differential cross section and the total transition amplitude. Finally, the differential cross section is integrated over the angular variables, and the total cross section is obtained as a function of the momentum transferred during the collision. It was found that this computational result is within a factor of 2 of the lowest measured cross section, and within a factor of 5 of the average of the experimental measurements.

Transition Amplitude

Format of Solution

The coordinate system used for the calculation of the total transition amplitude was given in Figure 7.2. Because the dependence of the total transition amplitude upon the relative orientation of the Ar coordinate system was removed, this same coordinate

system represents the solution space for the calculation, as well. Note that quite often the vector space defined by the set of reaction coordinates does not necessarily correspond to actual configuration space. Although the registration of the solution space with the configuration space will aid in the interpretation of the data, it is important to realize that the two are distinct.

Since the total transition amplitude is dependent upon three dimensions, conveying the results, in an intelligible format, is a rather awkward process. The solution space consists of the total transition amplitude of the Ar-N_2 system for a set of separation vectors. Thus, each location in the solution space corresponds to an energy of interaction that is observed in the physical system when the Ar and N_2 have the same separation vector. The approach taken here is to display two-dimensional cuts, or sheets, through the solution space across planes of constant z value. The sheets are displayed as surface maps, in which the x and y axes of the map correspond to the physical x, y plane, and the z axis of the map corresponds to the total transition amplitude, measured in atomic energy units, at that particular point. For example, Figure 8.1 is a sheet of the total transition amplitude for $z = -18.89$ au. Thus, each point on the map corresponds to the energy of interaction between the Ar and N_2 in physical space, when separated by a vector corresponding to the coordinates of the mapping. In other words, this map represents the interaction when the Ar is confined to move in a plane specified by $z = -18.89$ au, and the N_2 is fixed with its internuclear midpoint at the origin.

Numerical Results

Figures 8.2 through 8.32 complete the entire set of z sheets for the interaction. A mental assimilation of all 32 sheets leads to a reconstruction of the three-dimensional interaction. It is interesting to note the gentle, symmetric features of Figure 8.1.

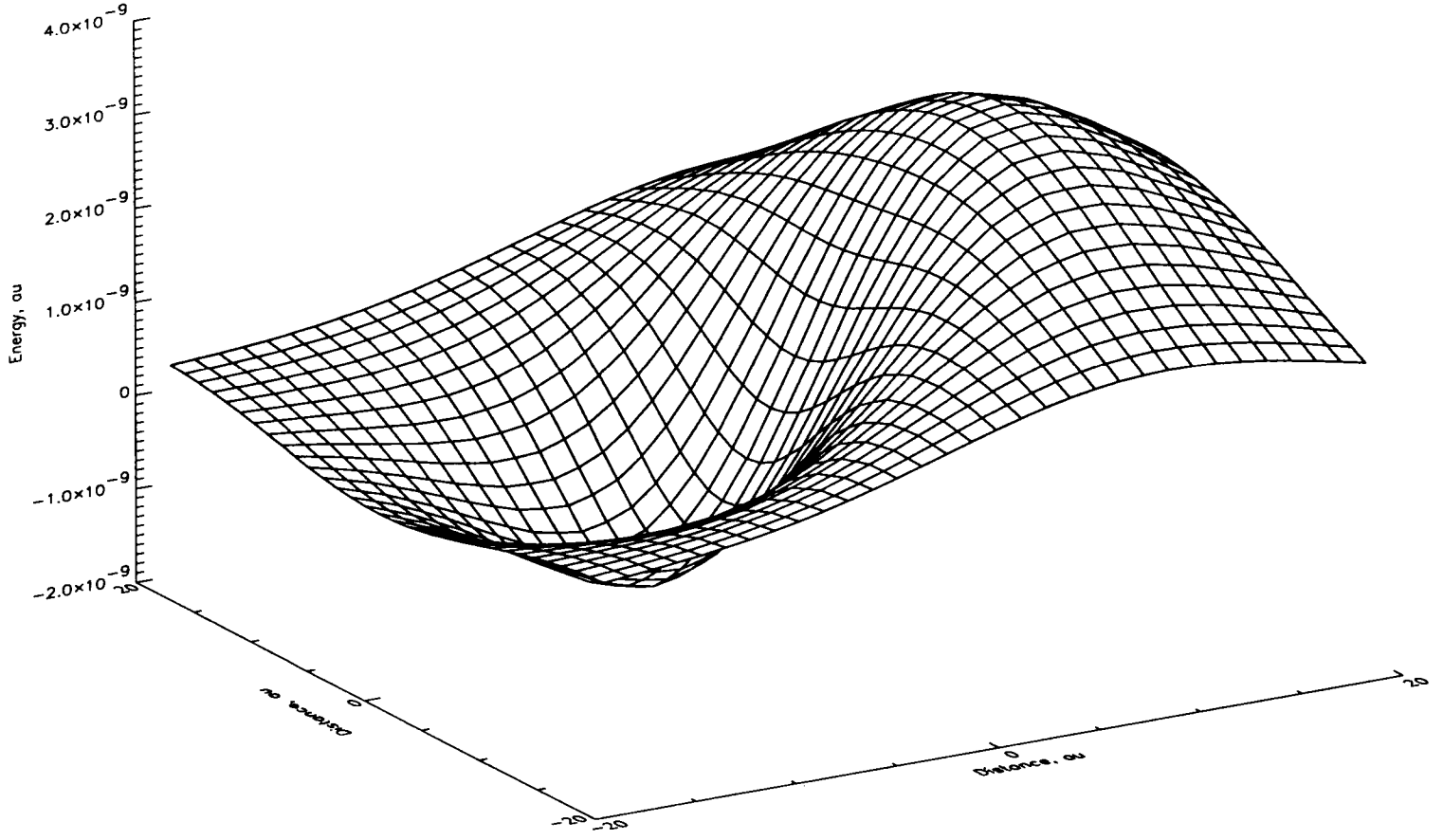

Figure 8.1 Total Transition Probability Amplitude for z = -18.90 au

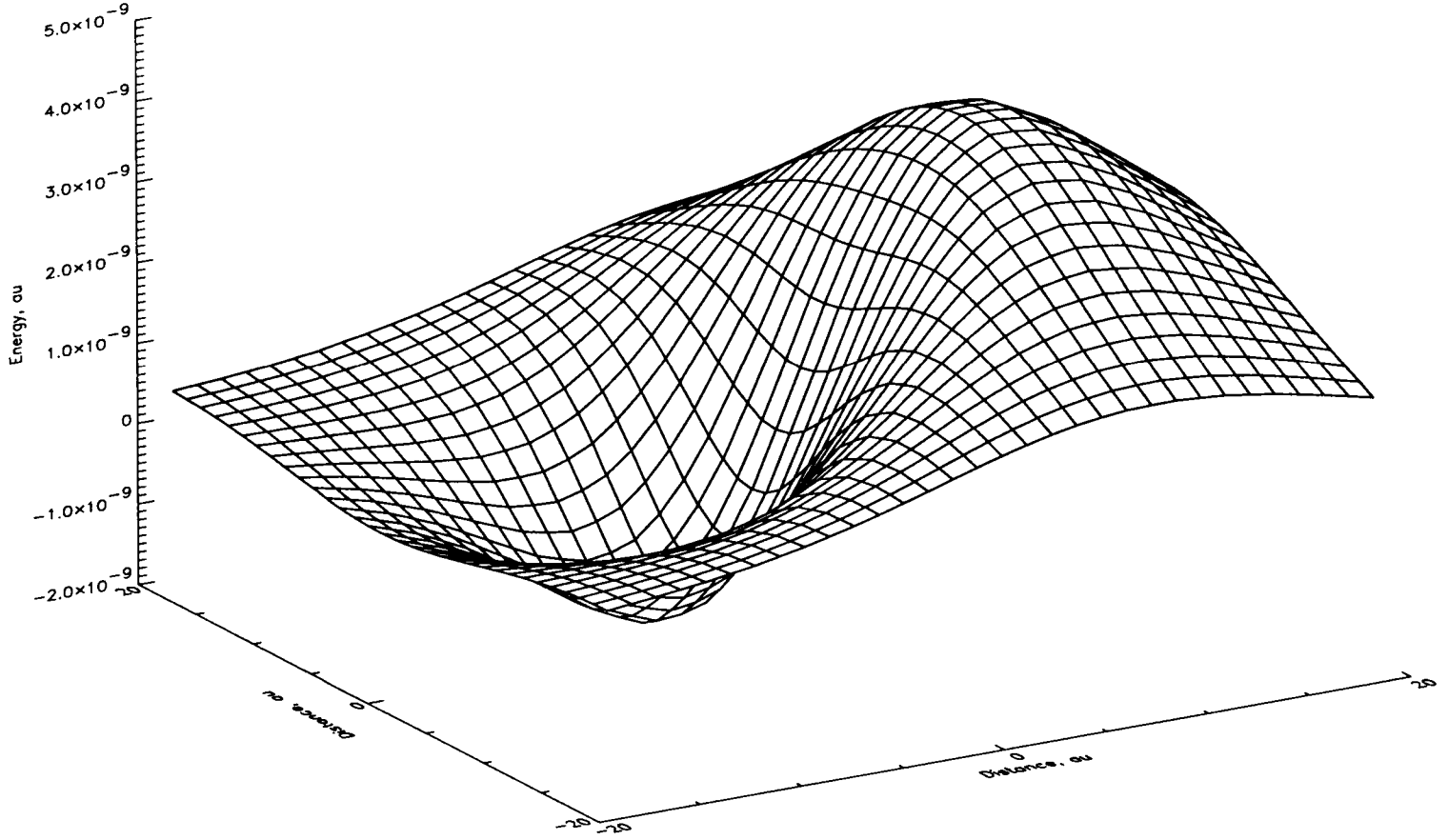

Figure 8.2 Total Transition Probability Amplitude for z = -17.68 au

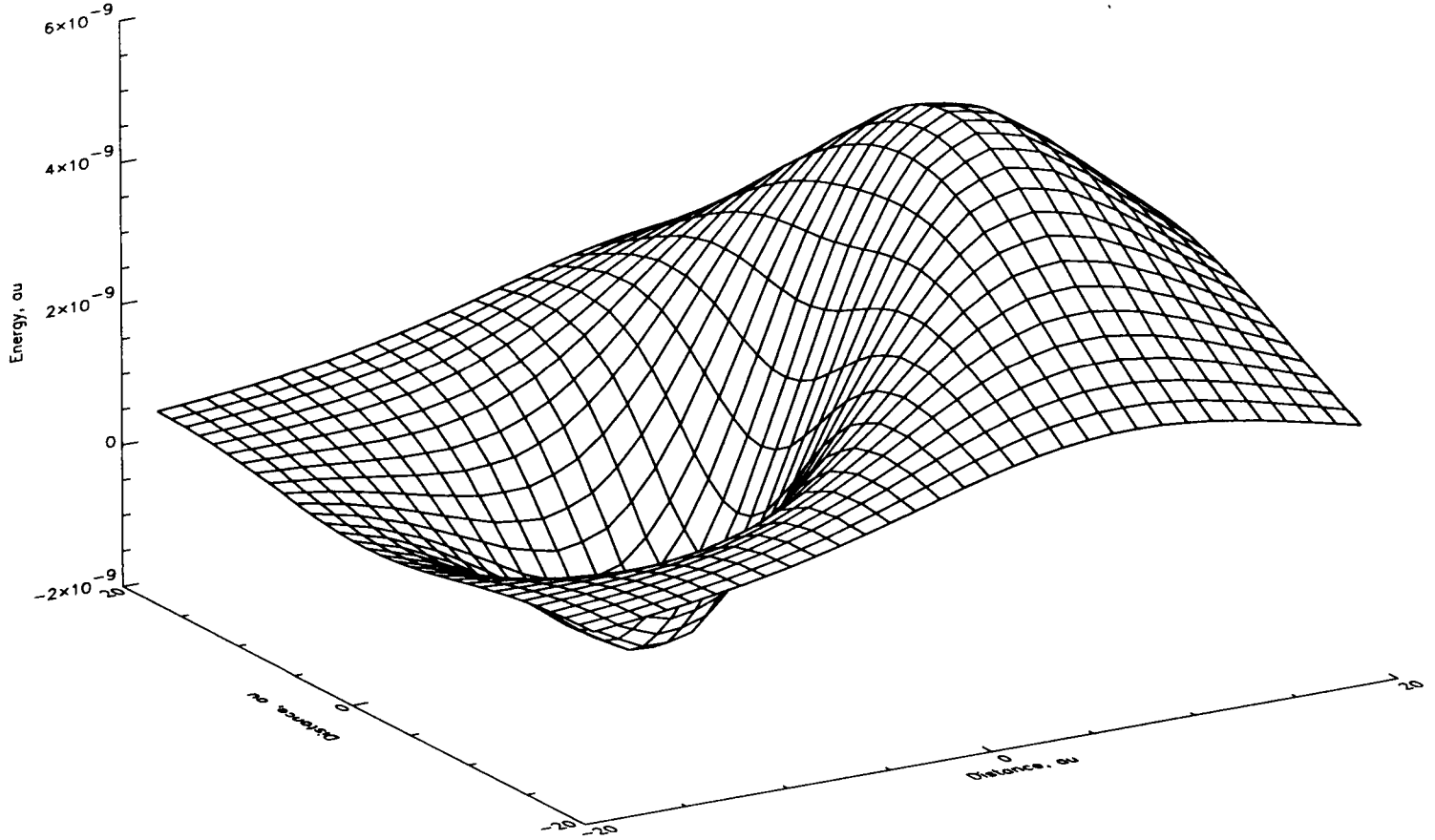

Figure 8.3 Total Transition Probability Amplitude for z = -16.46 au

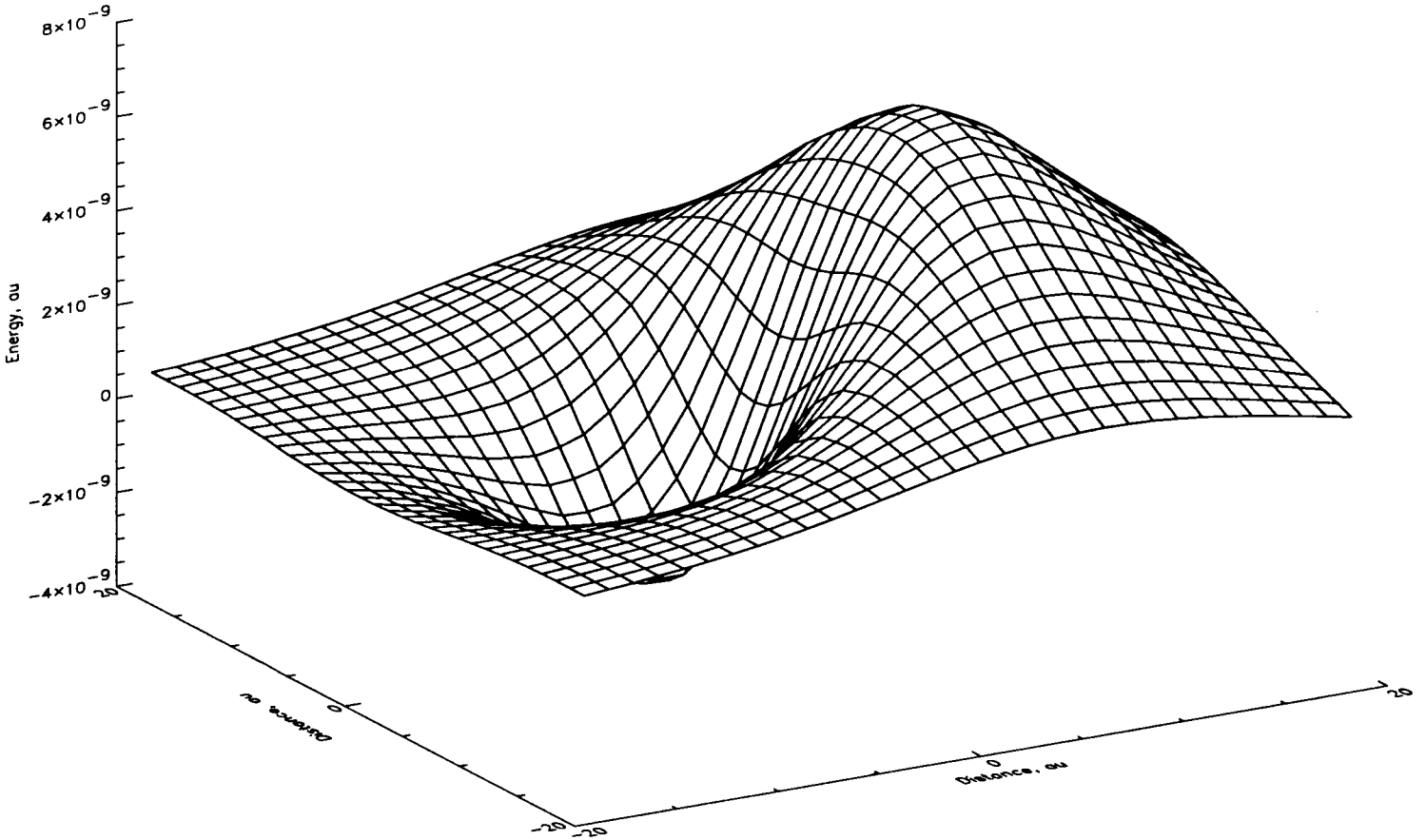

Figure 8.4 Total Transition Probability Amplitude for z = -15.24 au

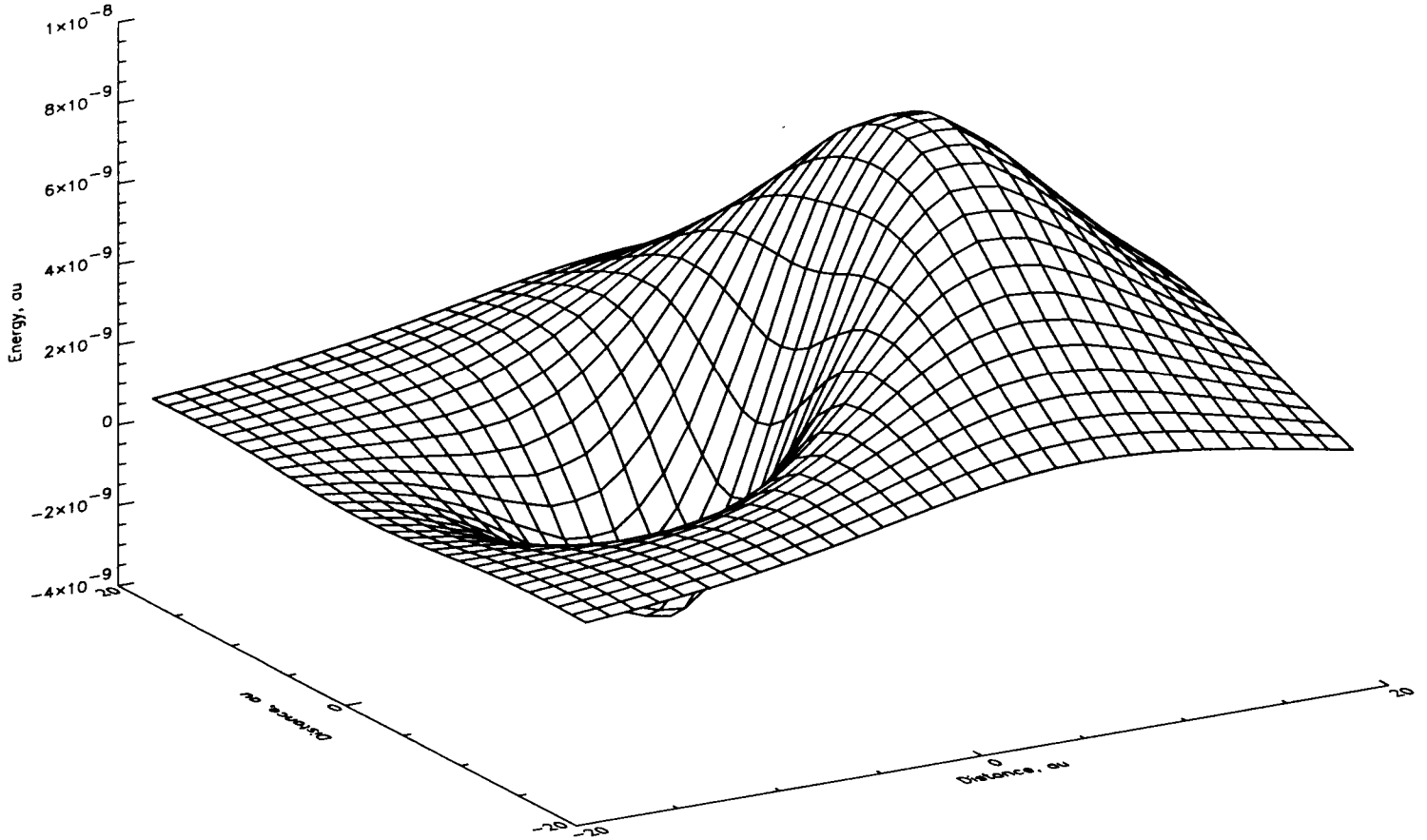

Figure 8.5 Total Transition Probability Amplitude for z = -14.02 au

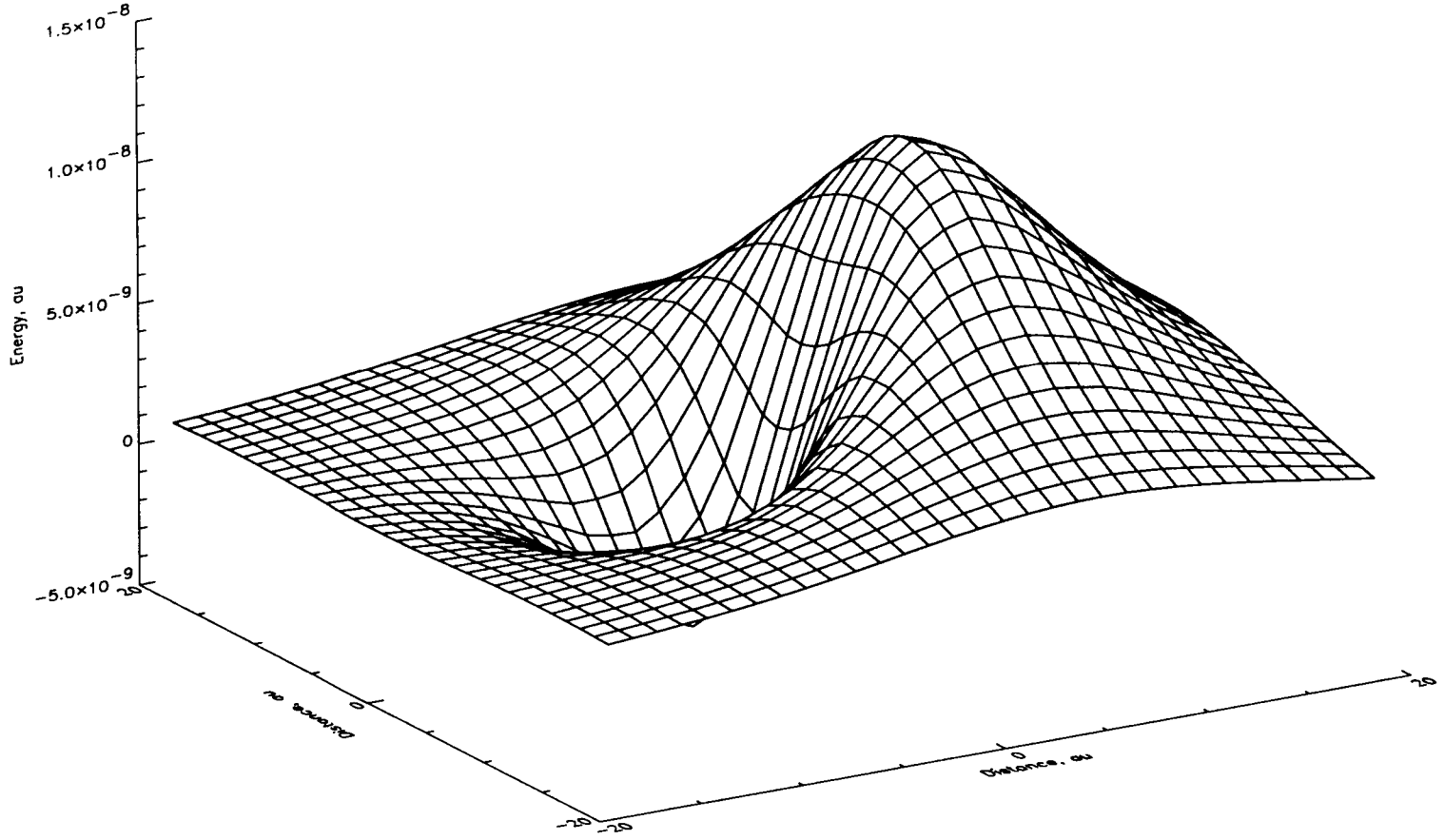

Figure 8.6 Total Transition Probability Amplitude for z = -12.80 au

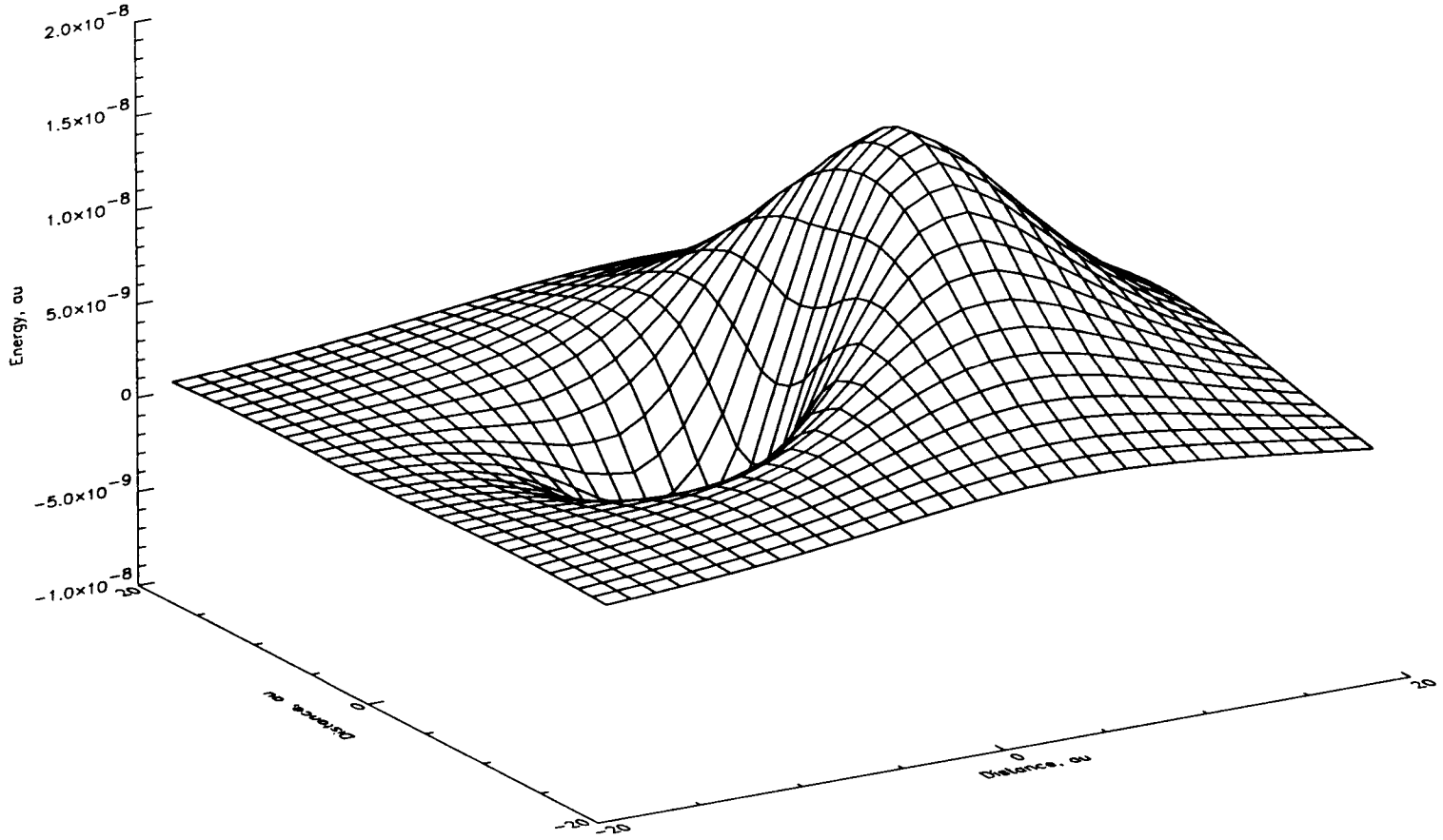

Figure 8.7 Total Transition Probability Amplitude for z = -11.58 au

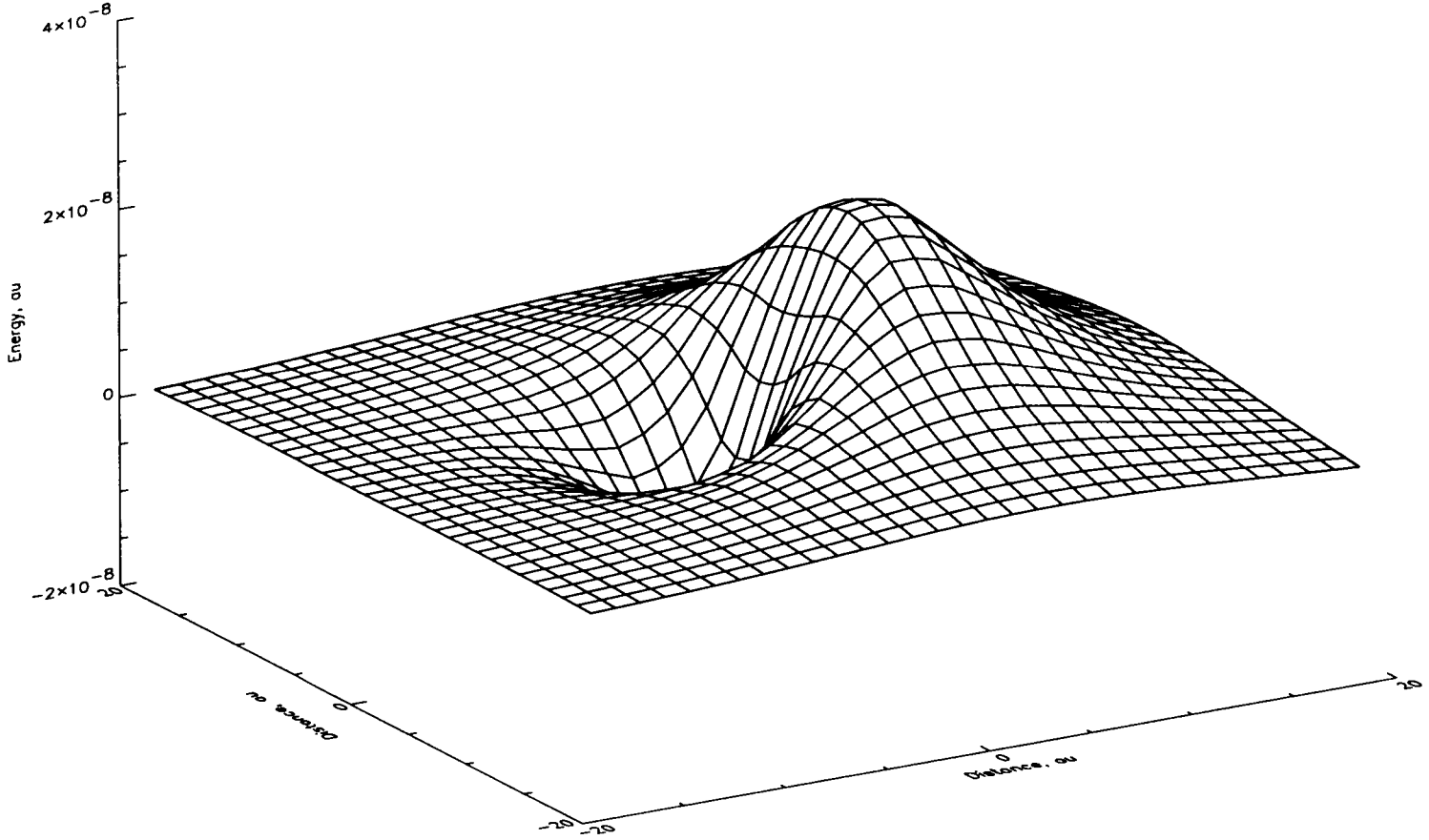

Figure 8.8 Total Transition Probability Amplitude for z = -10.36 au

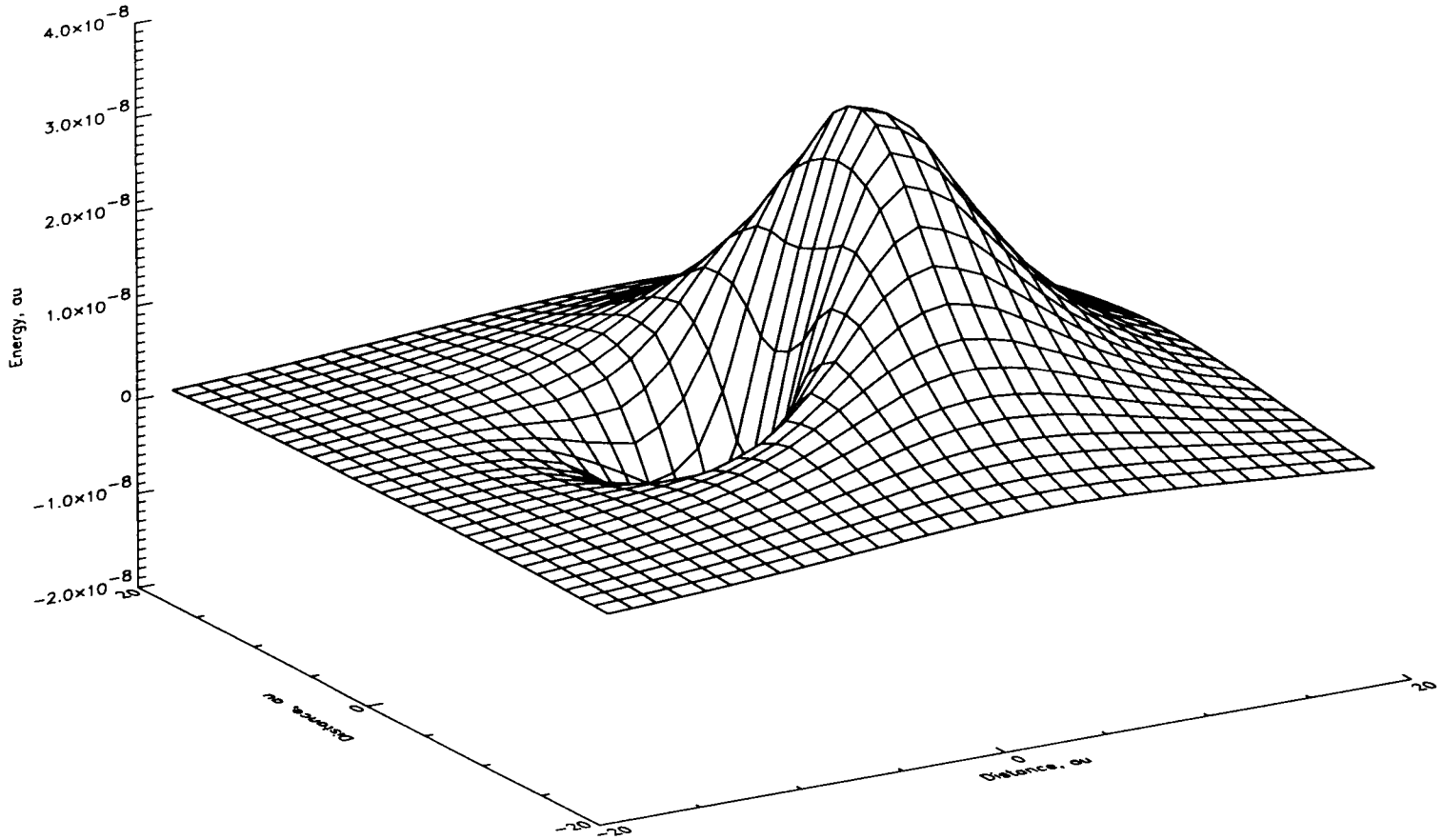

Figure 8.9 Total Transition Probability Amplitude for z = -9.14 au

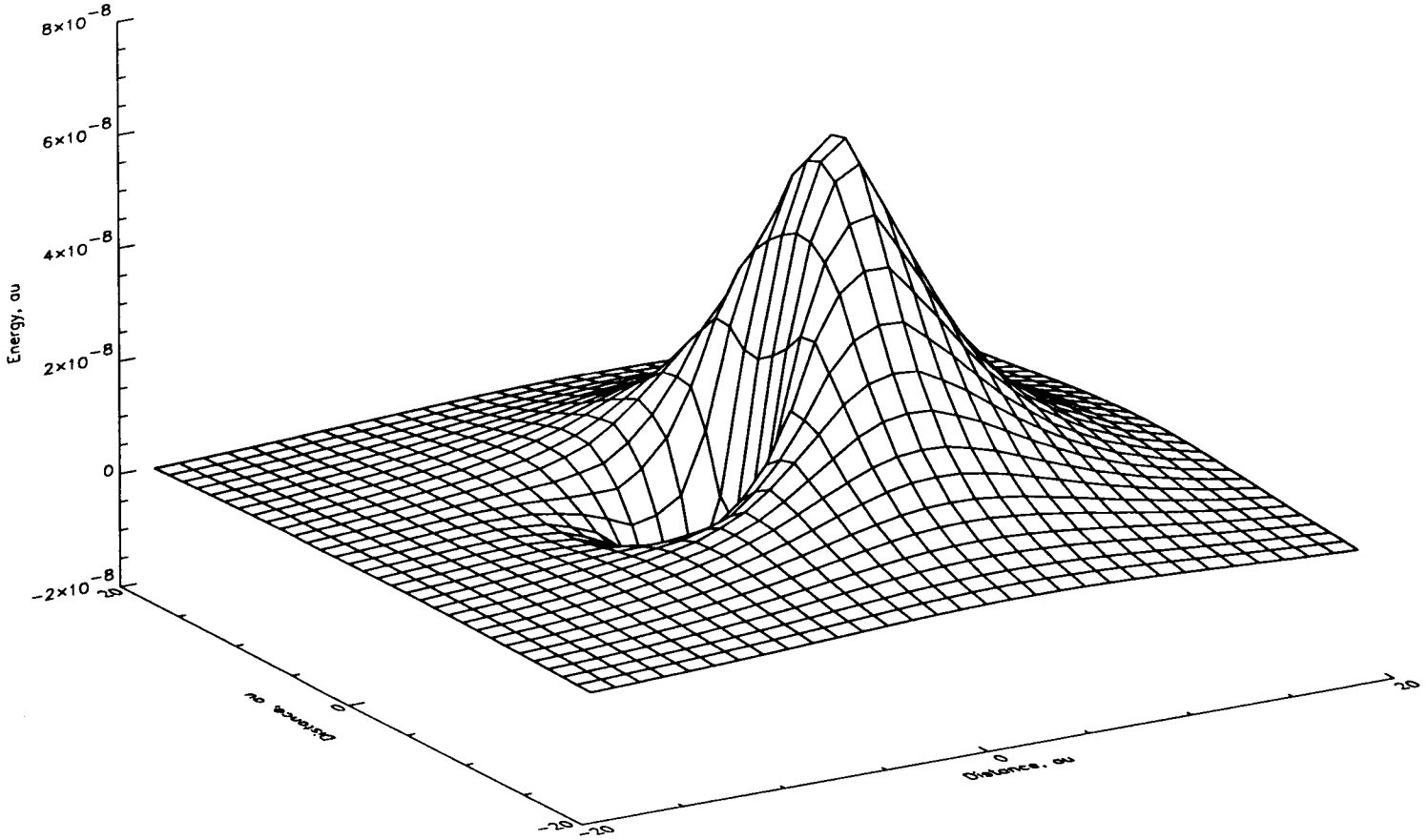

Figure 8.10 Total Transition Probability Amplitude for z = -7.92 au

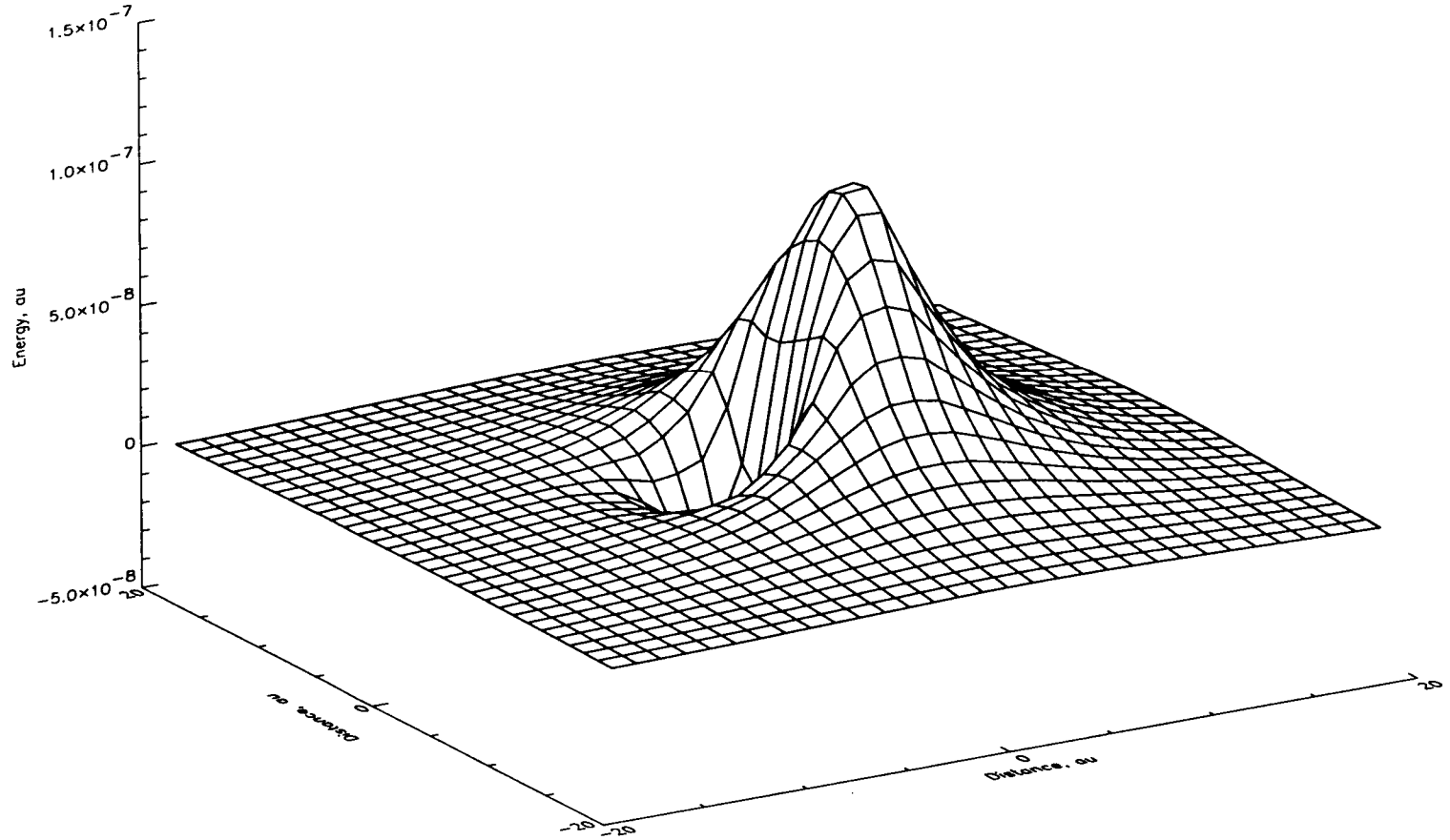

Figure 8.11 Total Transition Probability Amplitude for z = -6.71 au

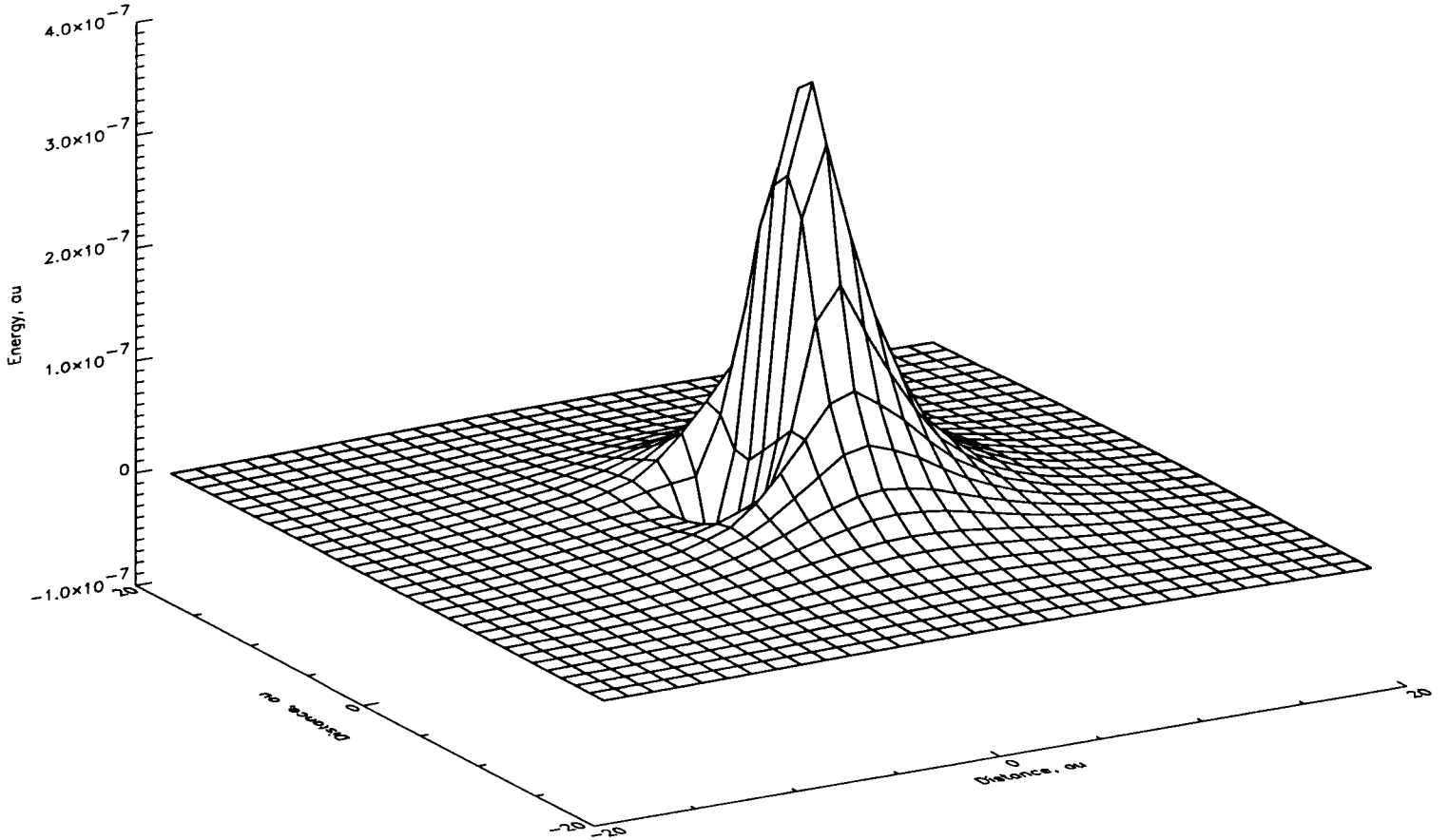

Figure 8.12 Total Transition Probability Amplitude for z = -5.49 au

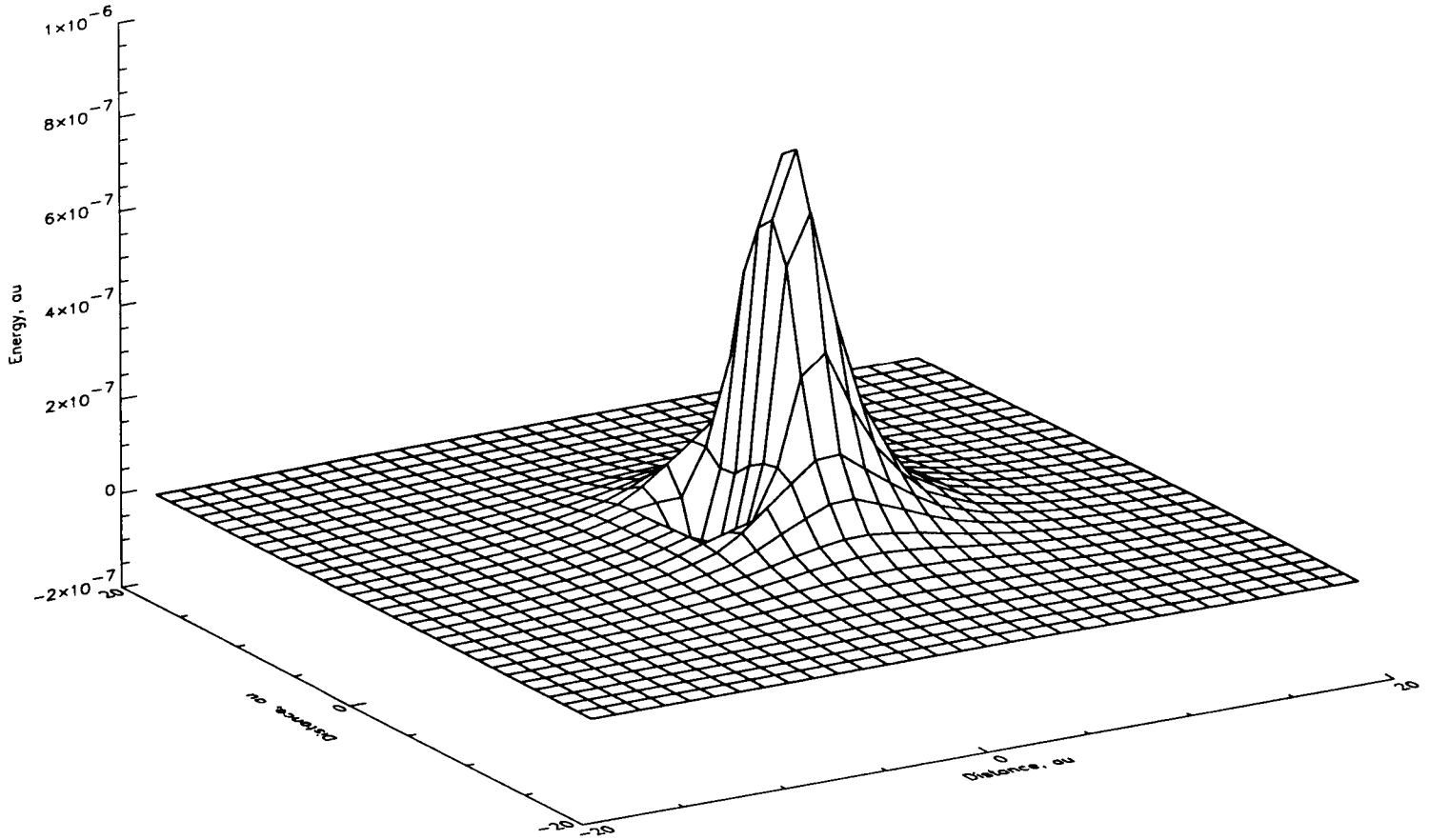

Figure 8.13 Total Transition Probability Amplitude for z = -4.27 au

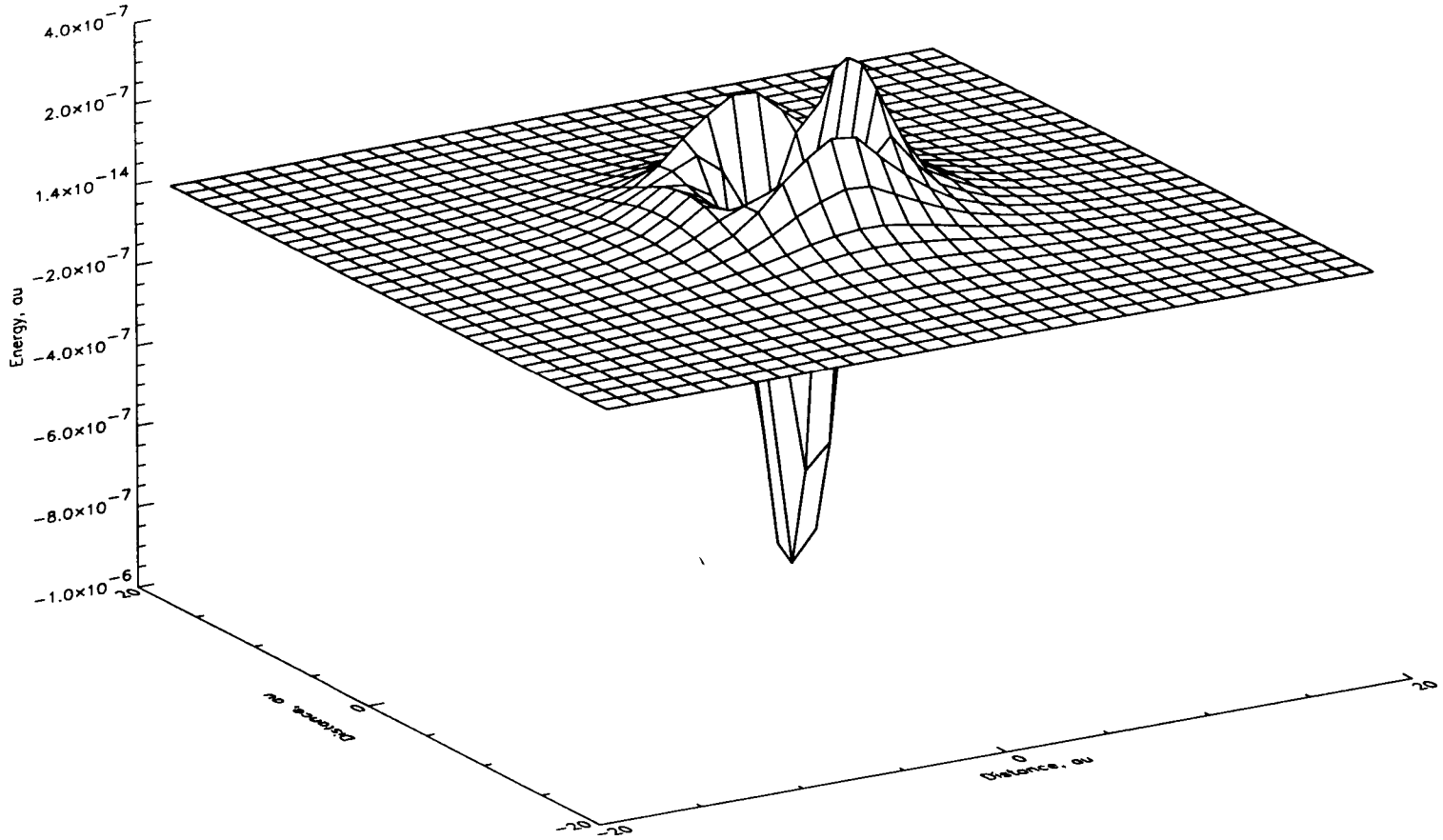

Figure 8.14 Total Transition Probability Amplitude for z = -3.05 au

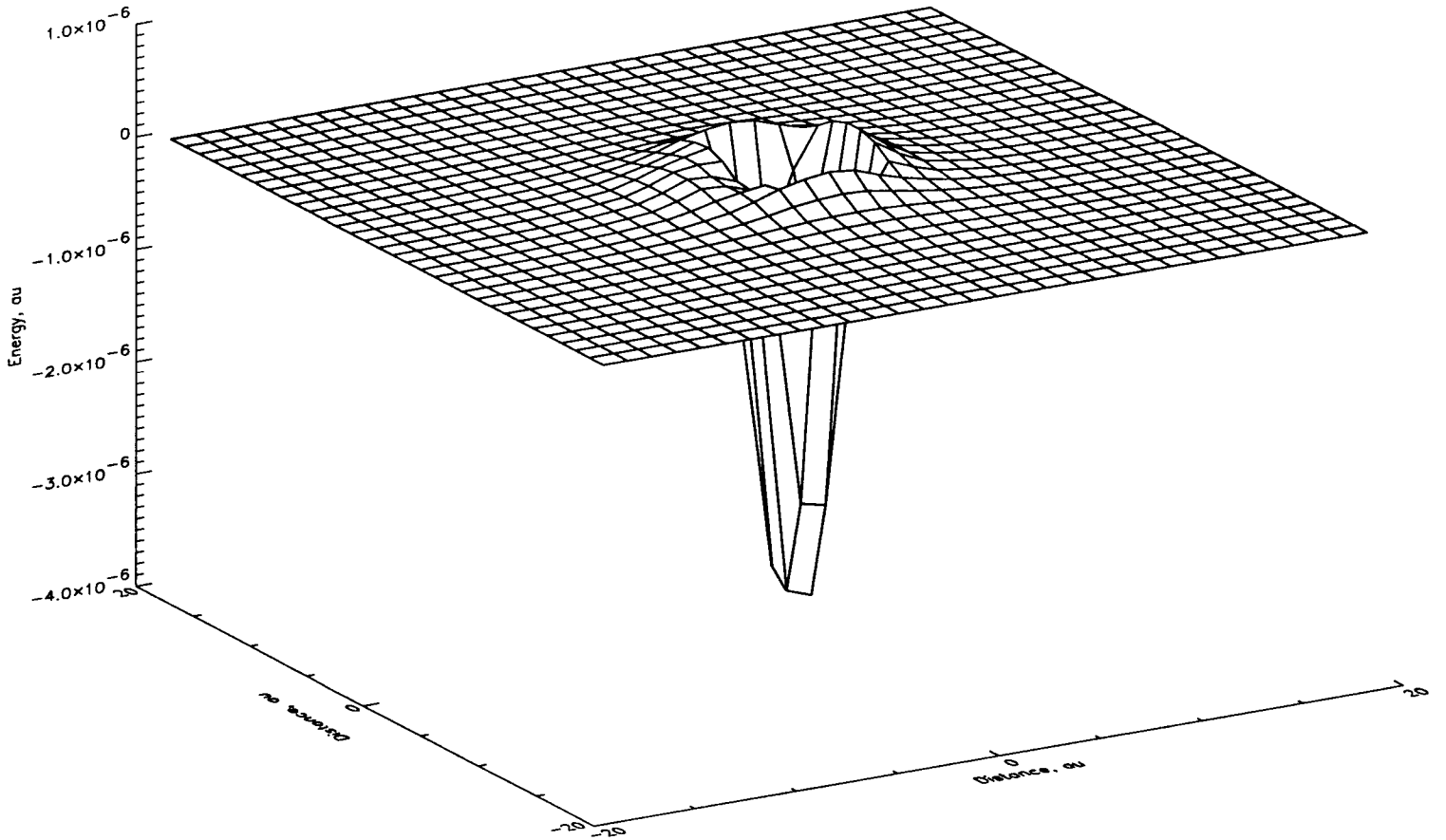

Figure 8.15 Total Transition Probability Amplitude for z = -1.83 au

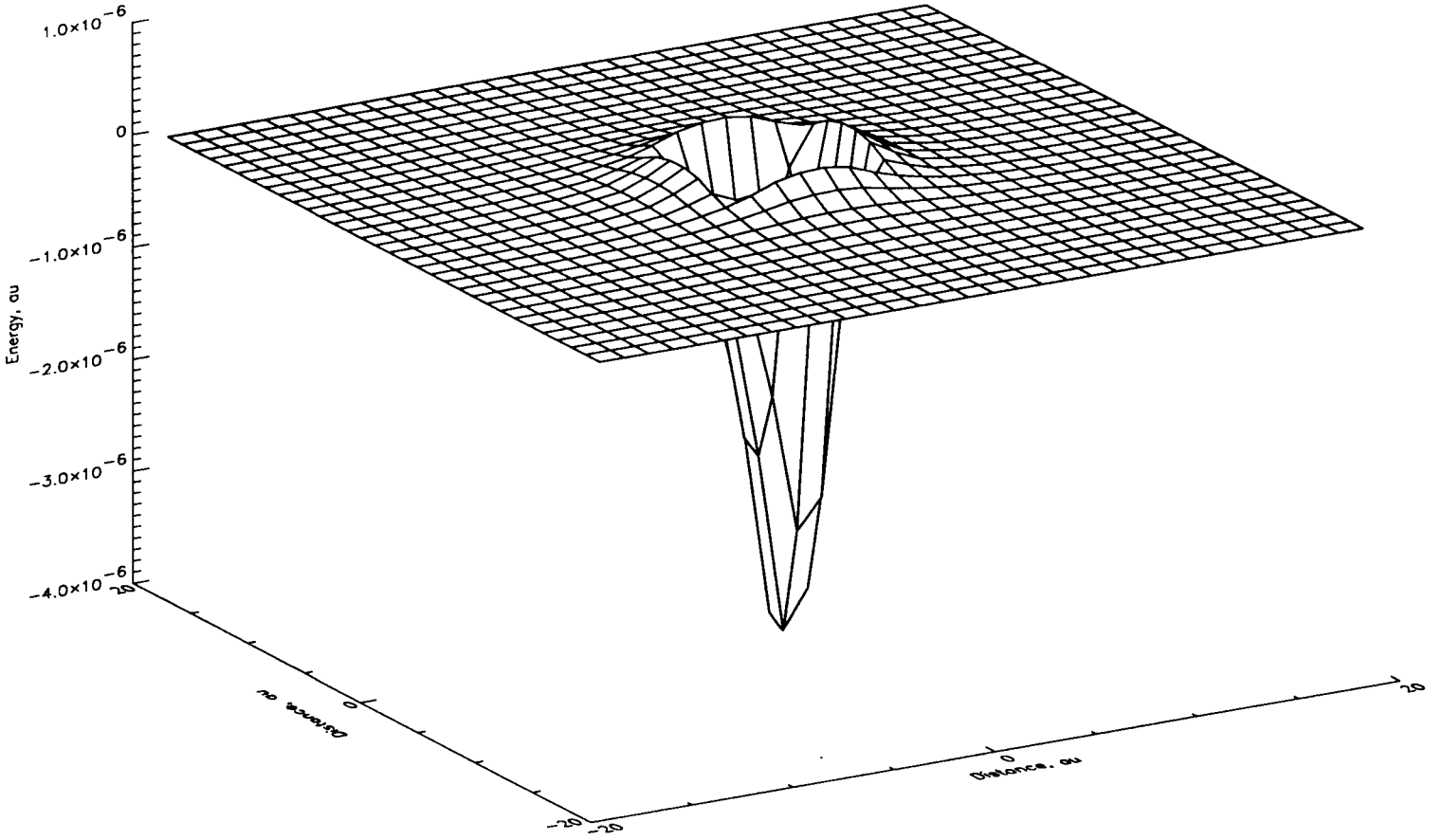

Figure 8.16 Total Transition Probability Amplitude for z = -0.61 au

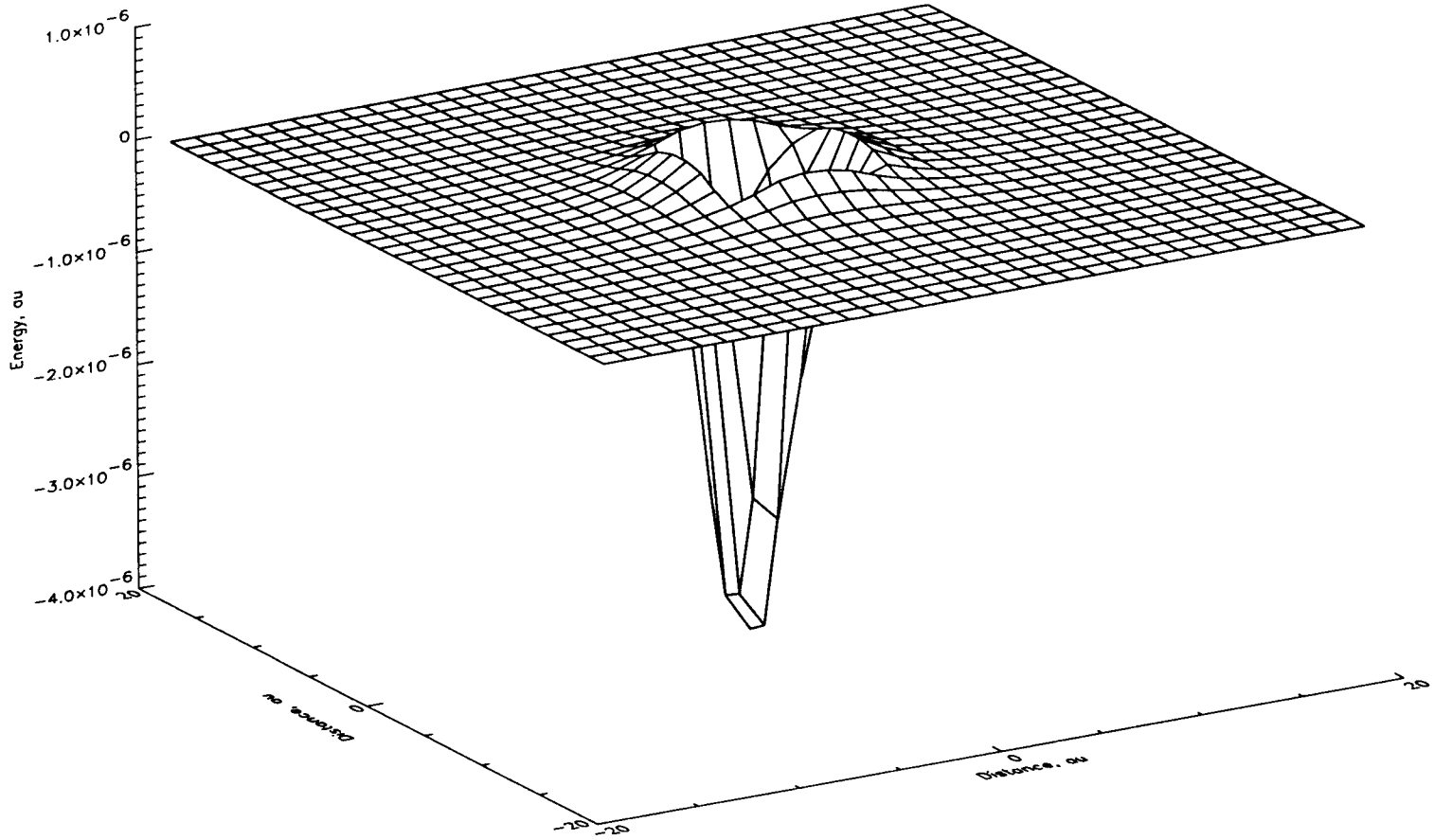

Figure 8.17 Total Transition Probability Amplitude for z = 0.61 au

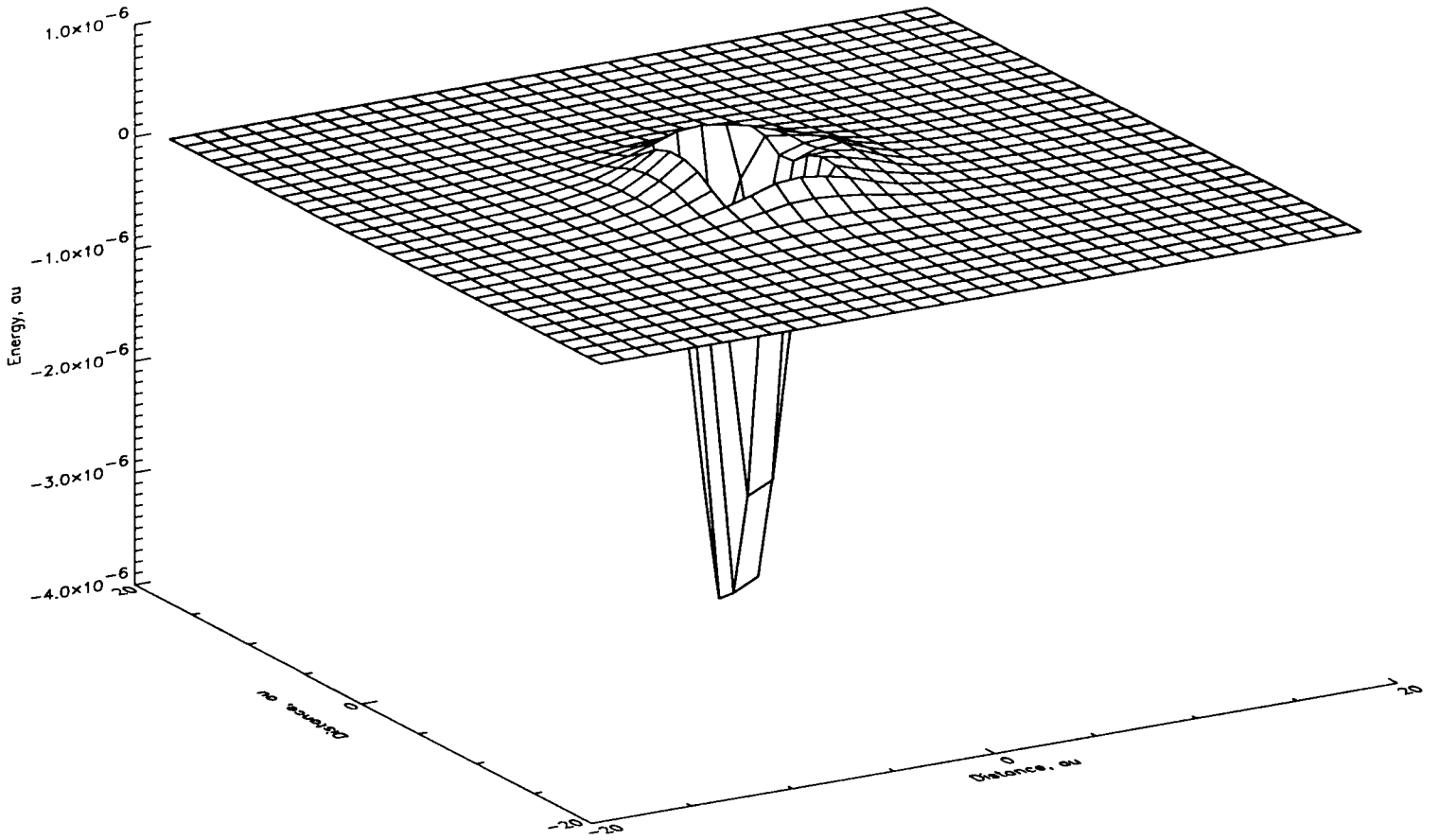

Figure 8.18 Total Transition Probability Amplitude for z = 1.83 au

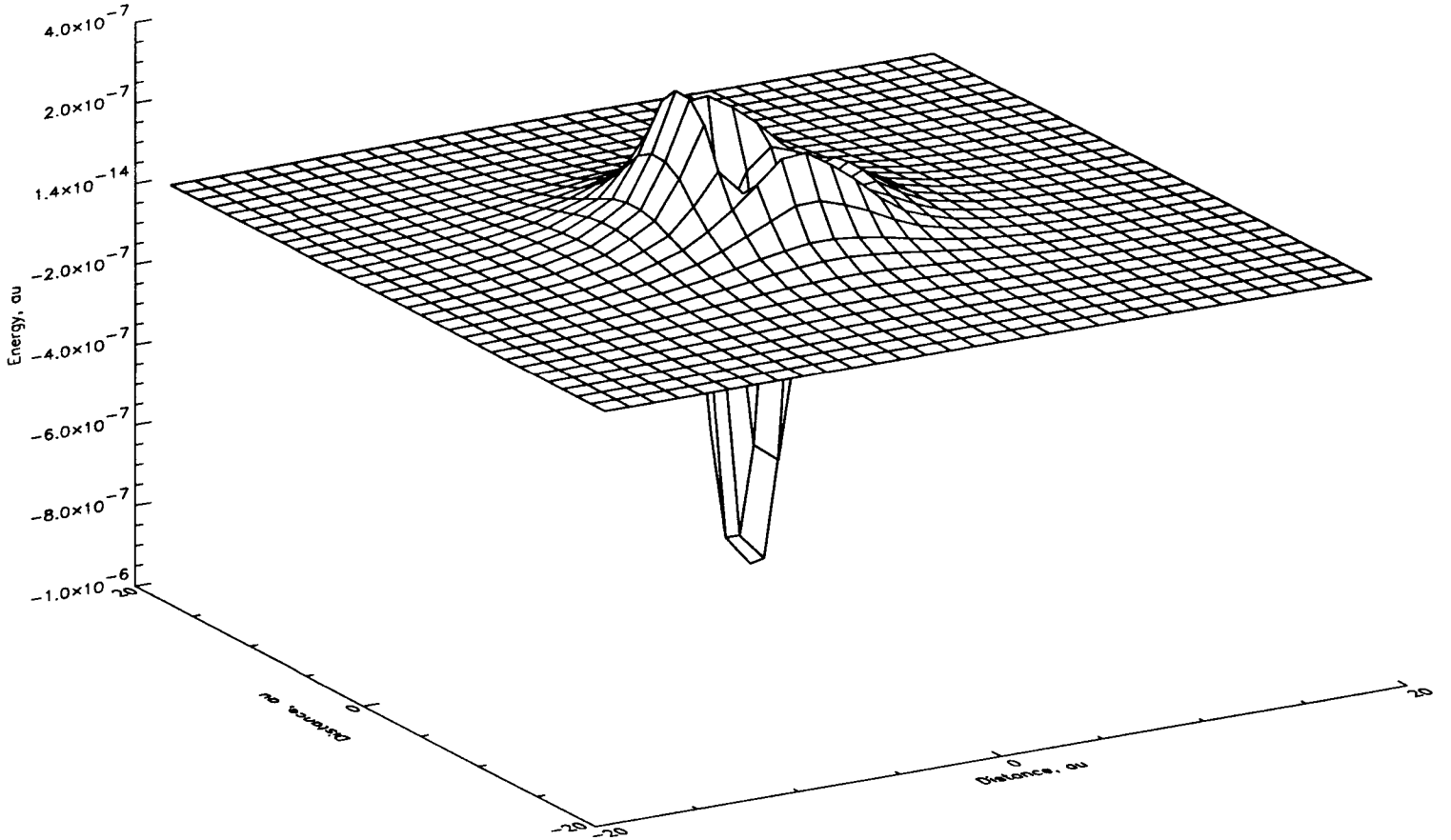

Figure 8.19 Total Transition Probability Amplitude for z = 3.05 au

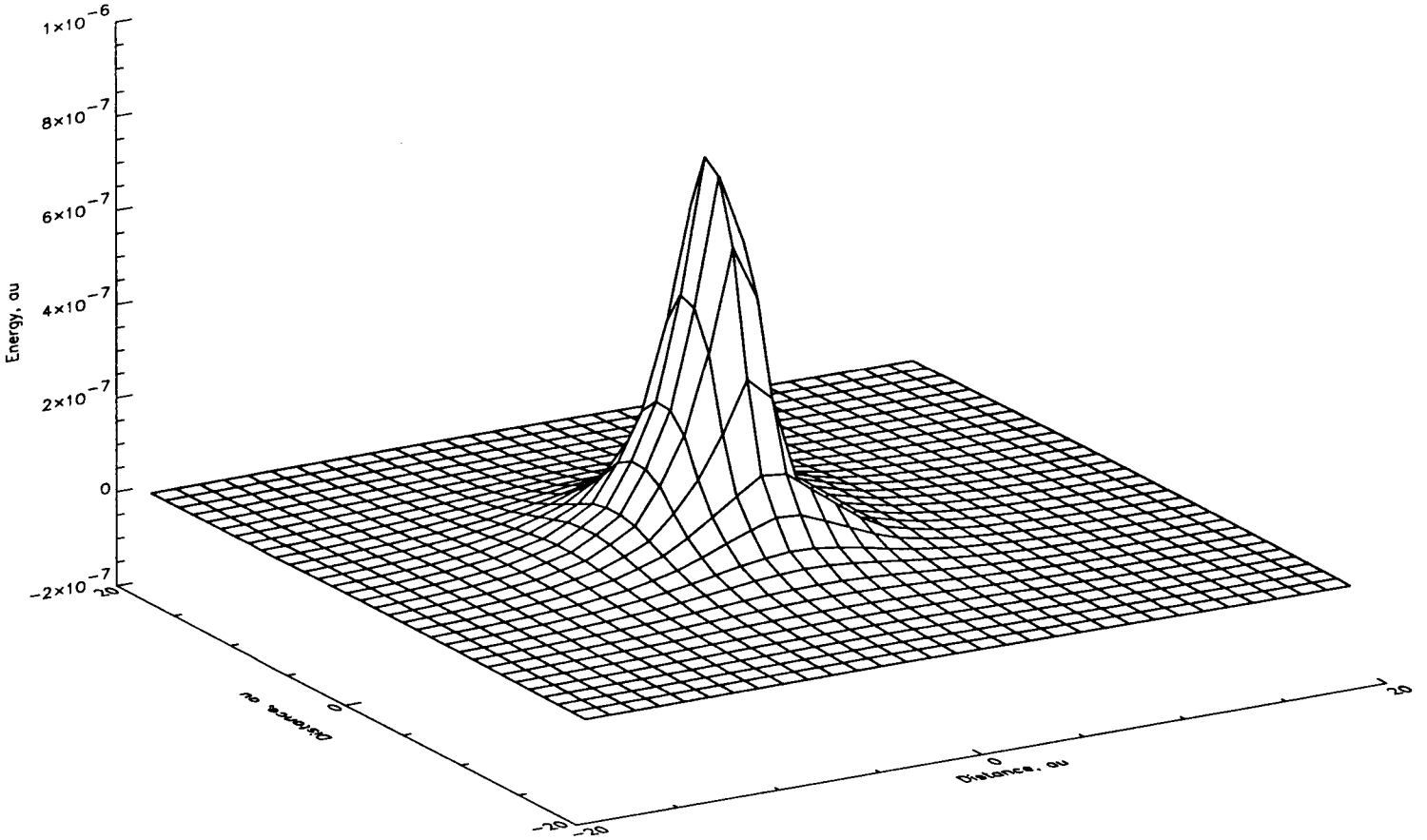

Figure 8.20 Total Transition Probability Amplitude for z = 4.27 au

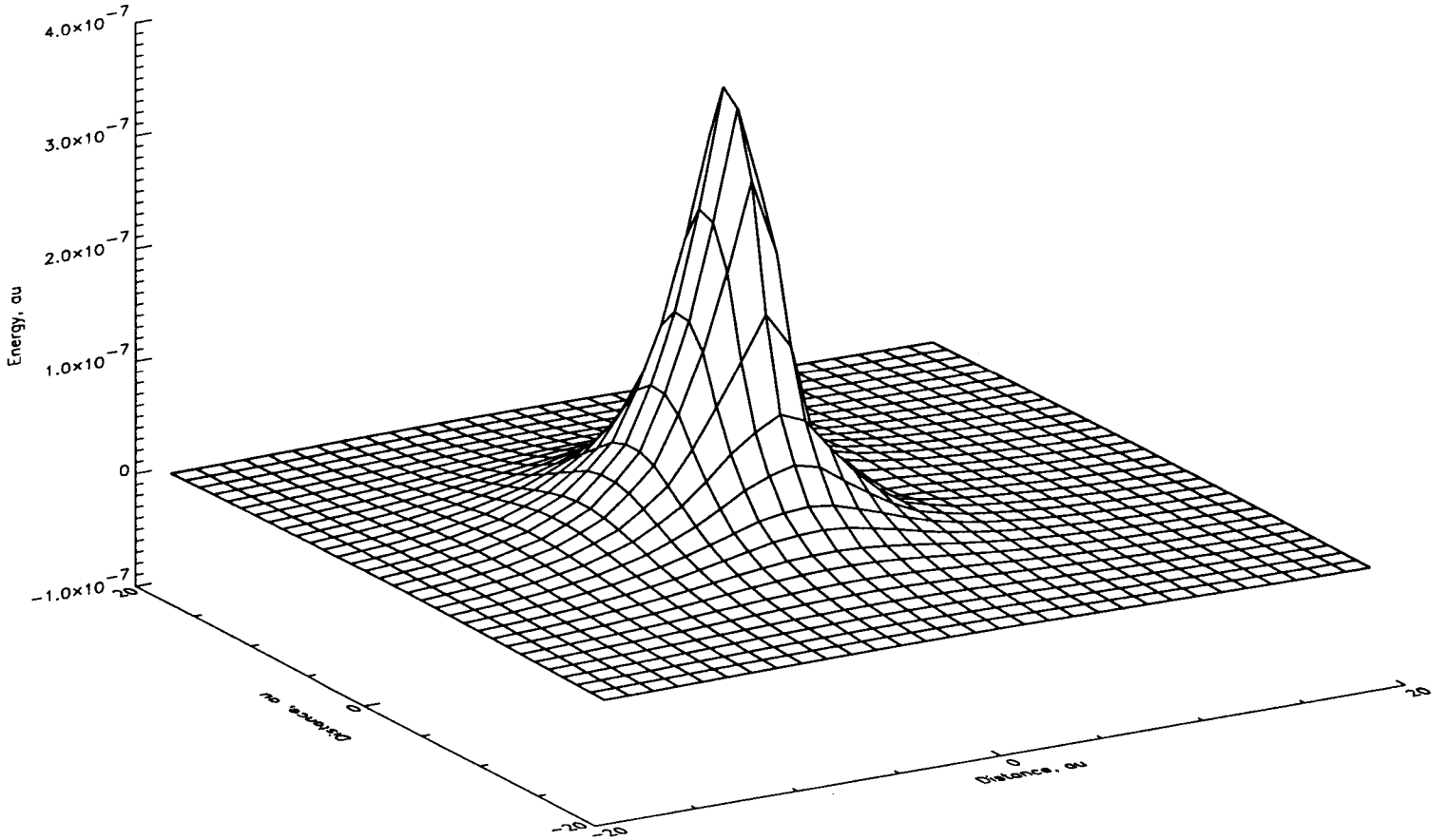

Figure 8.21 Total Transition Probability Amplitude for z = 5.49 au

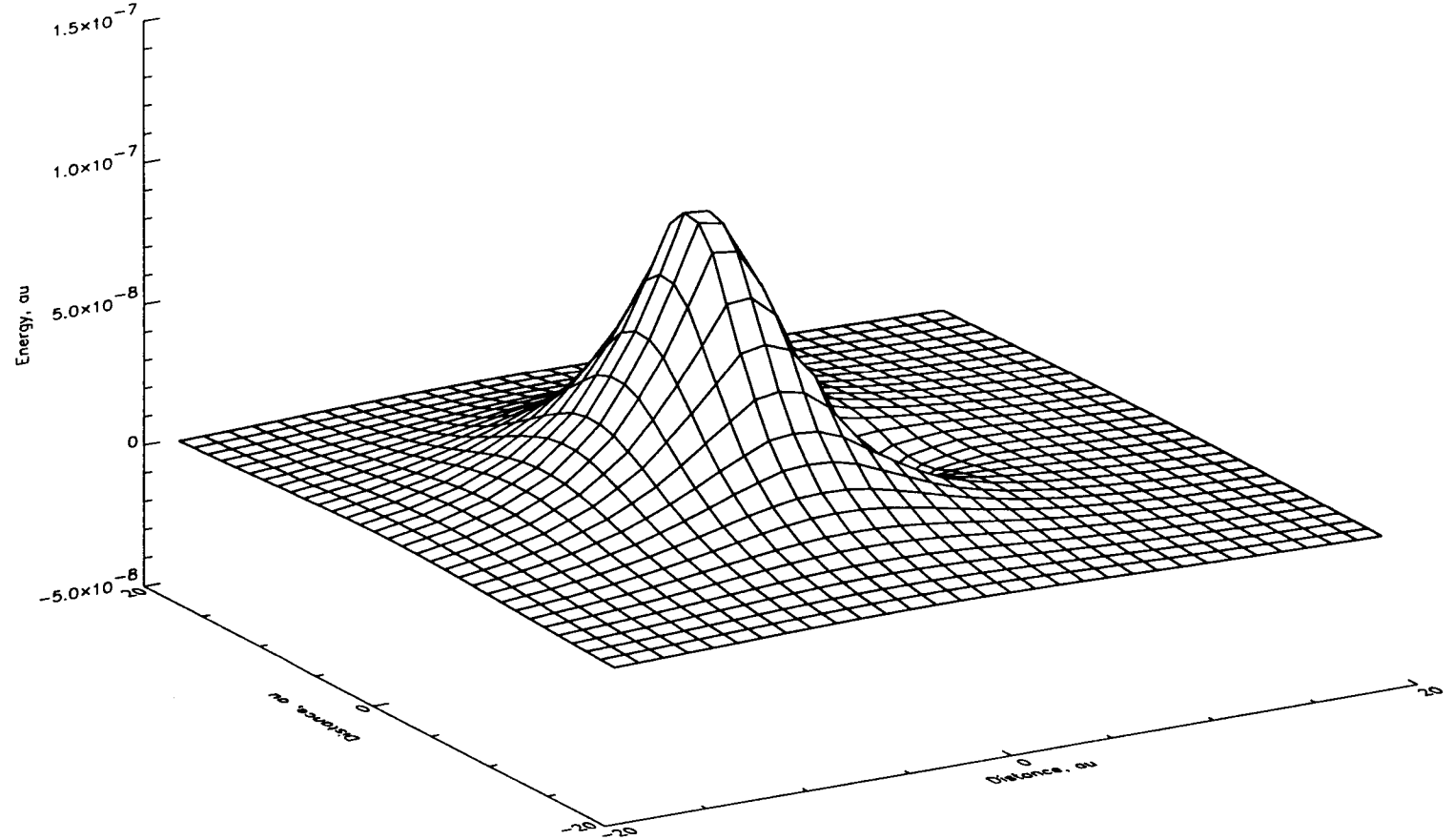

Figure 8.22 Total Transition Probability Amplitude for z = 6.71 au

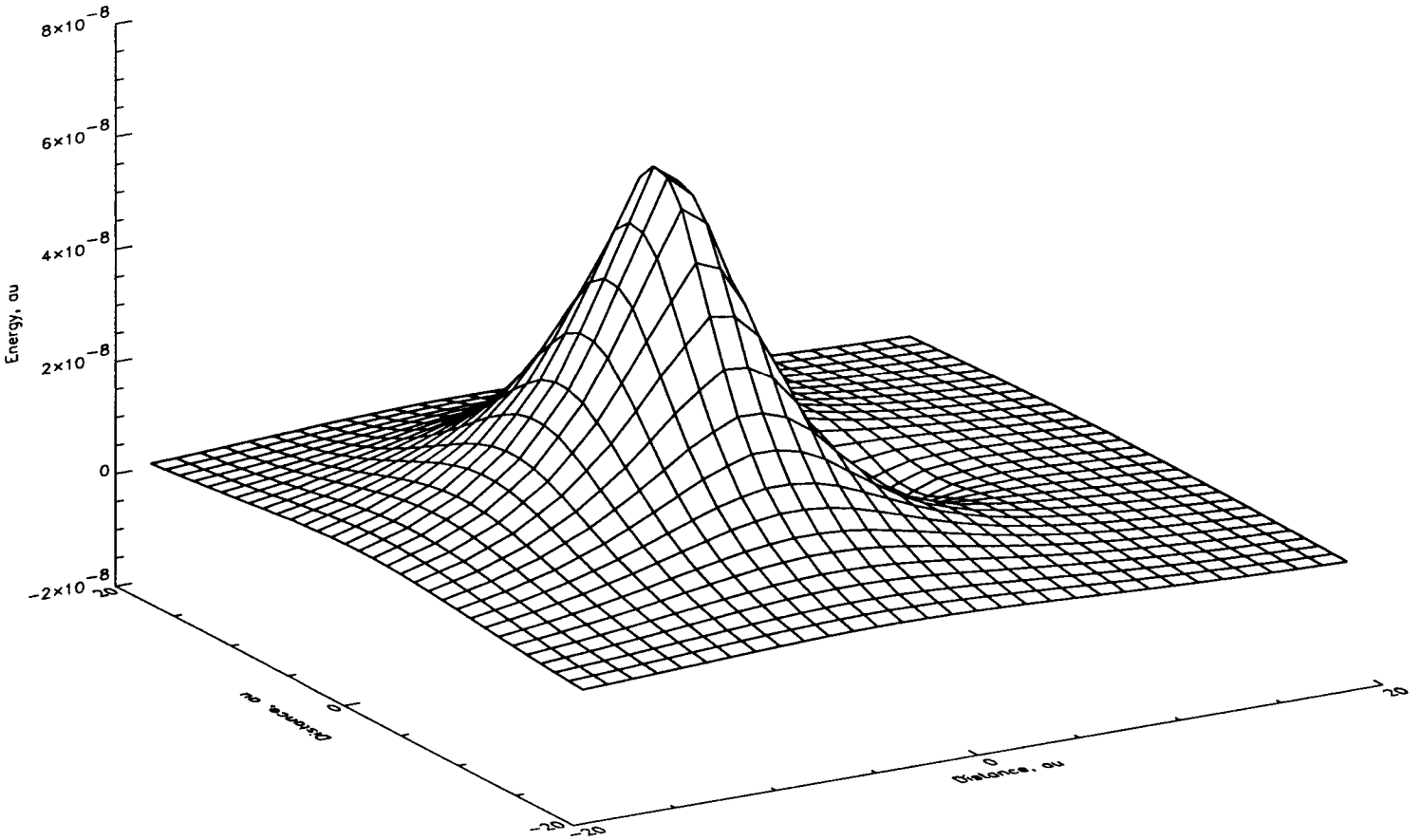

Figure 8.23 Total Transition Probability Amplitude for z = 7.92 au

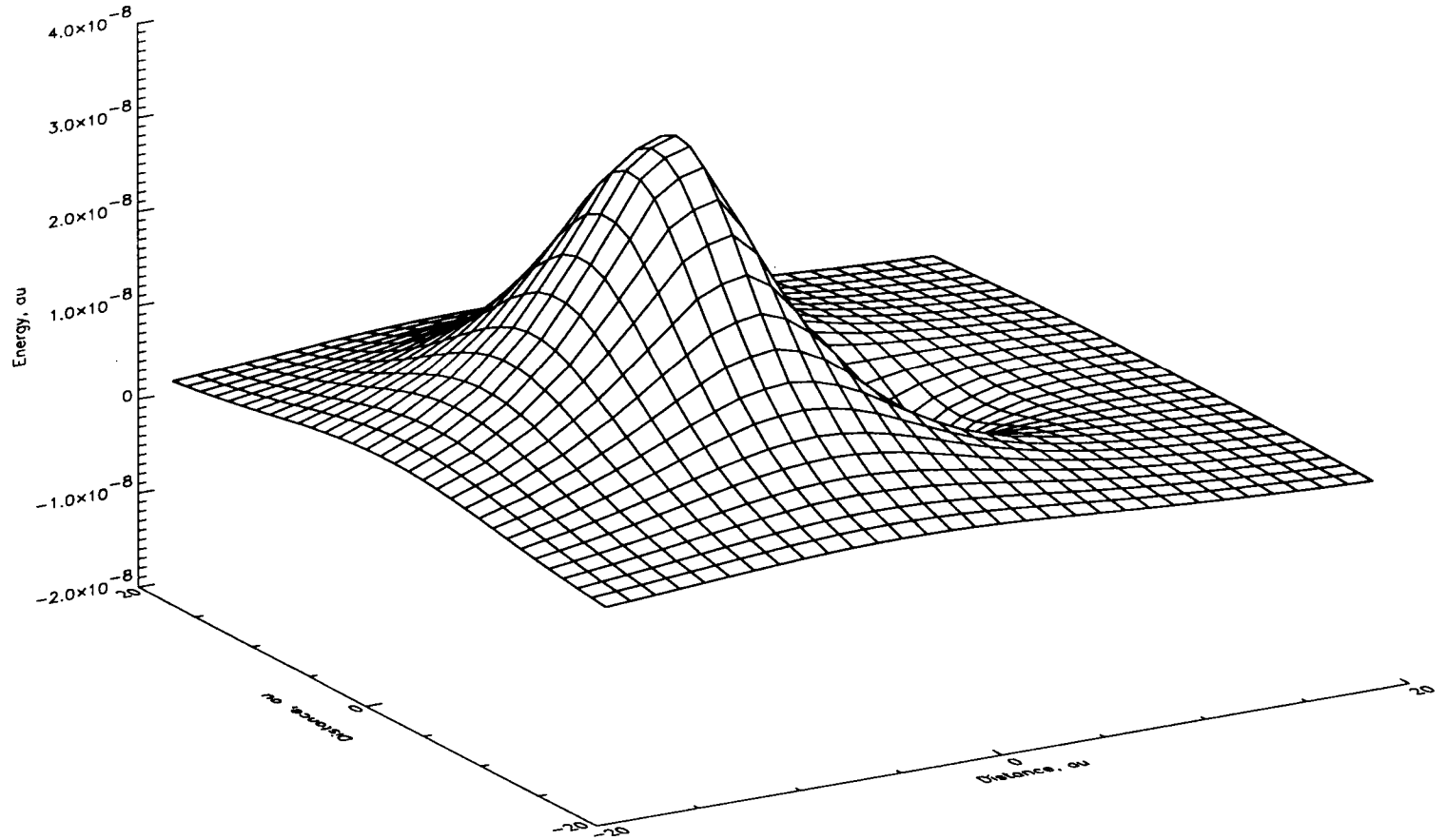

Figure 8.24 Total Transition Probability Amplitude for z = 9.14 au

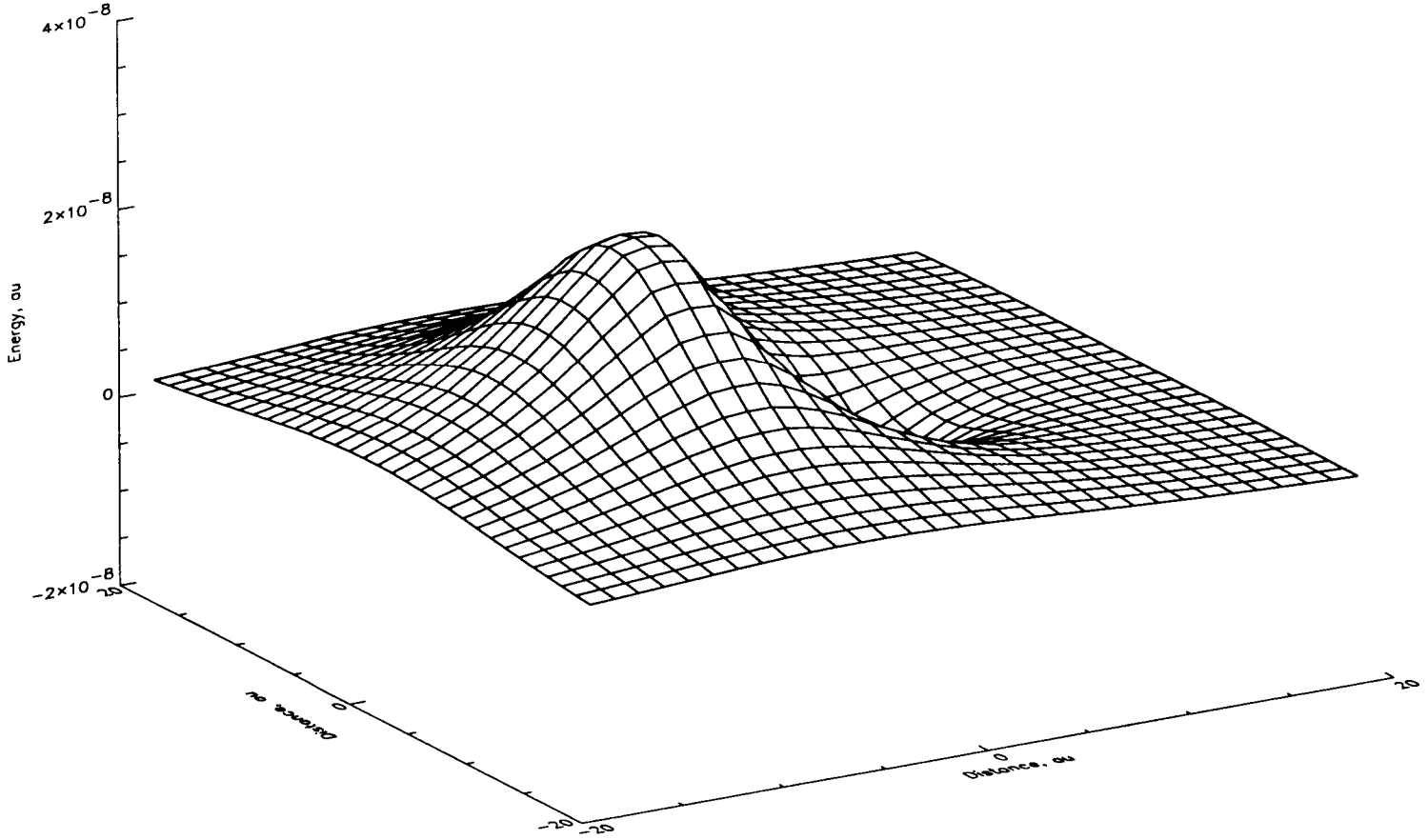

Figure 8.25 Total Transition Probability Amplitude for z = 10.36 au

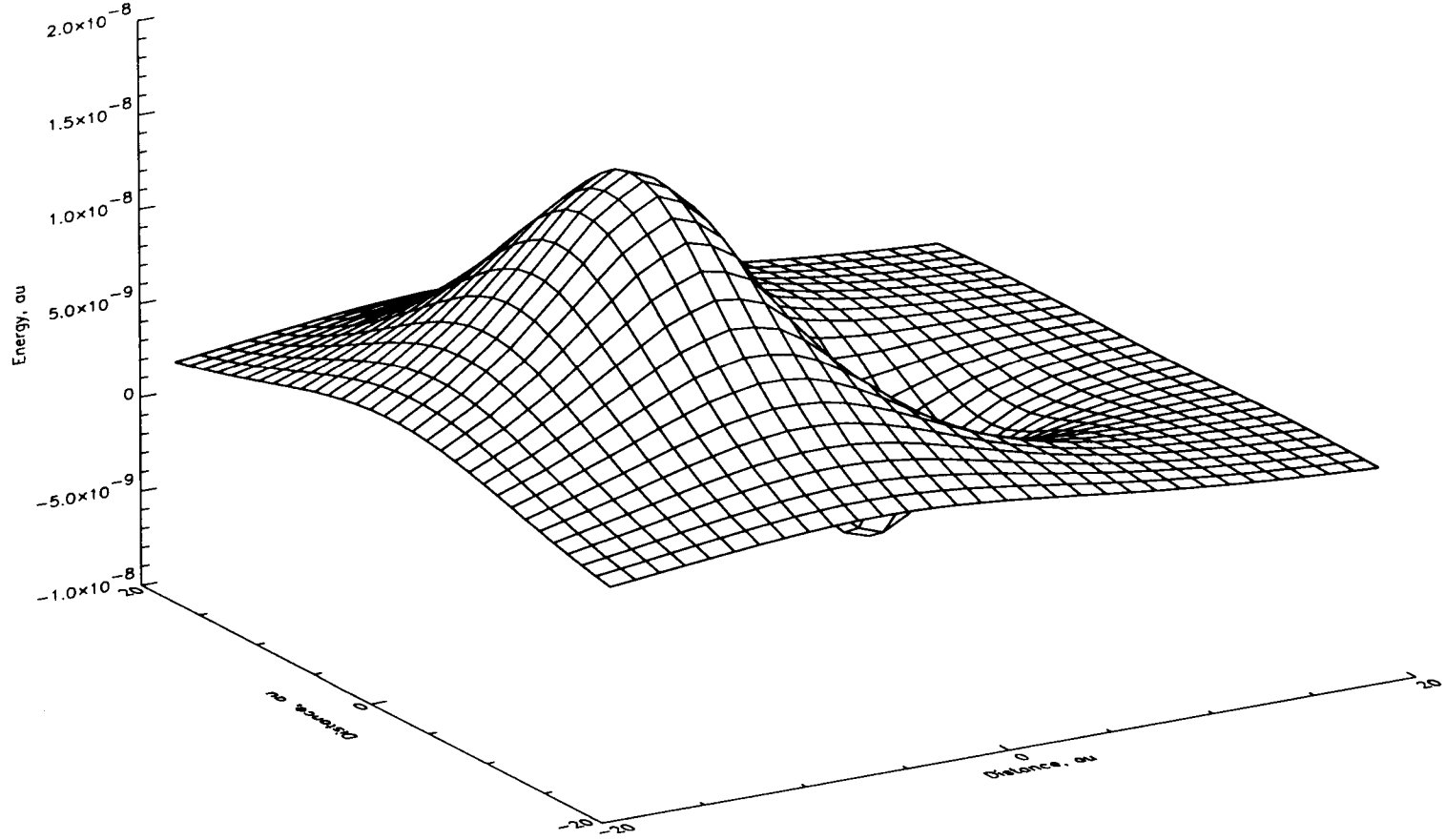

Figure 8.26 Total Transition Probability Amplitude for z = 11.58 au

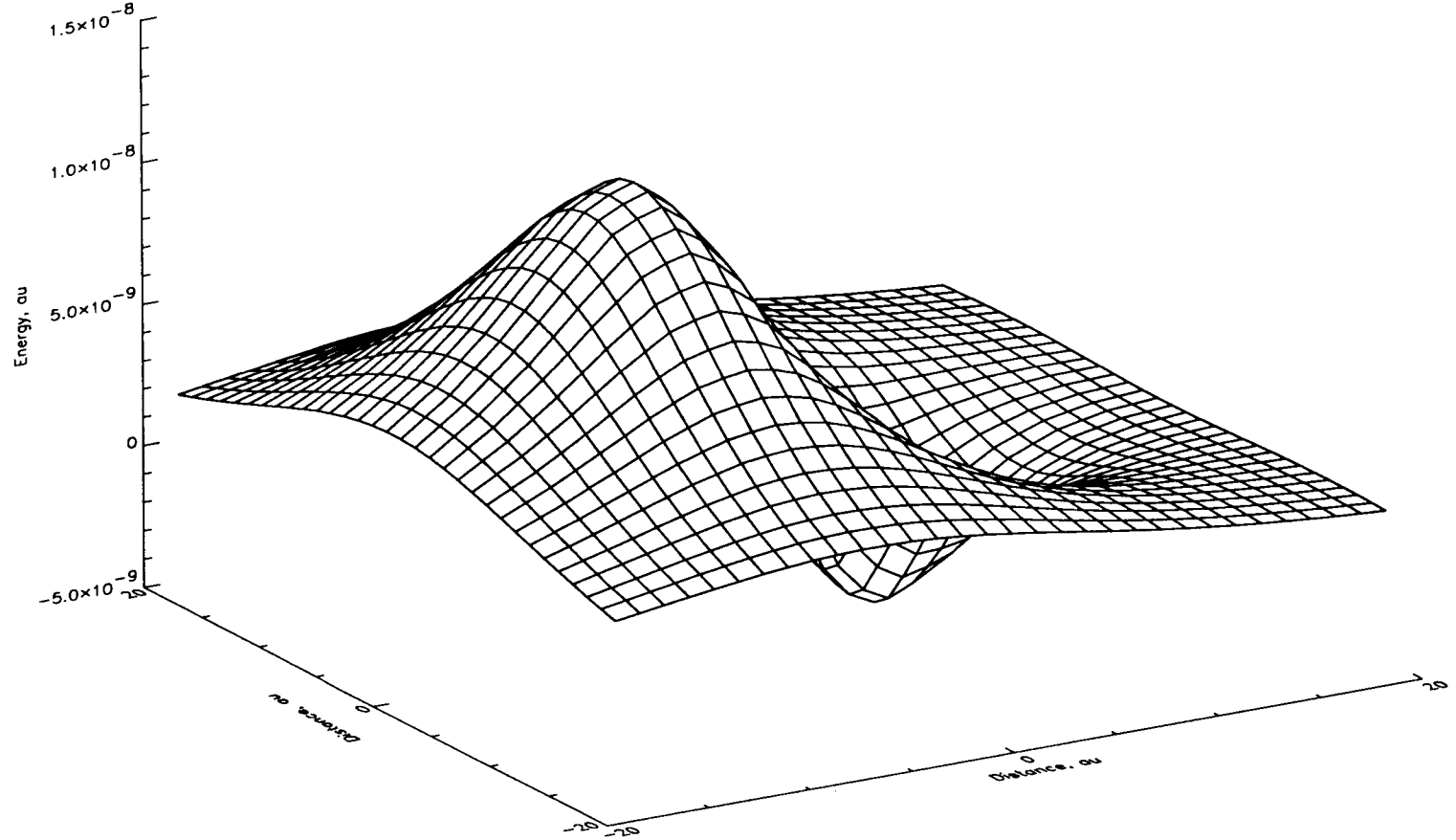

Figure 8.27 Total Transition Probability Amplitude for z = 12.80 au

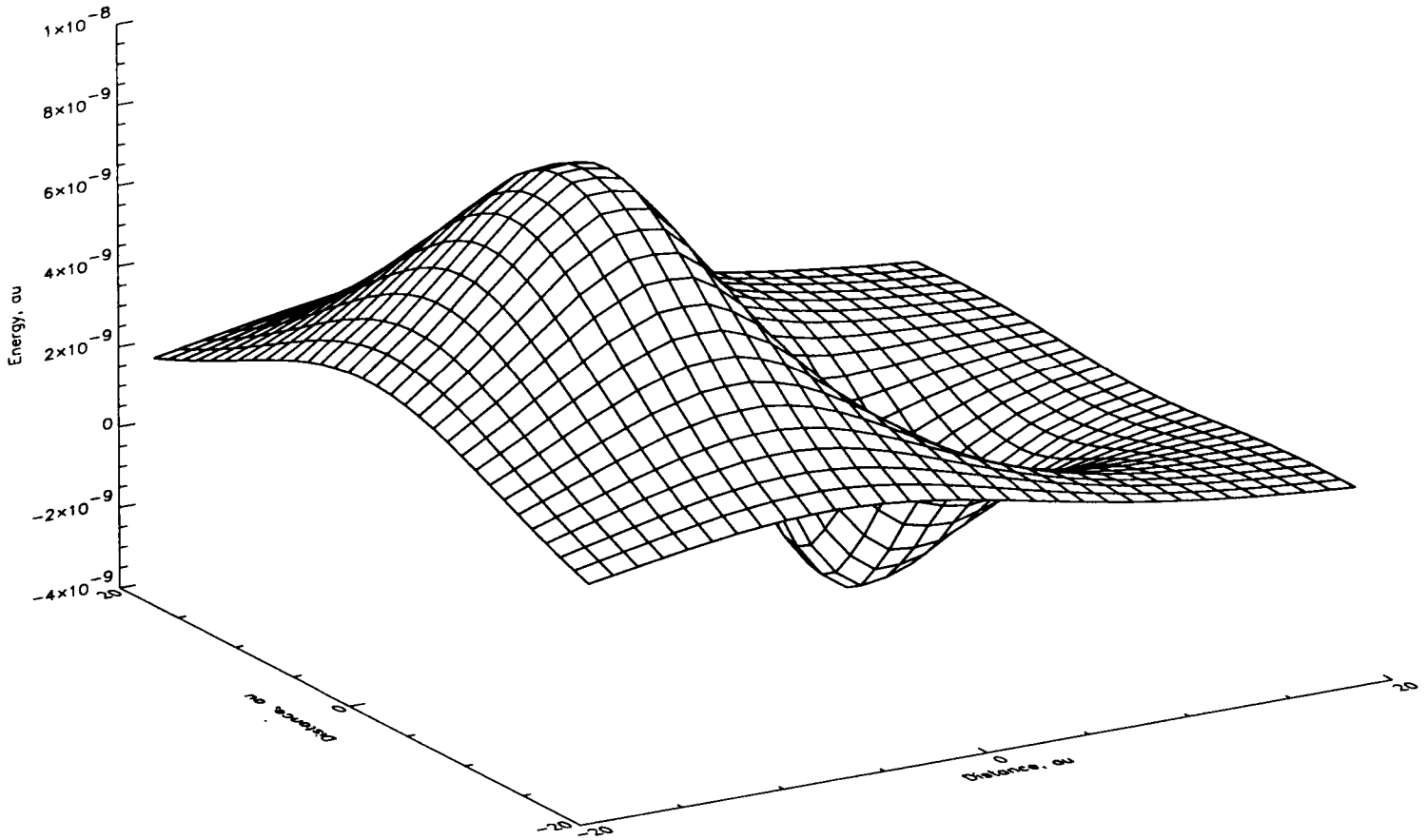

Figure 8.28 Total Transition Probability Amplitude for z = 14.02 au

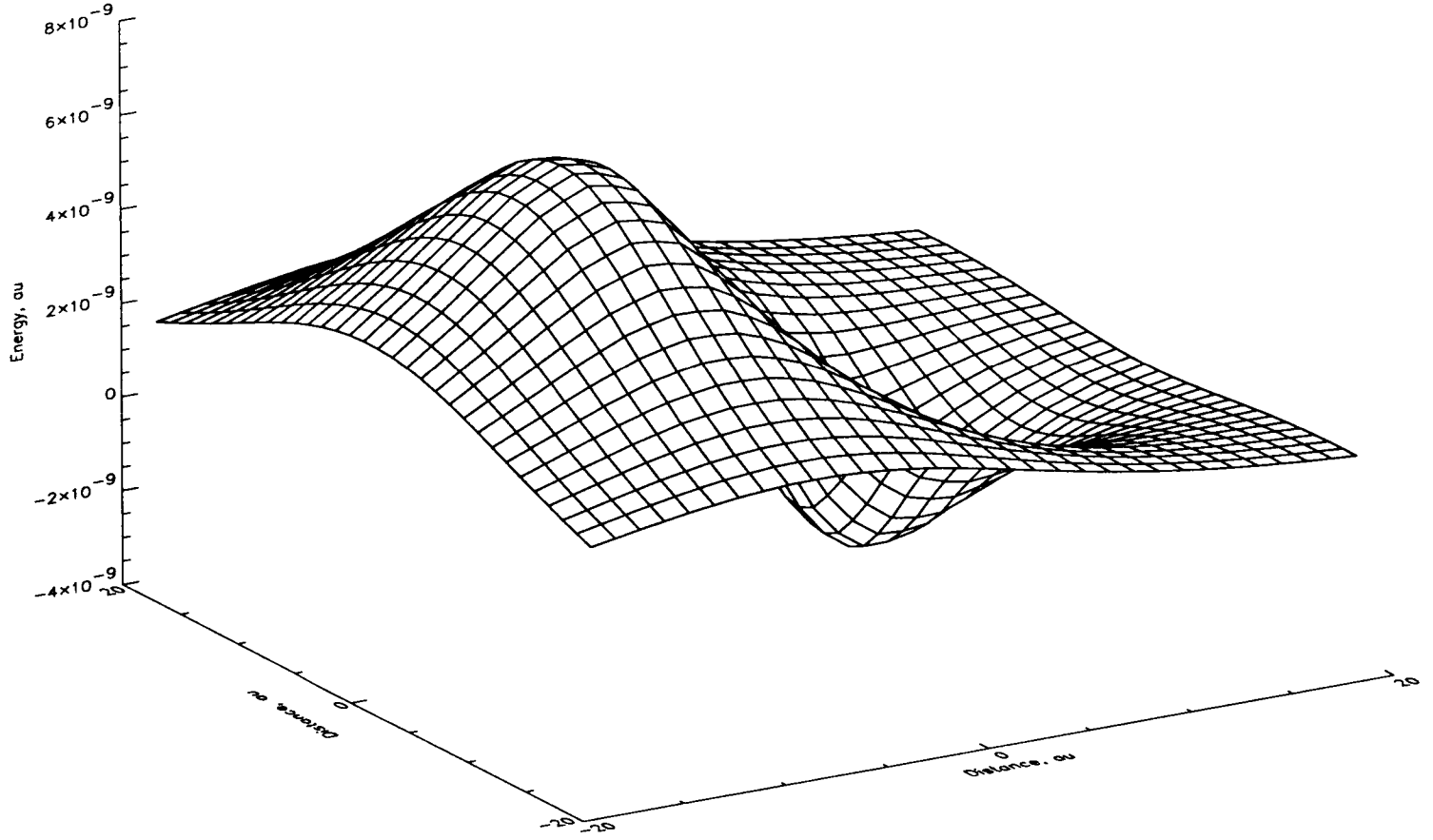

Figure 8.29 Total Transition Probability Amplitude for z = 15.24 au

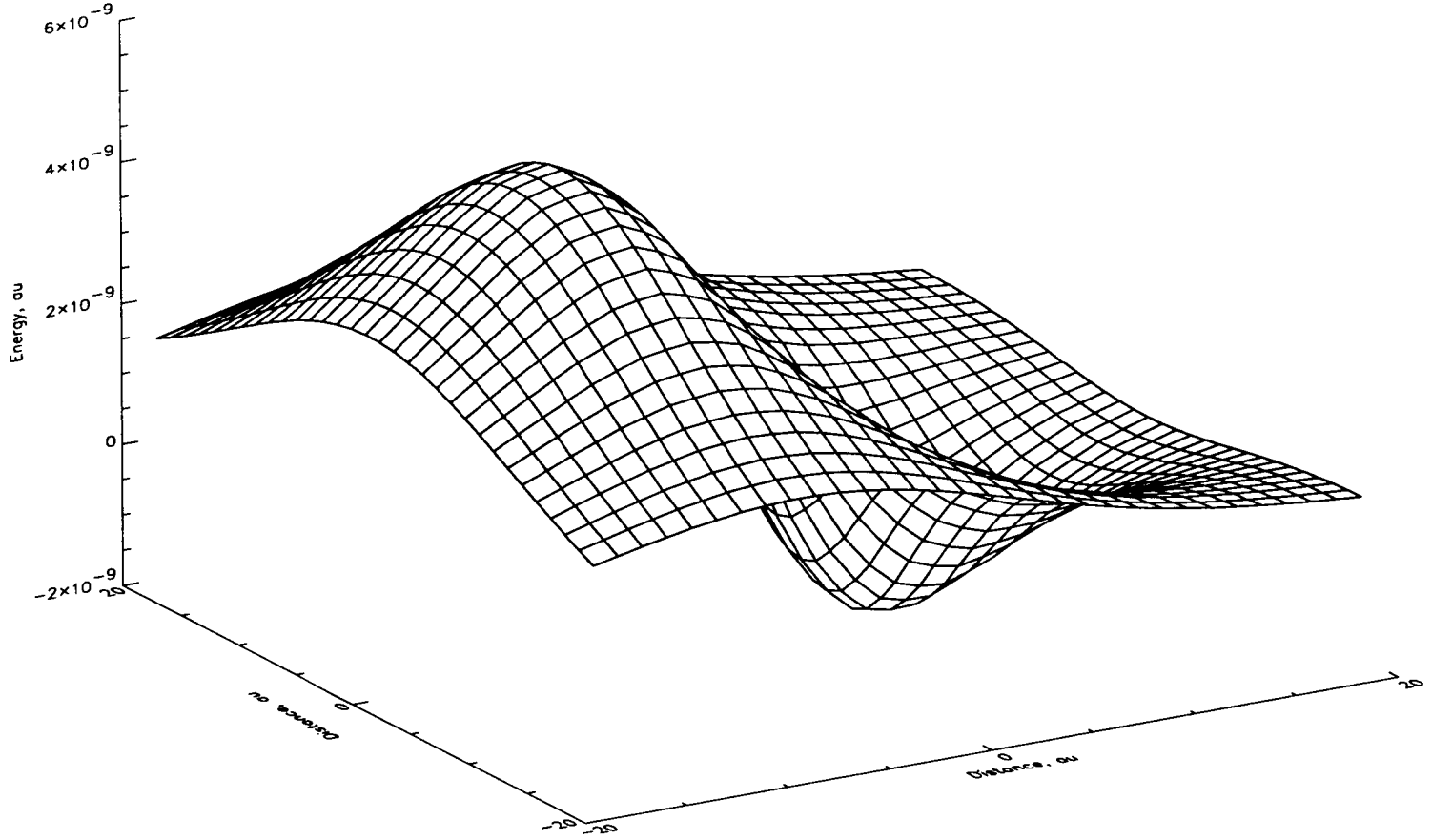

Figure 8.30 Total Transition Probability Amplitude for z = 16.46 au

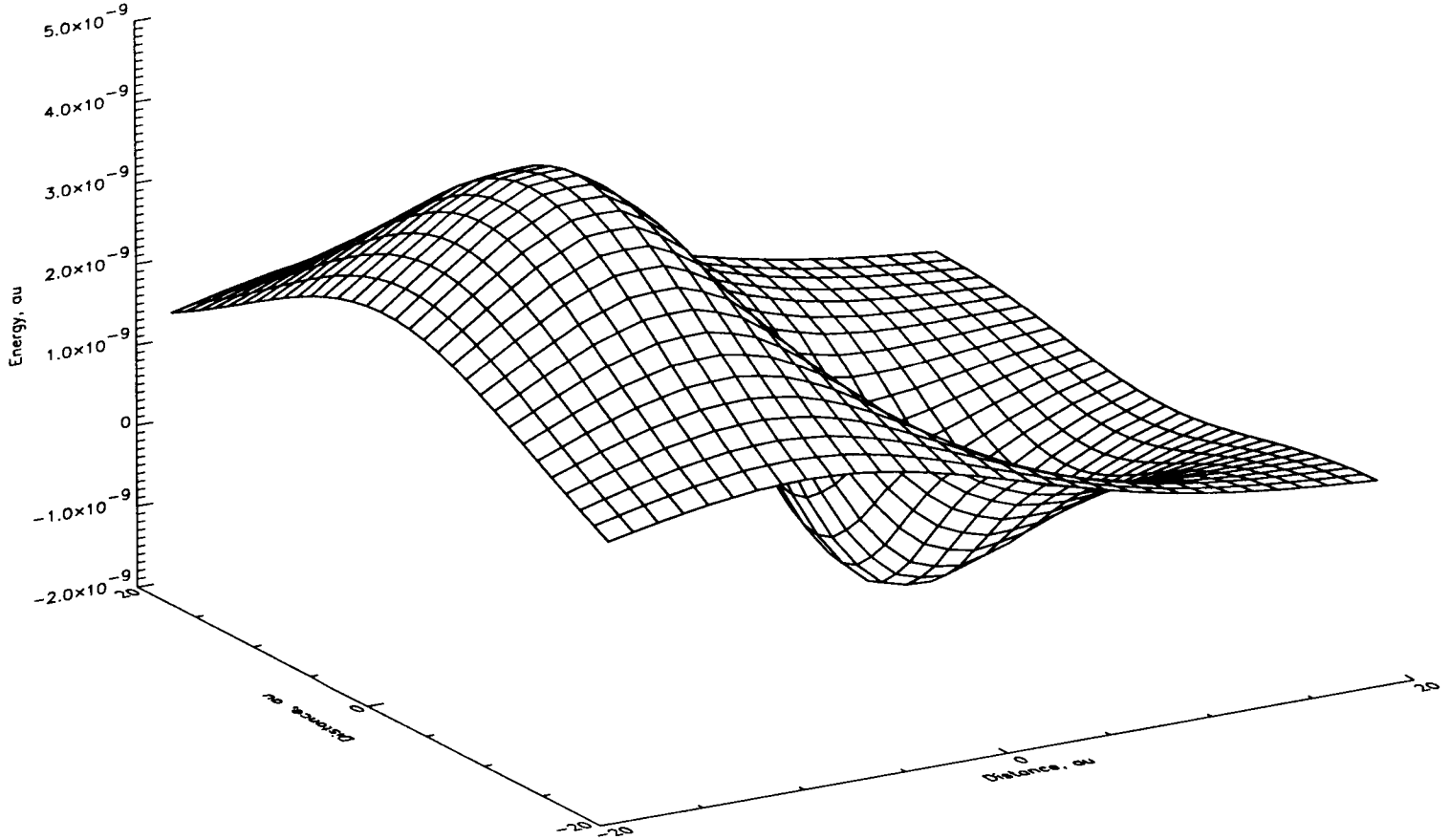

Figure 8.31 Total Transition Probability Amplitude for z = 17.68 au

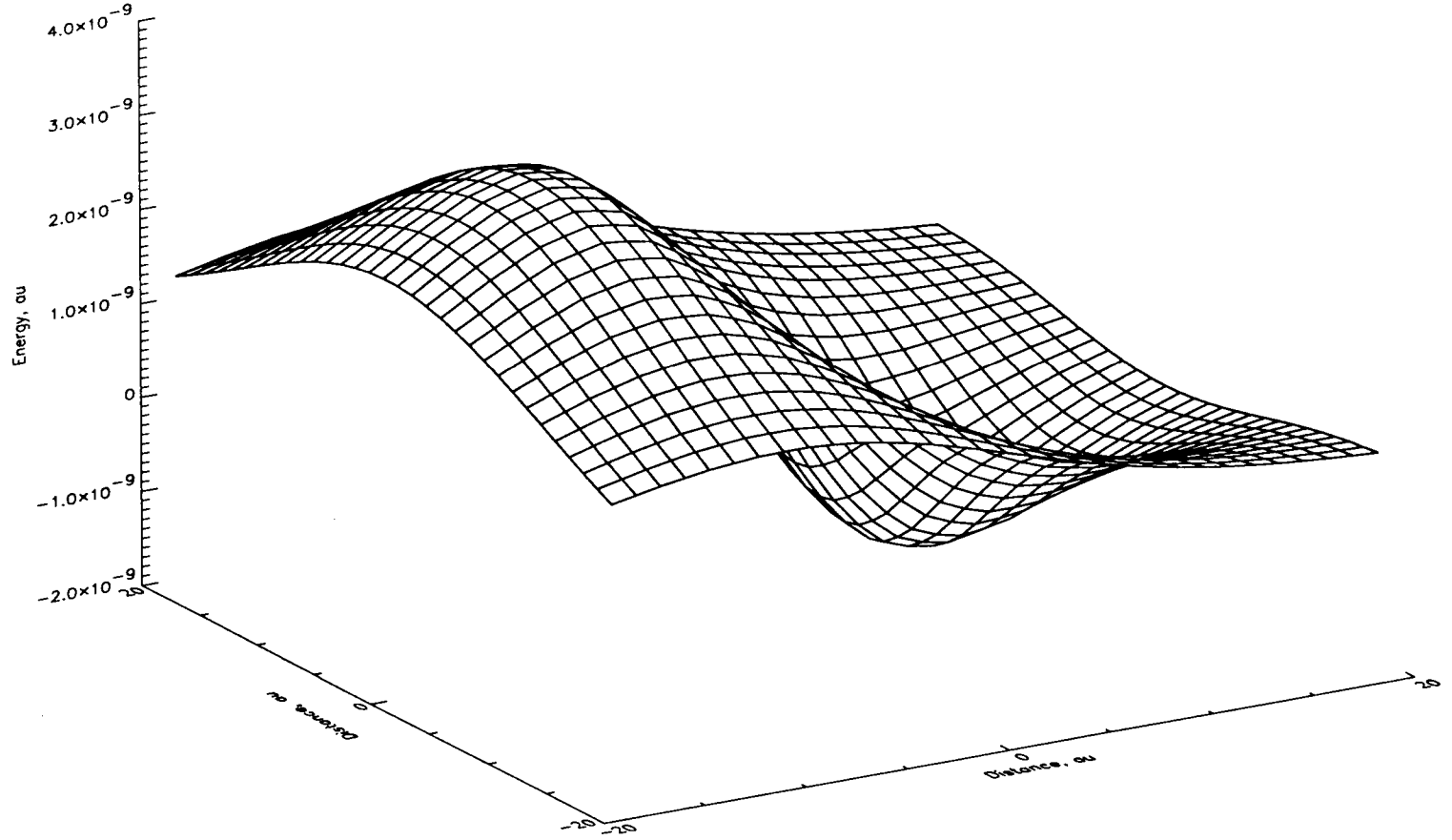

Figure 8.32 Total Transition Probability Amplitude for z = 18.90 au

These features persist for higher z sheets up to z = -6.71 au, Figure 8.11. At that point, distortion begins to break the apparent symmetry of the surface. Also, note that for large positive z, the same symmetric features, albeit inverted, are evident. This can be seen for z = 18.89 au, in Figure 8.32, down to z = 6.71 au, displayed in Figure 8.22.

Since the total transition amplitude is displayed with the Ar orientational dependence removed, any features present must be due to the spatial character of the N_2 orbitals. Furthermore, since the $2\sigma_u$ orbital is cylindrically symmetric about the z axis, any features observed within a plane of constant z must be due to the $1\pi_g$ orbital. As noted in Table 7.4, there are two degenerate $1\pi_g$ orbitals to be considered, denoted as $1\pi_g$(a) and $1\pi_g$(b). The relative orientation and sign can be determined from the g90 calculation results.

The coefficients of Table 7.4 show that the $1\pi_g$(a) orbital is largely composed of equal amounts of atomic 2px and 2py orbitals. Recall that these orbitals behave spatially as x and y, respectively. For example, the 2px orbital is positive for x > 0 and negative for x < 0. Table 7.4 lists the contribution from the upper N atom, at +0.55 au, as -0.29 2px +0.33 2py, while for the lower N atom, at -0.55 au, the contribution is +0.29 2px - 0.33 2py. Thus, the nodal plane of the $1\pi_g$(a) orbital contains the internuclear axis and satisfies the equation 0 = -0.29x + 0.33 y in both the lower half-space, i.e. z < 0, and the upper half-space, i.e. z > 0. In the lower half-space, the wavefunction is positive for points satisfying 0.29 x - 0.33 y > 0, while for points satisfying 0.29 x - 0.33 y < 0 the wavefunction is negative. Figure 8.33(a) is a sketch of the wavefunction sign in the lower half-space.

The second $1\pi_g$ orbital can be examined in a similar manner. The g90 coefficients listed in Table 7.4 show that, in the lower half-space, $1\pi_g$(b) orbital is composed of -0.33 2px - 0.29 2py. Thus, the nodal plane of the $1\pi_g$(b) orbital is perpendicular to that of the $1\pi_g$(a) orbital, which is as expected if the $1\pi_g$(a) and the

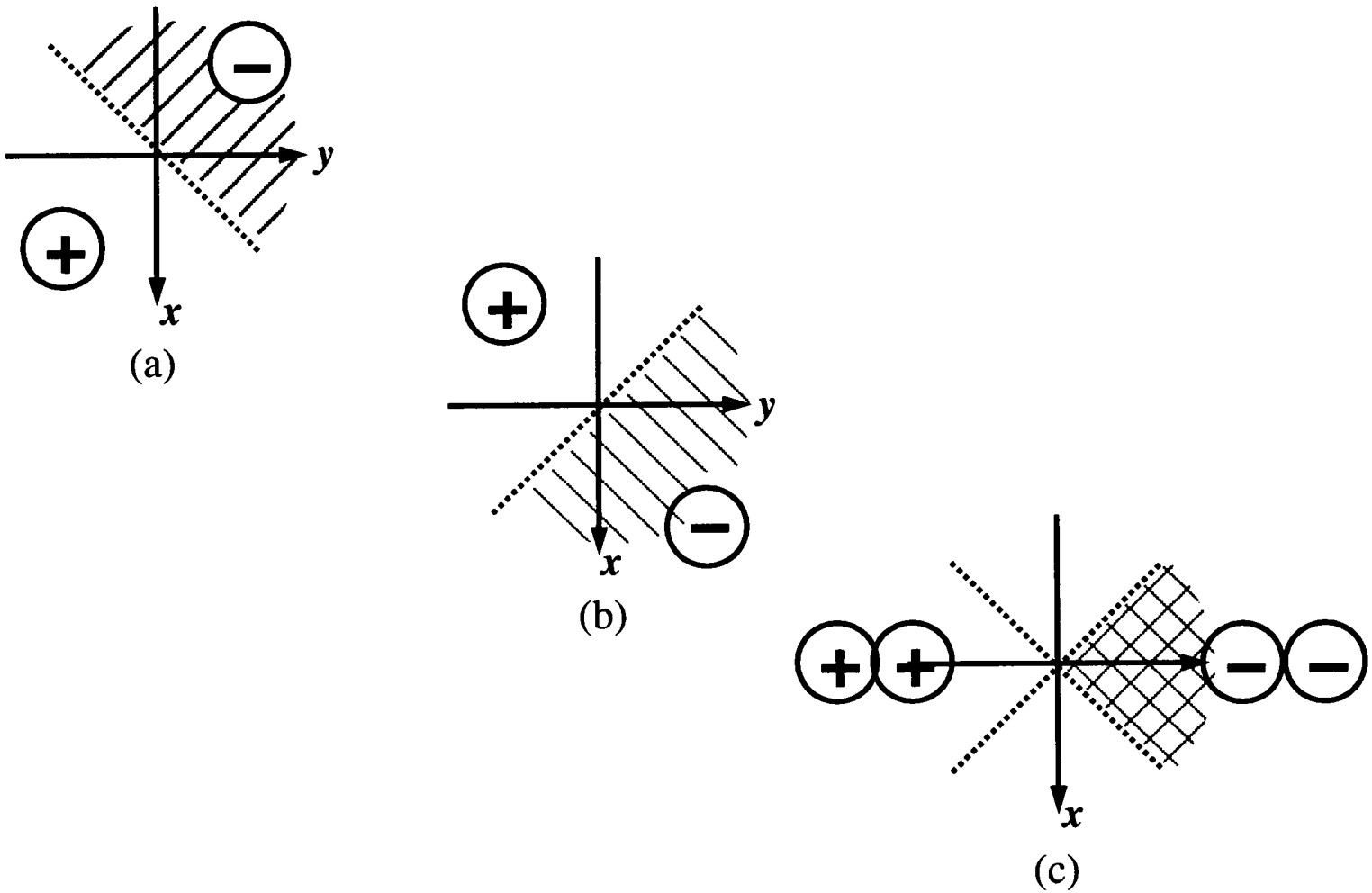

Figure 8.33 Wavefunction Sign in the Lower Half Space for a) $1\pi_g a$, b) $1\pi_g b$, and c) $1\pi_g a + 1\pi_g b$

$1\pi_g$(b) are to be orthogonal. Figure 8.33(b) shows a sketch of the orbital sign for the lower half-space of the $1\pi_g$(b) orbital. Note that the direction of the maximal amplitude of the $1\pi_g$(a) and $1\pi_g$(b) orbitals is simply rotated from the x and y coordinate axes by roughly 45 degrees. This choice was specified by the g90 calculation and has no physical meaning.

The resultant interaction depends upon the sum of the two $1\pi_g$ orbitals, as discussed in Chapter 7. The sign of the sum of the orbitals is sketched in Figure 8.33(c). Notice that this matches the shape of the total transition amplitude displayed in Figures 8.1 through 8.11, with the exception of the overall sign. This can be accounted for by examining the sign of the $2\sigma_u$ orbital. First, note that the $2\sigma_u$ orbital is composed primarily of 2s atomic orbitals, and that the sign of the 2s orbital is always positive. In the lower half-space, the $2\sigma_u$ is due to a negative contribution of the 2s orbital, i.e. from Table 7.4 the 2s coefficient is -0.55. Hence, the sign of the $2\sigma_u$ orbital in the lower half-space is negative, as illustrated in Figure 6.2. Therefore, the total transition amplitude has the same symmetry properties as the product of the $1\pi_g$ and $2\sigma_u$ orbitals. Recall that the general form of the interaction is

(8.1) $$H' \propto V_{1\pi,3p,4s,2\sigma} - V_{1\pi,3p,2\sigma,4s}$$

The first term is a coulomb term in which the integration is performed on orbitals of like centers, while the second term is an exchange term and relies upon the overlap of the orbitals of different centers. Hence, at large distances, it is reasonable that the second term should be inconsequential to the interaction. Since the sign of the interaction can be accounted for by the coulomb term, this leads to the important discovery that for large distances only the coulomb interaction influences the energy transfer between Ar and N_2.

The symmetry of the total transition amplitude provides another clue to the long range interaction. The form of the coulomb term is a double integral,

(8.2) $$V_{1\pi,3p,4s,2\sigma} \propto \int d^3r\, \phi_{1\pi}(\underline{r})\phi_{2\sigma}(\underline{r}) \int d^3r'\, \phi_{3p}(\underline{r}')\phi_{4s}(\underline{r}') \frac{1}{|\underline{r}-\underline{r}'|}$$

where $V_{1\pi,3p,4s,2\sigma}$ is actually an implicit function of the separation vector, $\underline{R}$, through the Ar orbitals. Indeed, as the separation becomes large, the difference between $\underline{R}$ and $\underline{r}'$ dwindles since both vectors originate from the N_2 reference frame. The coulomb potential can be replaced by $1/|\underline{r}-\underline{R}|$, which can then be pulled through the Ar integral. The Ar integral then becomes an effective charge integral, yielding some small constant ε . Note that if the removal of the coulomb potential were exact, then the resulting Ar integral would be zero due to orthogonality. Because $\underline{R}$ is so large, the only significant contribution to the N_2 integral will be for values of $\underline{r} \approx \underline{R}$. The result is that $V_{1\pi,3p,4s,2\sigma}$ has an asymptotic form,

(8.3) $$V_{1\pi,3p,4s,2\sigma} \propto \frac{1}{R}\phi_{1\pi}(\underline{R})\phi_{2\sigma}(\underline{R})\varepsilon_{3p,4s} \qquad (large\ R)$$

which is essentially a statement of Coulomb's Law for charged particles. Thus, it is reasonable to find the symmetry of the N_2 orbitals present in the total transition amplitude for large separation distances, in part because the Ar dependence has been averaged out.

In addition to the important mechanistic information about the long range interaction, i.e. that the interaction is solely coulomb, practical information concerning the calculational technique can also be inferred. Because of the asymptotic form of the transition amplitude, it is clear that the computational grid is sufficient to capture the entire spatial extent of the electron exchange mechanism. This allows for the determination of the interaction length scale.

The asymptotic behavior of the total transition amplitude can be used as a marker for the dominant term in (8.1). Indeed, not only is it possible to detect the absence of the exchange due to the symmetry of the total transition amplitude, more importantly, it is

also possible to detect the onset of exchange behavior. It was mentioned above that the long range symmetry was present up to z = -6.71 au, Figure 8.11, whereupon there is noticeable distortion of the symmetry of the peaks and valleys. Based upon the above findings, this distortion must be due to the gradual enhancement of the exchange term as the separation vector decreases in magnitude. Indeed, taken as a sequence in increasing z, Figures 8.11, 8.12, and 8.13, having z values of -6.71, -5.49, and -4.27 au, respectively, display an increasingly asymmetric coulomb barrier. The magnitude of the coulomb barrier increases by roughly a factor of 6 over this range to a peak value of 8 x 10^{-7} au. However, with the next z sheet, z = -3.05 au, shown in Figure 8.14, a critical transition occurs. At this z location, the interaction is dominated by a deep well, while the magnitude of the coulomb barrier drops to 4 x 10^{-7} au. The well depth is roughly -8 x 10^{-7} au. The critical distance scale, ≈3 - 4 au, correlates with the expected spatial extent of the Ar and N_2 wavefunctions. Recall Figure 7.6 showed the Ar 4s orbital peaking at about 4.5 au from the atomic center. Thus, the appearance of the negative energy well must be due to the commencement of the exchange interaction, with an onset length scale between 3 and 4 au.

The computational gridding provided two additional negative z sheets, Figures 8.15 and 8.16, where z = -1.83 and -0.61 au, respectively. The behavior of the interaction remains essentially steady. Although the coulomb barrier remains constant, the exchange well deepens to nearly -4 x 10^{-6} au. It should be noted that in physical space, the individual N atoms are positioned at ±1.04 au on the z axis. Thus, the calculation of the total transition amplitude for z = ±0.61 au with x, y = 0 places the Ar on the internuclear axis between the two N atoms. However, there is little significant difference between the exchange well for the z-sheet at -1.83 au and the z-sheet for -0.61 au.

Potential Well Model

Because of its prominence, the observed attractive well merits further attention. However, it is difficult to analyze a fully three-dimensional potential. To assist the interpretation of the data, reduction of the spatial dimensionality is helpful. An estimation of the character of the well can be obtained by finding the minimum value of the total transition amplitude as a function of the z value of each planar sheet. For example, for every sheet displayed in Figures 8.1 through 8.32, the minimum value of the interaction is recorded as a function of z. This function is presented in Figure 8.34. However, since this method discards information about the x and y location of the minimum for every z sheet, two additional reduction functions are also useful, one for the x-direction and one for the y-direction. Thus, the well is roughly mapped out by three functions, which are displayed in Figure 8.34. The shape of the well strikingly resembles a square well in all three directions. For distances greater then 4.3 au, there is essentially no attractive potential energy. However, as the distance from the origin decreases to below 4.3 au, the potential energy drops sharply to the value of -4×10^{-6} au.

Because of this spatial behavior, a good model of the attractive portion of the total transition amplitude would be a spherical potential well. The adoption of spherical symmetry is desirable since the full regiment of central force analysis tools may be invoked, including partial wave analysis of the scattering process.

However, the curves of Figure 8.34 only addressed the minimum at every sheet. To monitor the spatial extent of the repulsive potential barrier, an analogous set of functions may be defined which map the maximal value of every sheet for all three spatial directions. This set of functions is displayed in Figure 8.35. In contrast to the agreement of the three curves of Figure 8.34, the maximal functions show considerable deviation from one another. Indeed, in the z-direction, the maximal barrier height peaks occur at

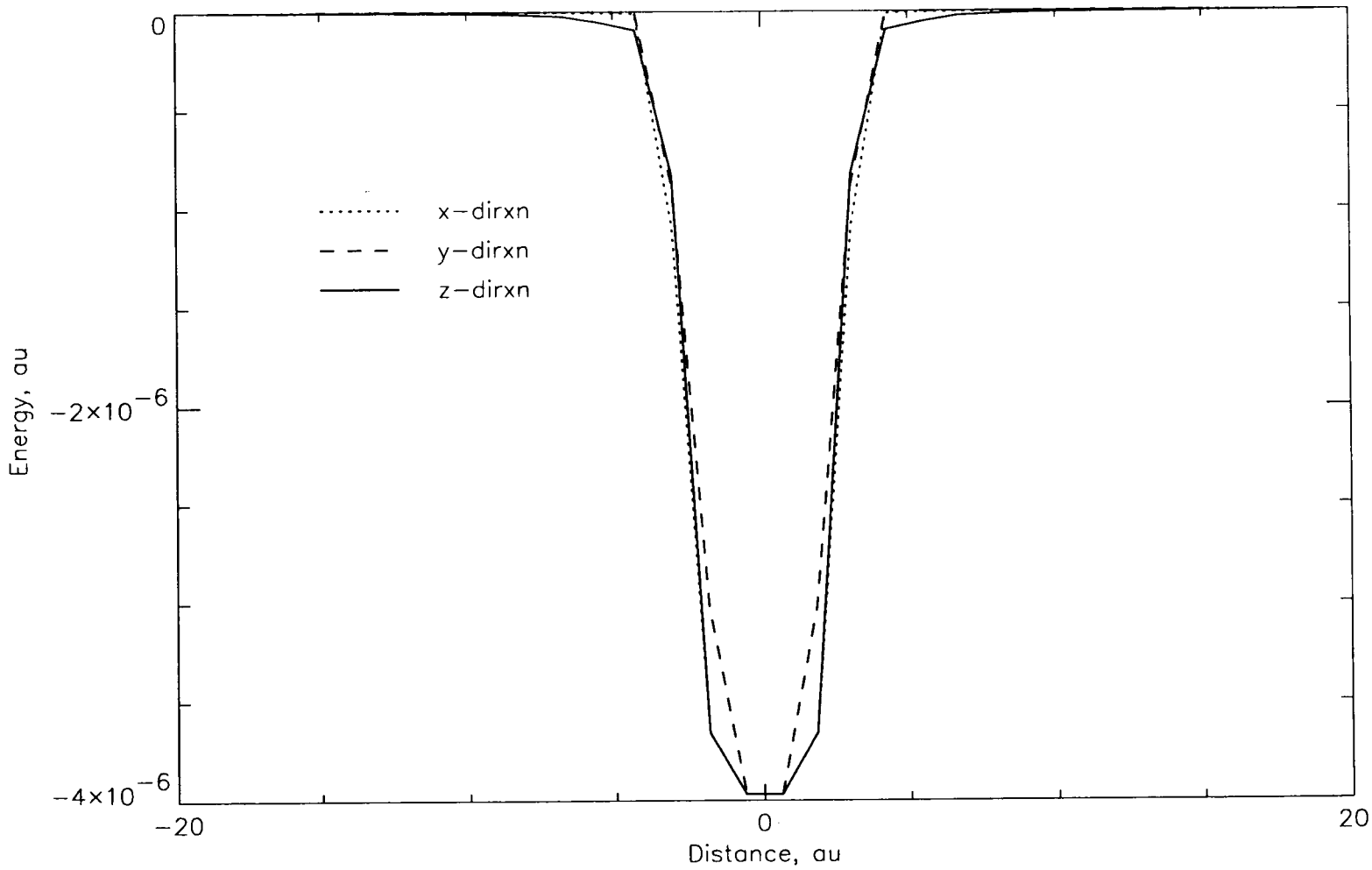

Figure 8.34 Spatial Estimation of the Attractive Potential Well

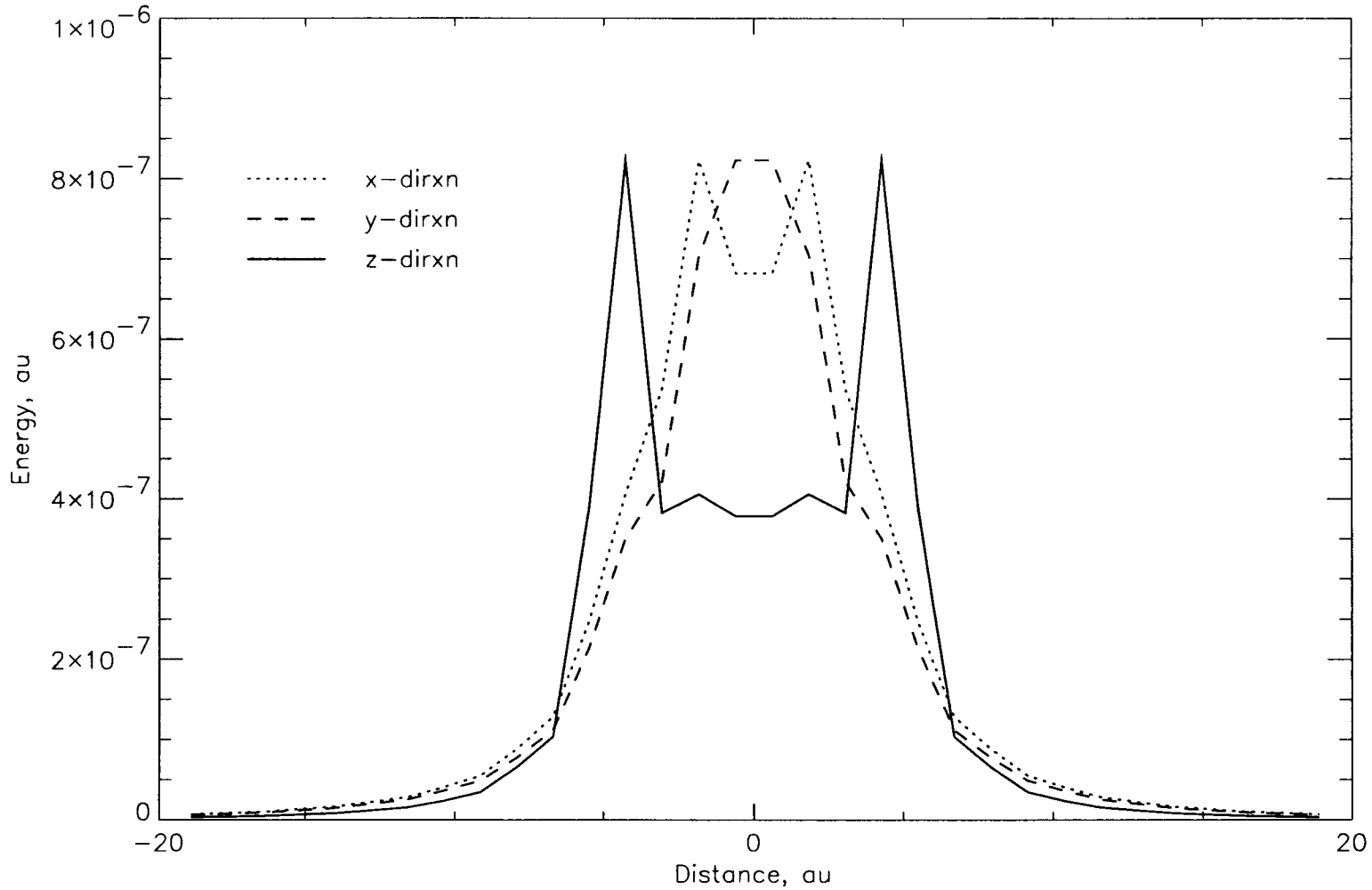

Figure 8.35 Spatial Estimation of the Repulsive Potential Barrier

$\pm$ 4.3 au, whereas in the x-direction, the peak is not reached until $x = \pm 1.83$ au. In keeping with the modeling of the attractive well, a simple model of the spatial extent of the potential barrier is along the lines of a three-dimensional ellipsoid, with the major axis along the z axis, and having nonequal minor axes along the x and y axes. From the actual data, it can be seen that the barrier spans a greater width than the width of the attractive well. For example, in Figure 8.16, the barrier is seen to surround the lip of the attractive well. This suggests a crude model of the transition amplitude as a combination of a spherical square well potential, rimmed by a spherical potential barrier. A schematic of the model is shown in Figure 8.36. As will be discussed below, the fact that the well width is smaller than the total barrier span is important to the scattering amplitude.

Although the model of the potential may appear contrived, it serves to illustrate perhaps the most important aspect of the computed total transition amplitude, the lack of spherical symmetry. If the total transition amplitude were spherically symmetric, then much physical intuition could be extracted from the numerical solutions, such as angular momentum, etc. Without spherical symmetry, the interaction is not a central potential, which means that Schrödinger's equation for the motion of the system is not separable into radial and angular solutions. Hence, a model which preserves this symmetry is worthwhile for qualitative understanding, even at the expense of the accuracy of the model. The full impact of the lack of spherical symmetry in the transition amplitude becomes apparent in the calculation of the differential cross section.

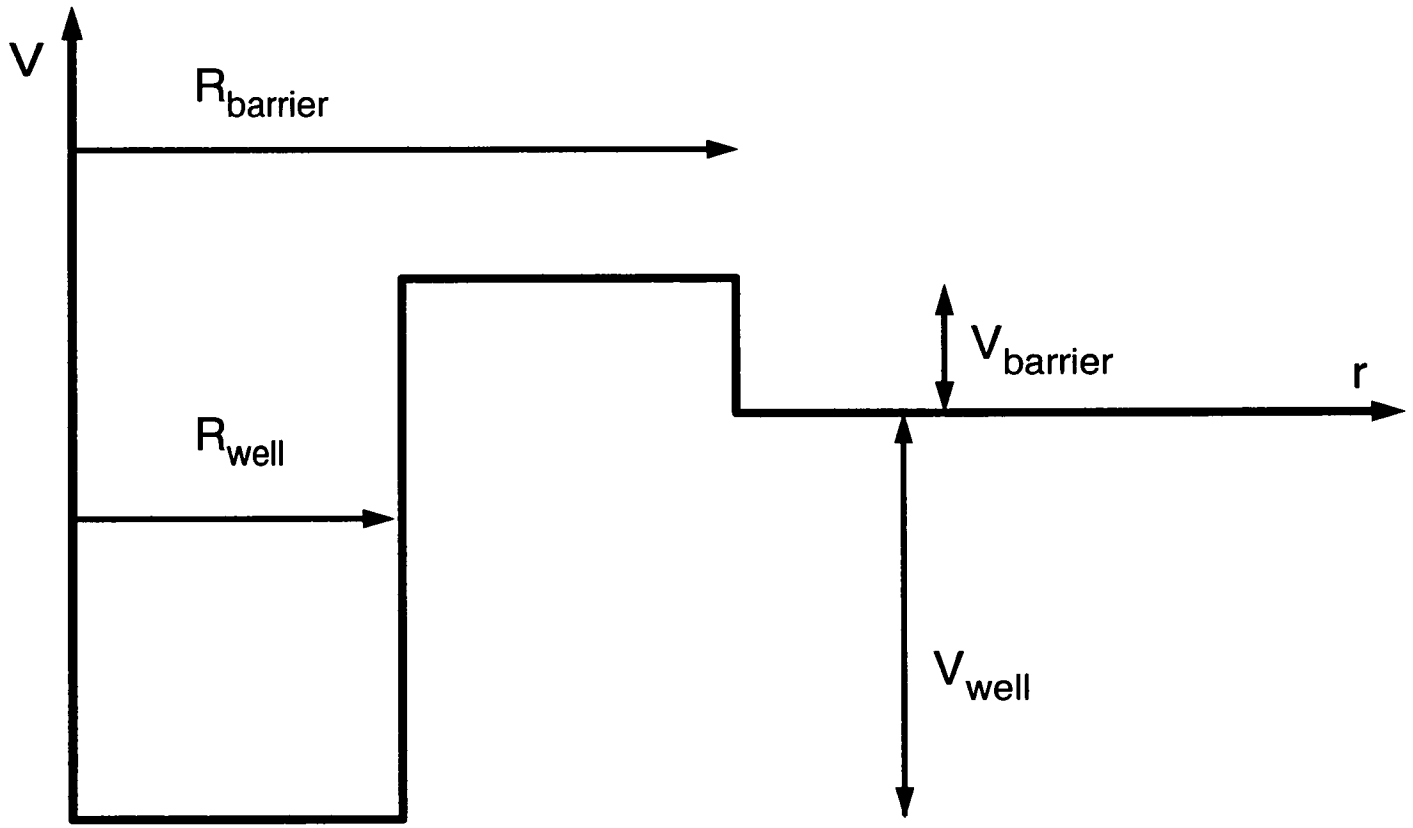

Figure 8.36 Qualitative Model of the Transition Amplitude

Differential Cross Section

Born Approximation Results

As discussed in Chapter 7, the differential cross section was calculated from the results of (7.21) using the first Born approximation. Numerically, this was not a taxing exercise since the FFT technique can be used to calculate the result. There are two technical items worth noting, however. The first is that the functional dependence of the differential cross section is upon the momentum transferred during the collision. There is no dependence upon the initial or final momentum explicitly. Hence, the differential cross section is constant for all initial momenta, which can be related to the initial center of mass kinetic energy. Thus, the Born approximation cannot model the slight collision energy dependence observed in the experimental data.

The second point worth noting is that the momentum difference is a vector quantity given by $\underline{q} = \underline{k_i} - \underline{k_f}$. Furthermore, the momentum transfer vector is registered with the position vector in the form of the Fourier transform. This means that the angular variables referred to in the differential cross section are identical to the angular variables of the configuration space.

The results of the numerical calculation of the differential cross section, as a function of q, may be broken into four regimes. The first regime is for very low momentum transfers, the second is for moderate momentum transfers, the third regime concerns large momentum transfers, and the last regime is for very large momentum transfers.

At very low momentum transfers, i.e. for q very small, the interaction amplitude is essentially sampled for spatially large topographic features. Alternatively, for small q the expression for the differential cross section is roughly a simple volume integral of the

interaction energy over all space. Figure 8.37 shows the results of the numerical calculation of the differential cross section using the computed total transition amplitude. The magnitude for the momentum transfer is 0.08 au. The x-axis of the surface plot refers to the polar angle, θ, and the y-axis refers to the azimuthal angle, ϕ. Note that the periodicity of the azimuthal angle must be reflected by the result of the calculation. Of course, the polar angle has no such restriction.

Two items concerning this data need to be noted. First, the differential cross section is clearly a function of the azimuthal angle. This is due to the fact that the transition amplitude lacks even cylindrical symmetry. There is also a strong dependence of the differential cross section upon the polar angle, although this is usually the case for most central force problems. The second important point is that the momentum transfer for the data of Figure 8.37 has an equivalent wavelength of 12.5 au. In other words, any feature present in the transition amplitude which possesses a length scale less than 12.5 au will be smeared out at this momentum transfer. Referring back to Figures 8.1 through 8.32, the only features with spatial dimensions of this size are the small fluctuations in the long range interaction, such as displayed in Figure 8.1. Note that the amplitude of the fluctuations is roughly 10^{-3} of the attractive well depth. There is no feature of significant amplitude in the data which has a spatial dimension of 12.5 au. From Figures 8.34 and 8.35, the repulsive barrier has a radial length scale of roughly 5 au, while the attractive well is on the order of 2.5 au in radius. Thus, the smoothness of the differential cross section shown in Figure 8.37 is due to a long wavelength averaging of the sharp features of the transition amplitude.

The second momentum transfer regime is typified by the differential cross section shown in Figure 8.38. The data of this plot has a momentum transfer magnitude of 0.48 au. Clearly, there is some structure in the differential cross section, but the features are not distinctive in comparison with the overall level of the data. The polar angle

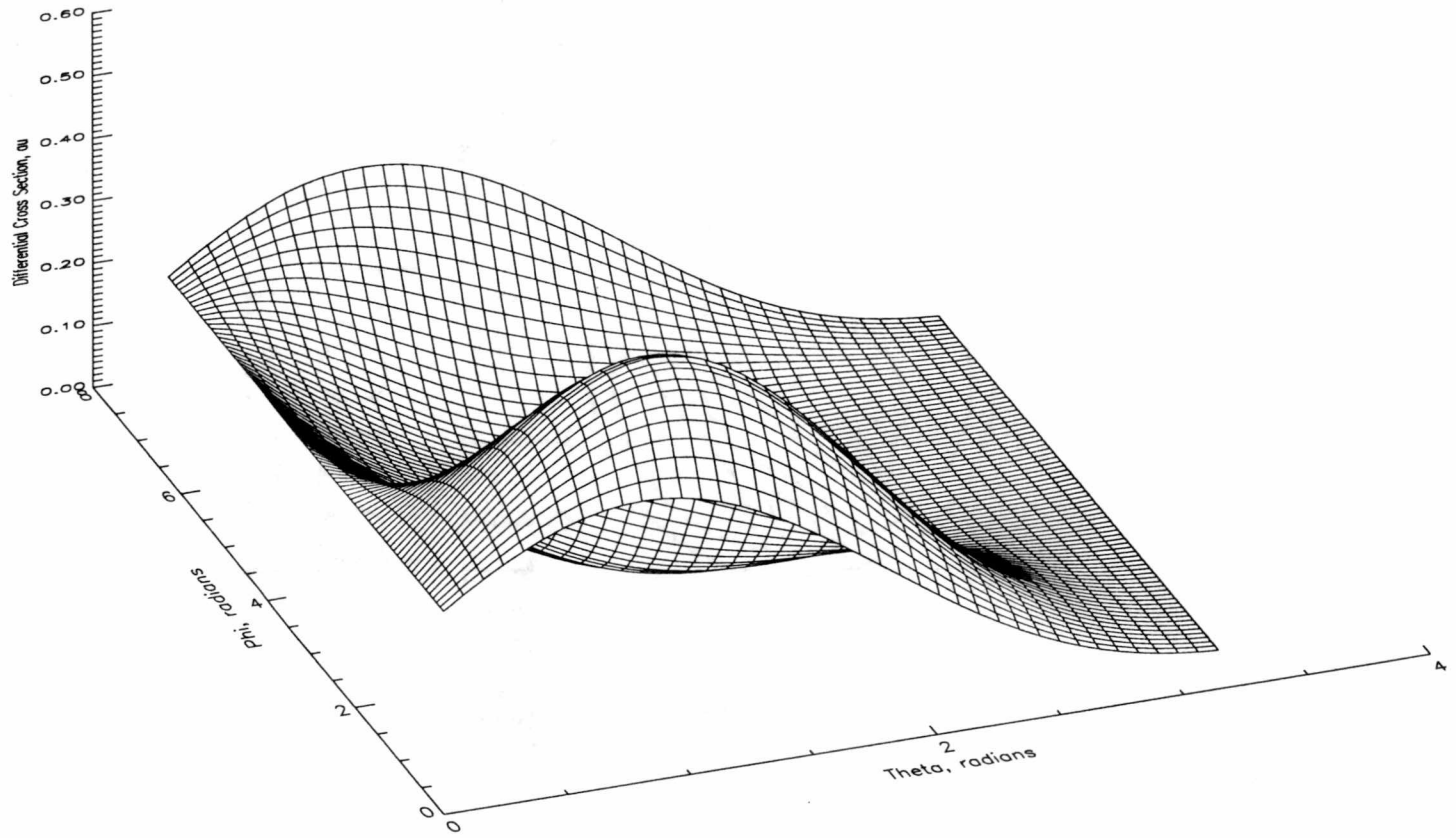

Figure 8.37 Differential Cross Section for $q = 0.08$ au

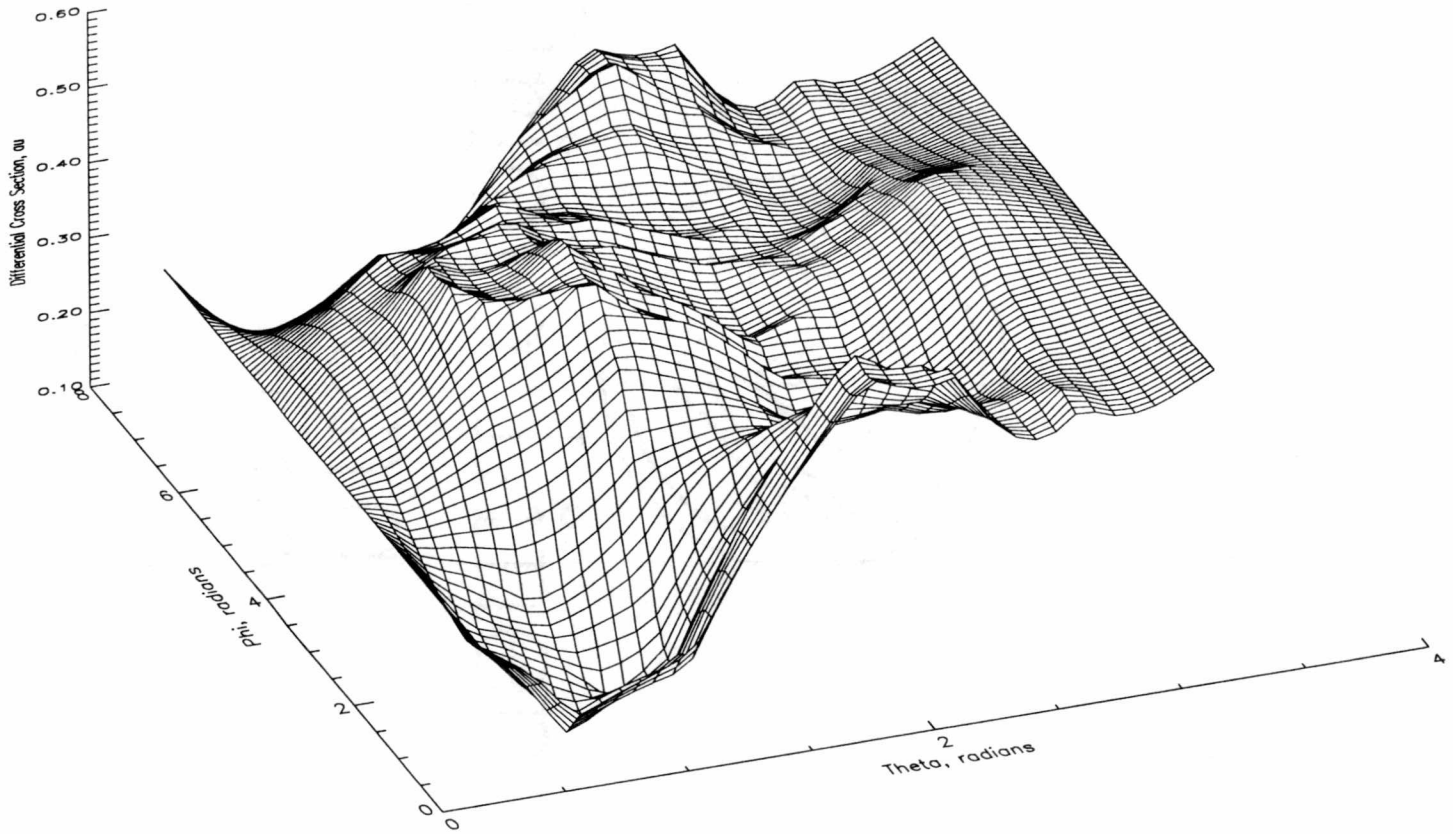

Figure 8.38 Differential Cross Section for $q = 0.48$ au

dependence is rather flat, with the exception for the forward angles, roughly $\theta < \pi/3$. Indeed, the azimuthal dependence for larger polar angles also seems to diminish. The effective length scale probed by the momentum transfer in this regime is on the order of 2 au.

The third momentum transfer regime is characterized by the appearance of definite structure in the differential cross section and is characterized by the data shown in Figure 8.39. The momentum transfer for this data is 0.96 au. There are two clear maxima in the differential cross section. One occurs for a polar angle of roughly $3\pi/4$ and an azimuthal angle of π. The second feature occurs for near zero azimuthal angle and a polar angle of roughly $\pi/4$. The effective length scale for this momentum transfer is approximately 1.04 au.

The very large momentum transfer regime is exemplified by the data shown in Figure 8.40, in which q = 1.53 au. In addition to the peaks observed in Figure 8.39 at $(\theta,\phi) = (\pi/4, 0)$ and $(3\pi/4, \pi)$, there are two additional peaks in the differential cross section located at $(\theta,\phi) = (\pi/4, \pi)$ and $(3\pi/4, 0)$. Hence, the differential cross section of this regime is the most symmetric of all. The effective length scale probed by this momentum transfer is 0.6 au.

The gain in symmetry as the momentum transfer is increased would seem to imply that the transition amplitude essentially becomes more and more spherical to the collision system for larger momentum transfers. For a spherical potential, the scattering amplitude may be resolved into partial waves of angular momentum. The standard expression for the partial wave amplitude is given by [92],

$$f_l(\theta) = \frac{1}{q}\sqrt{4\pi(2l+1)}\, e^{i\delta_l} \sin\delta_l\, Y_{l0}(\theta,\phi) \tag{8.4}$$

where δ_l is the phase shift of the spherical waves due to the presence of the potential. When appropriate, the differential cross section can be calculated from (8.4) by the

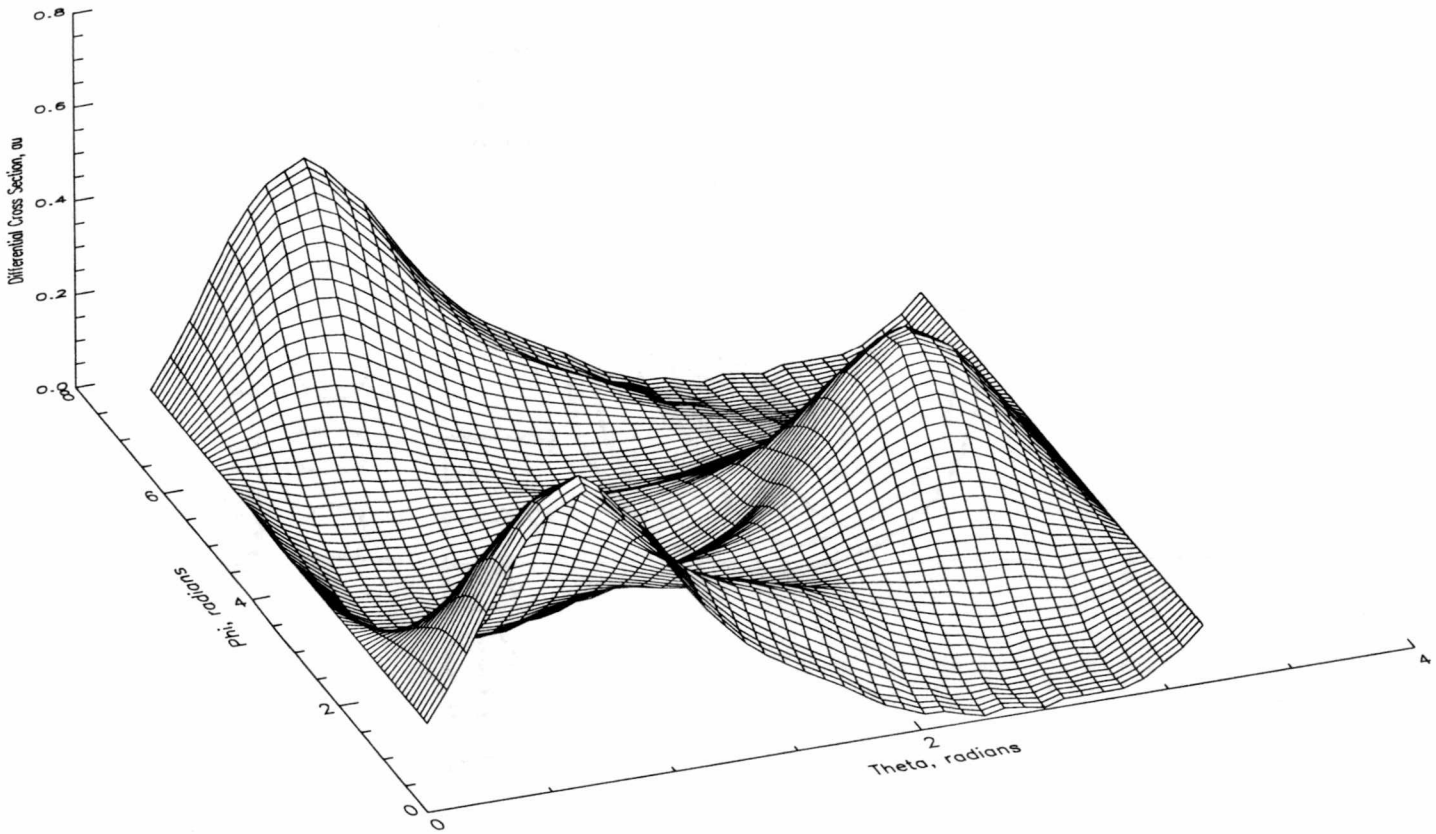

Figure 8.39 Differential Cross Section for $q = 0.96$ au

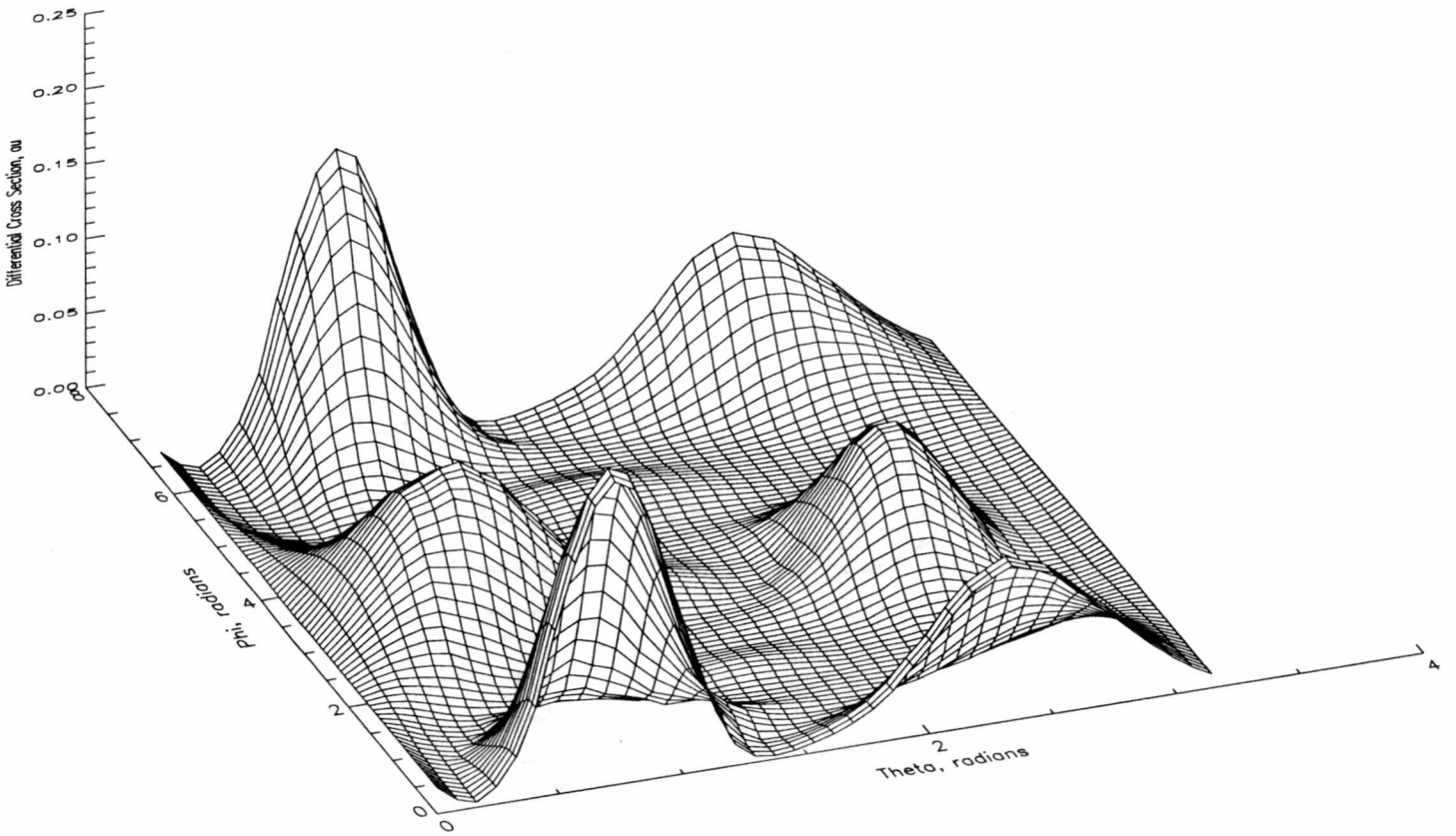

Figure 8.40 Differential Cross Section for q = 1.53 au

equation,

$$\frac{d\sigma}{d\Omega} = \left| \sum_l f_l(\theta) \right|^2 \tag{8.5}$$

The dependence of the scattering amplitude upon the spherical harmonic suggests that the periodicity in θ exhibited by the data in Figure 8.40 might be due to a partial wave effect. Tables of the spherical harmonics are available in most standard texts [63], but for the present purposes it is important to note their functional forms,

$$Y_{00} = 1/\sqrt{4\pi} \tag{8.6}$$

$$Y_{10} = \sqrt{\frac{3}{4\pi}} \cos\theta\,; \qquad Y_{1\pm1} = \mp\sqrt{\frac{3}{8\pi}} \sin\theta\, e^{\pm i\phi} \tag{8.7}$$

$$Y_{20} = \sqrt{\frac{5}{4\pi}}\left(\frac{3}{2}\cos^2\theta - \frac{1}{2}\right); \quad Y_{2\pm1} = \mp 3\sqrt{\frac{5}{24\pi}} \sin\theta\cos\theta\, e^{\pm i\phi}\,; \quad Y_{2\pm2} = 3\sqrt{\frac{5}{96\pi}} \sin^2\theta\, e^{\pm 2i\phi} \tag{8.8}$$

The differential cross section data of Figures 8.39 and 8.40 can be loosely correlated with (8.4) and (8.5) on the basis of the location of the peaks as a function of the polar angle. The azimuthal dependence of the differential cross section is most likely due to cross terms in the partial wave expansion. This would imply that there is no particular angular momentum which dominates the partial wave expansion. In other words, at higher momentum transfer, the transition amplitude appears more spherical, but with a strong azimuthal feature. The data of Figure 8.40, which is the regime of very large momentum transfers, has peaks at $\theta = \pi/4$ and $3\pi/4$, with $\phi = 0,\ \pi$. From (8.8), this is roughly the behavior of $Y_{2\pm1}$ and $Y_{2\pm2}$. The peaks in the data of Figure 8.39, which are at lower energy transfer, correlate with the number of azimuthal peaks present in $Y_{1\pm1}$.

Therefore, at sufficiently high momentum transfers, the transition amplitude effectively loses much of its irregular nature.

Total Cross Section

Results of Numerical Integration

Once the differential cross section is obtained, it is a straightforward matter to determine the total cross by direct numerical integration. No further approximations are necessary. The culmination of this study is presented in Figure 8.41, in which the computed total cross section is given as a function of momentum transfer.

The first item to note is the absolute magnitude of the cross section. The present calculation determines the cross section as 5.96 au, or 1.67 A^2. Before comparing this value to the measured values of Chapter 6, it is instructive to attempt to understand the momentum transfer dependence of the total cross section.

Qualitative Features of the Cross Section

The key to interpreting Figure 8.41 has been alluded to above. It was found that the length scale of the momentum transfer effectively changes the transition amplitude that a plane wave of particular momentum will scatter from. From the above, it was determined that for high momentum transfers, the transition amplitude effectively became more regular in shape. However, since the peak in the total cross section occurs for lower momentum transfers, it is important to understand the phenomenon occurring in that regime.

In fact, describing the low momentum transfer regime was the prime motivation for introducing the qualitative amplitude model of Figure 8.36. Recall that for the lowest momentum transfers, the probe length was on the order of 12.5 au, much larger than any

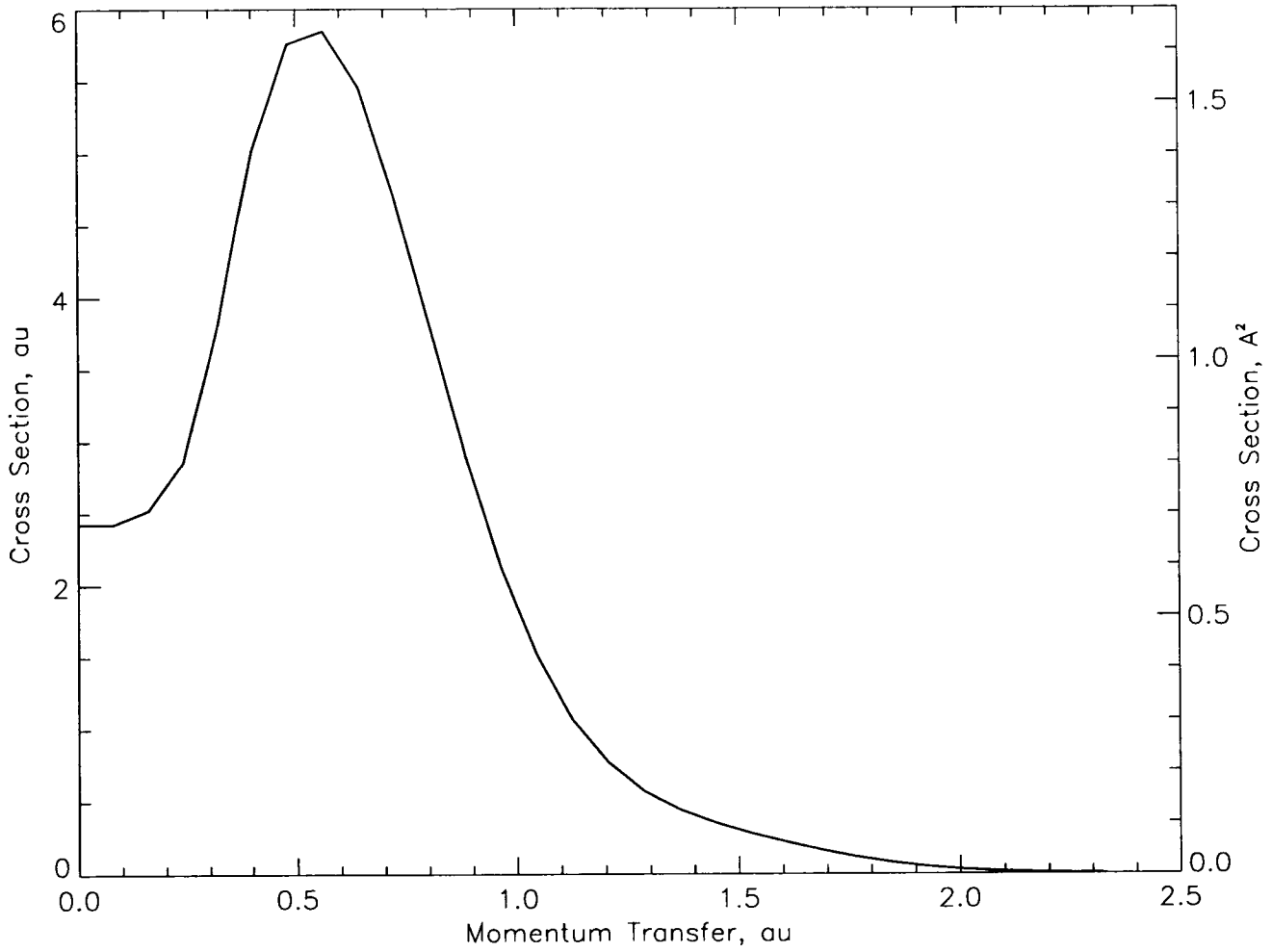

Figure 8.41 Total Scattering Cross Section for Ar-N_2 Energy Transfer

feature in the transition amplitude data. As the momentum transfer increases, the first significant feature to be "seen" is the coulomb barrier. In order to understand the behavior of the total cross section at low momentum transfers, it will be sufficient to solve the qualitative model of Figure 8.36.

The theory of scattering from spherical barriers and wells is discussed in most standard texts. The important aspects are the application of partial waves (8.4), the determination of the phase shift, and the summation of the waves to obtain the cross section (8.5). Although the topic is well developed, it can provide a wealth of insight. Repulsive potential barriers lead to negative shifts in the phase of incoming spherical waves with respect to the outgoing spherical waves. The extent of the shift depends upon the width and height of the barrier. Beginning with the lowest momentum transfer, the transition amplitude appears as a solid potential barrier. Assuming that the system energy (in this instance, the momentum transfer defines the energy scale) is larger than the barrier height, the solution for the scattering phase shift is a transcendental function of the momentum transfer. If Figure 8.36 is used to model the actual coulomb barrier, it can be estimated that the barrier height is 4×10^{-7} au, and the width is approximately 5.0 au. Note that for sufficiently long wavelengths, the inner attractive well is too narrow to create significant scattering. Furthermore, for low momentum transfers, it is usually sufficient to calculate only the $l = 0$ quantities.

The result of calculating the $l = 0$ scattering phase shift for this case is shown in Figure 8.42. First of all, note that the phase shift is negative. This is true, in general, for all repulsive barriers. Also, note that it tends to zero as q goes to zero. However, the momentum transfer may not fall below a level corresponding to the barrier height. The total cross section may be obtained from the phase shift via [51,92]

$$\sigma = \frac{4\pi}{q^2} \sin^2 \delta_0 \tag{8.9}$$

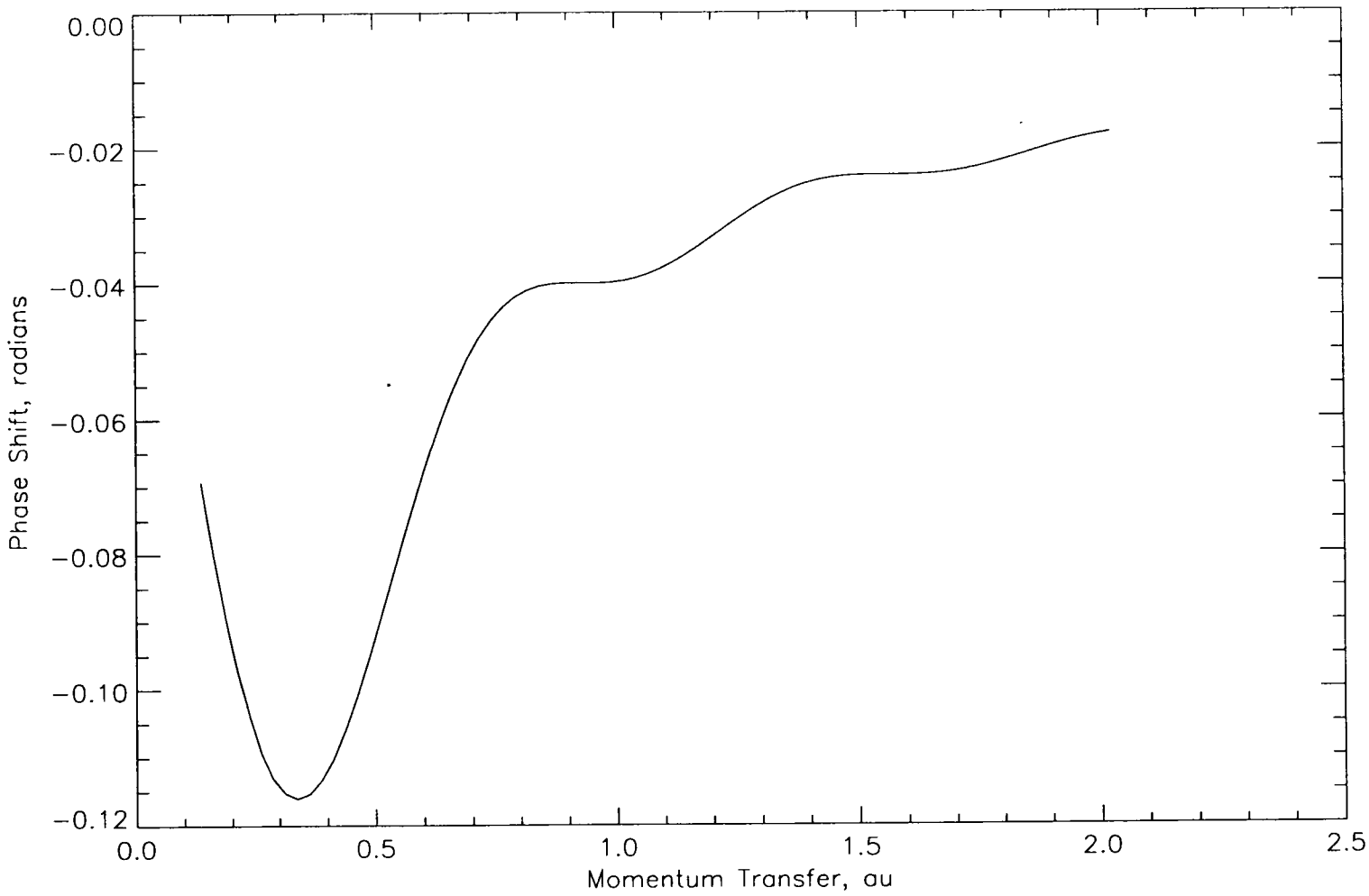

Figure 8.42 Scattering Phase Shift using the Model Potential Barrier

where $\delta_0 = \delta_0(q)$ as mentioned above. Based upon the data of Figure 8.42, the total cross section for the qualitative model was calculated by (8.9). The result is displayed in Figure 8.43, where only the low momentum transfer values are of interest. Comparing the barrier model cross section with the result of the actual computation shown in Figure 8.41 reveals striking agreement for the lowest momentum transfers. Whereas the complete calculation predicts a cross section of 2.4 au at $q = 0.1$ au, the model predicts 3.3 au. This is roughly a 40 percent disagreement. It should also be noted that from Figure 8.35 the description of the barrier as spherically symmetric was not a particularly good one.

Obviously, the barrier model calculation fails in comparison to the actual calculation for momentum transfers much larger than 0.1 au. However, it did illustrate the fact that the system was blind to details in the transition amplitude smaller than 5 au. As the momentum transfer increases, though, it is possible to detect the presence of the potential well embedded within the barrier. Indeed, the depth of the well is large enough to overshadow the coulomb barrier. A calculation of the phase shift due to the attractive well was performed for two well widths. One calculation used the width of the actual well near the top, which was taken from Figure 8.34 as 4.3 au. The second calculation attempted to consider the fact that the actual well of Figure 8.34 is narrower at the bottom than at the top. Thus, the width, 2.5 au, at the half-height position was used. In both instances the model well depth was -4×10^{-6} au.

The resulting scattering phase shift is shown in Figure 8.44 for both model well widths. Note that both phase shifts are positive, as is true, in general, for attractive wells. The result for the 2.5 au width shows that the phase shift peaks for momentum values near 0.5 au, and goes to zero for both low and high momentum transfer values. The phase shift using the 4.3 au well width, however, tends to π as q goes to zero. This result is rather intriguing because it indicates the presence of a bound state. Further

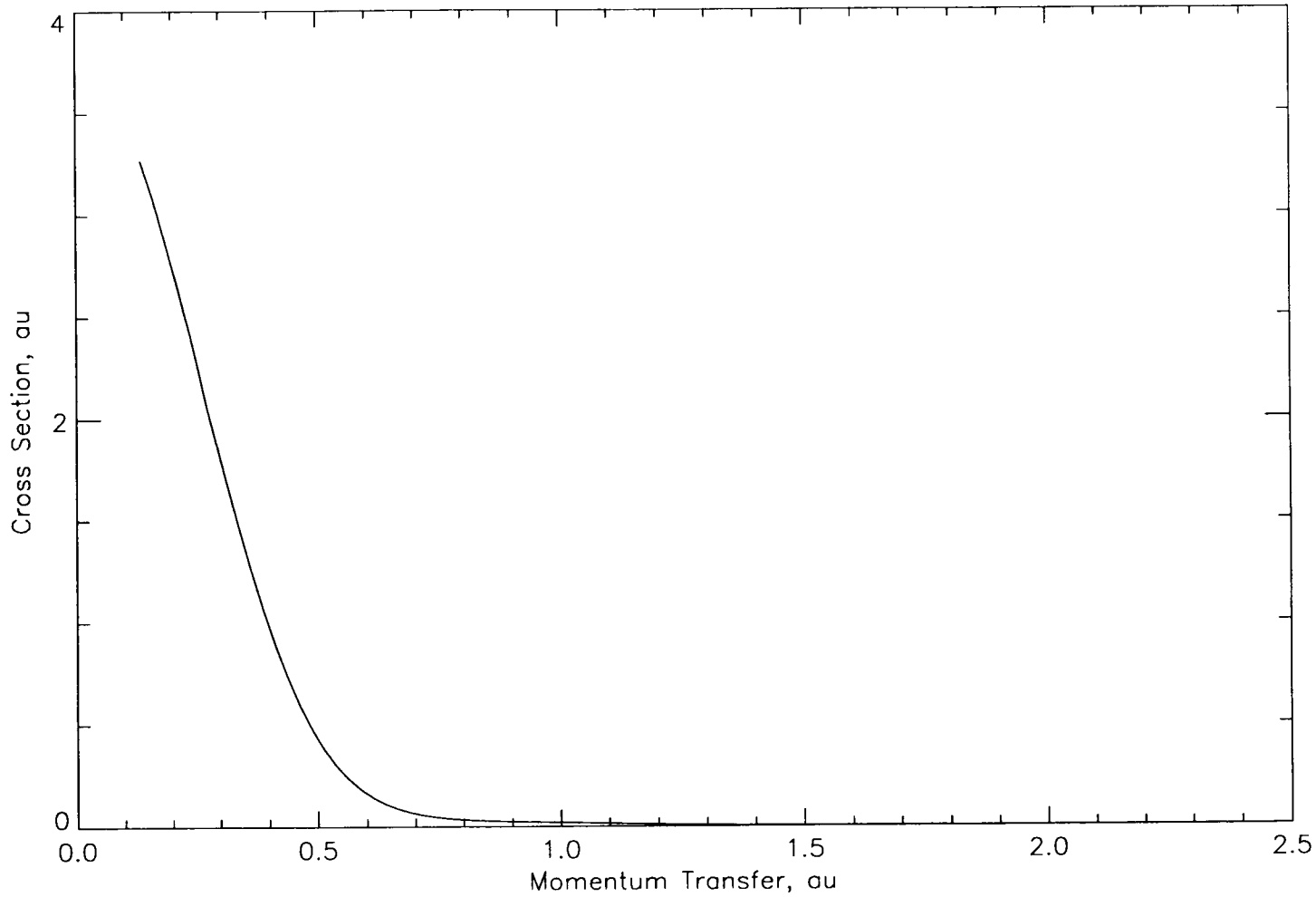

Figure 8.43 Total Scattering Cross Section using the Model Potential Barrier

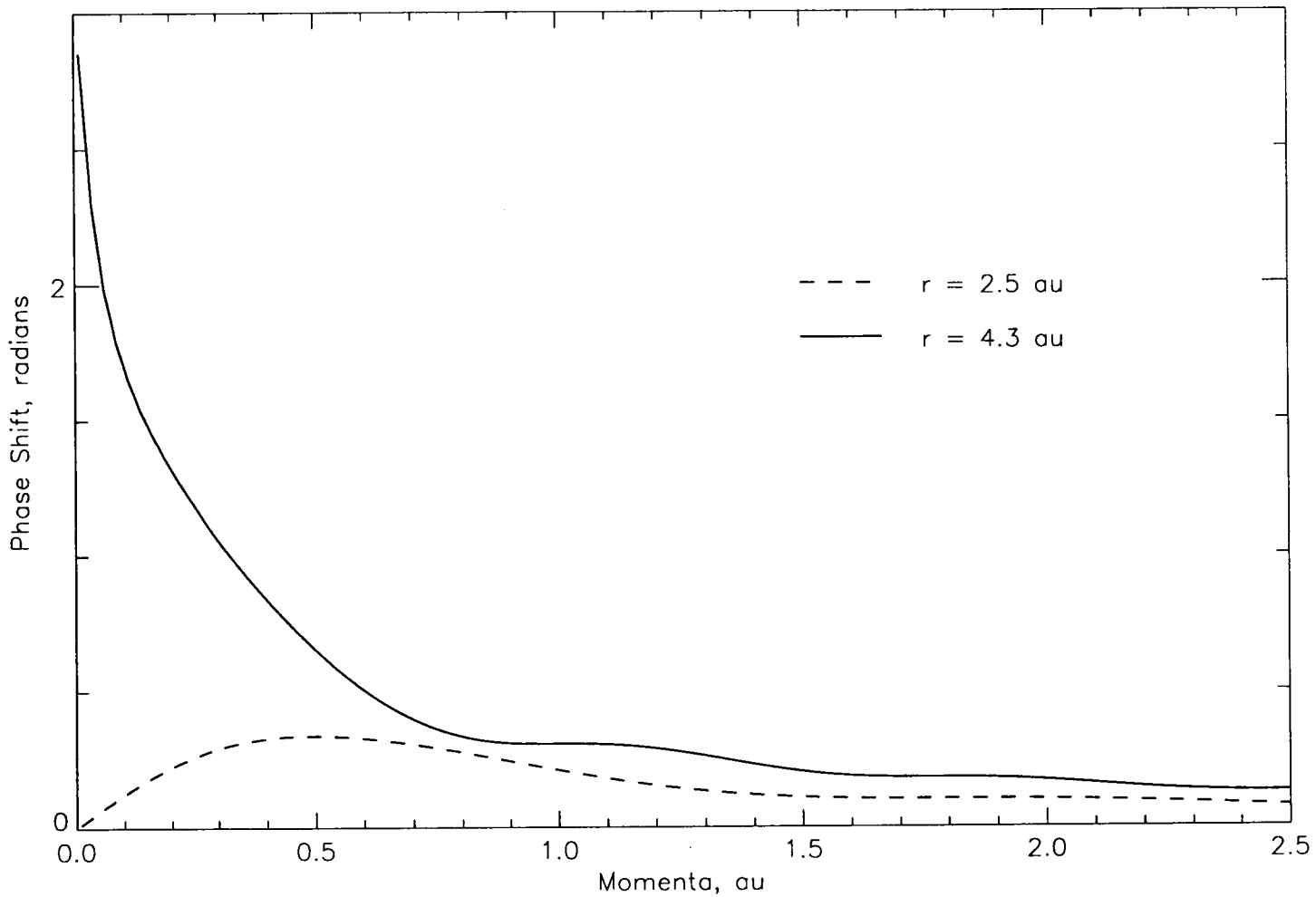

Figure 8.44 Scattering Phase Shift using the Model Potential Well

analysis shows that, for the well depth of -4×10^{-6} au, there exists a critical radius of 4.0 au which determines whether a bound state will exist.

To the extent that this simple model represents the actual transition amplitude for the Ar-N_2 reaction, it is not outrageous to assert that an ionic bridge may form between the reactants during the collision. Indeed, Vredenbregt, et al., [83] recently proposed this phenomenon to explain their seemingly large experimental cross section data. It is interesting that this possibility would arise from this study.

As a measure of the quality of the model well in representing the actual transition amplitude, the total cross section was calculated via (8.9) and the results are shown in Figure 8.45. In comparing the model well calculation with the actual cross section, it is clear that the 4.3 au width well is not a good representation of the actual transition amplitude. However, the 2.3 au width well yields surprisingly good agreement with the complete calculation in the appropriate momentum transfer region. The model well cross section at $q_.= 0.5$ au is 5.2 au, compared with 5.9 au for the complete transition amplitude computation, or roughly a 12 percent difference. Given the gross oversimplification of the true transition amplitude by the model well, the agreement is remarkable.

The purpose of introducing a spherical model of the computed transition amplitude was to discern the physical meaning of the variation of the resulting cross section with momentum transfer. Clearly, this objective has been met. At very low momentum transfers, the coulomb barrier dominates the scattering. As the momentum transfer increases, the attractive well due to the exchange-like term of the complete interaction Hamiltonian starts to scatter incoming waves. This channel-opening is responsible for the rise in the total cross section to the value of 5.97 au. Finally, as the momentum transfer continues to increase, the irregular features of the transition amplitude become less important to the scattering process. At this point, the probe

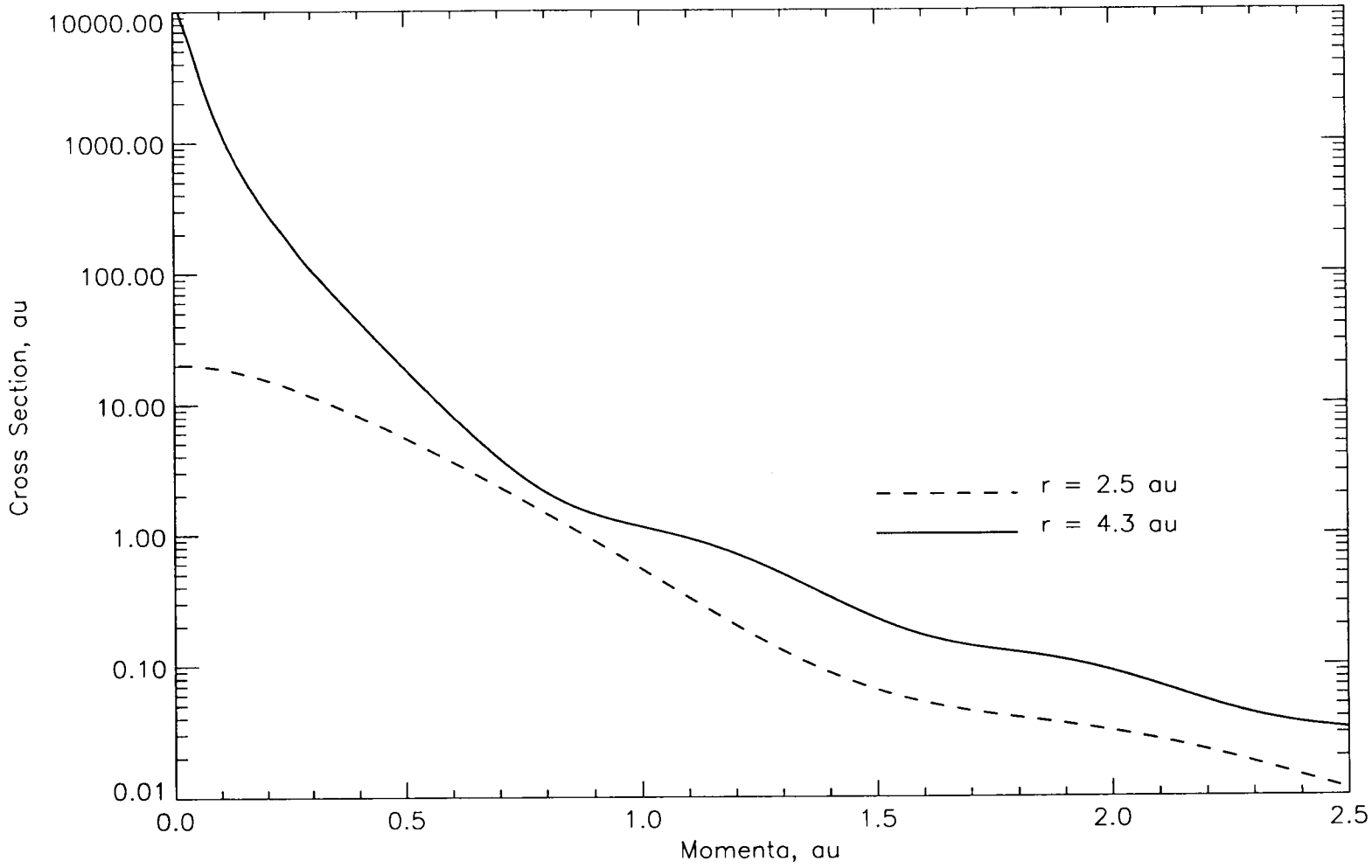

Figure 8.45 Total Scattering Cross Section using the Model Potential Well

length is much shorter than any significant feature of the transition amplitude, and the scattering is due to the near spherical attractive well. At the higher momentum transfer values, the differential cross section has a strong azimuthal dependence due to the cross terms in the partial wave expansion.

Comparison to Experimental Data

Although the model potential yielded a great deal of insight, the comparison of the calculated cross section to the experimental measurements is the true test. The experimental data has been thoroughly discussed in Chapter 6, and the results are summarized in Table 6.3. Ten measurements of the cross section are listed with values ranging from 2.7 to 18 A^2. The publication by Parr and Martin [72] of their inference of the data of Kolts [9] can be discarded because of the subsequent correction by Tyndall, et al., [74]. After dropping the highest and the lowest value, the number of measurements is reduced to seven. Without regard to the collision energy of the measurement, the mean value is 9.0 ± 3.5 A^2. The peak value in the calculated cross section is 1.67 A^2, which is roughly a factor of 5 lower than the mean experimental cross, and a factor of 3.3 lower than the lower bound of the mean, i.e. 5.5 A^2.

As a rule, the cross sections determined from the crossed beam experiments tend to yield greater values than the other techniques. The mean cross section as determined from the crossed beam experiments is 12.2 ± 4.4 A^2. The mean cross section measured by the remaining techniques, with the removal of the Parr and Martin value, is 5.7 ± 2.7 A^2. This is a factor of 2 lower than the crossed beam measurements. Since the crossed beam measurements occur at much higher center-of-mass energies than, for example, a discharge flow tube, it is reasonable to infer that the cross section has a dependence upon the system collision energy. A comparison of the calculated cross section with the data from the non-crossed beams experiments shows that the calculated cross section is

roughly a factor of 3.5 lower than the mean, and a factor of 1.8 lower than the lower bound to the mean. A comparison to the crossed beam experiments shows that the calculated cross section is a factor of 7.3 lower than the mean and a factor of 4.7 lower than the lower bound of the mean.

The fact that the calculated cross section agrees better with the low energy data than it does with the high energy data is somewhat surprising. To put it in the proper perspective, though, the low energy data was recorded at ambient temperatures such that the energy scale is 0.025 eV. This is only one order of magnitude difference from the beam data.

Typically, the Born approximation tends to agree better with higher energy data. It is worthwhile to assess the validity of the Born approximation now that the magnitude and length scale of the interaction are known. Using $k = \sqrt{2\mu E}$, the Born criteria given in (5.68) can be rewritten as

(8.10) $$E >> 2\mu R^2 |H'|^2$$

From above, $|H'| = 4 \times 10^{-6}$ au and $R = 2.5$ au. Substituting these values into (8.10) along with the value of the reduced mass, $\mu = 1.89 \times 10^4$ au, sets the energy scale as

(8.11) $$E >> 3.8 \times 10^{-6} \text{ au}$$

The crossed beam experiments have energies on the order of 10^{-3} au, while the discharge reactor experiments have energies on the order of 10^{-4} au. Thus, while the experimental energy scales are greater than 10^{-6} au, it is not clear that they are greater by a sufficient amount.

As mentioned in Chapter 7, the choice was made to pursue the Born approximation to prove the concept of the two-electron exchange mechanism. Clearly, the most significant drawback of the Born approximation, as mentioned in Chapter 5, is that the system does not evolve due to the interaction Hamiltonian. Physically, the replacemet of the correct solution to the interaction Hamiltonian by a solution to the free

Hamiltonian is tantamount to restricting the scattering process to a single point in the space, i.e. it is an impulse approximation. The transition amplitude data displayed in Figures 8.1 through 8.32 show that the interaction has a significant spatial extent. The Born approximation is incapable of fully describing this spatial extent because the wavefunctions are not free to realign as they system moves over the interaction potential. This result clearly points out that a desirable refinement of the present technique is a distorted Born wave approximation. By using coulomb waves, rather than plane waves, the description of the long range scattering will improve. Thus, this will tend to increase the predicted scattering cross section because they waves will be able to scatter from the outer portions of the interaction potential.

Estimation of Computational Uncertainty

The numerical technique used to calculate the cross section was rather involved. A legitimate question, in the light of the comparison to the experimental data, is the accuracy of the computation. To resolve that issue, an investigation was made into the numerical method used to calculate the cross section. First, note that in the flowchart of Figure 7.1, there is one theoretical block and three numerical blocks. Thus, it is assumed that the computational error will be due primarily to three sources: 1) the computation of the interaction Hamiltonian and the transition amplitude, 2) the FFT used to calculate the differential cross section in the Born approximation, and 3) the numerical integration of the differential cross section to obtain the total cross section.

The simplest computational step to assess is the last one. The integration of the differential cross section over the solid angle at a given radius was done by using Simpson's Rule with 40 points in both the θ and ϕ directions. The truncation error associated with Simpson's Rule is estimated by [63],

(8.11) $$\varepsilon = -h^5 \frac{f''''(\xi)}{90}$$

where ξ is some point within the integration interval. For the purpose of error assessment, it can be assumed from the above discussion of the differential cross section, that the differential cross section can be considered as proportional to a sine or cosine function. Thus, the fourth order derivative on θ and ϕ will also be proportional to a sine or cosine function. Because the spherical harmonic coefficients are all less than one, the evaluation of the fourth order derivative at some point in the interval has an upper bound of unity. The value of $h^5/90$ for the calculation parameters is 3×10^{-8}. Note that the calculation was done in double precision. Hence, the contribution of the numerical integration to the global numerical uncertainty of the total cross section is less than 3×10^{-8} au.

The first step of the computational chain required some additional effort in order to quantify the numerical error. This was not a straightforward task, due to the intricacies involved in actually computing the transition amplitude. The FORTRAN code structure is based upon a set of 18 nested DO loops which mimics (7.34). At the inner most loop, a subroutine with the name four_gip, in reference to the fact that it solves the inner product of four primitive gaussians, is called to determine the atomic orbital integral given in (7.56). Prior to the four_gip call, the set of DO loops primarily serves to define a given grouping of expansion coefficients, indices, and exponents. After the program returns from four_gip, the DO loops accumulate the results.

The entire program was modified to count the number of instructions performed in four_gip, the number of times that four_gip was called, and the number of accumulations in the DO loops. Independent tallies of the simple math operations and exponentiations were kept, based upon the general assumption that the numerical uncertainty of exponentiation is greater than that of addition, subtraction, or

multiplication. The result of the instruction counting was that the total number of exponentiations required to calculate a single grid point was roughly 10^8 operations. The total number of simple math operations was on the order of 10^7 operations. The entire program utilized double precision. Simple math operations are uncertain in the fifteenth digit, while exponentiations are uncertain in the fourteenth digit. An estimate of the cumulative propagation of numerical uncertainty of the final result for the transition amplitude at given grid point is determined by multiplying the uncertainty level of a single operation with the number of operations used in the grid point calculation. By this method, the numerical uncertainty of the transition amplitude lies in the sixth digit.

Estimating the numerical uncertainty of the intermediate step, the calculation of the differential cross section was less direct than for the other two steps because a commercial package was used to calculate the FFT. Since access to the source code was impossible, an empirical approach to the numerical uncertainty was taken. Conceptually, it may be outlined as follows. Suppose there exists a quantity, α, which undergoes a transformation, $f(\alpha)$, such that, for infinite precision, $f(\alpha)=\beta$. If there is computational uncertainty present, then the result of the transformation upon α will be given by $f(\alpha)=\beta+\Delta\beta$. The task is then to determine the value of $\Delta\beta$. It follows that a small variation of α may be used to probe the scale of $\Delta\beta$ by letting $\alpha+\delta\alpha$ undergo the transformation and defining $f(\alpha+\delta\alpha)\equiv\beta'$. In the event that $f(\alpha)$ is a linear transformation, the process is simplified because $f(\alpha+\delta\alpha)=(\beta+\Delta\beta)+(\delta\beta+\Delta\delta\beta)$. By neglecting second order variations, it is possible to estimate $\Delta\beta$ as

$$\Delta\beta=\lim_{\delta\alpha\to 0}\{f(\alpha+\delta\alpha)-f(\alpha)\} \tag{8.12}$$

To determine this relationship for the commercial FFT would have been cumbersome in practice. A more practical approach to the numerical uncertainty was taken, although it was still based on (8.12).

The experimental data of Table 6.3 lists values which are certain in the first and second digits. Thus, a comparison to a calculation which is certain in the tenth digit is excessive. Since it was determined that the first and third steps of the overall calculation have numerical uncertainties in the eighth and sixth digits, respectively, it was only necessary to ensure that the FFT algorithm was certain to a level better than the second digit. Suppose that $\delta\alpha = 0.01\alpha$, then it is necessary that the residual $\Delta\beta$ be no greater than 0.01β if the FFT is to be certain to better than the second digit. This was, in fact, calculated using the computed transition amplitude result with a 1 percent variation. The FFT was performed for both the transition amplitude and the transition amplitude combined with 1 percent noise. Since it was known that the numerical integration over spherical angles was accurate in the eighth digit, the total cross section was calculated in order to simplify the determination of the residual. Hence, the total cross sections with and without 1 percent noise added to the transition amplitude were subtracted to find $\Delta\beta$ as a function of the momentum transfer. The result is shown in Figure 8.46 and it is clear that the residual is much less than 1 percent for all but the largest momentum transfers. At $q = 2.3$ au, the residual becomes greater than 1 percent. Note that this does not indicate that the computational uncertainty is greater than 1 percent for $q \geq 2.3$ au. It merely indicates that a finer variation in the amplitude is required to determine a bound of the uncertainty.

Since the transition amplitude has an estimated uncertainty of 10^{-6}, the uncertainty due to it can be neglected in comparison to the exercise using a 1 percent variation of the FFT. Thus, the numerical uncertainty of the overall calculation can be confidently given as less than 1 percent for momentum transfer values less than 2.3 au.

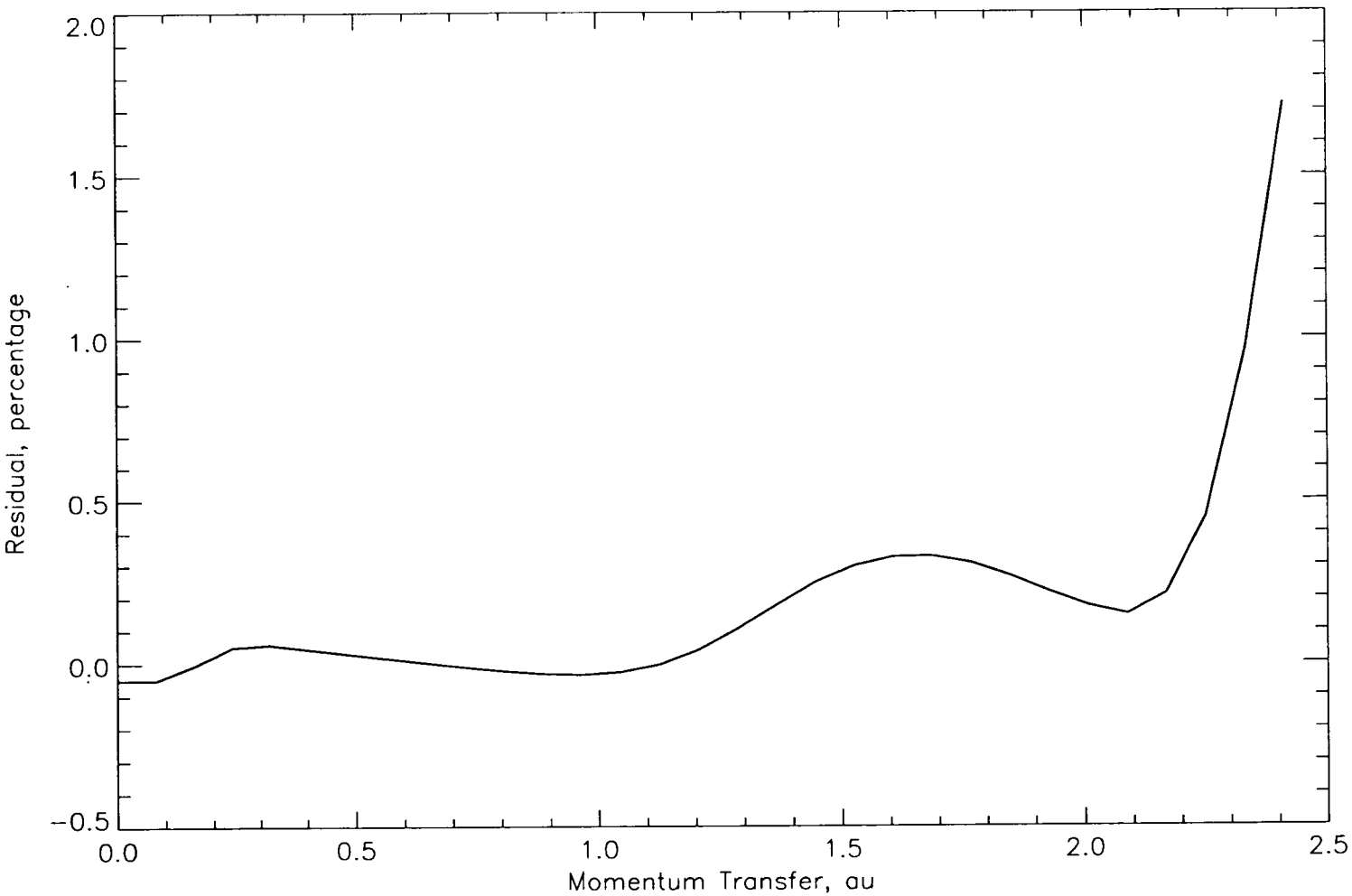

Figure 8.46 Residual of the FFT Calculation of the Transition Amplitude with a 1 Percent Noise Level

Chapter 9

Summary

This final chapter is intended to concisely reiterate the results obtained during this research, list the assumptions made in order to obtain the results, and specify some future research directions.

Results

Four primary results were obtained during this research. Two of these are related to scientific advancement of the description of fast, spin-forbidden energy transfer reactions. The remaining two results are of a more technical nature, relating to advances in current techniques of established fields of research. They are summarized below in a list format. A complete discussion occurs in the preceding Chapters.

1. A first principles derivation of the two-electron exchange mechanism for bimolecular collisions was presented in Chapter 3. Driven by the unique physical arrangement of the colliding reactants, and the inability of standard molecular quantum electrodynamics to describe the collision process adequately, a hypothesis was proposed which effectively replaced the photon as the collision intermediary by the electron.

2. The fast, spin-forbidden energy transfer reaction,

$$Ar(^3P_{0,2}) + N_2(X^1\Sigma_g^+) \rightarrow Ar(^1S_0) + N_2(C^3\Pi_u)$$

was modeled numerically using the theoretical results above. It was found that the cross section predicted by the two-electron exchange mechanism was

1.67 A^2. This value is roughly a factor of 5 lower than the average of the experimental measurements, which range from 2.7 to 18 A^2.

3. In quantum chemistry, the solution of two-electron integrals is a key element in the study of chemical structures. Typically, they are calculated using numerical quadrature. This research developed an approach to solve the two-electron integrals analytically. The analytic solutions were then used in the numerical modeling of the Ar-N_2 reaction.

4. Because the numerical modeling of the Ar-N_2 reaction was computationally stressing, a workstation cluster was developed to perform the calculation. The technology of distributed processing, i.e. clustering, is rapidly being developed by the computational science community. The present research represents a unique application of that technology.

Assumptions

In assessing the results of any analysis, it is important to know the limits placed upon the solution by the underlying assumptions. This research relied upon several assumptions about the nature of physical systems, in general, and the Ar-N_2 reaction in particular. There were three crucial approximations applied during the research presented herein. They were explicitly discussed in the text and are briefly listed below. This research used many standard techniques of *ab initio* quantum chemistry during the application of the two-electron exchange mechanism theory to the Ar-N_2 system. There were many implicit assumptions within these numerical techniques, and a short listing of the most important of these is also given. Further discussion of their impact upon *ab*

initio quantum chemistry calculations is relegated to the appropriate references.

1. The most important assumption made was that quantum field theory can provide an adequate description of physical systems on the molecular length and energy scales.

2. The application of the two-electron mechanism to the Ar-N_2 system invoked the assumption that the initial and final states could be described by ignoring all but the participating electrons. Thus, any impact that the inner shell electrons of Ar and N_2 might have upon the final cross section calculation has been ignored.

3. The kinematics of the Ar-N_2 reaction were described using the first Born approximation. A crude estimate of the ratio of the time the system spends under the influence of the interaction to the time required for the interaction Hamiltonian to appreciably alter the free eigenstate manifold indicates that the Born approximation should be valid.

4. The molecular structures were modeled by *ab initio* quantum chemistry. Quantum chemistry, in general, assumes an efficient numerical fit to the self-consistent field solutions for the electronic wavefunctions of the atoms which compose the molecule of interest.

5. This research used one type of *ab initio* theory, the Hartree-Fock model. This inherently assumed that the molecular structure of N_2 could be described by a single Slater determinant of appropriate molecular orbitals, as opposed to

multiple Slater determinants.

6. This research assumed that the expansion modes of the electron field operator could be identified with the molecular orbitals of the noninteracting molecules. This is only true if there is no coupling between molecular electronic, vibrational, rotational, and kinematic modes. Hence, the Born-Oppenheimer approximation was implicitly invoked.

Recommendations

Based upon the results of this research, several suggestions for the improvement of this effort, as well as for future efforts may be made. The most important are listed below.

1. From Figure 7.11 it is apparent that there is a slight discrepancy between the radial amplitude of the Ar 4s orbital as predicted by numerical Hartree-Fock program as opposed to the g90 program. Since the g90 code uses an approximate fit to the atomic orbitals, i.e. the 6-31G basis, the Hartree-Fock code should produce a more accurate description of atomic orbital wavefunctions because it solves for the orbitals directly. One method to improve the description of the 4s orbital would be to incorporate the Hartree-Fock result.

2. The first Born approximation may be a factor preventing better agreement of the predicted Ar-N_2 cross section with the experimental measurements, although a rough estimation indicates that the Born approximation should be

appropriate. It is recommended that the kinematic calculation be taken to the level of a distorted Born wave approximation.

3. The results of the entire calculation reside upon a numerical grid which was chosen with little information about the nature of the Ar-N_2 interaction. Now that the present results are known, the numerical gridding of the interaction should be refined to concentrate more points near the edge of the potential well, roughly 2 to 6 au.

4. The present research is purely theoretical, based upon the quantized Lagrangian for interacting electron and radiation fields. Since the electronic wavefunctions are determined by an *ab initio* calculation, without empirical parameters of any kind, their inclusion does not degrade the pristine nature of the calculation. In light of this, the fact that the predicted cross section for the Ar-N_2 reaction is low by a factor of 5 of the experimental mean, while the data itself varies by a factor of 6, should be considered as a successful application of the theory. Based upon the results of the present research, it is recommended that the two-electron exchange mechanism be applied to other chemical reactions exhibiting the same unusual combination of spin-forbidden transitions and fast reaction rates. Reactions (1.1) and (1.2) would be excellent candidates for future analysis.

Bibliography

Bibliography

1. Piper, L.G., Cowles, L.M., and Rawlins, W.T., *J. Chem. Phys.*, **85**, 3369 (1986).
2. Huber, K.P., and Herzberg, G., *Molecular Spectra and Molecular Structure. IV. Constants of Diatomic Molecules*, Van Nostrand Reinhold (1979).
3. Herzberg, G., *Molecular Spectra and Molecular Structure. I. Spectra of Diatomic Molecules*, Krieger (1989).
4. Slanger, T.G., and Black, G., *J. Chem. Phys.*, **55**, 2164 (1971).
5. Young, R.A., and Van Volkenburgh, G., *J. Chem. Phys.*, **55**, 2990 (1971).
6. Taylor, G.W., and Setser, D.W., *J. Chem. Phys.*, **58**, 4840 (1973).
7. Katayama, D.H, and Thomas, J.M., *J. Chem. Phys.*, **94**, 4797 (1991).
8. Gaydon, A.G., and Wolfhard, H.G., *Flames*, Chapman and Hall (1979).
9. Kolts, J.H., Brashears, H.C., Setser, D.W., *J. Chem. Phys.*, **67**, 2931 (1977).
10. Mott, N.F., and Massey, H.S.W., *The Theory of Atomic Collisions*, Oxford (1965).
11. Massey, H.S.W., and Burhop, E.H.S., *Electronic and Ionic Impact Phenomena*, Oxford (1969).
12. McDaniel, E.W., Cermak, V., Dalgarno, A., Ferguson, E.E., Friedman, L., *Ion-Molecule Reactions*, Wiley-Interscience (1970).
13. Sauerbrey, R., Liegel, J., Schatzlein, E., and Langhoff, H., *Appl. Phys.*, **25**, 283 (1981).
14. Power, E.A., and Thirunamachandran, T., *Phys. Rev. A*, **28** 2649 (1983).
15. Power, E.A., and Thirunamachandran, T., *Phys. Rev. A*, **28** 2663 (1983).
16. Power, E.A., and Thirunamachandran, T., *Phys. Rev. A*, **28** 2671 (1983).
17. Power, E.A., and Thirunamachandran, T., *Phys. Rev. A*, **45** 2671 (1992).
18. Craig, D.P. and Thirunamachandran, T., *Molecular Quantum Electrodynamics*, Academic (1984).

19. Craig, D.P. and Thirunamachandran, T., *Chem. Phys.*, **167**, 229 (1992).

20. Panofsky, W.K.H., and Phillips, M., *Classical Electricity and Magnetism*, Addison-Wesley (1962).

21. Wooley, R.G., Proc. R. Soc., **A321**, 557 (1971).

22. Loudon, R., *The Quantum Theory of Light*, Clarendon Press (1983).

23. Atkins, P.W., and R.G. Wooley, Proc. R. Soc., **A319**, 549 (1970).

24. Power, E.A., and S. Zienau, Phil. Trans. Roy. Soc. London, **A251**, 427 (1959).

25. Baym, G., *Lectures on Quantum Mechanics*, Benjamin/Cummings (1969).

26. Cohen-Tannoudji, C., Dupont-Roc, J., Grynberg, G., *Atom-Photon Interactions*, Wiley-Interscience (1992).

27. Cohen-Tannoudji, C., Dupont-Roc, J., Grynberg, G., *Atom-Photon Interactions*, Wiley-Interscience (1992).

28. Scholes, G.D., Clayton, A.H.A., and Ghiggino, K.P., J. Chem. Phys., **97**, 7405, (1992).

29. Lee, T.D., *Particle Physics and Introduction to Field Theory*, Harwood (1988).

30. Aitchison, I.J.R., and Hey, A.J.G., *Gauge Theories of Particle Physics*, Adam Hilger (1989).

31. Sakurai, J.J., *Advanced Quantum Mechanics*, Addison-Wesley (1967).

32. Akhiezer, A.I., and Berestetskii, V.B., *Elements of Quantum Electrodynamics*, Oldbourne (1962).

33. Bjorken, J.D., and Drell, S.D., *Relativistic Quantum Mechanics*, McGraww-Hill (1964).

34. Gasiorowicz, S., *Elementary Particle Physics*, Wiley, (1966).

35. Fetter, A.L., and Walecka, J.D., *Quantum Theory of Many-Particle Systems*, McGraw-Hill, (1971).

36. McWeeny, R., *Methods of Molecular Quantum Mechanics*, Academic, (1989).

37. Ziman, J.M., *Elements of Advanced Quantum Theory*, Cambridge University Press, (1969).

38. Wilson, S., and Diercksen, G.H.F., *Methods in Computational Molecular Physics*, Plenum, (1992).

39. Brandsen, B.H., and Joachain, C.J., *Physics of Atoms and Molecules*, Longman (1983).

40. Fetter, A.L., and Walecka, J.D., *Theoretical Mechanics of Particles and Continua*, McGraw-Hill (1980).

41. Froese-Fischer, C., *The Hartree-Fock Method for Atoms*, Wiley-Interscience (1977).

42. Hehre, W.J., Radom, L., Schleyer, P.v.R., Pople, J.A., *ab initio Molecular Orbital Theory*, Wiley-Interscience (1989).

43. Boys, S.F., *Proc. Roy. Soc. (London)*, **A200**, 542 (1950).

44. GAUSSIAN 70, Hehre, W.J., Lathan, W.A., Newton, M.D., Ditchfield, R., and Pople, J.A., Program No. 236, Quantum Chemistry Program Exchange, Indiana University, Bloomington, IN.

45. Hehre, W.J., Stewart, R.F., and Pople, J.A., *J. Chem. Phys.*. **51**, 2657 (1969).

46. Hehre, W.J., Ditchfield, R., and Pople, J.A., *J. Chem. Phys.*, **56**, 2257 (1972).

47. Binkley, J.S., and Pople, J.A., *J. Chem. Phys.*, **66**, 879 (1977).

48. Francl, M.M., Pietro, W.J., Hehre, W.J., Binkley, J.S., Gordon, M.S., DeFrees, D.J., and Pople, J.A., *J. Chem. Phys.*, **77**, 3654 (1982).

49. GAUSSIAN90, Frisch, M.J., Head-Gordon, M., Trucks, G.W., Foresman, J.B., Schlegel, H.B., Raghavachari, K., Robb, M.A., Binkley, J.S., Gonzalez, C., Defrees, D.J., Fox, D.J., Whiteside, R.A., Seeger, R., Melius, C.F., Baker, J., Martin, R.L., Kahn, L.R., Stewart, J.J.P., Topiol, S., and Pople, J.A., Gaussian, Inc. (1990).

50. Newton, R.G., *Scattering Theory of Waves and Particles*, Springer Verlag (1982).

51. Goldberger, M.L., and Watson, K.M., *Collision Theory*, Wiley (1964).

52. Messiah, A., *Quantum Mechanics*, Wiley (1963).

53. Merzbacher, E., *Quantum Mechanics*, Wiley (1961).

54. Bennet, W.R., *Annals Phys.*, **18**, 367 (1962).

55. Heard, H.G., *Bull. Am. Phys. Soc.*, **9**, 65 (1964).

56. Bennett, W.R., in *Applied Optics Supplement 2 on Chemical Lasers*, edited by Schuler, K. and Bennett, W.R., Optical Society of America (1965).

57. Puech, V., Collier, F., and Cottin, P., *J. Chem. Phys.*, **67**, 2887 (1977).

58. Ernst, W.E., Tittel, F.K., Wilson, W.L., Marosky, G., *J. Appl. Phys.*, **50**, 3879 (1979).

59. Sauerbrey, R., and Langhoff, H., *Appl. Phys.*, **22**, 393 (1980).

60. Searles, S.K., *Appl. Phys. Lett.*, **25**, 735 (1974).

61. Searles, S.K., and Hart, G.A., *Appl. Phys. Lett.*, **25**, 74 (1974).

62. Basov, N.G., Danilychev, V.A., Dolgikh,V.A., Kerimov, O.M., Dobanov, A.N., and Suchkov, A.F., *JETP Lett.*, **20**, 53 (1974).

63. Arfken, G., *Mathematical Methods for Physicists*, Academic (1985).

64. Lentz, J., "An Examination of the Spectral Radiation (NH, H, and A) Produced by Collisions of NH_3 Molecules with Argon Metastable Atoms," Ph.D dissertation, The University of Tennessee (1970).

65. Herzberg, G., *Atomic Spectra and Atomic Structure*, Dover (1944).

66. Chisholm, C.D.H., *Group Theoretical Techniques in Quantum Chemistry*, Academic Press (1976).

67. Cotton, F.A., *Chemical Applications of Group Theory*, Interscience (1963).

68. Jaffe, H.H., and Orchin, M., *Theory and Applications of Ultraviolet Spectroscopy*, Wiley (1964).

69. Lofthus, A., and Krupenie, P.H., *J. Phys. Chem. Ref. Data*, **6**, 113 (1977).

70. Schultz, H.A., *J. Chem. Phys.*, **44**, 377 (1966).

71. McGregor, W.K., *Proceedings of the 9 th International Conference on Phenomena in Ionized Gases*, Bucharest, Romania, Editura Academiei Republicii Socialiste Romania, 33 (1969).

72. Parr, T.P., and Martin, R.M., *J. Chem. Phys.*, **69**, 1613 (1978).

73. Sadegi, N., and Setser, D.W., *Chem. Phys. Lett.*, **82**, 44 (1981).

74. Tyndall, G.W., de Vries, M.S., Cobb, C.L., and Martin, R.,M., *J. Chem. Phys.*, **87**, 5830 (1987).

75. Bennett, W.R., and Flint, J., *Physical Review A*,.**18**, 2527 (1978).

76. Cutshall, E.R., and Muschlitz, E.E., *J. Chem. Phys.*, **70**, 3171 (1978).

77. Sanders, R.A., Schweid, AN., Weiss, M., and Muschlitz, E.E., *J. Chem. Phys.*, **65**, 2700 (1976).

78. Hardy, K.A., and Sheldon, J.W., *Physical Review A*, **37**, 2689 (1988).

79. Winicur, D.H., and Fraites, J.L., *J. Chem. Phys.*, **61**, 1548 (1973).

80. Lee, W., and Martin, R.M., *J. Chem. Phys.*, **63**, 962 (1975).

81. Piper, L.G., Velazco, J.E., and Setser, D.W., *J. Chem. Phys.*, **59**, 3323 (1973).

82. Tabayashi, K., and Shobatake, K., *J. Chem. Phys.*, **84**, 4919 (1986).

83. Vredenbregt, E.J.D., Boom, W., van Gerwen, R.J.F., and Beijerinck, H.C.W., *Chemical Phys.*, **145**, 267 (1990).

84. Goldstein, H., *Classical Mechanics*, Addison-Wesley (1980).

85. Wolfram Research, Inc., *Mathematica*, Version 2.2 (1993).

86. Geller, M., and Griffith, R.W., *J. Chem. Phys.*, **40**, 2309 (1964).

87. Sakurai, J.J., *Modern Quantum Mechanics*, Benjamin/Cummings (1985).

88. Gradshteyn, I.S., and Ryzhik, I.M., *Tables of Integrals, Series, and Products*, Academic (1980).

89. Parasoft Corporation, Inc., *Express*, Version 3.2.5 (1993).

90. Precision Visual, Inc., *PV-Wave Reference Manual* (1993).

91. Cohen-Tannoudji, C., Diu, B., and Laloe, F., *Quantum Mechanics*, Wiley (1977).

92. *Handbook of Physics*, Condon, E.U., and Odishaw, H., Eds., McGraw-Hill (1967).

Appendices

Appendix I

Derivation of the Differential Scattering Cross Section

The scattering cross section is a measurable quantity which parametrizes the relative efficiency of a collision. The discussion which follows is included for completeness only, and has been extracted largely from four sources, Newton [50], Goldberger [51], Sakurai [87], and Cohen-Tannoudji [91].

To obtain physical intuition, consider a picture in which a beam of N_b particles impinges upon a target of area A having N_t scattering centers. Each scattering center will present an effective area, σ , to the impinging beam. The probability, P, that a beam particle will collide with a target particle is simply

(AI.1) $$P = \frac{N_t \sigma}{A}$$

The total number of collisions experienced by the beam is $N_c = P\, N_b$. The effective area per scattering center follows as

(AI.2) $$\sigma = \frac{N_c A}{N_b N_t}$$

It is useful to express the particle numbers as fluxes. Suppose that the beam has a duration of t, then the volume of the beam which passes through the target is given by $V = (vt)A$. Thus, the number of beam particles undergoing collisions is $N_b = \rho V = \rho vtA$, where ρ is the beam density. Then the cross section may be written as

$$\sigma = \frac{(N_c/t)}{(N_b/t)N_t} A$$
$$= \frac{1}{\rho v} \frac{(N_c/t)}{N_t} \qquad \text{(AI.3)}$$

This shows that the cross section may be clearly thought of as the transition rate per target, per unit incoming flux.

The differential cross section relates the probability that the system will undergo a state-altering collision and subsequently scatter into a specified solid angle in phase space, given that the system was prepared in a defined initial state. This is simply the probability that the system has a particular out state, given a well defined in state. Consider the in state as propagating as a wave packet in the barycentric, or center-of-mass, frame. Furthermore, let the overall system be described by two momentum amplitude functions, $g^{CM}(\underline{p})$ and $g(\underline{p})$, which describe the center of mass and the relative momentum, respectively, of the wave packet. For a well-defined state, the amplitude functions will be very sharply peaked at a center of mass momentum $\underline{P_i}$ and a relative momentum $\underline{p_i}$ and have widths Δ^{CM} and Δ such that $\Delta^{CM} << \left|\underline{P_i}\right|$ and $\Delta << \left|\underline{p_i}\right|$. The translational energies corresponding to the peak momenta are E_i^{CM} and E_i respectively. Also, let the wave packets be centered at a spatial position corresponding to an impact parameter, $\underline{b}$. The in state may be explicitly written as

$$\Psi_{in}(\underline{b}, \alpha, \underline{P}, \underline{p}; t) = g^{CM}(\underline{P}) e^{-i(\underline{P}\cdot\underline{b} + E^{CM}t)}\, g(\underline{p}) e^{-i(\underline{p}\cdot\underline{b} + Et)} |\alpha\rangle \qquad \text{(AI.4)}$$

where the ket describes all the remaining quantum numbers. The center of mass and relative translational energies are given by

(AI.5)
$$E^{CM} = \frac{P^2}{2M}$$
$$E = \frac{p^2}{2\mu}$$

where M represents the total system mass and μ represents the reduced mass of the collision partners. Furthermore, the amplitude functions are normalized as

(AI.6) $$\int d\underline{p}\ |g(\underline{p})|^2 = 1$$

From (5.46) the out state is determined from the in state by the scattering matrix, or function. This can be written in the present context as

(AI.7) $$\Psi_{out}(\beta, \underline{P}, \underline{p}; t) = \iint d\underline{P'}\, d\underline{p'}\, S(\beta, \underline{P}, \underline{p}; \alpha, \underline{P'}, \underline{p'})\, \Psi_{in}(\underline{b}, \alpha, \underline{P'}, \underline{p'}; t)$$

The scattering matrix for the center of mass can be written as in (5.51),

(AI.8)
$$S(\beta, \underline{P}, \underline{p}; \alpha, \underline{P'}, \underline{p'}) = \delta_{\beta\alpha} - 2\pi i \delta(E_\beta + E^{CM} + E - (E_\alpha + E'^{CM} + E'))$$
$$\cdot \delta(\underline{P} - \underline{P'})\, T_{\beta\alpha}(E, \underline{P}, \underline{P'}, \underline{p}, \underline{p'})$$

The delta function $\delta(\underline{P} - \underline{P'})$ explicitly conserves the overall center of mass momentum. Furthermore, note that $T_{\beta\alpha}(E, \underline{P}, \underline{P'}, \underline{p}, \underline{p'})$ is written only as a function of the energy due to the relative momenta of the collision, $E = p^2/2\mu$, and not as a function of the energy due to the motion of the center of mass of the system. This is because it is assumed that the interaction Hamiltonian is translationally invariant over all space. It is likely, though, for the collision to depend upon the available energy due to the relative momentum of the collision partners.

Substituting (AI.8) into (AI.7) generates an expression for $\Psi_{out}(\beta, \underline{P}, \underline{p}; t)$ when $\beta \neq \alpha$,

$$\Psi_{out}(\beta,\underline{P},\underline{p};t) = -2\pi i \iint d\underline{P'}\, d\underline{p'}\ \delta(E_\beta - E_\alpha + E^{CM} - E'^{CM} + E - E')$$

(AI.9)
$$\delta(\underline{P}-\underline{P'})\, T_{\beta\alpha}(E,\underline{P},\underline{P'},\underline{p},\underline{p'})$$
$$g^{CM}(\underline{P'})e^{-i(\underline{P'}\cdot\underline{b}+E'^{CM}t)}\ g(\underline{p'})e^{-i(\underline{p'}\cdot\underline{b}+E't)}|\beta\rangle$$

The probability that the system will enter a solid angle centered at $\underline{P_i}$ and $\underline{p_i}$ in the two respective momentum spaces is given by

(AI.10)
$$\chi(\underline{b}) = \int d\underline{P}\int d\underline{p}\ \left|\Psi_{out}(\beta,\underline{P},\underline{p};t)\right|^2$$

By assuming that all impact parameters are equally likely, the total probability of a collision which sends the system into cones centered at $\underline{P_i}$ and $\underline{p_i}$ is the integral of (AI.10) over all impact parameters within the plane which is defined by interaction cross-sectional area, A. For impact parameters outside A, the integration is null, so the integration in the $\underline{b}$ plane may be allowed to extend over the entire plane perpendicular to the momentum vectors. Use is then made of the result,

(AI.11)
$$\int_{\substack{plane\perp\\ to\ \underline{p_i}}} d\underline{b}\, e^{i\underline{b}\cdot(\underline{p''}-\underline{p'})} = (2\pi)^2\delta(\underline{p''_\perp}-\underline{p'_\perp})$$

where the momentum vectors $\underline{p'_\perp}$ and $\underline{p''_\perp}$ are perpendicular to $\underline{p_i}$, which was the initial momentum vector of the system. Using (AI.11) in the extension of (AI.10) reduces the probability to

$$\chi = \frac{(2\pi)^4}{A}\int_{C^{CM}} d\underline{P}\left|g^{CM}(\underline{P})\right|^2 \int_C d\underline{p}\iint d\underline{p'}\, d\underline{p''}\ \delta(E_\beta - E_\alpha + E - E')$$

(AI.12)
$$\cdot\delta(E_\beta - E_\alpha + E - E')T^*_{\beta\alpha}(E,\underline{P},\underline{p},\underline{p'})\, T_{\beta\alpha}(E,\underline{P},\underline{p},\underline{p''})$$
$$\cdot g^*(\underline{p'})g(\underline{p''})\,\delta(\underline{p''_\perp}-\underline{p'_\perp})$$

where the delta function $\delta(\underline{P}-\underline{P'})$ has been used to reduce the intermediate center of mass momentum integrations. Note that the delta functions retain the original meaning if they are rewritten as

$$\delta(E_\beta - E_\alpha + E - E')\delta(E_\beta - E_\alpha + E - E') = \delta(E_\beta - E_\alpha + E - E')\delta(E' - E'') \tag{AI.13}$$

It is possible to rewrite the delta function $\delta(E'-E'')$ as a delta function over the momentum components parallel to $\underline{p_i}$, which can be used to combine with the delta function of the perpendicular momentum components to create a single delta function relating the integration momentum vectors. The probability then becomes,

$$\chi = \frac{(2\pi)^4}{A}\frac{\mu_i}{p_i}\int_{C^{CM}} d\underline{P}\left|g^{CM}(\underline{P})\right|^2 \int_C d\underline{p}\int d\underline{p'}\,\delta(E_\beta - E_\alpha + E - E') \cdot\left|T_{\beta\alpha}(E,\underline{P},\underline{p},\underline{p'})\right|^2 \cdot\left|g(\underline{p'})\right|^2 \tag{AI.14}$$

where μ_i and p_i are the initial reduced mass and momentum modulus respectively. The final step uses the assertion that $g(\underline{p})$ is so sharply peaked about the initial momentum vector that the scattering matrix and the delta function may be evaluated at the initial momentum, e.g. $T_{\beta\alpha}(E,\underline{P},\underline{p},\underline{p'}) \approx T_{\beta\alpha}(E,\underline{P},\underline{p},\underline{p_i})$. Then the normalization of $g(\underline{p})$ is used to further simplify the integral. A similar assertion is used for the center of mass integration, where in the barycentric system $\underline{P_i} = \mathbf{0}$, leading to the following form for the probability,

$$\chi = \frac{(2\pi)^4}{A}\frac{\mu_i}{p_i}\int_C d\underline{p}\,\delta(E_\beta - E_\alpha + E - E_i)\left|T_{\beta\alpha}(E,\underline{p},\underline{p_i})\right|^2 = \frac{(2\pi)^4}{A}\frac{\mu_i}{p_i}\mu_f p_f \int_C d\hat{p}\,\left|T_{\beta\alpha}(E,\underline{p},\underline{p_i})\right|^2 \tag{AI.15}$$

where the initial and final mass and momenta are explicit. The explicit notation of the momenta of the center of mass has been dropped for clarity. In the event of an elastic collision, $p_i = p_f$. The relative beam flux is equal to $(At)^{-1} \equiv F$, where t is the beam duration time. In accord with the concept of AI.3, the scattering cross section can be written in a differential form as the ratio of the transition rate per solid angle per unit flux. Defining χ / t as the transition rate we obtain,

$$\begin{aligned} \frac{\chi/t}{F} &= \int_C d\hat{p}\,(2\pi)^4 \mu_i \mu_f \frac{p_f}{p_i} \left| T_{\beta\alpha}(E, \underline{p}, \underline{p_i}) \right|^2 \\ &\equiv \int d\Omega \frac{d\sigma}{d\Omega} \end{aligned} \tag{AI.16}$$

Thus, in the case of an elastic collision where $\mu_i = \mu_f$ and $p_i = p_f$, the differential cross section is

$$\frac{d\sigma}{d\Omega} = (2\pi)^4 \mu^2 \left| T_{\beta\alpha}(E_i, \underline{p}, \underline{p_i}) \right|^2 \tag{AI.17}$$

Since the initial momentum is usually a well defined quantity, the differential cross section may be written in terms of the momentum transfer, $\underline{p} - \underline{p_i} \equiv \underline{q}$, allowing the differential cross section to be rewritten as [50],

$$\frac{d\sigma_{\beta\alpha}}{d\Omega}(\underline{q}) = (2\pi)^4 \mu^2 \left| T_{\beta\alpha}(E_i, \underline{p_i}, \underline{q}) \right|^2 \tag{AI.18}$$

The total cross section is then simply the angular integral of (AI.18).

$$\sigma_{\beta\alpha}(q) = (2\pi)^4 \mu^2 \int d\Omega \left| T_{\beta\alpha}(E_i, \underline{p_i}, q, \Omega) \right|^2 \tag{AI.19}$$

where $E_i = p_i^2 / 2\mu_i$.

Appendix II

Atomic Units

The set of atomic units was developed to facilitate computations of atomic and molecular physics and chemistry. All atoms and molecules are roughly the same size, have roughly the same charge, and roughly the same mass. Atomic units, also called Hartree units, address these similarities by assigning the dimensionless value of unity to three fundamental constants, [92]

(AII.1) $$\hbar = c = m_e \equiv 1$$

The first constant is Planck's constant, the second is the speed of light in a vacuum, and the third is the rest mass of the electron.

There are two ramifications of the assignments (AII.1). The first is that the important equations, such as Schrödinger's equation, are freed from the clutter of extra constants. The second is that the dynamical variables themselves must account for the proper dimensional behavior. Thus, a standard unit of length, charge, mass, velocity, energy, momentum, angular momentum, and even time are defined. These units represent useful scaling parameters for physical phenomena.

A list of the values of the most relevant atomic units is given in Table AII.1.

Table AII.1 A Listing of Useful Atomic Units

Physical Entity	Unit Name	Relation to Fundamental Constants	Numerical Value in Other Common Unit Systems
Length	bohr, a_o	$\frac{\hbar^2}{m_e e^2}$	0.529177 Angstroms
Energy	hartree	$\frac{m_e e^4}{\hbar^2}$	27.2116 eV
Velocity	---	$\frac{e^2}{\hbar}$	2.18769×10^{6} m-s^{-1}
Momentum	---	$\frac{m_e e^2}{\hbar}$	1.99288×10^{-24} kg-m-s^{-1}
Angular Momentum	---	$\hbar$	1.05459×10^{-34}J-s
Time	---	$\frac{\hbar^3}{m_e e^4}$	2.41889×10^{-17} s

Appendix III

Proof of (7.54)

The development of the analytic solution to the intermolecular potential hinged upon a closed form solution to (7.54),

$$\int d^3k\, e^{i\underline{k}\cdot\underline{W}} \frac{e^{-\lambda^2 k^2}}{k^2} = \frac{2\pi^2}{W} erf\left(\frac{W}{2\lambda}\right) \tag{7.54}$$

The proof of this identity may be determined by examining the left side of the equation in more detail. Utilizing spherical coordinates, the integral may be expressed as

$$\begin{aligned} \int d^3k\, e^{i\underline{k}\cdot\underline{W}} \frac{e^{-\lambda^2 k^2}}{k^2} &= 2\pi \int_0^{\infty} dk \int_0^{\pi} d\theta\, sin\theta\, e^{ikWcos\theta} e^{-\lambda^2 k^2} \\ &= 2\pi \int_0^{\infty} dk\, e^{-\lambda^2 k^2} \int_{-1}^{1} dx\, e^{ikWx} \\ &= 4\pi \int_0^{\infty} dk\, e^{-\lambda^2 k^2} \frac{sin(kW)}{kW} \end{aligned} \tag{AIII.1}$$

By introducing the spherical Bessel function, $j_0(kW) = \frac{sin(kW)}{kW} = \sqrt{\frac{\pi}{2kW}} J_{1/2}(kW)$, the integral can be written as

$$\int d^3k\, e^{i\underline{k}\cdot\underline{W}} \frac{e^{-\lambda^2 k^2}}{k^2} = 4\pi \sqrt{\frac{\pi}{2W}} \int_0^{\infty} dk\, e^{-\lambda^2 k^2} \frac{J_{1/2}(kW)}{\sqrt{k}} \tag{AIII.2}$$

The right side may be evaluated using standard integration tables [88],

$$\int_0^{\infty} dx\, x^{\nu-1} e^{-\alpha x^2} J_{\nu}(\beta x) = 2^{\nu-1} \beta^{-\nu} \gamma\left(\nu, \frac{\beta^2}{4\alpha}\right) \tag{AIII.3}$$

where $\gamma\left(\nu, \frac{\beta^2}{4\alpha}\right)$ refers to the incomplete gamma function [63]. Letting $\nu = 1/2$, $\beta = W$, and $\alpha = \lambda^2$ yields for (AIII.2),

$$\int_0^\infty dk\, e^{-\lambda^2 k^2} \frac{J_{1/2}(kW)}{\sqrt{k}} = \sqrt{\frac{\pi}{2W}} 2^{-1/2} W^{-1/2} \gamma\left(\frac{1}{2}, \frac{W^2}{4\lambda^2}\right) \tag{AIII.4}$$

Thus, (AIII.2) may be written as

$$\int d^3k\, e^{i\underline{k}\cdot\underline{W}} \frac{e^{-\lambda^2 k^2}}{k^2} = \frac{2\pi^{3/2}}{W} \gamma\left(\frac{1}{2}, \frac{W^2}{4\lambda^2}\right) \tag{AIII.5}$$

The incomplete gamma function can be related to the error function in the event that $\nu = 1/2$, i.e.,

$$erf(z) = \frac{1}{\sqrt{\pi}} \gamma\left(\frac{1}{2}, z^2\right) \tag{AIII.6}$$

Upon substituting (AIII.6) into (AIII.5), one arrives at the desired result,

$$\int d^3k\, e^{i\underline{k}\cdot\underline{W}} \frac{e^{-\lambda^2 k^2}}{k^2} = \frac{2\pi^2}{W} erf\left(\frac{W}{2\lambda}\right) \tag{AIII.7}$$

VITA

James Alan Drakes was born in the small agricultural community of North East, Pennsylvania, which lies on the southern shore of Lake Erie in the middle of a 30 mile stretch of grape vineyards known for producing Welch's grape juice and a host of fine wines. He attended North East High School, graduating in 1981. He went on to study physics at the University of Dayton, graduating with a B.S. degree in the spring of 1985. He was a member of the Society of Physics Students, Sigma Pi Sigma honor society, and a member and officer of Chi Sigma Alpha fraternity.

In the fall of 1985, he enrolled into the University of Tennessee Space Institute. He was given the opportunity to fulfill his research assistantship under the tutelage of the Technology branch of Sverdrup Technology, Inc., technical contractor to the United States Air Force Arnold Engineering Development Center. During that time, his research was focused in the area of radiative transfer in rocket plumes. He graduated with a M.S. degree in Physics in the spring of 1987.

At that time he enrolled in the Ph.D. program at Penn State University, with an emphasis on condensed matter physics. After two years of experimenting with critical phenomena of monolayers of fluid and superfluid helium, he decided to accept a full-time position with Sverdrup Technology, Inc., where he is presently employed. Upon his return to Tennessee, he re-enrolled in the University of Tennessee Space Institute and began his studies in the chemical physics of combustion exhausts. His experimental and theoretical research was conducted at the facilities of AEDC, under the joint direction of Dr. A. A. Mason and Dr. W. K. McGregor. He finished his Ph.D. program in physics in the spring of 1994.

He is currently a member of the American Physical Society, and a senior member of the American Institute of Aeronautics and Astronautics.

He married the former Nancy Ollinger, daughter of Mary Ollinger and the late Charles Ollinger, also of North East, Pennsylvania on July 20, 1985. They reside in Manchester, Tennessee and have two sons, James Charles and Dylan Joseph.